Assessment of novel utilisation pathways for biogas and nitrogenous waste streams at wastewater treatment plants

Oliver Richard Grasham

Submitted in accordance with the requirements for the degree of Doctor of Philosophy as part of the integrated PhD with MSc in Bioenergy

April 2019

Centre for Doctoral Training

School of Chemical and Process Engineering

University of Leeds

Declaration of Authorship

The candidate confirms that the work submitted is his own, except where work, which has formed part of jointly authored publications, has been included. The contribution of the candidate and the other authors to this work has been explicitly indicated below. The candidate confirms that appropriate credit has been given within the thesis where reference has been made to the work of others.

Much of the work contained in Chapter 5 is based on the following publication:

Grasham O, Dupont V, Camargo-Valero MA, García-Gutiérrez P, Cockerill T. Combined ammonia recovery and solid oxide fuel cell use at wastewater treatment plants for energy and greenhouse gas emission improvements. *Applied Energy* 2019;240:698–708.

As lead author, the candidate performed all numerical modelling, process modelling, data analysis and the candidate also wrote the manuscript. The remaining authors provided supervision, guidance and corrections to the manuscript.

Acknowledgements

First and foremost, I would like to express my profound gratitude to Dr. Valerie Dupont, Dr. Miller Alonso Camargo-Valero and Prof. Timothy Cockerill for their supervisory and moral support during my PhD. Without Dr. Dupont's initial encouragement to apply for the Bioenergy Centre for Doctoral Training, I would not be submitting this thesis, or any thesis at all. Her weekly meetings since have been a constant source of encouragement, motivation and insight. For this I am truly grateful.

There are other University of Leeds staff members I would also like to thank for their expertise and assistance, including; Emily Bryan-Kinns, James McKay, Karine Alves Thorne, Dr. David Elliot, Sheena Bennett, Kevin Dyer, Scott Prichard and Ed Woodhouse. Without whom, this submission would be happening many, many months in the future. On a similar note, I would like to reserve special thanks to Dr. Christian Aragon Briceño, Cigdem Oz and Dr. Tande Lifita Nguve whose patience, humour and training in the lab unequivocally enhanced my aptitude and enjoyment. A special mention also to the staff at Esholt WWTP and Yorkshire Water for their help and willingness to assist me with data and sample collection.

My appreciation extends to the EPSRC for their funding via the Bioenergy Centre for Doctoral Training and NWaste2H2 grant - making this entire process possible. I have spent much of the last three and a half years with Dr. Lee Roberts, Robert White, Hana Mandova, Kiran Palmer, Charlotte Stead, Diarmaid Cleary, Andy Dyer and Gillian Finnerty. From day one, the surrounding wit, passion and drive, bettered me as a researcher but more so as a person. Further recognition to Dr. Douglas Phillips, Dr. Dave Allen, Daisy Thomas, Andy Price and Fernando Barba whose friendship has been an invaluable distraction.

Outside of the University; Rory Dormer, Matt Jakeman, Jack Hutchinson, Lizi Gilham, Martin Ashcroft, Nicole Ashcroft, Fin Boyter, Joe Gumb, Matt Quigley and Gavin Schofield have been a constant crutch and you have my lifelong appreciation of your friendship. Catriona Dunn has been there every step of the

way with me, your love and laughter has kept me going. I cannot thank you enough. I am indebted to you and hope I can replicate the support you have given me during your PhD.

My mother Clare, my father Nigel, my sisters Patricia and Victoria, my Nan Betty and those no longer here, have been and continue to be my inspiration. Thank you.

Missy, this is for you.

Abstract

A combination of process modelling, numerical modelling, economic analysis and experimental techniques have been used to analyse novel utilisation pathways for biogas and nitrogenous waste streams at wastewater treatment plants. An assessment of a large wastewater treatment plant serving a population equivalent of 750,000 people was carried out including compositional analysis of various streams at the facility. This facilitated three key findings that function as the bedrock for the rest of study: the facility's greenhouse gas footprint, its energy balance and its digestate liquor ammonia concentration.

Aspen Plus process modelling software was used to develop a system that recovers ammonia in a way that prepares it for thermochemical decomposition to hydrogen and nitrogen. Sensitivity analysis showed that air stripping was energetically preferable to steam stripping as the base recovery technology. This was proceeded by an absorption step that uses a water-only solvent and finally a distillation step that was found to be energetically preferential to flash separation. The modelling showcased an ability to recover 91% of ammonia contained in the digestate liquor. Ordinarily, the wastewater treatment plant would recycle the liquor back into its conventional process. By recovering the ammonia, and diverting it away from conventional treatment, it is proposed that the plant will experience significant reductions in energy consumption and GHG emissions.

Aspen Plus was used to develop a process model that combines the recovery of ammonia with the operation of an internally reforming solid oxide fuel cell stack, which uses a blend of biomethane and ammonia as its fuel. A numerical model was developed that precisely calculates its power production potential, based on a commercially available solid oxide fuel cell stack. It was found to operate at a net electrical efficiency of 48% and if implemented at the referenced wastewater treatment plant, would increase the site's power production by 45%. It was also proposed that the site's lifecycle GHG emissions would reduce by 7.7% due to a combination of ammonia diversion and reduced grid electricity consumption. An economic study showed that it would be

financially viable to implement this technology at the site with a positive net present value facilitated after eight years of operation.

A process model was developed which utilises recovered ammonia and biomethane as feedstock for a thermochemical H_2 production system. Steam to carbon ratios of 2, 3 and 4 were analysed to assess their impact on H_2 production, energetics and financial viability. The scenario with a steam to carbon ratio of 3 showcased the best economic potential with net present value becoming positive during its 14^{th} year of operation. It was proposed that if the H_2 produced was used as a vehicle fuel for bus transportation the process implementation would reduce the facility's lifecycle GHG emissions by 25%.

An H_2-rich syngas was generated experimentally using ammonia, methane and steam feeds in a fixed-bed reactor holding a conventional Ni-Al catalyst. Ammonia, methane and carbon monoxide conversions were less than predicted via equilibrium calculations. However, the general selectivity of products closely resembled that of equilibrium equivalents – showcasing an ability to combine the steam reforming of methane and the decomposition of ammonia in a single reactor.

Table of Contents

List of Tables

Table of Figures

Abbreviations

ACT	Advanced conversion technology
AD	Anaerobic digestion
ADBA	Anaerobic Digestion & Bioresources Association
AFC	Alkaline fuel cell
APEA	Aspen Process Economic Analyzer
ASP	Activated sludge process
BOD	Biological oxygen demand
CfD	Contracts for Difference
CHP	Combined heat and power
COD	Chemical oxygen demand
CV	Cell voltage (V)
CSD	Compression, storage and dispensing technology
FCEV	Fuel cell electric vehicle
FCHJU	Fuel Cells and Hydrogen Joint Undertaking
FiT	Feed in tariff
GC	Gas chromatograph
GHG	Greenhouse gas
GHSV	Gas hourly space velocity
GWP	Global warming potential
HHV	Higher heating value
HPS	High pressure scrubbing
HTS	High temperature shift
HT-SOFC	High temperature solid oxide fuel cell
IT-SOFC	Intermediate temperature solid oxide fuel cell
IR-SOFC	Internally reforming solid oxide fuel cell
LTS	Low temperature shift
MCFC	Molten carbonate fuel cell
MLVSS	Mixed liquor volatile suspended solids
NH3-DEC	Ammonia decomposition reaction
NPV	Net present value

ONS	Office for national statistics
PAFC	Phosphoric acid fuel cell
PEMFC	Proton exchange membrane fuel cell
PSA	Pressure swing adsorption
RAS	Return activated sludge
RHI	Renewable heat incentive
RO	Renewables obligation
ROC	Renewables obligation certificate
RPI	Retail price index
SAS	Surplus activated sludge
S:C	Steam to carbon ratio
SMR	Steam methane reforming reaction
SOFC	Solid oxide fuel cell
SPGI	Siemens Power Generation, Inc
SS	Suspended solids
TAN	Total ammoniacal nitrogen
TCD	Thermal conductivity dectectors
TKN	Total kjeldahl nitrogen
TN	Total nitrogen
TP	Total phosphorus
TPB	Triple Phase Boundary
TSS	Total suspended solids
UWWTD	Urban Wastewater Treatment Directive
VSS	Volatile suspended solids
WAS	Waste activated sludge
WGS	Water gas shift reaction
WHSV	Weight hourly space velocity
WWTP	Wastewater treatment plant
YSZ	Yttria-stabilised zirconia

Nomenclature

A_{cell}	Cell active area (m^2)
β	*A*pparent charge transfer coefficient
ΔH	Enthalpy change of reactions (kJ)
D_{eff}	Effective diffusivity ($m^2\ s^{-1}$)
D_{O_2}	Oxygen ordinary diffusivity ($m^2\ s^{-1}$)
ε	Porosity of electrode material
E	Nernst voltage potential (V)
E_a	Activation energy (J)
E_o	Reference voltage (V)
F	Faraday constant (96,48 C mol^{-1})
δ_a	Component thickness (m)
i	Discount rate (10%)
I	Current (A)
j	Current density (A m^{-2})
j_l	Limiting current densities (A m^{-2})
j_0	Exchange current density (A m^{-2})
$\dot{m}_x$	Mass flow rate of species *x* (kg h^{-1})
M_x	Molar mass of species *x* (g mol^{-1})
$\dot{n}_x$	Mole flow rate of species *x* (kmol h^{-1})
n	Number of participating electrons
n_{act}	Activation loss (V)
$n_{CHP,\,net}$	Net cogeneration efficiency
$n_{elect,\,net}$	Net electrical efficiency
n_{ohm}	Ohmic loss(V)
n_{conc}	Concentration loss (V)
n_{therm}	Thermal efficiency
N	Plant lifetime (yr)
N_{OL}	Number of operators per shift
N_{np}	Number of non-particulate processing steps
ρ	Anode material resistivity (Ω m)

p_x	Partial pressure of component *x* (bar)
$P_{AC,net}$	Net AC system power (kW)
P_{cell}	Cell operating pressure (bar)
P_P	Number of processing steps
p.e.	Population equivalent
P_{gross}	Cell output power (kW)
Q_L	Heat loss from cell (kW)
Q_R	System heat output
Q_{trans}	Heat transfer across cell (kW)
R	Universal gas constant (8.314 J mol^{-1} K^{-1})
R_{ohmic}	Global internal resistance (Ω m^2)
R_t	Net cashflow for the year
τ	Tortuosity of electrode porous material
T_{cell}	Cell Temperature (K)
t_{exp}	Experiment length (h)
U_F	Fuel Utilisation (fraction)
$\dot{V}_x$	Volume flow of species *x* (l h^{-1})
γ_a	Anode activation barrier overpotential coefficient (A m^{-2})
γ_c	Cathode activation barrier overpotential coefficient (A m^{-2})
y_x	Mole fraction of species *x*

1 Introduction

1.1 Opening Remarks & Rationale

1.1.1 Climate Change and UK Policy

Over the time period in which this body of work has been carried out, the planet has experienced the four hottest years on record (2015-2018) [1,2]. The unprecedented change in the earth's climate has been determined, irrefutably, as anthropogenically induced due to emission of greenhouse gases (GHGs). The consequences are, and will continue to be, devastating. Global efforts to combat climate change began in 1992 at the Rio Earth Summit and led to multiple international treaties committing governments to limit their GHG emissions [3]. 23 years after the Rio Earth Summit, 195 countries adopted the first legally binding universal global climate change deal, at COP21 in Paris, which aims to keep average global warming well below 2°C above pre-industrial levels [4].

The UK, one of these 195 nations, has also constitutionally pledged to reduce GHG emissions by 80% on 1990 levels by 2050, under the Climate Change Act [5]. The Carbon Plan [6] has set out a framework in order to achieve these targets, focussing on key areas such as; energy efficiency, low carbon heating, electricity, transport, industry and waste management. However, it is the UK's policy towards bioenergy, waste management and hydrogen deployment within this framework that is of particular relevance to this research. The carbon plan highlights the key role bioenergy will play in the UK's energy infrastructure to 2050, and led to the development of a 'UK Bioenergy Strategy' [7]. This blueprint suggests that 12% of the UK's primary energy demand will

be met through bioenergy in 2050 via a series of pathways that include: waste, heat, transport and electricity.

Waste-derived energy is expected to make up a considerable proportion of UK renewable and bio energy over the coming years. One of the primary methods this will be achieved is via anaerobic digestion (AD) of waste material. Feedstocks for AD include; sewage sludge, food waste, farm manures and slurries [7,8]. AD generates a 'biogas' composed mostly of methane (55-70%) and carbon dioxide (30-45%) [9]. The 'biomethane' fraction of biogas makes for its satisfactory use as a fuel. As such, it is generally utilised as a fuel for internal combustion combined heat and power (CHP) units or can be scrubbed of its impurities and used as a vehicular fuel or for injection to the natural gas grid. The anaerobic digestion of sewage sludge is already extensively used in the UK with over 80% of sewage treated by AD [10] and delivers roughly 30% of AD-derived energy [11].

1.1.1 Nitrogen removal at wastewater treatment plants – energy use and GHG emissions

Before wastewater management was integrated as an indispensable part of human society, the apathetic disposal of wastewater resulted in serious ramifications for the environment and human health [12]. From the late 19th century, advancement in wastewater treatment technology and process development erupted [12]. By the 1960s Ludzack and Ettinger proposed the use of an anoxic zone to achieve biological denitrification (conversion of nitrite to gaseous nitrogen) in the now well established activated sludge process [13]. A decade later, James Barnard patented a process that applies both nitrification (conversion of ammonium to nitrite) and denitrification that could achieve almost total destruction of nitrogen present in wastewater [14].

When the EU placed strict limits on the discharge of ammonia and nitrites to water-courses under the Urban Wastewater Treatment Directive (91/271/EEC) [15] and the Water Framework Directive (2000/60/EC) [16], it was the de/nitrification process that was most widely implemented in order to

meet restrictions. Although significantly improving the health of aquatic ecosystems affected by wastewater induced eutrophication, nitrogen removal resulted in unfavourable impacts for plant operators. Firstly, the aerobic bacteria involved in nitrification require the pumping of vast quantities of oxygen, which increases the electricity consumption of the plant. Secondly, nitrous oxide (N_2O) is often emitted due to its formation as an intermediary and side-product during de/nitrification [17]. N_2O is a fierce GHG with 298 times the global warming potential of CO_2. In essence, not only does nitrogen removal increase plant operational costs but also deepens its GHG footprint.

One key contributor of total nitrogen in wastewater plants is the digestate liquor from AD units which is recycled back to the head of the treatment works. The nitrogen contained in digestate liquor originates from the assimilation of nitrogen by activated sludge bacteria or retention in solid fractions of the wastewater which are internally retained until the plant's anaerobic digester. Here, a significant volume of ammonium is formed during biological processing. The liquid fraction of the digestate produced during AD, known as liquor, is often logistically too difficult to be sold for land application and is recycled back into the conventional treatment process. However, it is estimated that this stream contains 15-20% of a facility's nitrogen load [18,19], thus, significantly impacting on plant GHG emissions and energy consumption.

In support of attempts to close nutrient cycles and recuperate valued products from waste, ammonia recovery from digestate liquor has received considerable attention from industry and academia [20–26]. A wide variety of options are available such as, membrane filtration, adsorption techniques, struvite precipitation and stripping with absorption [20,23]. In the vast majority of cases, ammonia is being recovered for use as a fertiliser. However, ammonia, comprising ¾ of hydrogen on a molar basis, can also be used for energy recovery [27] or as a hydrogen storage medium [28]. Regardless of the desired end use, the diversion of ammonia from conventional treatment has the potential to significantly impact the sustainability of wastewater management.

1.1.2 H_2 Potential

Hydrogen has long been touted as an energy vector for the future, due to its unparalleled energy/weight ratios, the potential for long-term storage and for pollution free emissions. However, interest has surged recently with the view that green hydrogen has an important part to play in the global transition to carbon-free economies [29–32]. Hydrogen's flexibility seems to be its unique selling point, with an ability to penetrate all energy sectors; heat, power, transport and storage.

There is vast interest in the use of green hydrogen as a replacement or addition to the natural gas grid for decarbonisation of the heat sector. In the UK, Northern Gas Networks are researching the potential of converting the gas grid of Leeds, in the UK, to 100% hydrogen [33]. The concept is that natural gas is converted to hydrogen via steam reforming with attached carbon capture and storage technology. Meanwhile, the collaborative project, 'HyDeploy', involving a consortium consisting of members such as Cadent Gas Limited and ITM Power are pilot testing the addition of hydrogen in the gas grid of Keele University by up to 20% in order to better understand the implications of partial injection [34]. A recent consortium including Northern Gas Networks and Cadent is now looking at expanding the scope of 100% H_2 penetration of the UK's gas grid in the North of England into heat for industrial, commercial and domestic heat but also power generation and transport (H21 North of England).

Due to the intermittency of renewable electricity production from wind and solar and the inefficiency and cost of battery storage, 'power to gas' schemes have generated vast global interest. The hope is to use hydrogen as an energy storage medium, produced from excess renewable electricity via electrolysis, and either directly inject it into gas grids or store and use it for electricity generation via fuel cells during times of grid deficits [35–37]. RWE's 'power-to-gas' project, launched in 2015, is producing hydrogen for gas injection from a PEM electrolyser at a competitive overall efficiency of 86% [38].

Hydrogen has long been recognised as a plausible transport fuel of the future. Its lightweight properties and pollution-free emissions at the point of use mean this vision is starting to be realised. It is envisaged that 800,000 fuel cell electric

vehicles will be on the road in Japan by 2030 [39] and 37,000 in California by 2023 [40]. Meanwhile, the UK government announced the roll-out of 200 new hydrogen powered police cars and taxis in March 2018 [41] a year after the announcement of a £23 million fund to aid development of FCEV infrastructure [42]. The indication here is that green hydrogen may play an important role in decarbonising the transport sector for years to come.

1.1.3 Energy Recovery at wastewater treatment plants

In general, WWTPs use the anaerobic digestion of sewage sludge to recover energy used during the treatment process. The biogas produced, which generally contains 55-65% methane is used as fuel for combustion-based combined heat and power (CHP) units [43]. However, more often than not, the energy demand for the facility is not matched by the renewable power generated onsite. Resultantly, treatment plants must purchase grid-based electricity, which adds to both operational costs and lifecycle greenhouse gas emissions.

Providing solutions to these sustainability issues at WWTPs is becoming an increasingly important issue. The consequences of climate change have had and will continue to impact on the global security of supply of fresh water due to changes in hydrological cycle patterns [44]. Combined with the growing global population and the mass migration from rural areas to cities, there is more pressure than ever for sustainable wastewater treatment to maintain a secure supply of clean, fresh water sustainably.

The research drive to overcome energy deficits at WWTPs is extensive and wide-ranging [45–52]. One frequently discussed option is the replacement of existing CHP units with fuel cells which operate at superior electrical efficiencies. Several studies have analysed the implementation of sewage-biogas operated solid oxide fuel cells (SOFCs), modelling electrical efficiencies of over 50% [53–55]. This demonstrates the potential to make vast improvements on the current electrical efficiencies of standard CHP units typically used in the industry which stand at around 35%.

One important advantage of SOFCs is their flexibility of potential fuel options [56]. Their high temperature operation means they are capable of carrying out thermochemical reactions internally such as steam methane reforming (SMR), water-gas-shift, partial oxidation of hydrocarbons and ammonia decomposition to produce a hydrogen rich syngas (a gas mixture composed mainly of hydrogen and carbon monoxide). The hydrogen is then utilised electrochemically in the SOFC with oxygen from an air supply to generate electrical power. Due to their capability of carrying out both SMR and ammonia decomposition, in theory, both recovered ammonia and biogas from WWTPs could be used as direct fuel inputs for SOFC operation.

1.1.4 Research Problem

There are three key research problems this work will address. The first is the need to address GHG emissions from wastewater treatment. The second is whether the energetic balance of wastewater treatment can be improved via proposed process designs. The third is developing a novel method of sustainable hydrogen production. Each topic is of abundant academic and commercial interest, whilst their combination fulfils an academic niche.

During sewage treatment, nitrogen is removed from wastewater via biological processing in a WWTP's activated sludge process. It is a problematic process for two key reasons.

(1) The aeration required contributes to roughly ¼ of a WWTP energy demand [57].

(2) The biological transformation generates substantial N_2O emissions; a powerful GHG [58,59].

As such, WWTP operators are under increasing pressure to reduce both the energy demand and the GHG emissions while meeting stringent ammonium discharge constraints. Thus, source separation and diversion of nitrogenous material from the activated sludge process is an obvious method of preventing the use of energy and emissions of GHGs. Digestate liquor is often promoted for

diversion and ammonia recovery but with the aim of producing agricultural products, which are uncompetitive in the well-established commercial fertiliser market [21]. Alternatively, this research proposes the use of recovered ammonia from this waste stream along with biomethane for either hydrogen production or use in a SOFC. It will then be determined whether the processes can address the research problems discussed.

1.1.5 Research Gap

Hydrogen production from biogas and biomethane has been the focus of research for several years. It has been identified as a far more sustainable method of H_2 production compared to conventional steam reforming of natural gas; with roughly half the lifecycle emissions of GHGs [60]. There have also been examples of pilot testing of bio-methane steam reforming at a WWTP in Germany, where it is seen as an important component in a future hydrogen infrastructure [61].

However, examples of unconventional reagent use in the steam reforming process are extremely limited. Zin et al. (2015) assessed the production of hydrogen via the reforming of ethanol with the aqueous fraction of bio-oil produced from fast pyrolysis and liquefaction of pine wood. In Zin et al.'s study (2015), the aqueous fraction acted as both a conventional steam reagent and a supplementary source of hydrocarbon-produced hydrogen and was systematically advantageous. There exists a clear knowledge gap in the use of ammonia recovered from wastewater treatment waste streams as a feedstock, alongside biomethane for hydrogen production.

There are reports of research carried out on the use of ammonia in fuel cells [63–66]. However, limited examples of combining ammonia and biogas as inputs for SOFCs exist and fewer that have discussed the extended impacts of recovering ammonia from wastewater treatment plants or other renewable sources for such use. Thus, by combining process modelling, energetic analysis, GHG emission analysis, financial analysis and experimental validation, a robust understanding of the feasibility of the proposed processes will be achieved.

1.2 Aims, Scope, Objectives

1.2.1 Aims

With the identification of the discussed research gaps, a number of aims have been constructed to help plug them: 1) determine the feasibility and impact of recovering ammonia from digestate liquor generated at wastewater treatment facilities in a manner that is acceptable for the following two aims; 2) assess the feasibility and impact of utilising the recovered ammonia for use, alongside biomethane, as fuel for a solid oxide fuel cell; 3) evaluate the feasibility and impact of employing the recovered ammonia, alongside biomethane, as a feedstock for thermochemical hydrogen production.

1.2.2 Objectives

To achieve these aims, the following four key research objectives (listed below in italics) have been generated and encompass a number of research activities (displayed below under each key objective).

Key objective #1: Assessment of reference wastewater treatment plant for mass flows, energy balance and GHG emissions.

1. Thorough sampling of various process streams at Esholt wastewater treatment plant over a one-year period.
2. Compositional analysis of samples. Characterisation of: Kjeldahl Nitrogen (TKN), Ammoniacal-nitrogen (NH3-N), Chemical Oxygen Demand (COD), Total Suspended Solids (TSS), Volatile Suspended Solids (VSS), Total Phosphorus (TP), Total Reactive Phosphorus (PO_4^{3-}).
3. Development of a mass flow diagram by applying the above concentrations to anticipated total flows of wastewater throughout treatment process.
4. Determination of the plant energy balance, informed by data gathered in activities 1-3 and external sources.

5. Determination of plant GHG footprint, informed by data gathered in activities 1-3 and external sources.

Key objective #2: Perform process modelling of ammonia recovery, SOFC processing and thermochemical hydrogen production systems.

1. Perform thorough literature review of current ammonia recovery options.
2. Use mean ammonia concentration found in Esholt's digestate liquor stream as input to Aspen Plus process modelling software.
3. Calculate the quantity of lime required to convert ammonium to ammonia.
4. Perform energy-based sensitivity analysis, using Aspen Plus, on technology options for ammonia recovery: stripping, absorption, flash separation, distillation.
5. Select highest performing recovery technology options and operational conditions for the final process.
6. Review thoroughly the literature on solid oxide fuel cell process modelling.
7. Develop a Microsoft Excel-based numerical model for robust power production data.
8. Develop integrated process flow for solid oxide fuel cell system using Aspen Plus
9. Perform energy-based sensitivity with heat integration alongside ammonia recovery process for selection of optimum operational conditions.
10. Assess energetic and GHG emission impacts for SOFC process implementation at Esholt WWTP.
11. Review thoroughly the literature on steam reforming-based process for hydrogen production.
12. Develop integrated process flow for hydrogen production system using Aspen Plus.

13. Perform energy-based sensitivity with heat integration alongside ammonia recovery process for selection of optimum operational conditions.
14. Assess energetic and GHG emission impacts for SOFC process implementation at Esholt WWTP.

Key objective #3: Perform economic assessments for the introduction of ammonia recovery, solid oxide fuel cell and hydrogen production systems in the WWTP.

1. Cost the equipment based on Aspen Plus process diagrams for each system including biogas purification step.
2. Cost the installation costs of equipment.
3. Determine operational costs for each system.
4. Identify eligible renewable incentives.
5. Identify revenue options for each process, including offset energy costs.
6. Perform net present value analysis to evaluate the financial attractiveness of the different processes.
7. Thorough sensitivity analysis, covering a range of realistic scenarios.

Key objective #4: Experimentally analyse the production of hydrogen via combined ammonia decomposition and steam methane reforming.

1. Review thoroughly the literature of catalysts that can be used for both steam methane reforming and ammonia decomposition.
2. Identify ammonia concentrations to be used for experimental input, based on results of process model.
3. Perform analysis for feed molar steam to carbon ratios 2, 3 and 4.
4. Perform analysis for temperatures 700°C, 750°C and 800°C
5. Perform runs with and without the presence of ammonia
6. Determine catalyst carbon deposition on catalyst via CHNS tests
7. Analyse ammonia decomposition via HACH LCK 303, ammonium cuvette tests.
8. Compare experimental results with equilibrium model.

1.3 Thesis Structure

This thesis contains eight Chapters. Please note that due to the interdisciplinary nature of this thesis, each results chapter contains an individual outline of research methods rather than an overarching methodology thesis chapter.

Chapter 1 aims to introduce the research topic, provide rationale for the study and outline the investigation's aims and objectives.

Chapter 2 contains a comprehensive review of literature encompassing each key research topic. It aims to inform the reader of fundamental theories behind: wastewater treatment; the influence of nitrogen on the energetics and emission of greenhouse gases from wastewater treatment; the role of anaerobic digestion in producing biogas and ammonia-containing digestate liquor; ammonia recovery techniques, fuel cells for the production of heat and power; hydrogen production techniques and feedstock options; and the current status of UK financial incentives for renewable energy. The chapter also critically identifies the current status of research amongst these themes and showcases the gaps which have led to this study taking place and helped highlight its novelty. Furthermore, the literature discussed will be consistently referred to throughout subsequent chapters to place the author's work in context.

Chapter 3 covers the assessment performed for the reference plant. It acts as the foundation for each of the subsequent chapters, detailing mass flows, energetics and GHG emission data that are used as an inventory for everything from model inputs to critical analysis and determination of process implementation feasibility.

Chapter 4 focusses on process identification, modelling and optimisation of ammonia recovery from digestate liquor. It utilises flow and compositional data found in Chapter 3 to match real-life operation as best as possible. An economic assessment of the process has been carried out to indicate whether it is financially worthwhile in the context of systems set up downstream of the ammonia recovery unit.

Chapter 5 synthesises a number of analysis techniques to facilitate a thorough investigation into the feasibility and impact of implementing a combined

ammonia recovery and biomethane-ammonia fuelled SOFC process at the referenced wastewater treatment plant. A numerical model has been developed to calculate the power production potential of a SOFC stack based on a real operational module. The numerical model results feed into a process model, developed on Aspen Plus which integrates both ammonia recovery and SOFC processing. Effective heat integration has also been employed that provides robust indications of thermal power production potentials. A thorough economic study has been carried out detailing investment and operational costs, income flows, expense savings, payback periods and net present value. An economic sensitivity analysis has also been carried out via evaluation of a number of hypothesised scenarios to justify its true financial viability.

Chapter 6 details the process model developed which combines the ammonia system from Chapter 4 with the thermochemical production of hydrogen. Thorough sensitivity analysis has been carried out on the process model to optimise system efficiency and analyse the impact of temperatures, pressures and feed molar steam to carbon ratios in the reformer. It contains an evaluation of the potential impact on the energetics and GHG footprint of the reference facility. The work in Chapter 6 is finalised with an economic study, utilising similar methods as employed during Chapter 5 to demonstrate the financial viability of process implementation and evaluate which process is the more monetarily attractive.

Chapter 7 covers the research activities detailed under the final thesis Objective displayed in Section 1.2.2. It book-ends the results chapters with the experimental validation of the use of a singular packed-bed reactor for the production of a hydrogen rich syngas facilitated by a combination of ammonia decomposition, steam methane reforming and water-gas-shift reactions.

Chapter 8 concludes the thesis with a summary of its findings, a comprehensive critical analysis of the research methodologies and identification of gaps in which future work can be developed.

2 Literature Review

2.1 Anthropogenic Nitrogen Balance

Diet depending, humans consume between 20-100g of protein daily per capita [67]. The nitrogen contained in this protein enters the food-chain via initial vegetational uptake from soil, and makes up the entirety of nitrogen processed by humans. The consequential metabolic breakdown augments the release of N-containing products in urine as urea and in faeces as unassimilated protein. The quantity of N in human waste is estimated to be on average 13g of nitrogen per capita per day [67] and is carried through sewage systems and eventually to WWTPs.

If soluble nitrogen in wastewater is left untreated, a plethora of issues may occur. For example, the final plant effluent will discharge ammonium ions (NH_4^+) which are toxic to fish, cause eutrophication and oxidise to undesirable nitrates. Nitrogen, alongside phosphorus and potassium, is a key determining nutrient for the status of water-based trophic communities. If NH_4^+ is released from WWTPs, its bioavailability facilitates overactive biological activity; causing algal blooms and excessive growth of aquatic plants [68]. Eutrophication is the resultant blockage of light and depletion of dissolved oxygen, which can devastate entire habitats.

In response to these environmental concerns, the EU has placed strict limits on nutrient emissions from WWTPs to land water bodies. Under the Urban Waste Water Treatment Directive (UWWTD) (91/271/EEC) and the Water Framework Directive (2000/60/EC) [15,16], all large WWTPs located in areas with 'sensitive' waters, in member states, must reduce the overall load of N and P entering the facilities by at least 75%. Smaller plants are not exempt either,

but with local environmental regulators enforcing limitations. From these directives came the introduction of tertiary (nutrient removal) treatments to wastewater plants in order to transform N and P to more favourable forms. This is most frequently done either through biological processing in upgraded activated sludge processes and/or through chemical precipitation [69].

However, tertiary treatment has led to undesired consequences for WWTP operators. For example, energy consumption in the activated sludge process can be increased by 60-80% with the introduction of nitrogen removal [18]. Meanwhile, amplified capital expenditure is required for chemicals for P-precipitation or additional carbon for intensified biological activity. These problems not only impact on the financial stability of a facility, but also its lifecycle greenhouse gas (GHG) emissions. The latter is further augmented by nitrous oxide (N_2O) emissions affiliated with biological nitrogen removal [59]. N_2O is a potent GHG with a global warming potential (GWP) 298 times that of CO_2 over a 100 year period [58]. It has also been proven as the most important ozone-depleting substance during the 21st century [70]. Moreover, the IPCC [58] calculated that 2.8% of anthropogenic N_2O emissions originate from WWTPs.

2.2 Wastewater treatment plant design and sewage system

Figure 2-1 illustrates a conventional WWTP design. Sewage enters the plant and is pre-treated via screening and grit removal to limit equipment damage downstream. A percentage of suspended solids present in the wastewater are then allowed to settle in a primary clarifier, forming a sludge. The sludge is removed and dewatered before being anaerobically digested. The liquid effluent from the primary clarifier is sent to the activated sludge process (ASP) for biological processing and secondary settlement. The water from the secondary clarifier is ordinarily clean enough to be placed into a water source. A proportion of the sludge from the secondary clarifier is recycled back through the ASP as it contains the bacterial matter required in the aeration basin. The rest is dewatered for anaerobic digestion with the primary sludge. The

anaerobic digester produces a methane-rich biogas, which is sometimes scrubbed for methane purification for use in a combined heat and power (CHP) unit; providing heat and electricity for the plant. Alternatively, if the biogas has been upgraded to biomethane via scrubbing, it can be sent into the natural gas grid or compressed for use as a transport fuel.

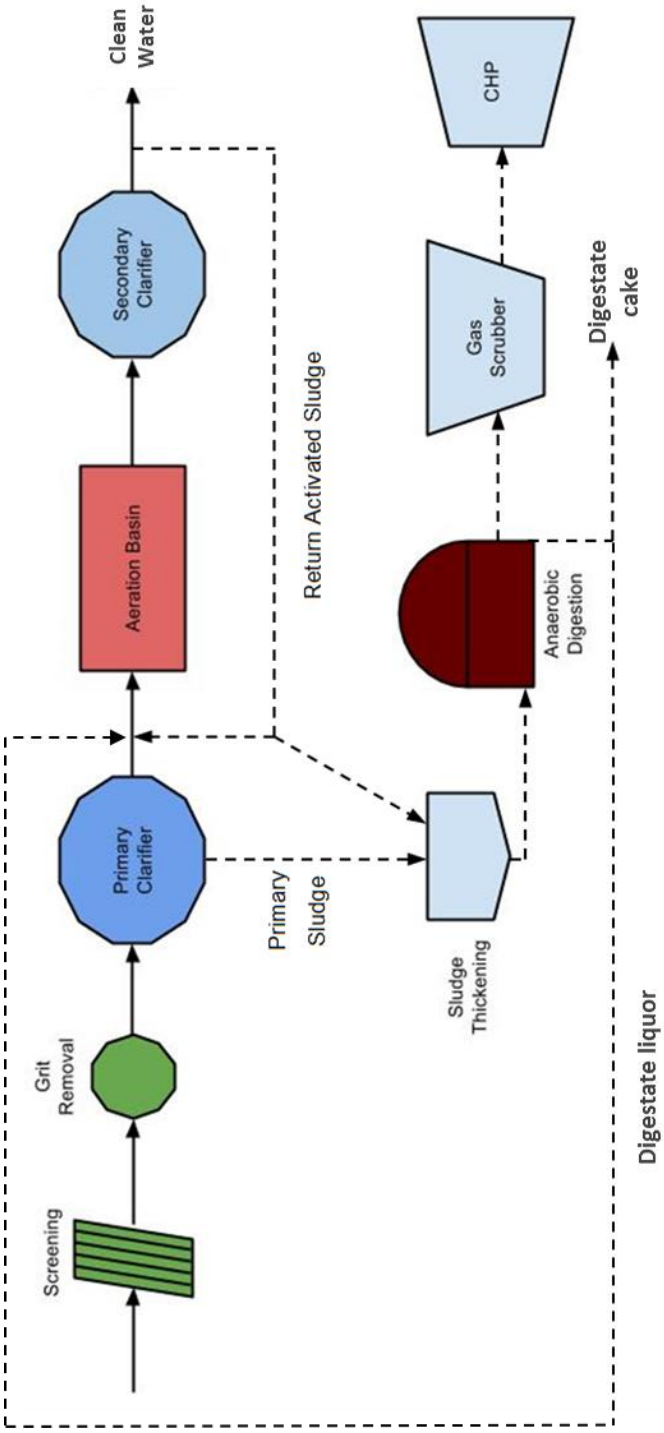

Figure 2-1. *Typical WWT process flow diagram.*

2.2.1 Pre-treatment

The preliminary stage in most wastewater treatment involves the removal of gross solids from the influent. For efficient biological processing later, problematic contraries such as plastics, rags and rubber must be withdrawn. Table **2-1** shows the typical composition of screenings; ordinarily removed via centrifugation or filtration and pressing. There are energy costs during the screening with additional energy demand associated with their removal from site, conventionally via road transport [71].

Table 2-1. *Typical Screening Composition* [72]

Component	Concentration (%dw)
Paper	20-50
Rags	15-30
Plastic	5-20
Rubber	0-5
Vegetable Matter	0-5
Faecal Matter	0-5

As illustrated in Figure 2-1, the second stage of pre-treatment comprises of the removal of grit. Here, influent flow velocity is reduced to ~0.3 m/s to allow inorganic grit to settle in a specific chamber, of which grit channels and detritors are the most common options in the UK [71].

Primary clarifiers, or primary sedimentation tanks, act to remove 60-70% of suspended solids (SS) in the wastewater. The SS contain around 30-35% of the Biochemical Oxygen Demand (BOD) due to the high organic nature of the solid fraction; thus making an effective feedstock for anaerobic digestion [71]. Primary sedimentation most commonly occurs in horizontal flow or radial flow tanks. The target for both is to allow the settlement of heavy solids for removal by scrapers and to clear the scum that forms on the surface-water, composed of mostly fats, oils and grease. The settled material, known as primary sludge, can then be thickened/dewatered and transferred for anaerobic digestion

treatment. The supernatant (liquor) from sludge thickening is sent for activated sludge processing.

2.2.2 Activated Sludge Process

The activated sludge process (ASP) is the most common wastewater 'secondary' treatment system in the UK. Biological activity is used to degrade organic material and remove phosphorus or nitrogen-containing products in the final effluent. The ASP is ordinarily comprised of an aeration basin, a secondary clarifier and a recycling system (Figure 2-1). The primary clarifier effluent and recycled sludge from the secondary clarifier is first transferred to an aeration basin where it meets air and biomass (bacteria and protozoa). The aim is for full degradation of carbonaceous waste by bacteria which utilise the embedded carbon for energy [73]. The biomass, along with the degraded organic material (known as activated sludge) is then allowed to settle in a secondary clarifier, before being recycled back into the aeration basin. The biomass can, in essence, be re-used to continue degrading waste entering the treatment facility. However, surplus sludge is generated as the biomass reproduce and multiply. Thus, fractions are siphoned off and mixed with primary sludge for anaerobic digestion. The treated liquid effluent is then passed through for disinfection or, more likely, placed straight into a water-course.

2.2.3 Nitrification/Denitrification during ASP

In order to comply with national and international regulations on the discharge of nitrogen-containing compounds to water-courses, a series of steps have been incorporated to the activated sludge process to remove them. Nitrogen contained in the food humans consume is mostly emitted into sewers in the form of urea and some organic nitrogen held in proteins. However, much of this is quickly transformed into ammonium ions, as amino acids undergo deamination and urea is hydrolysed. The result, is that by the time wastewater

reaches a treatment facility, roughly 40% of the total N is in ammonium form [73,74].

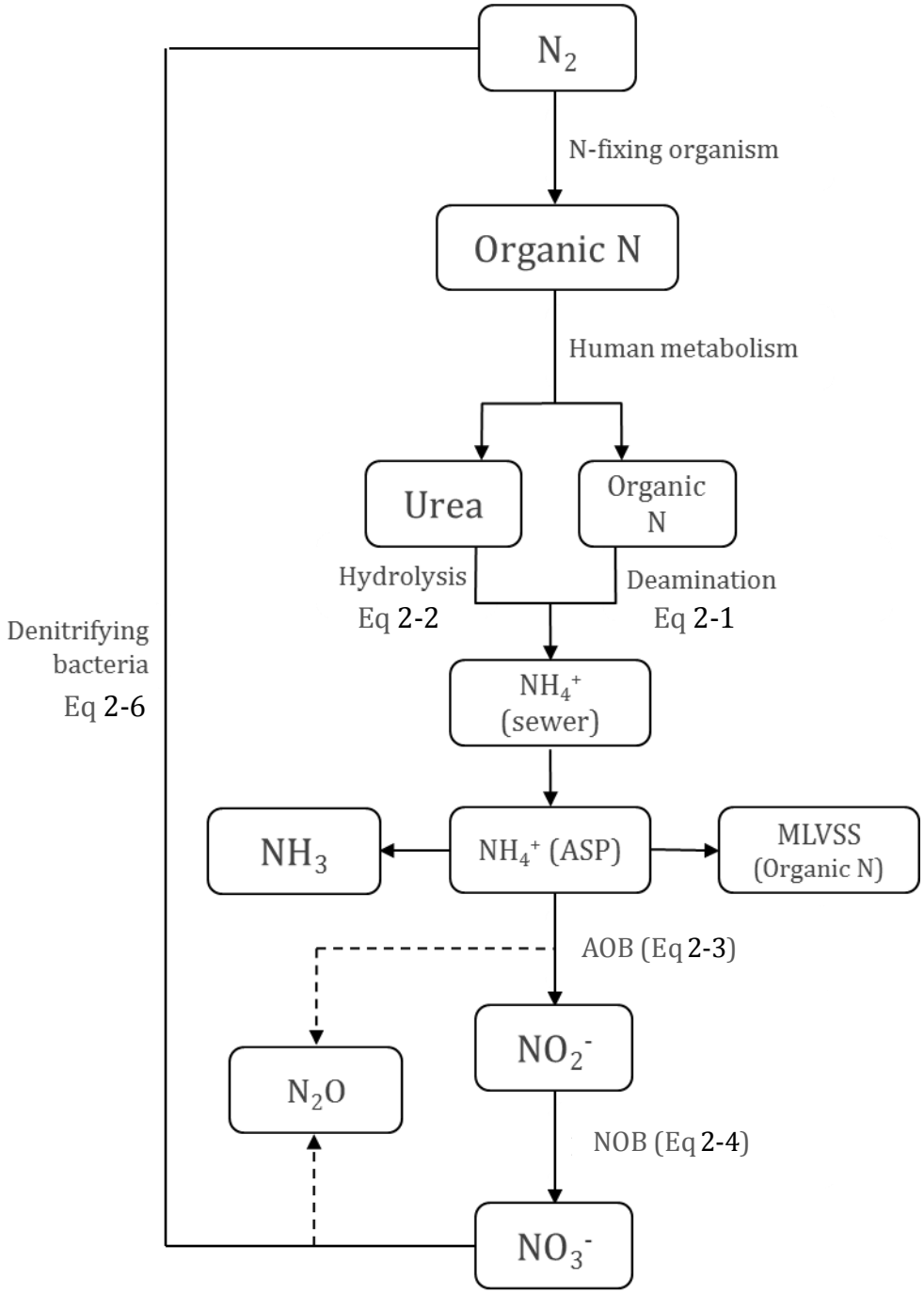

Figure 2-2. *Wastewater nitrogen cycle. Interpreted from:* [73]

As Figure 2-2 shows, the elimination of total nitrogen (TN) occurs in 4 transformative steps. The first is the deamination of amino acids to ammonium ions and the hydrolysis by bacteria of urea to ammonia (Eq 2-1 & Eq 2-2).

Amino acid – *organotrophs*	→	NH_4^+ + Acid	**2-1**
$NH_2COHN_2 + H_2O$ – *Citrobacteria*	→	$2NH_3 + CO_2$	**2-2**

In addition to materialising in sewage pipes, ammonification is promoted in the aeration basin. There are then three potential chemical routes ammonium ions can take [73]:

1. Used as a N-nutrient source by organotrophs and nitrifying bacteria (nitrogen assimilation)
2. Air stripped as NH_3 in high pH conditions
3. Oxidised to nitrite ions (NO_2^-)

Whilst N can be lost to the atmosphere as ammonia, under a typical temperature range of 10-20^{0}C and a pH between 7-8.5, roughly 95% of the reduced form of nitrogen will remain as ammonium for conversion to nitrite (Equation 2-3). Alternatively they could be used nutritionally by the bacteria and trapped as organic-N in the mixed liquor volatile suspended solids (MLVSS). In total, approximately 14% of the nitrogen entering a wastewater plant will be assimilated by bacteria [73].

The nitrification process begins with the oxidation of ammonium to nitrite (Eq 2-3) by ammonium-oxidising bacteria (AOB) [17,73]. The AOB's use ammonia and CO_2 as energy and carbon sources respectively. The nitrite ions are then quickly oxidised to nitrate (NO_3^-) (Eq 2-4) by nitrate-oxidising bacteria (NOB) in other text [17]. Combined, these processes complete the nitrification process, providing the equation displayed in Eq 2-5.

$NH_4^+ + 1.5\ O_2$ AOB	→	$NO_2^- + 2H^+ + H_2O$	**2-3**
$NO_2^- + 0.5\ O_2$ - NOB	→	NO_3^-	**2-4**
$NH_4^+ + 2O_2$ - *Nitrifiers*	→	$NO_3^- + 2H^+ + H_2O$	**2-5**
$C_5H_{10}O_5 + 4NO_3^- + 4H^+$	→	$5CO_2 + 7H_2O + 2N_2$	**2-6**

This process occurs in the aeration basin with a greater than stoichiometric quantity of dissolved oxygen (DO) available. Forster [71] suggests that "good nitrification" will occur with a DO of ≥ 2mg/l for sludge aged 10 days or more at 10^0C. Greater aeration also limits N_2O emissions [75]. For these reasons, the energy required for aeration for nitrogen elimination makes up around 27% of a treatment facility's energy demand [57].

Nitrate ions are used as substrate by denitrifying bacteria; where nitrate is reduced to molecular nitrogen (equation 2-6). There are a number of intermediate steps in the denitrification process where nitrate is converted to NO_2, then to NO, followed by N_2O and finally to nitrogen gas. But, essentially heterotrophic denitrifying bacteria utilise nitrate in the absence of DO to degrade organic carbon (cBOD) for energy; e.g. lyxose as shown in equation 2-6. Thus, in order for effective denitrification to occur, there are three major requirements: firstly, an abundant population of denitrifying bacteria, secondly an anoxic environment, and finally, sufficient presence of soluble cBOD. Some of the nitrate-N is nutritionally used by bacteria, whilst the N_2 generated as a metabolic bi-product is removed totally from the system, escaping to the atmosphere in gaseous form.

As Figure 2-2 indicates, nitrous oxide (N_2O) forms as an intermediary product of denitrification and is emitted to the atmosphere. Thus, if full denitrification is not achieved, substantial nitrous oxide will be emitted. As such, N_2O emissions can be limited by maintaining low O_2/DO levels and high COD:N ratios in the anaerobic basin [17]. N_2O can also be formed during nitrification by autotrophic and heterotrophic oxidising bacteria alike. However, unlike during denitrification, N_2O is not an intermediate in the catabolic pathway [17]. Contrary to the denitrification step, limited O_2 will facilitate N_2O production by

AOB during nitrification. AOB will attempt to save oxygen and use nitrite as an electron donor instead and generate N_2O preferentially over NO_2. This may also occur if nitrite is not converted to nitrate quickly enough, leaving high concentrations of NO_2 in the nitrification tank [76].

The emissions of N_2O from WWTPs contribute an estimated 2.8% of total anthropogenic N_2O emissions [58] and roughly 26% of the total GHG emissions from the water chain; including drinking water production, water transport, wastewater and sludge treatment and discharge [17]. Because there are many different parameters that can facilitate N_2O emissions, it is difficult to estimate the exact quantity of nitrogen that will be emitted in this form. Kampschreur et al. [17] reviewed numerous studies in the literature and found huge variations in N_2O emissions as a % of wastewater N-load at lab scale (0-95% N-load) and full scale (0-14.6% N-load).

2.2.4 Activated Sludge Process Design

A number of N-removal design options are available for WWTPs. Initially, designs focussed on following the sequential flows of the biochemical reactions, where nitrification precedes denitrification (Figure 2-3). However, an external carbon source (often as methanol) is required to supply sufficient carbonaceous material for the denitrifying bacteria, adding significantly to system costs and environmental impact. Resultantly, pre-denitrification options were developed where cBOD is supplied by the return activatedsludge (RAS) from the secondary clarifier and the incoming wastewater from the primary clarifier (Figure 2-4). Typically the process, also known as the Ludzack-Ettinger process, can see improved N-removal efficiencies by incorporating an internal recycle of mixed liquor from the aerobic zone, allowing more contact with nitrified material [77].

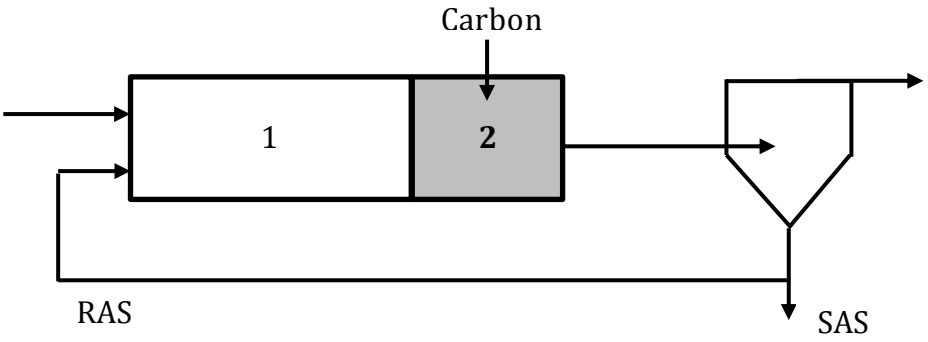

Figure 2-3. *Conventional nitrogen removal process (1 aerobic/nitrification zone; 2 anoxic/denitrification zone).*

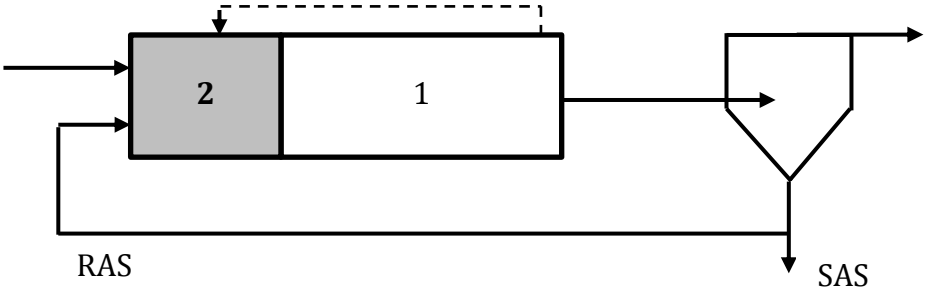

Figure 2-4. 2-*stage pre-denitrification (1 aerobic/nitrification zone; 2 anoxic/denitrification zone)*

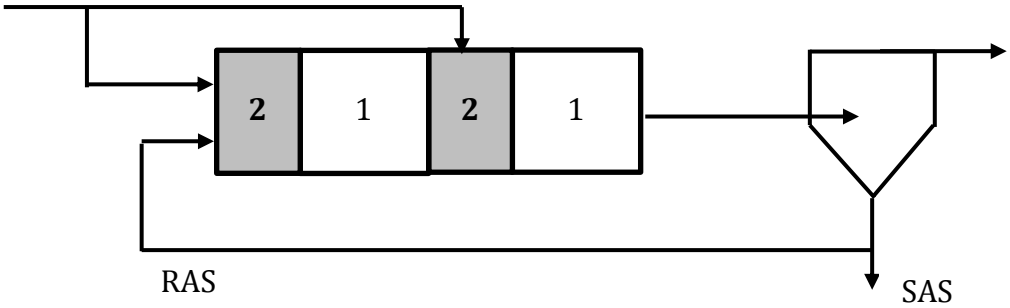

Figure 2-5. 4-*stage pre-denitrification (1 aerobic/nitrification zone; 2 anoxic/denitrification zone)*

Alternatively, a 4-stage process may be used (**Figure 2-5**), also known as the Bardenpho process [77]. Here, the incoming sludge from the primary clarifier is split between the two denitrification zones and encourages high nitrogen removal. Anammox

The anaerobic ammonium oxidation (anammox) process, discovered by Strous et al. [78] is a further nitrogen removal option. It is becoming an increasingly attractive option for WWTPs as it does not require an organic carbon source and considerably reduces the energy input for aeration [51]. Here, ammonium is used as the electron donor as nitrite is converted to nitrogen gas (Equation 2-7).

$$NH_4^+ + NO_2^- \rightarrow N_2 + 2\,H_2O \qquad \textbf{2-7}$$

The autotrophic nature of the catalysing bacteria means this can occur without additional COD/methanol [79]. Anammox is argued by some as a more effective option for nitrogen removal compared to the others discussed [80]. However, these bacteria have a slow growth rate of roughly 11 days doubling time; thus, reducing the quantity of sludge and therefore biogas [79]. It also means there can be long start-up times associated with the reactor. Furthermore, Anammox generates more GHG emissions comparatively as the partial nitrification that occurs generates excessive N_2O [80].

2.3 Anaerobic Digestion

2.3.1 Overview

In the UK, around 80% of all sewage sludge generated at WWTPs is anaerobically digested, equating to 24.5 million wet tonnes per annum [10]. The result is the production of 4,950 m^3 of biogas per hour; almost ¼ of the nation's total [43]. Anaerobic Digestion (AD) is essentially the microbial breakdown of organic matter in the absence of oxygen [81,82]. Anaerobic bacteria utilise oxidised compounds for metabolic processes, converting organic matter to methane, carbon dioxide, ammonia and hydrogen sulphide (Table 2-2). The combination of these gases is colloquially known as biogas. The primary and secondary sludge provided by their associated clarifiers are first thickened/dewatered in order to lessen the load entering the digesters.

The liquor from this process contains much less organic matter volumetrically and is sent back upstream to the primary clarifier or activated sludge process. The dewatered sludge is then ready for digestion.

Table 2-2 Biogas chemical composition [9]

Composition	Concentration
CH_4	55-70 (vol%)
CO_2	30-45 (vol%)
H_2S	500-4000 (ppm)
NH_3	100-800 (ppm)
H_2	<1 (vol %)
O_2	<1 (vol %)
H_2O	<1 (vol %)

The Buswell equation (Eq 2-8) describes the collective reactions that breakdown organic matter ($C_cH_hN_nS_s$) to biogas during anaerobic digestion [83,84].

$$C_cH_hN_nS_s + \tfrac{1}{4}(4c - h - 2o + 3n + 2s)\ H_2O \rightarrow \tfrac{1}{8}(4c - h - 2o + 3n + 2s)\ CO_2 + \tfrac{1}{8}(4c - h - 2o + 3n + 2s)\ CH_4 + nNH_3 + sH_2S \quad \textbf{2-8}$$

A series of steps occur during AD to achieve the full degradation of organic matter shown in the Buswell equation. This includes: 1) 'hydrolysis' which converts carbohydrates, proteins and fats to sugars, amino acids and fatty acids; 2) 'fermentation' which converts the products of hydrolysis to acetic acid, volatile fatty acids (VFAs), H_2 and CO_2; 3) 'acetogenesis' which converts VFAs to acetic acid, H_2 and CO_2; 4) 'methanogenesis' which converts acetic acid, H_2 and CO_2 to mostly methane and CO_2 [81]. Each stage is carried out by particular microbial communities with differing biochemical processes and preferential conditions. They run near-on sequentially, where the product of one becomes the substrate for the next. The Buswell equation assumes 100% metabolic breakdown, thus can be used to infer the composition of biogas but

not the volume. However, from simple stoichiometric analysis, it can simply be assumed that every kg of CH_4 generated took the removal of 4kg of COD [57].

The energy content of the methane contained in biogas (Table 2-2) makes for satisfactory use of biogas as a fuel. Currently, around 60% of biogas produced at WWTPs is used for onsite electricity and heat using combustion-based cogeneration technology [43]. However, other properties of biogas can prove problematic. As Table 2-2 shows, the other major components of biogas are CO_2, hydrogen sulphide, ammonia and saturated with water vapour. CO_2 lowers the energy content, ammonia can be inhibitory and facilitate NO_x emissions, whilst H_2S converts to SO_2 and H_2SO_4 which are highly corrosive and hazardous [85–87]. Furthermore, biogas often contains siloxanes (not shown in Table 2-2), which are silicon-bearing volatile compounds and form micro-crystaline silica during combustion that can cause considerable damage to energy recovery equipment [87,88]. As such, in many cases biogas is purified in order to remove some or all of these components.

2.3.2 Biogas Purification

There are a number of technology options that can be utilised to purify biogas and separate CO_2 and other impurities such as H_2S from biomethane. These have been extensively reviewed in literature, exemplified by Abatzoglou and Boivin [89] and Awe et al. [90]. Discussed options include: physical and chemical absorption, pressure swing adsorption, chemical adsorption and membrane separation.

2.3.2.1 Physical Absorption

The preferred method utilised in industry is water scrubbing with a 41% share of the market at the time of the IEA's 2014 market report on biomethane [91]. Water scrubbing works on the principle that the solubility of CO_2 is 26 times that of CH_4 (at 25°C). H_2S solubility is greater than that of CO_2 and is often removed prior to CO_2 in a separate column due to its corrosiveness [90]. The

biogas is often pressurised anywhere between 4-12 bar [92] before being fed into the column. This contributes significantly to the energy demand of the process which can be comparatively greater than competing options [93]. However, the comparatively lower maintenance costs of water stripping dwarf any energetic disadvantages, justifying industry's technology preference. Water scrubbers generally facilitate a biomethane product containing >96% of CH_4 and <2% of CO_2 [94].

Organic solvents, such as methanol and dimethyl ethers of polyethylene glycol (DMPEG), can be used in place of water due to the comparative high solubility of CO_2 and H_2S over CH_4 in them [90]. Organic solvents of choice exhibit higher affinity to the biogas impurities, meaning a smaller volume flow of scrubbing liquid is required. This has the potential benefit of reduced equipment size and operating costs. However, regeneration of the organic solvents can be an energetically costly process [95]. Hence, there is a general preference for water scrubbing in the AD industry [96]. Organic solvent scrubbers generally produce a biomethane product of purity between 96-98.5% [94]. It is detailed in Munoz et al. [96], that both water and organic solvent scrubbers generally results in methane losses under 2%.

2.3.2.2 Chemical Absorption

Chemical absorption/scrubbing utilises CO_2-reactive absorbents such as alkanol amines and alkali aqueous solutions to separate CO_2 from CH_4 contained in the biogas. As with the discussed physical absorption techniques, it involves the transfer of CO_2 from gas to liquid but via chemical reactions. However, unlike water scrubbing, H_2S must be carried out separately in order to eliminate the chance of H_2S-amine poisoning [90]. The use of chemical absorption enables the recovery of over 99% of biomethane due to the high reaction selectivity with CO_2 [90]. The process can also make sure little to no CO_2 remains present in the biomethane product [96]. Similarly to organic solvent scrubbing, the process incurs high regeneration costs, reasoning its limited (22%) share of the biogas upgrading market [91].

2.3.2.3 Pressure Swing Adsorption

Pressure swing adsorption (PSA) units manipulate molecular characteristics in order to separate species according to their molecule size [92]. Water vapour within the biogas must initially be condensed before the biogas is pressurised and passed through adsorptive media, typically in the form of activated carbon and/or zeolites. The smaller particle size of CH_4 allows for its passage through the material's pores, whereas CO_2 is adsorbed to its surface. When the biomethane has been partitioned off, the pressure inside the PSA is dropped, releasing CO_2 from the, now re-useable, adsorptive material [93]. PSA can achieve over 97% CH_4 enrichment but at high energetic costs. The high pressures required dictates that every ton of CO_2 removed requires 915 MJ electricity. In addition to the removal of water vapour, any H_2S must also be eliminated before PSA activity because its low sorbent characteristics means it will remain in the biogas.

2.3.2.4 Chemical Adsorption

Chemical adsorption is a popular technology for the reduction of H_2S concentration in biogas. Fe_2O_3, $Fe(OH)_3$, ZnO and activated carbon are all potential adsorptive media options [96]. However, the high costs of regeneration and replacement limits the technology to large-scale applications [89]. The adsorption can be described via the following stoichiometry:

$$Fe_2O_3 + 3H_2S \rightarrow Fe_2S_3 + 3H_2O \quad (2\text{-}9)$$

$$2Fe(OH)_3 + 3H_2S \rightarrow Fe_2S_3 + 6H_2O \quad (2\text{-}10)$$

$$2Fe_2S_3 + 3O_2 \rightarrow 2Fe_2O_3 + 6S \quad (2\text{-}11)$$

Despite the high costs, chemical adsorption remains a well-used option because of its simplicity and ability to reduce concentrations of species other than CO_2 and CH_4 down to 1ppm [96]. The use of such adsorption technology has

recently been tested at pilot scale for the removal of H_2S from biogas at a wastewater treatment plant in Spain as a pre-treatment for SOFC processing [97] with great effect. However, if CO_2 removal is required, it must be combined with an alternative technology such as water scrubbing.

2.3.2.5 Membrane Separation

Conventional membrane systems work under the principle of preferential permeation of CO_2, H_2S, O_2 and H_2O and the retention of CH_4 and N_2 across a semi-permeable membrane [98]. Membrane upgrading can occur in low pressure (atmospheric) gas-liquid modules or high pressure (>20bar) gas-gas modules [96]. CH_4 concentrations of 92-94% are typical for single-pass gas-gas units [98]. However, 96-98% CH_4 concentrations are guaranteed by standard gas-liquid modules or in multi-stage gas-gas units [98]. Maintenance costs are typically more than water scrubbing but less than other options discussed [92]. High energy costs can result from the pressurisation or heating with membrane technology, yet as a mature option it still holds a market share of 10 % [93,98][93,98].

2.3.3 Digestate

Digestate is the digested effluent from AD, i.e. what is left of the feedstock material after biogas extraction plus the mix of microbial biomass responsible for the biogas production. Thus, the composition of the digestate is highly dependent on that of the initial feedstock, maintaining all of the original nitrogen, phosphorus and potassium (NPK). These nutrients are the foundation of biological growth, making it suitable for use as a fertiliser.

However, the nature of wastewater as a product of human and industrial waste has led to varying opinions on the use of digestate from WWTPs as a fertiliser. Direct application of primary and secondary sludge has brought about no instances of human, animal or crop contamination [99]. However, concerns regarding toxic substances and harmful micro-organisms has led to varying

acceptance and a ban in Switzerland on the use of sludge as a fertiliser [100]. These concerns have trickled down to application of digestate from sludge digestion. Furthermore, in the UK, both sewage sludge, through the European directive 86/278/EEC, and digestate, through PAS 110 [101] are regulated for land application. As such, digestate often doesn't meet these standards and significantly limits the market for digestate in the UK.

2.3.4 Digestate Separation

In the AD industry, digestate is most often dewatered to produce a solid (fibre/cake) and liquid (liquor) fraction. The wastewater industry most commonly refers to the solid fraction as cake [102], thus, it will be referred to as such from here-on. Separation is done for a number of reasons. Firstly, the cake fraction is far smaller by mass and volume, making it easier to store, transport and apply as a fertiliser. Furthermore, the cake retains more of the phosphorus contained whilst the liquor contains the majority of nitrogen from the whole digestate [103]. The distribution of these factors can be viewed in Figure 2-6.

As aforementioned, there is an increasing flux of phosphorus from rural to urban areas [104–106]. A such, there is a higher demand for the phosphorus-rich cake, justifying further why transport of cake over liquor is often favoured [103]. A number of methods for dewatering are used in industry that range between biological, mechanical and thermal techniques. A review of these technologies can be found in ADBA [102] and Drosg et al. [107]. The most popular options include: screw press, centrifuge, belt filters, membrane filtration and evaporation.

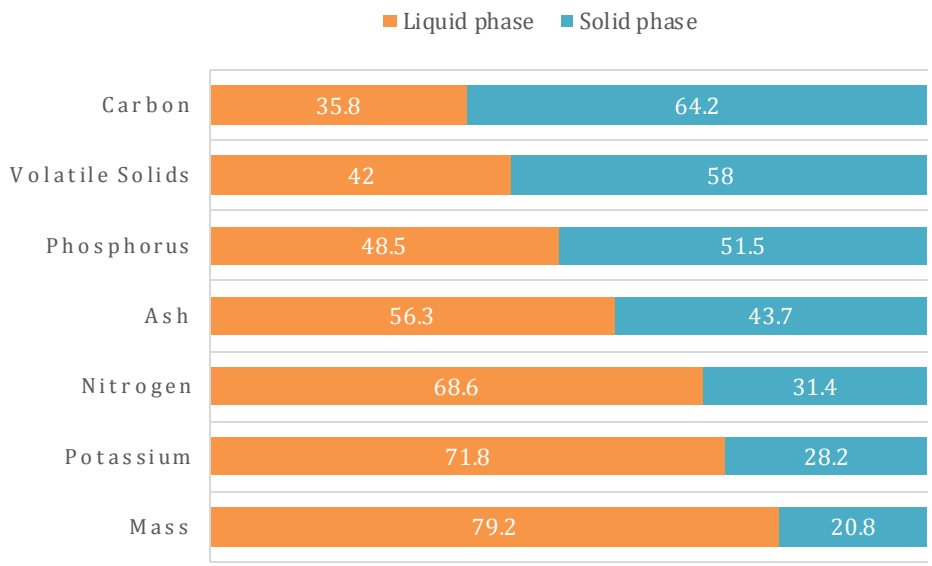

Figure 2-6. *Distribution (%) of various factors after liquid-solid separation by rotary screen separator and screw extractor. Source:* Bauer et al. [108].

In the wastewater industry, digestate liquor is often recycled back into the treatment process for activated sludge conditioning [19]. The recycling of digestate liquor contains 15-20% of a plant's N-load [18,19]. Resultantly, it significantly contributes to the energy demand and carbon footprint of a wastewater treatment system due to the forcing of having an increased nitrogen plant load.

2.4 Energy at wastewater treatment plants

Conventional wastewater treatment facilities both recover and use energy. However, with the exception of a handful of cases [50,57], more energy is consumed than generated. The specific energy use varies drastically amongst regions and facilities. Comparisons can be made between plants by calculating electricity use as a function of influent flow, known as the 'source electrical energy use intensity' (EUI). This variation can be seen displayed in Table 2-3, ranging from 0.30-0.78 kWh /m^3 treated wastewater.

Table 2-3. *Average EUI values from literature for respective regions*

Region	Average EUI (kWh/m^3 treated sewage)	Reference
USA	0.78	[109]
Canada	0.35	[110]
Flanders	0.30	[111]
Austria	0.30	[112]
Sweden	0.47	[112]

Displayed in Figure 2-7 are the primary formats in which electricity is used at WWTPs and makes up the EUI's shown in Table 2-3. The largest share of demand is that associated with aeration, with an average share of 54%. As discussed in sections 2.2.2 and 2.2.3, aeration is required in ASP for the biological processing of nitrogen and organic carbon. According to the stoichiometry of Eq 2-5, the conventional nitrification process requires 4.57 kg O_2 /kg oxidised-N. Aeration efficiency varies between 1-2 kg O_2 /kWh therefore energy requirements lie between 4.57-9.14 kWh /kg oxidised-N [57,67]. According to calculations in [57], conventional removal of nitrogen (via predenitrification) accounts for roughly 27% of a WWTP's total energy demand.

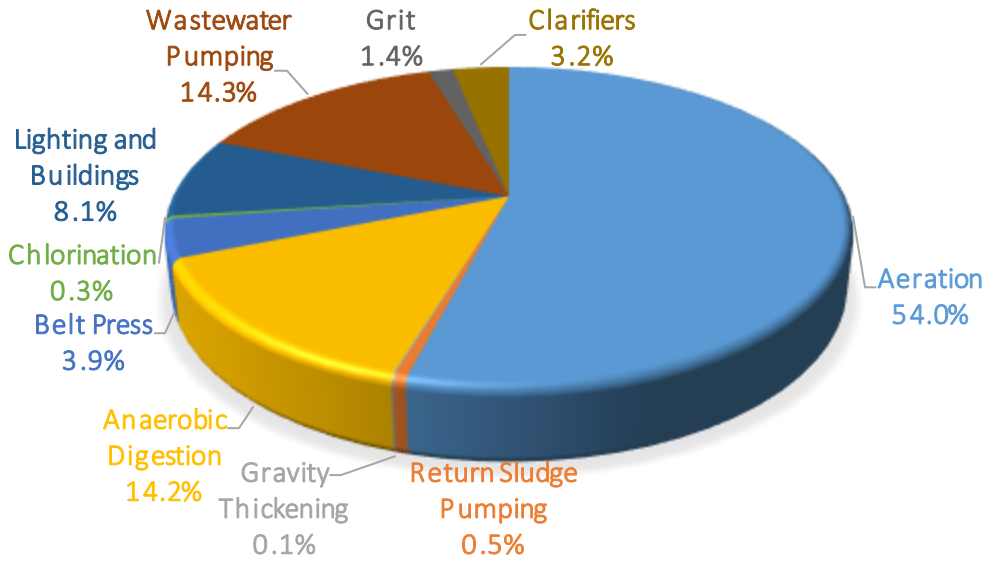

Figure 2-7. E*nergy demand breakdown at conventional WWTPs data derived from* [52].

Energy is conventionally recovered through anaerobic digestion of primary secondary sludge in most wastewater treatment facilities in the UK [43]. AD is a way to convert the energy stored in organic compounds to a biogas which can be combusted in CHP units. The composition of biogas is shown in Table 2-2. Methane (CH_4) has a high energy content, with a heat of combustion of 55.53 kJ/ g CH_4 [113]. Spark ignition internal combustion engines are almost exclusively used with biogas for CHP applications and run with varying electrical (37-42 %) and thermal efficiencies (35-43 %) [114].

2.5 Hydrogen

2.5.1 Hydrogen Background

The origins of producing an electric current when combining hydrogen and oxygen i.e. the fuel cell effect, can be traced back to the early 19th century [115]. This electrochemical conversion and/or its combustion has the ability to provide energy whilst emitting no GHGs or pollutants, just water (Equation 2-12):

$$H_2 + ½\ O_2 \quad \rightarrow \quad H_2O \qquad \textbf{2-12}.$$

H_2 has a greater energy density by mass than any other fuel, with an energy content of 141.78 MJ/kg [116]. This is more than double that of liquefied natural gas (54.4 MJ/kg) and more than triple that of automotive gasoline (46.4 MJ/kg) [116]. Hydrogen is also the most simple and abundant element in the universe. However, accessing/extracting it sustainably in its pure form has been the most important stumbling block for the uptake of hydrogen energy technologies.

On earth's surface, the majority of hydrogen is found combined with oxygen in water or carbon in hydrocarbons. Water's abundance makes it a near-perfect feedstock at face-value, but its thermodynamic stability means dissociation requires vast quantities of energy [117]. Instead, the preferred method of industrial hydrogen production is through steam methane reforming (SMR) [118]. However, high temperatures are still required to crack the CH_4, which makes it an expensive process with limited thermal efficiencies. Resultantly, the majority of hydrogen is used for industrial processes such as ammonia production, oil refining, and methanol production, rather than as fuel [119,120].

The notion of an energy system broadly based on molecular hydrogen has been touted since the early 1970's with Bockris [121] coining the term 'Hydrogen Economy'. However, despite vast swathes of research and enough molecular hydrogen produced every year to power 600 million fuel cell cars [122], it plays a miniscule role in current energy infrastructure. This boils down to 4 main reasons (1) the energy intensive nature of its production, (2) safety concerns, (3) storage problems, (4) lack of a sustainable feedstock.

2.5.2 Safety

Many properties of H_2 facilitate concerns over the safety of its use and have been extensively researched and reviewed in literature such as Rigas & Amyotte (2013) [123] and Crowl & Jo [124]. Its high energy content and combustion efficiency are the crux of both the resistance and attraction of its use as a fuel. Historical high profile disasters involving hydrogen gas such as the Hindenburg zeppelin fire of 1937, the Pasadena chemical plant explosion of 1989 and the Sodegaura refinery explosion of 1992 killed 36, 23 and 10 people respectively [123]. Hydrogen requires a very small amount of energy to ignite and just a small electrostatic spark is enough to enable its combustion [125]. Furthermore, in broad daylight, flames during its combustion are near-invisible to the naked eye, making them hard to locate, extinguish or avoid. The burning velocity is also much greater than other fuels, meaning ignition in a confined space will likely lead to an explosion [125].

The public's fear of these hazards has been coined 'Hindenburg syndrome' after the disaster in 1937 where a zeppelin containing 200,000m^3 fuel ignited whilst flying over New Jersey, USA. However, questions over hydrogen's comparative risk to other fuels or whether Hindenburg syndrome is felt universally have been questioned. Hydrogen may represent a greater hazard over natural gas and gasoline for its higher deflagration index, wider flammability limits and lower ignition energy as shown by Crowl & Jo [124]. However, hydrogen happens to be the lightest element in nature meaning, unless it is ignited in a contained space, it will disperse into the atmosphere before any damage can be done. This is significant if comparing H_2 to traditional vehicle fuels such as gasoline which, unlike hydrogen, would leak over a long period of time; increasing the chance of fire [125]. Furthermore, hydrogen is often compared to methane as a potential pollution free, light-weight transport fuel for the future, but it too, requires very little energy to ignite. Study by Kiwa found it to be just another flammable gas.

Despite 'social concern' continually expressed as a key reason for the lack of hydrogen uptake [126,127], critical reviews of public perception studies carried out in Ricci et al. [128] and Yetano Roche et al. [129] have questioned

this. They found the Hindenburg disaster, along with the aforementioned related events, are seldom associated with hydrogen by the public and positive views of hydrogen far outweigh negative ones. However, both studies did illustrate the widespread lack of understanding and awareness of hydrogen/fuel cells and they also displayed the varied outlooks towards public willingness to pay more for hydrogen fuel or vehicles.

2.6 Current hydrogen production methods

2.6.1 Steam Reforming

Steam reforming of natural gas, often referred to as steam methane reforming (SMR) is the most widely used method of hydrogen production. In principle, super-heated steam is used to separate natural gas into its individual hydrocarbon components; resulting in a syngas of hydrogen and carbon monoxide (Equation 2-13). The reaction is highly endothermic with a standard enthalpy of formation (ΔH_{298}) of +206 KJ mol_{CH4}^{-1}. Resultantly, temperatures of ~850-900^{o}C are used by industry for this process [130].

$CH_4 + H_2O$	⇆	$CO + 3H_2$	**2-13**.
$2CO$	⇆	$C + CO_2$	**2-14**.
CH_4	⇆	$C + 2H_2$	**2-15**.
$C + H_2O$	⇆	$CO + H_2$	**2-16**.
$CO + H_2O$	⇆	$CO_2 + H_2$	**2-17.**
$CH_4 + CO_2$	⇆	$2H_2 + 2CO$	**2-18**.

Equation 2-13 indicates that 2 moles of reactants are used to produce 4 moles of syngas. Therefore, under Le Chatelier's Principle, a forward reaction would hold a preference for lower pressures. However, high pressures of 20-30 bar are usually used in industry due to space saving, and synthesis loop requirements (in the case of ammonia production) [130]. Equation 2-13 also shows under stoichiometric conditions an equimolar feed ratio of steam to

carbon (S:C) of 1:1. However, S:C ratios of 2.5 to 3 are more commonly used to prevent coke deposition on the catalysts [131]. Elemental carbon (coke) can form through Equation 2-14 and Equation 2-15. Thus, excess steam is used in order to keep the reaction shown in Equation 2-16 going forward.

The hydrogen production process doesn't stop there in an SMR plant, however. The reforming stage is followed by a mildly exothermic (ΔH_{298} = -41 KJ mol_{CO}^{-1}) 'water gas shift' (WGS) (Equation 2-17) that is used to maximise H_2 yields. By facilitating the reaction of steam with the carbon monoxide in the syngas, it is possible to dissociate hydrogen bonds held in water.

The syngas is rapidly cooled to 350°C, before entering the WGS reactor. However, the reaction's exothermicity increases the temperature, which aids the catalysts and increases the rate of reaction [130]. However, this shifts the equilibrium leftwards which limits hydrogen formation. To bypass this, two reactors can be used, with a high temperature shift (HTS) and low temperature shift (LTS) reactor. However, the LTS step has become obsolete in recent years due to the introduction of pressure swing adsorption (PSA) units [130] which are used to separate hydrogen from the unconverted CH_4 and carbon dioxide product by manipulating adsorption properties for differing partial pressures [132].

2.6.1.1 SMR Catalysts and deactivation

Catalysts are agents used to accelerate the rate of reaction and lower required activation energy without being consumed themselves [133]. Metals such as nickel, ruthenium, rhodium, iridium cobalt, platinum and palladium (amongst others) can and have been used as catalysts in SMR [134–136]. Despite less favourable activity per unit weight, nickel-based catalysts are most commonly used due to their financial advantages of production [135,136].

The steam reforming reaction must take place on the surface of Ni catalysts for it to be catalytically influential, making the available surface area an important factor of catalysis. As such, nickel is dispersed as small crystallites on a strong 'support' with good porosity, to allow a stable and large active surface area

whilst being able to withstand great heights of its own weight [135]. Commonly used supports include aluminium oxide (Al_2O_3), magnesium oxide (MgO), calcium oxide (CaO), magnesium aluminate ($MgAl_2O_4$) and silicon dioxide (SiO_2) [135,136]. The support material must fit a number of criteria: allow the dispersion of Ni; prevent particle migration; allow access of reactants; not interfere with reactivity or catalyse side reactions [136].

Ni-based catalysts can undergo physical decay via the agglomeration of crystallites, often referred to as 'sintering' [137]. Agglomeration results in a loss of surface area, which as aforementioned, is a quintessential component for the effectiveness of a catalyst. Elevated temperatures, the presence of water and an inadequate support to prevent particle migration are known to be the most important factors to enhance sintering [135,136]. In fact, without an effective support, extensive and deactivating sintering would occur in seconds [136].

Catalyst poisons work by blocking active surface sites and/or by changing atomic surface structures whereby reducing catalytic activity [135]. Sulphur can be considered as the most important poison for Ni-based catalysts. It is both a powerful poison and present in most naturally occurring feedstocks, such as natural gas [136]. Sulphur binds to metal sites after decomposing from H_2S and forms stable compounds with all transition metals [138,139]. This not only coats the nickel surface but also alters its structure [140]. It is widely regarded that concentrations of <0.5 ppm are acceptable in the feed gas for reforming [136]. However, above this and desulphurisation methods should be implemented.

'Coking' is a common form of poisoning in the steam reforming of hydrocarbon compounds. Coking describes the process of elemental carbon deposition which causes both operational instability and deactivation of catalysts [141]. As discussed in section 2.6, coke forms during intermediate reactions of the reforming process (Eq 2-14 and Eq 2-15) and proceeds to diffuse and dissolve into Ni catalysts. It has been found that coking is more susceptible on nickel-based catalysts than on noble metal counterparts, temperatures above ~450°C and low S:C ratios [135]. Thus, in order to prevent coking, greater than

stoichiometric quantities of H_2O are used, which often equates to S:C ratios >2.5. Alternative noble metal-based catalysts may also be used, such as ruthenium and rhodium, which are generally considered to facilitate less carbon formation[141]. However, financial costs rarely outweigh the benefits. Furthermore, trace amounts of sulphur in feed streams have been found to minimise coking by restricting the space for formation to occur on Ni catalyst surfaces [141].

2.6.1.2 Desulphurisation

Both chemical reaction technologies and adsorptive technologies can be used for the removal of sulphur [118]. The most widely used for large-scale applications is hydrodesulphurisation (HDS) [118], which is only used on hydrocarbon feedstock containing chemically bound sulphur in the form of sulphides, mercaptans, thiophene and benzo-thiophenes, commonly present in petroleum crudes. A chemical reaction technology, it uses H_2 (often recycled) to hydrogenate sulphur to release H_2S under elevated temperatures and pressures [142,143]. It is able to reduce sulphur levels to several ppm, but is energy intensive; running at temperatures of (300-340^oC) and pressures (20-100 atm) [143].

For gaseous feedstocks contaminated with H_2S, adsorption processes are similar to those described in section 2.3.2. Whereby a reaction takes place between a reduced metal and sulphur, forming a metal sulphide [142]. The sorbent is continuously regenerated and recycled which is advantageous but chemical costs still remain expensive [96,142].

2.6.2 Water Electrolysis

Simply put, water electrolysis is the separation of hydrogen and oxygen from water via the use of an electric current [118,144]. The process occurs in an electrolytic cell, which is configured of three main elements; two electrodes, a diaphragm and an electrolyte [144]. In the cell, electrodes are submerged in an

electrolyte which facilitates strong ionic conductivity. The diaphragm divides the two electrodes and ensures hydrogen and oxygen do not recombine once separated. The flow of electrons creates a positively polarised cathode and a negatively polarised anode. Water is normally introduced at the cathode (in alkaline electrolysers) and decomposes to hydrogen and OH^- [145]. The OH^- ions travel across the electrolyte to the anode where O_2 is formed [145]. The process is essentially the conversion of electric and thermal energy to chemical energy (in the form of molecular hydrogen):

$$H_2O \rightarrow H_2(g) + \tfrac{1}{2}O_2(g) \qquad \textbf{2-19}$$

The electrolyte material used will dictate the operational conditions used and create different classifications of electrolysers. The main options of which include; alkaline electrolysers, proton exchange membrane electrolysers and solid oxide electrolysers that can be seen reviewed extensively in Ursua et al. and Holladay et al. [118,144]. Water electrolysis holds roughly 4% of the market share of hydrogen production [144]. One of its main advantages is the potential to obtain unparalleled high purity H_2. However, the requirement of electricity is where it comparatively falls short of other technologies for a number of reasons. Firstly, it facilitates low exergetic efficiency, it is expensive and (in most part) non-renewable [146]. However, there are scattered examples of large-scale plants using inexpensive and renewable electricity from hydro-electric dams [146].

2.6.3 Dark fermentation

Dark fermentation involves the microbial degradation of organic material in anaerobic environments to generate an H_2 rich biogas [147]. The process works under similar fundamentals to anaerobic digestion (see section 2.3.1), but conditions are catered for bio-hydrogen production rather than bio-methane. This is done by manipulating a number of parameters such as temperature, pH, organic loading rate, type of reactor, pre-treatment, solids

retention time to name a few [148]. By doing this, one can promote hydrogen production pathways and limit its consumption. However, this is problematic as by limiting particular biochemical routes, a large proportion of substrate will be left in the fermenter/digester [149]. As such, in practice only a third of the theoretical H_2 can be generated, equating to 4 mol H_2/mol glucose, known as the Thauer limit [148,150].

Despite its flaws, system efficiencies range between 60-80 % [151]. Furthermore, the remaining substrate can be used for standard anaerobic digestion [152]. Under this scenario, bio-hydrogen and biomethane could be generated sequentially using the same feedstock. However, dark fermentation is yet to see commercial uptake and is likely to be the case until significant process optimisation is achieved.

2.6.4 Ammonia-based hydrogen studies

Due to issues in storing hydrogen, ammonia has been touted as a carrier of hydrogen that can be used for chemical storage. Ammonia contains a high quantity of hydrogen (17.6 wt%) and has multiple sustainable storage options [153]. Thus, the release of its hydrogen via catalytic decomposition has received much attention as can be seen in reviews by Bell & Torrente-Murciano [153], Yin et al. [154] and Schüth et al. [155]. Ammonia decomposes under the reverse Haber-Bosch process (Equation 2-20):

$$2NH_3(g) \leftrightarrow 3H_2 + N_2 \qquad \textbf{2-20}$$

With a ΔH of +92.4 kJ mol^{-1}, it is an endothermic reaction and is thermodynamically limited at low temperatures. Under equilibrium conditions ammonia conversion at 1atm and 773K is 99.1%, exponentially decreasing with lower temperatures [154]. In real systems, decomposition is heavily dependent on the type of catalyst being used. It is widely accepted that Ruthenium(Ru)-based catalysts are the most active for ammonia

decomposition [154,155]. However, Ru is a rare and expensive material, making cheaper metals such as iron, cobalt and nickel more attractive [153].

Ni/Al_2O_3 has been found to provide competitive rate of reactions for ammonia decomposition [153,155]. It is also a common catalyst used in steam methane reforming (SMR) reactors and the anode of internal reforming solid oxide fuel cells (SOFCs). An investigation by Wang et al. [156] found that ammonia, when mixed with methane and used as fuel for a SOFC with a Ni/Al_2O_3 anode catalyst, significantly suppressed carbon deposition. They found at an ammonia concentration of 33.3% with methane, coke formation decreased by 71%, whilst maintaining high conversions of both methane and ammonia.

There are few other cases of in-situ combined SMR and ammonia decomposition. However, one exception is a study carried out by Xu et al. [157], whom experimentally analysed the recovery of ammonia from landfill leachate for use alongside biogas in a SOFC. The anode, consisting of NiO + $(ZrO2)_{0.92}(Y2O3)_{0.08}$ (YSZ, NiO: YSZ = 6:4 by weight) was able to perform both ammonia decomposition and SMR.

2.6.5 Steam reforming with unconventional reagents

Zin et al. [62] investigated the potential of using a reagent that could simultaneously act as a source of steam and a supplementary hydrogen feedstock in the reforming of ethanol. In their experiments, waste aqueous bio-oil from fast pyrolysis was used in replacement of pure steam. It was shown to have an organic content of 7.1 wt%; with the remaining 92.9 wt% water. At temperatures of 600°C the water content conventionally reformed ethanol, whilst the organic fraction broke down, boosting final H_2 yields. As of yet, it is the only paper to have replaced steam in conventional hydrocarbon reforming.

2.6.6 Hydrogen generation at wastewater treatment plants

Producing H_2 from biogas generated at WWTP was first proposed by Shiga et al. [158] in 1998. Since, however, only scattered examples of hydrogen

production at wastewater treatment works can be found in literature and even fewer real applications. The Emschergenossenschaft's Bottrop wastewater treatment facility was recently chosen as the location for the EuWaK project, where a pilot-scale operation involving the processing of biogas to bio-methane and hydrogen has been implemented [61]. As at most WWTPs, sewage sludge is anaerobically digested to generate biogas. The biogas is then scrubbed of CO_2 and other impurities within a PSA unit, generating high quality biomethane. The biomethane supply is then split between a biogas filling station and a conventional SMR process. A review of the project by Reinders et al. [61] has discussed the operation which generates high-purity hydrogen for use in a H_2 combined heat and power (CHP) unit to supply a local school and swimming pool with electricity and heat. This is the only example in literature that could be found for a pilot-scale thermochemical hydrogen production system based at a wastewater treatment facility. However, a study by Hajjaji [60] found that a steam biomethane reforming hydrogen production facility would have half the lifeycle emissions of a conventional SMR plant. It is also important to note findings from Appari et al. [159] and Chattanathan et al. [160], which describe the importance of H_2S removal prior to any reforming by highlighting the detrimental impacts of only small quantities of H_2S in biogas for the operation of catalysts during steam reforming.

Due to the presence of CO_2 in biogas, dry reforming has been considered an option for hydrogen production at wastewater treatment and AD plants. The dry reforming reaction (CO_2 reforming of methane) can be seen in Eq 2-18 and involves the reaction of methane and carbon dioxide to produce a syngas of hydrogen and carbon monoxide. Studies such as Cruz et al. [161] have found competitive exergetic efficiencies of around 55%. Wheeldon et al. [162], showcased a process modelling-based study for the implementation of biogas dry reforming technology at WWTPs. They were able to determine potential flow-rates and system efficiencies but omitted mentioning some of the technological barriers which have hindered market uptake of this technology. This has been largely due to catalytic issues such as coke formation and poor catalytic activity with affordable catalyst options [163,164].

Another potential route for hydrogen production at wastewater treatment plants is via biological processing of sludge. Ordinarily, sludge is anaerobically digested to generate a methane-rich biogas, a technology extensively used in WWTPs globally. However, by manipulating the bacteria present in the digester, it is possible to generate an H_2 rich gas, instead, via dark fermentation. An extensive review of biohydrogen production can be found in Ntaikou et al. [147], whilst a review in its application with multiple wastewater streams can be found in Lin et al. [165]. The prevention of bacterial methane production, however, leaves a considerable amount of substrate in the digestate which can be used for conventional anaerobic digestion [152]. As such, it is possible to produce both bio-hydrogen and biomethane with the same sludge feedstock. However, dark fermentation is yet to be utilised on a large scale in WWTPs.

A further option for hydrogen production at WWTPs discussed in literature is the use of microbial electrolysis cells (MECs). These work by the oxidation of organic material present in wastewater by electrochemically active bacteria to produce electrons and protons [166]. The electrons are passed through a circuit from the anode to the cathode, whilst the protons are released into solution. Simultaneously, an external voltage is applied which enables the production of hydrogen at the MEC's cathode via the combination of protons (H^+) and electrons (e^-). It is considered a promising technology due to the relatively low energy input of 0.2-0.8 V compared to water electrolysis' requirement of 1.23-1.8 V [166]. There are further benefits, considering their use facilitates the destruction of COD simultaneously. The potential impact of MEC implementation has been discussed in studies such as Zou & Zhen [167] and Khan et al. [168]. Scale-up rates and pilot testing have been slow due to high internal resistances, contaminated electrodes and product gas and capital investment costs [166]. A partnership between Northumbrian Water and Newcastle University have been carrying out pilot tests as discussed in Cotterill et al. [169]. However, it is concluded that significant research and development is required before full-scale implementation can be realised.

2.7 Ammonia Recovery Options

2.7.1 Stripping

Stripping is a desorption technique, relying on the principle of liquid to gas mass transfer. It is the most popular method of recovering ammonia from waste streams such as digestate liquor, landfill leachate, farm slurry and urine [22,170–172]. There are two main stripping agents used in industry, air and steam [173]. Air is generally the preferred method for the fact that steam generation is energetically more intensive than heating air to required temperatures.

In the case of both air and steam stripping, ammonia should be present in its un-ionised (free) form of NH_3 over its ionised form of NH_4^+ (ammonium). This allows the ammonia to be in its more volatile form, thus increasing the chances of it being successfully stripped. The equilibrium between ammonium and ammonia is temperature and pH dependent, as described in Equation 2-21:

$$[NH_3] = \frac{[NH_3 + NH_4^+]}{1 + [H^+]/K_a} \qquad 2\text{-}21$$

$$pK_a = 4 \times 10^{-8} T^3 + 9 \times 10^{-5} T^2 + 0.0356T + 10.072 \qquad 2\text{-}22$$

where, $[NH_3]$, $[NH_3 + NH_4^+]$ and $[H^+]$ are the free ammonia, total ammonia and hydrogen ion concentrations respectively and K_a is the acid ionisation constant for ammonia. The pK_a can be calculated via Equation 2-22 which has been derived in Bonmatí & Flotats [174] by polynomial regression of data from Lide [175]. In essence, together, they show that the higher the temperature and pH, the more ammonia will be present in its free form. Caustic soda is often used to increase the pH of the liquor. However, there is a balance between boosting pH and keeping the cost of recovery down. It was found by Hidalgo et al. [176] that when pH is increased to above 10.5, the extra costs of purchasing alkali products are not balanced out by the marginal increase potential of ammonia

recovery. Alongside alkali doping, carbon-dioxide stripping is often carried out as a pre-treatment, as it also helps to boost the pH of the remaining liquor [177].

Dissolved CO_2 reduces the pH of solution, thus its removal acts inversely. This has been experimentally demonstrated in Lei at al. [178]. CO_2 has roughly one thousand times the volatility of ammonia, meaning CO_2 stripping can be completed without significant increases in operational costs, requiring less than 5% of the air required for ammonia stripping [177]. In most cases of ammonia recovery from digestate liquor, stripping is followed by an absorption step to form a product that can compete with industrial fertilisers. Sulphuric acid (H_2SO_4) and nitric acid (HNO_3) are popularly used as absorption agents [20]. A concentrated solution of ammonium sulphate ($(NH_4)_2SO_4$; AmS) can be generated with the addition of sulphuric acid. AmS has been used as a fertiliser for over 150 years [179] and still holds roughly a 3% share of the nitrogen-based fertiliser market [180]. Ammonium nitrate (NH_4NO_3) can alternatively be generated with the use of nitric acid during absorption [20], which currently holds roughly a 6% share of the nitrogen-based fertiliser market [180].

2.7.1.1 Air Stripping

Air stripping is normally carried out in stripping towers where a liquid stream is trickled from the top, travelling through spaces in a packing material where it meets air blown from the bottom. The amount of ammonia removed from liquid is dependent on a number of factors, one of the most important being the flow of air used. Effectively, the more air used, the more ammonia that will be stripped. At low concentrations, such as those found in digestate liquor, this is dictated by Henry's law (Equation 2-23). This describes the distribution of volatile compounds between gas and water phase at thermodynamic equilibrium, where solubility is directly proportional to the partial pressure of a gas above a liquid [181].

$$\mathbf{H} = \frac{\mathbf{P}_a}{C_a} \qquad 2\text{-}23$$

where, H is the proportionality constant (bar.L.mol^{-1}), P_a is the partial pressure of the solute (in this case ammonia) in gas phase (bar) and C_a is the concentration of the solute in the liquid (mol l^{-1}). Thus, solubility lowers with partial pressure which can be achieved by increasing the flow of air.

Temperature is another factor which influences the effectiveness of stripping. This is because it is a property of the Henry proportionality constant (H) which follows Van't Hoff's relationship Equation 2-24:

$$\mathbf{logH} = \left(\frac{-\mathbf{H^o}}{\mathbf{RT}}\right) + \boldsymbol{k} \qquad 2\text{-}24$$

where H^o is the standard enthalpy of reaction for the dissolution of ammonia (kJ mol^{-1}), R is the ideal gas constant (kJ K^{-1} mol^{-1}), T is absolute temperature (K) and k is an empirically derived compound dependent constant. The solubility of ammonia, as with most substances, decreases with temperature [181]. As such, boosting the temperature of the liquor and air being used will aid the stripper's capability.

It is not just temperature and air flow that control the rate at which ammonia can be stripped. The overall mass transfer coefficient (Equation 2-25) [182] describes other important factors such as packing material properties and physical properties of the liquid in question:

$$\boldsymbol{K_L a} = \boldsymbol{\alpha}\left(\frac{\boldsymbol{L_M}}{\boldsymbol{U_L}}\right)^{\boldsymbol{1-n}}\left(\frac{\boldsymbol{U_L}}{\boldsymbol{\rho_L D}}\right)^{\boldsymbol{0.5D}} \qquad \mathbf{2\text{-}25}$$

where α and n are packing-specific constants, L_M is the liquid mass flux rate (kg m^{-2}), U_L is the liquid's viscosity (Pa · s), ρ_L is the liquid's density (kg m^{-2}) and D is the molecular diffusion coefficient (m^2 s^{-1}) of ammonia in water. It is, therefore, important that appropriate packing material is used for effective ammonia stripping to occur due to the effect of packing-specific constants in

equation 2-25. Options are often made of polypropylene, PVC or ceramic and can be any size or shape from rings to saddles to spheres [183].

In a review by Kinidi et al. [184], seven packed bed ammonia stripping reactors were assessed from various types of industrial wastewater. Initial ammonia concentrations ranged from 12-5000 mg l^{-1}, stripping temperatures ranged from 14-60°C, pH ranged from 10-12 and the corresponding ammonia removal varied from 72 to 99%. Kinidi et al. noted the significant influence, temperature, pH and air-water ratios have on stripping capabilities. Theyalso note that at higher temperatures the air-water ratio is far less significant.

Other research has analysed the use of high temperature units (<60°C) such as Saracco and Genon [185] and Errico et al. [21]. Saracco and Genon studied air stripping of ammonia at temperatures between 40°C and 80°C, finding not only markedly improved performance at higher temperatures but also a reduction in capital cost projections. Capital costs for stripping carried out at 40°C was concluded to be twice those at 80°C due to the increased size of stripping and absorption units, pumps and fans required with a greater gas-liquid ratio used at lower temperatures. However, it was noted that operational costs were likely to increase with heating requirements, a sentiment also backed in Liu et al. [186]. On the other hand, Errico et al. found that heating requirements can be met internally with effective heat transfer with stripping temperatures up to 70°C.

The use of air stripping technology is limited at wastewater treatment works at present. However, there is an abundance of commercially available technology from various companies and countries of origin. Some manufacturers include: RVT [187] and ANAStrip® from Germany [188]; ACWA in the UK [189], Anaergia from Canada [190]; Monroe environmental [191], Branch Environmental Corp [192] and CECO Environmental [193] in the US; Nijhuis Industries (AECO-NAR process) [194] and Colsen (AMFER®) [195] from Holland; and CMI Group (RECOV'AMMONIA™) from Belgium [196]. The range of available technology demonstrates the readiness of the potential process implementation at UK wastewater treatment plants.

2.7.1.2 Steam Stripping

Steam stripping, like air stripping, is a liquid-gas mass transfer process but carried out at higher temperatures. One key benefit is that post-absorption doesn't have to be carried out, as the gaseous effluent can be condensed to produce a concentrated ammonia solution as shown by Teichgräber and Stein [197]. This in turn has the potential to reduce capital costs of the process. Zeng et al. [198] found that pH did not significantly impact on stripping efficiency due to natural increase of pH inside the stripper. If pH adjustments do not need to be made, then basic substances do not need to be purchased, which could reduce operational costs. However, one key reasons air stripping is industrially preferred is because the cost of raising steam is so much more intensive and expensive than raising the temperature of air [172,173].

2.7.2 Membrane Technology

Membrane technology is another method from which ammonia can be recovered from solution. Such options include reverse osmosis RO, forward osmosis (FO), membrane distillation (MD) and electrodialysis (ED) [20,199,200]. Reverse osmosis uses semi-permeable membranes and hydraulic pressure to overcome natural osmotic pressures in order to separate ions from water [201]. Thus, much like stripping requires a high pH in order to favour ammonia in its free gaseous form, RO requires a low pH so as to favour its ionised form (NH_4^+). However, use of RO for ammonia recovery is limited in industry for a number of reasons such as: high pressure (50 bar) requirements, scaling causing frequent down-times and extra operational costs, high retention of micropollutants and the need for additional separation processes such as ion exchange are required in order to recover ammonia without other components [107,202].

Forward osmosis (FO), like RO uses a semi-permeable membrane to allow the flow of water whilst retaining solutes such as ammonium. However, in FO a 'draw' solution is used which provides an osmotic pressure greater than that held in the wastewater [203]. It is seen as a promising alternative to RO because

direct hydraulic pressure is not required, reducing operational costs. However, FO is not without its issues. For example, there is often over-contamination in draw solutions and for pure ammonia removal it also needs to be paired with other separation technologies, which boosts operational and capital costs [204].

Membrane distillation (MD) uses a hydrophobic microporous membrane to separate a feed stream from distillate [204]. Heat is used in order to vaporise water and volatile components such as ammonia which pass through the membrane. MD regularly achieves ammonia recovery over 96% [204]. However, like most other membrane-based processes, fouling is a serious technological problem [205]. Due to the fact that it is a gas-liquid separation process, wetting of the membrane is also an issue, which results in direct liquid flow-through causing detrimental inorganic contamination [206].

In electrodialysis, an ion-exchange membrane is used to allow the movement of ionic compounds such as ammonium by electromigration under the driving force of an electrical potential created by a direct current field [25]. The current field allows the attraction of cations and anions to cathodes and anodes respectively [204]. Electrodialysis suffers from similar issues as other membrane technologies with persistent fouling and the need to be preceded or proceeded with other separation processes to generate a pure ammonia solution.

2.8 Fuel Cell Technology

Fuel cells enable the conversion of chemical energy in fuels directly to electrical energy. They tend to have greater electrical efficiencies compared to conventional power generation systems because they are not limited by Carnot efficiency or other thermodynamic obstructions experienced by combustion-based systems [56]. Fuel cells consist of an anode, a cathode and an electrolyte. Typically, fuel and an oxidant (usually oxygen in air) are fed continuously at the anode and cathode respectively. Electrochemical reactions take place causing

the movement of ions through an electrolyte, generating an electric current and, therefore, power.

Fuel cells are generally classified by the type of electrolyte in use. The most common of which include solid oxide fuel cell (SOFC), molten carbonate fuel cell (MCFC), phosphoric acid fuel cell (PAFC), alkaline fuel cell (AFC), proton exchanger membrane fuel cell (PEMFC) and polymer electrolyte fuel cell (PEFC) [56,207]. The electrolyte dictates the operating temperature range and, therefore, the type of fuel permitted and the quality of heat produced [56]. As such, this limits the type of fuel cell that can be used for CHP applications at wastewater treatment plants to SOFCs and MCFCs.

2.8.1 Solid oxide fuel cells

SOFCs use hard ceramic electrolytes operating at temperatures between 600-1000°C [207,208]. A crystal lattice, normally consisting of zirconium oxide and calcium oxide, forms the electrolyte [208]. The latticed nature of the electrolyte allows oxide ions (O^{2-}) to pass through to the anode, reacting with hydrogen to form water and electrons (Equation 2-26):

$$\boldsymbol{H_2 + O^{2-} \rightarrow H_2O + 2e^-} \qquad \text{2-26}$$

The reaction shown in Equation 2-26 is an exothermic one, which alongside the high temperatures used in the fuel cell produces a high quality heat stream. SOFCs have been found to generally operate at the highest electrical efficiencies of up to 60% and cogeneration efficiencies up to 90% [207]

2.8.1.1 Internal reforming capabilities

One key attribute of SOFC is their ability to handle a wide variety of fuels. The anode side of the fuel cell incorporates a catalyst, often nickel-based, which allows for steam reforming or gasification of hydrocarbons [209,210]. Accordingly, the most popular fuels for use in SOFCs have been natural gas or

methane which have been widely analysed in literature [208,210–212]. The internal reforming capabilities mean costs normally associated with external reforming reactors and separation technology are no longer required.

The high operating temperatures mean they can also reform other fuels, most notably ammonia. Ammonia will thermally crack on the anode side, generating hydrogen and inert nitrogen gas [213]. Ammonia has been analysed both as the sole fuel for SOFC in literature [63–66] and alongside other fuels [156,157,214]. It has been found that ammonia decomposes at a high rate, even at lower temperatures of 500°C [213].

Interestingly, it has also been found that using ammonia alongside methane significantly reduces coke formation in a study by Wang et al. [156]. The study found ammonia conversions over 96% above 750°C. Whilst, a mixture containing 33.3% ammonia reduced carbon formation by 71%. This demonstrates that it is not only possible to co-reform ammonia and methane directly in a SOFC but ammonia's presence could be operationally beneficial.

2.8.1.2 Use at wastewater treatment facilities

WWTPs are often net consumers of electricity [215]. As such, the use of SOFCs has been proposed as a way to enhance the power output of facilities and reduce net consumption [53–55]. A study by Gandiglio et al. [216] found that Castiglione WWTP in Italy can transform from producing just 50% of its energy demand to fulfilling all of it by co-digesting food waste and using a SOFC running off biogas made at the facility.

This highlights another important factor; that biogas containing both methane and CO_2 can be directly fed to a SOFC without scrubbing of the biogas. DEMOSOFC is a European project that will install a SOFC at SMAT Collegno WWTP in Turin and will be the largest SOFC system to run off biogas in Europe [217]. Many other authors have studied the use of using biogas in SOFC [53,54,97,157,207,218]. However, the fuel cell efficiency tends to be slightly impaired compared to pure bio-methane and pre-treatment to scrub H_2S is necessary due to its catalyst poisoning effects.

2.8.1.3 Modelling of SOFC systems

There has been an abundance of research carried out on the modelling of SOFC in literature. There are three key forms of modelling carried out, the first being numerical-based, the second being process modelling and the third fluid dynamics. A review of numerical modelling of SOFCs has been carried out by Hajimolana et al. [208]. Numerical modelling can illustrate the effect of important parameters such as current density, feed composition and operating conditions such as temperature and pressure on the overall cell voltage.

The fuel cell voltage is calculated via Equation 2-27:

$$CV = E - n_{act} - n_{ohm} - n_{conv} \qquad 2\text{-}27$$

where, E is the Nernst voltage potential which describes the theoretical cell voltage potential and n_{act}, n_{ohm} and n_{conv} are the activation, ohmic and concentration losses respectively. The calculation of each of these components forms the basis of numerical fuel cell modelling carried out in literature [53,63,157,208,212,219–224] because from here power production potential can be determined.

However, in order to understand the full efficiency and sustainability of the system, process modelling needs to be done. Process modelling allows investigation into the thermal power potential when heat transfer is taken into account. It also can be used to determine syngas compositions when externally or internally reforming hydrocarbons, the syngas compositions can then be used as inputs for variables required in numerical modelling. Aspen plus is frequently used to simulate mass and heat transfer for fuel cell systems [53,221,224–227].

2.8.1.4 Costing and Economics

Due to its fledgling market availability, techno-economic assessments of SOFCs have produced considerably varied results. For example, in the 2011

conference proceedings discussed by Colantoni et al. [228], a 2005 fuel cell stack cost of 2600 €/kW is presented. In this study, it was also projected that this figure would reduce to 501 €/kW by 2085 due to the influence of economies of scale and research and development. Data generated by the California Self-Generation Incentive Program (SGIP) and detailed in a study by Wei et al. [229] state that Bloom Energy's 200 kW base SOFC system has a capital cost of 7,000-8,000 $/kW and installation costs of 2,000-3,000 $/kW. However, it should be noted that the system cost also includes the price of equipment other than the fuel cell stack such as the AC/DC converter, burners, blowers etc. Colantoni et al. [228] state that the SOFC stack corresponds to roughly 39% of the total system costs. If this figure is used as an indicator of the SOFC capital cost from Wei et al. [229], the price would stand at 2,730-3,120 $/kW.

Siefert and Litster [230] suggest a stack cost of $1700 per m^2 of active area and indicate this would correspond to a capital cost of just 494 $/kW. This is significantly lower than any other figure discussed in literature and, thus, provokes questions over its reliability. MosayebNezhad et al. [54] discuss a number of SOFC capital cost scenarios dependent on the influence of the number of units manufactured by the company (i.e. economies of scale) based on findings by Ammerman et al. [231]. MosayebNezhad et al. [54] suggest that with the manufacture of 500 units per year, a 50 kW SOFC capital cost would be 5,656 €/kW. Whereas, at a manufacture rate of 5,000 units per year the CAPEX would be 2,326 €/kW. Furthermore, articles by Arsalis [232], Cheddie [233] and Naja et al [234] utilise Equation 2-28 to calculate the CAPEX for SOFC:

$$C_{SOFC} = A_{SOFC}\,(2.96T_{SOFC} - 1907) \qquad 2\text{-}28$$

where, C_{SOFC} is the capital cost ($), A_{SOFC} is the cell area (m^3) T_{SOFC} is the fuel cell's operating temperature (K). However, the source of this calculation has either been incorrectly referenced or omitted. Furthermore, the study by Arsalis [232] is over a decade in age. As such, a question hangs over its reliability as an effective method of estimating capital costs.

2.8.2 Molten Carbonate Fuel Cell

The electrolyte of MCFCs consist of a molten mix of carbonate salts, operating at roughly 650°C, they enable the transport of carbonate ions from the cathode to the anode [56,222]. Figure 2-8 illustrates the operation of an MCFC. On the cathode side, air is continuously fed alongside carbon dioxide. Oxygen reacts with carbon dioxide and incoming electrons Equation **2-29**. The carbonate ion generated (CO_3^{2-}), transports through the electrolyte and is used as the oxidant for the electrochemical reaction with hydrogen Equation **2-30**.

$$\frac{1}{2}O_2 + CO_2 + 2e^- \leftrightarrow CO_3^{2-} \qquad 2\text{-}29$$

$$H_2 + CO_3^{2-} \leftrightarrow H_2O + CO_2 + 2e^- \qquad 2\text{-}30$$

The electrons produced in Equation **2-30** enter an external circuit, producing electrical power before flowing back to the cathode for Equation **2-29**. It is general practice that CO_2 required at the cathode is sourced from the CO_2 generated on the anode side [56]. However, combusted gases from the anode or an alternate source altogether, may be used.

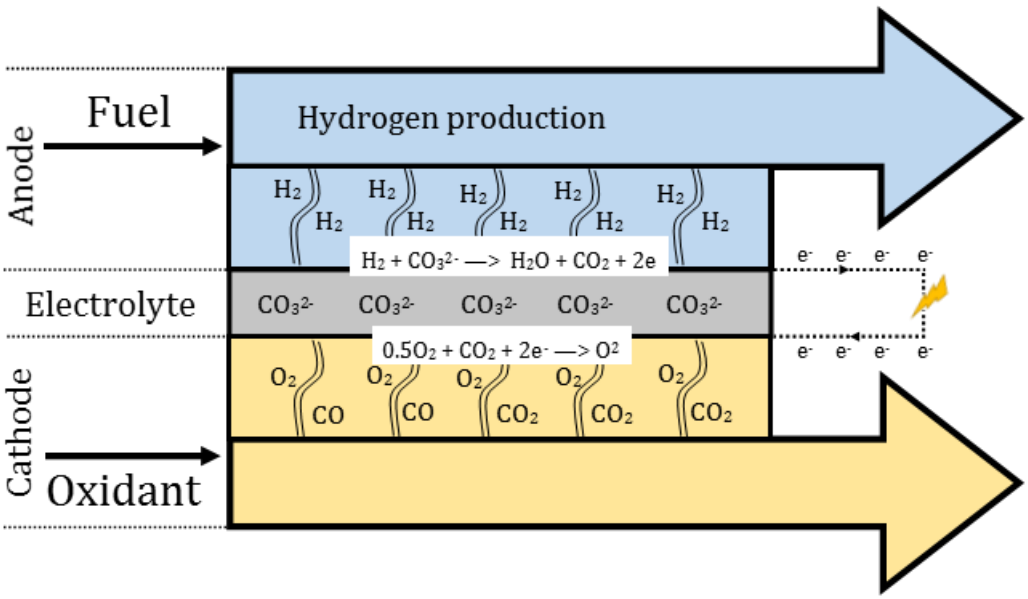

Figure 2-8. General operation of MCFC

Like SOFCs, MCFCs also have the capability of direct internal reforming due to the high temperatures used. They are also a more mature technology and stacks have been developed with greater power output than SOFC to date, as illustrated in Figure 2-9. For example Fuel Cell Energy Inc. based in Danbury, Connecticut have developed stacks rated at 2800 kW [235]. However, although competitive, they do not reach the electrical efficiency potential of SOFCs, as illustrated in Figure 2-9. This of significance in respect to applications where there is an electrical deficit. Furthermore, in an assessment carried out by Gabrielli et al. [236], it was found that the total annual costs for SOFCs was 60% that of MCFCs.

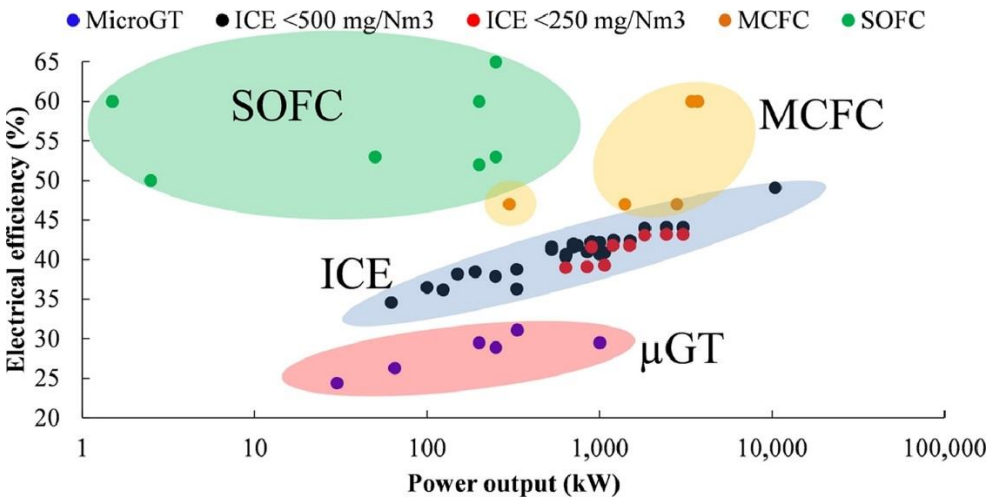

Figure 2-9. Comparison of performance between SOFCs, MCFCs, internal combustion engines (ICE) and micro-gas turbines (µGT). Taken from Lanzini et al. [237].

2.9 UK Renewables Incentives

If renewable technology is to penetrate the energy market in a capacity that will facilitate the achievement of GHG emission targets, financial incentives are absolutely essential. The UK and global economy is almost entirely reliant on a well-established fossil fuel-based infrastructure. As such, fledgling renewable

technology are often uncompetitive without incentive schemes to boost their investment potential. The UK has implemented a range of incentives schemes for renewable energy suppliers (RES) that are currently in an unquestionable state of flux.

2.9.1 Non-Domestic Renewables Obligation

The Renewables Obligation (RO) began in 2002 and has since been one of the key support mechanisms for UK renewable electricity generators (RES-E) [238]. Renewable Obligation Certificates (ROCs) are issued to providers that are able to substantiate the generation of green electricity. These certificates can then be traded at a premium price to RES-Es that are not meeting their renewable requirements. ROC's were first distributed per MWh but are now weighted depending on the technology-type's market readiness level [239]. For example, biogas-fuelled power production at wastewater treatment plants have received 0.5 ROCs per MWh since 2013. In contrast, advanced gasification technology sourced power has received between 1.8-2 ROCs per MWh in the same time period. This is because anaerobic digestion at WWTPs is a relatively mature practice that requires far less support to achieve market competitiveness. Conversely, advanced gasification technology with higher capital investment costs and limited applications needs a higher grade of support.

However, in July 2011, it was announced that the RO would close to new generators from 31 March 2017. The price of an ROC is determined via supply and demand forcings. For variable supply renewables, such as wind and solar, the uncertainty that this brought is thought to have affected the potential uptake of renewables [238,240]. For example, when renewable supply is high, income from both grid sales and ROC may lower. This uncertainty experienced under RO has led to the development of Contracts for Difference for a fundamental overhaul of RO.

2.9.2 Feed in Tariffs

In 2010 the Feed in Tariff (FiT) scheme was introduced for small scale <5 MW for wind, hydro and AD structures and microgenerators <2kW. The system provides a fix payment per unit of renewable electricity generation, adjusted for inflation which removed some of the uncertainty hindering small generators under the RO. However, FiT will be closed to new applicants from the 1st April 2019 [241]. The government claim that installation costs for small-scale RES-Es have been brought down enough via existing incentive schemes that will allow for continuing investment [242]. It is questionable whether the legitimacy of this hypothesis will stand the test of time.

2.9.3 Contracts for Difference

The Contracts for Difference (CfD) scheme was first proposed in 2011 under the Electricity Market Reform (EMR) which also announced the closing of the RO [243]. Figure 2-10 illustrates how the CfDsoperate and why they have been proposed as a replacement of RO. The strike price is contractually determined and represents the total income that will be provided by generating renewable electricity. The government will pay the difference between revenue generated from export to the grid and the contracted strike price. Figure 2-10 also demonstrates that if the market value of electricity overtakes the strike price, the operators will be obliged to pay the difference back to the government. By setting a constant value for the electricity generated, much of the market uncertainty experienced under the RO has been taken away. It is thought, investors will be far more willing to invest if clear calculations for income can be determined.

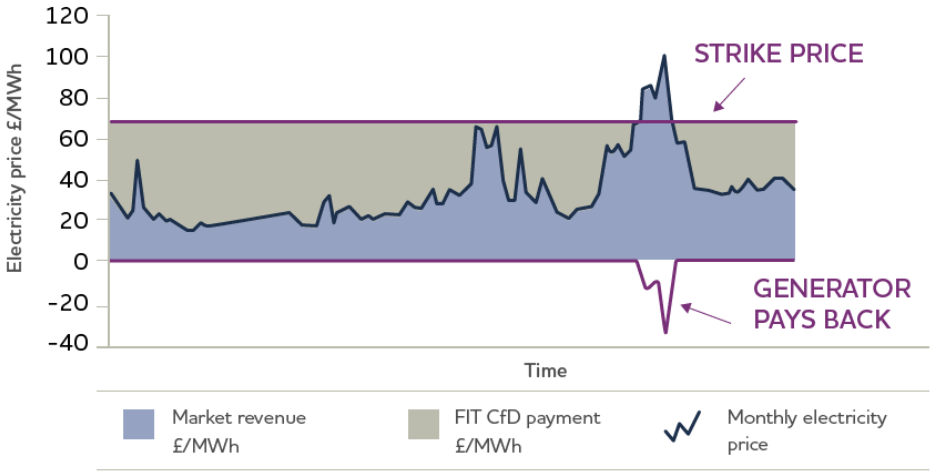

Figure 2-10. Operation of CfD renewables incentive scheme sourced from [243].

CfDs are distributed in allocation rounds (auctions), the first of which was held in 2015. The contracts are issued by a subsidiary private company to the government (The Low Carbon Contracts Company) and set the allocated strike price depending on technology type and market readiness. There are set 'Admin prices' which are pre-determined strike-price ceilings that can be allocated. However, these are often not met. For example, in the first auction an Admin price of £140 per MWh was set for advanced conversion technologies (ACTs), yet the highest allocated strike price was £119.89 [244]. Only time will tell of the CfD scheme can overcome some of the uptake shortfalls experienced under the RO.

2.9.4 Non-Domestic Renewable Heat Incentive

The non-domestic renewable heat incentive (RHI) was launched in 2011 to aid increasing the UK's share of renewable heat from 1% in 2010 to 12% by 2020 under its National Renewable Energy Action Plan [245]. The RHI operates in a similar fashion to the FiT, in that a fixed payment is made to renewable heat generators for each kWh_{th} produced. RHI payments are also banded depending on scale and technology type, as shown in Table 2-4.

Table 2-4. RHI tariff rates as of 1 January 2019 [246]

Tariff Name	Sizes	Tariff (p kWh_{th}^{-1})
Small commercial biomass	<200 kW_{th} (Tier 1)	3.05
	<200 kW_{th} (Tier 2)	2.14
Medium commercial biomass	200 – 1000 kW_{th} (Tier 1)	3.05
	200 – 1000 kW_{th} (Tier 2)	2.14
Large commercial biomass	>1 MW_{th} (Tier 1)	3.05
	>1 MW_{th} (Tier 2)	2.14
Solid biomass CHP systems	All	4.42
Water/Ground-source heat pumps	All (Tier 1)	9.36
	All (Tier 2)	2.79
Air-source heat pumps	All	2.69
Deep geothermal	All	5.38
All solar collectors	<200 kW_{th}	10.75
Biomethane injection	On the first 40,000 MWh	4.78
	Next 40,000 MWh	2.8
	Remaining MWh	2.16
Small biogas combustion	<200 kW_{th}	4.64
Medium biogas combustion	200 – 600 kW_{th}	3.64
Large biogas combustion	>600 kW_{th}	1.16

2.10 Concluding remarks

The literature review performed in this chapter has discussed the fundamentals and current status of key research topics investigated throughout the thesis. An assessment of standard wastewater treatment practices uncovered the substantial use of energy required for biological conversion of ammonia to nitrogen gas and the associated generation of the potent greenhouse gas, N_2O. Digestate liquor was revealed as a significant contributor of nitrogen to the wastewater treatment system and current practices for ammonia recovery from digestate liquor were evaluated.

Opportunities for H_2 production at wastewater treatment plants were examined with particular focus on catalytic processes such as biogas/biomethane steam reforming and ammonia decomposition. A review of

thermodynamic conditions and catalyst options concluded that nickel-based catalysts at high temperatures could be used to achieve H_2 production from both ammonia decomposition and steam reforming. However, examples in the literature of investigation into this form of co-reforming was limited.

Fuel cells that can produce heat and power were also explored. The study found that both solid oxide fuel cells (SOFCs) and molten carbonate fuel cells (MCFCs) were capable of internally reforming ammonia and methane whilst generating heat and power. However, it was found that SOFCs were capable of greater electrical efficiencies and have considerably lower operational costs than MCFCs. The literature indicated there has been some prior interest by WWTPs for on-site use of SOFCs but there is certainly a gap to fill analysing the use of both bio-methane and ammonia as fuel cell hydrogen carriers.

In addition to the aforementioned findings, the literature review presented in this chapter has highlighted the novelty of the investigations carried out in the following chapters. It can also be used as a toolbox for the overall understanding of the work and validating results with comparisons and verification. As such, several studies discussed here will be referenced throughout to highlight this thesis' position amongst existing literature.

3 Wastewater Treatment Plant Assessment

3.1 Introduction

Samples from different stages of the treatment process at Esholt WWTP in Yorkshire have been taken and analysed to generate a material flow diagram of the process. Determining and analysing component mass flows is crucial as GHG emissions and energy demand for different processes cannot be directly measured from the treatment facility. By producing a robust material flow dataset, the impacts of nitrogenous-waste diversion on GHG emissions and energy use can be interpreted. The compositional and volume flow of digestate liquor will also be used as inputs for ammonia recovery process modelling in chapters 4, 5 and 6. The material flow can also be used for future work, highlighting key streams for nutrient and/or energy recovery.

3.2 Process Description

Esholt WWTP, located in West Yorkshire, between the cities of Leeds and Bradford, serves a population equivalent to roughly 750,000 people. Operated by Yorkshire Water, it is the second largest of their treatment facilities. The process design is displayed in Figure 3-1. The process begins with initial screening of coarse and fine particles followed by a grit chamber. Duplicate

Archimidean screw generators then recover some power before primary clarification. The primary clarifiers consist of circular settlement tanks which allow solid material contained in the wastewater to fall with gravity and rotating arms scrape and remove the sediment. Colloquially termed 'primary' sludge, this material is sent for preparation for anaerobic digestion.

The clarified liquid from primary settlement is sent to the activated sludge process (ASP). Which consists of 12 aeration lanes, 7500 m^3 each and representing U-shaped plug flow reactors with diffused aeration. Oxic and anoxic zones allow sequential nitrification/denitrification alongside chemical oxygen demand (COD) and biological (BOD) destruction. The second part of the ASP consists of final clarification tanks, of the same description and operation as their primary counterparts. These prepare water for release into a nearby watercourse. The solid outlet of the final clarifiers (secondary sludge) is split in two. The sludge still contains useful bacteria required in the ASP. Thus, one stream returns to the beginning of the ASP and the second is prepared for AD along with the primary sludge.

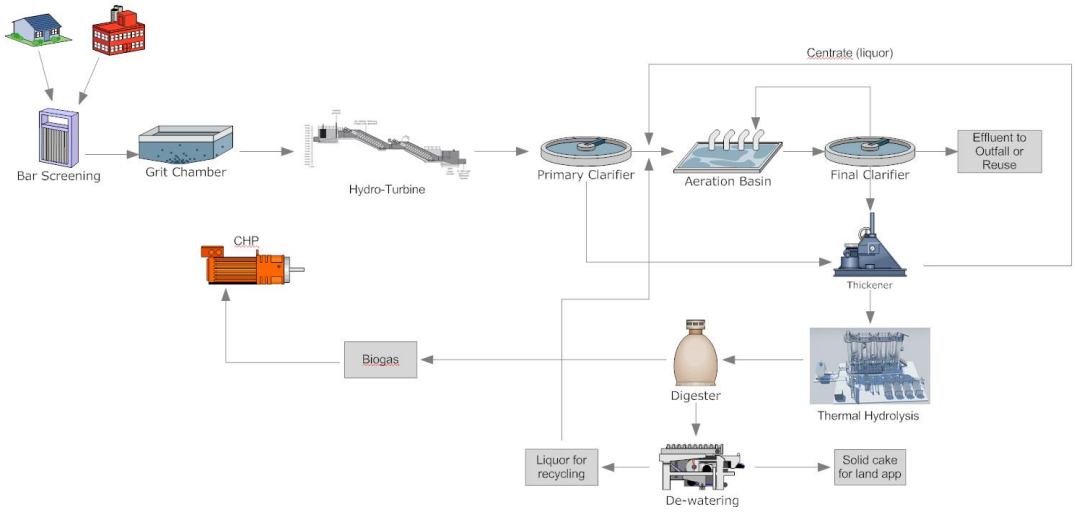

Figure 3-1. Process flow of Esholt WWTP

A thickening step is used to increase the concentration of carbonaceous material of the feedstock. This is followed by thermal hydrolysis, using a Veolia Biothelys® design, which pre-treats the sludge prior to AD. Utilising increases

in temperature and pressure, a significant amount of volatile suspended solids are dissolved, thus, boosting the feedstock's digestibility [87,247]. Four mesophilic digesters process this treated sludge with a retention time of 15 days, producing biogas and digestate. The biogas is used in four gas engines which provide heat and power for the site.

3.3 Wastewater Characterisation & Mass Balance Methodology

3.3.1 Sampling

Samples were taken monthly, along with other members of the BioResource Systems Research Group at the University of Leeds, from seven parts of the wastewater treatment process: the raw wastewater inlet, the primary clarifier, the activated sludge inlet, the activated sludge outlet, the anaerobic digester and the final effluent outlet. The samples were collected using a bucket on a rope and placed in clean sealed storage containers. The bucket collector was cleaned using acid wash and rinsed with distilled water after each collection to ensure no contamination.

3.3.2 Sample Preparation

Each sample was separated into three clean 500 ml containers. 0.4 ml and 1 ml of concentrated H_2SO_4 were added to two of the three containers to make 0.8 ml l^{-1} and 2 ml l^{-1} solutions. The acid was added to ensure preservation of the samples and prevent the volatilisation of ammonia. Two 200 ml of untreated sample and one 200 ml of each treated sample were centrifuged to remove the majority of suspended solids. Two 50 ml of 0.8 ml l^{-1} and one 50 ml of 2 ml l^{-1} sample were filtered through 9 cm GF/C filter paper for total solids removal.

3.3.3 Total Kjeldahl nitrogen (TKN) and total ammoniacal nitrogen (TAN)

Total Kjeldahl nitrogen (TKN) is the summation of inorganic nitrogen contained in ammonia and ammonium, along with nitrogen found in organic compounds. Total ammoniacal nitrogen (TAN) is the measure of the nitrogen present in ammonia in both its ionic and neutral state. Standard test 4500 C and 4500 B were used for determination of TKN and TAN respectively [248]. The procedure for both analyses is the same except total ammonia determination uses filtered samples.

The procedure begins with digestion, where all nitrogen containing compounds are broken down using sulphuric acid to liberate the nitrogen as ammonium sulphate ($(NH_4)_2SO_4$). Pre-determined sample sizes, as displayed in Table 3-1, were used depending on the expected concentration of nitrogen and only samples pre-treated with 0.8 ml l^{-1} sulphuric acid were used.

Table 3-1. Required sample size for TKN and TAN determination

Sample Location	TKN analysis sample size (ml)	TAN analysis sample size (ml)
Raw WW	25	50
Primary Settlement	50	50
Activated Sludge Inlet	25	50
Activated Sludge Outlet	10	50
Secondary Clarifier	50	50
Digestate	1	50
Digestate Liquor	1	1
Final Effluent	50	50

Each sample was placed in digestion tubes and topped up to 50ml with distilled water, where necessary. A control was also used with 50ml of distilled water. Glass beads, a copper catalyst and 10 ml of concentrated sulphuric acid were then added to each digestion tube. The samples were allowed to digest on a digestion rack at high temperature with a scrubber unit in place. After full digestion of samples had occurred and allowed to cool, distillation could begin.

The distillation was carried out using a Buchi (Switzerland) Distiller, where the concentrated acid mixture from the digestion step was diluted and NaOH added to make a strongly alkaline solution, which liberates ammonia (NH_3) as follows:

$$(NH_4)_2SO_4 + 2NaOH \rightarrow 2NH_3 + Na_2SO_4 + 2H_2O \quad 3\text{-}1$$

The ammonia was fed to a duran bottle containing 50ml of boric acid indicating solution. After distillation is complete the receiving arm contains an ammonium-borate complex (NH_4^+:$H_2BO_3^-$) which is ready for titration.

10mM sulphuric acid was used to neutralise the ammonium borate complex via reaction 3-2-3-2:

$$2NH_4H_2BO_3^- + H_2SO_4 \rightarrow (NH_4)_2SO_4 + 2H_3BO_3 \quad 3\text{-}2$$

The reaction facilitates a colour change from blue to lavender. The volume of titrant used when the colour change occurs was recorded. The concentration of TKN was calculated via equation 3-3:

$$\text{TKN (mg } l^{-1}) = \frac{(A-B) \times 280}{V} \quad 3\text{-}3$$

Where A is titrant volume for sample, B is titrant volume for control and V is volume of sample used.

3.3.4 Chemical Oxygen Demand (COD)

Standard test 5220 D was used to determine chemical oxygen demand (COD) [248]. Samples were first diluted using distilled water by the quantities shown in Table 3-2, dependent on the expected quantity of COD. 2.5ml of sample (in duplicate) and a blank of distilled water were added to digestion tubes containing 1.5ml digestion reagent (potassium dichromate solution), followed

by 3.5ml of catalyst reagent (sulphuric acid). The samples were left to digest for two hours at 160 ^{o}C before being ready for titration.

Table 3-2. Required sample dilution fraction for COD determination

Sample Location	Dilution fraction
Raw WW	1/100
Primary Settlement	1
Activated Sludge Inlet	1/10
Activated Sludge Outlet	1/100
Secondary Clarifier	1
Digestate	1/1000
Digestate Liquor	1/1000
Final Effluent	1

An undigested reference blank was formulated in a conical flask by adding 1.5ml COD digestion reagent, 15ml distilled water and 3.5 ml COD catalyst reagent. Two drops of ferroin indicator were added and titrated using Ferrous Ammonium Sulphate (FAS) solution. Samples were then transferred to conical flasks, two drop of ferroin indicator added to each and titrated with FAS solution. COD concentration were then calculated using equation 3-4.

$$\text{COD} = \frac{(B-S)}{T} \times D \times 1000 \qquad 3\text{-}4$$

Where B=Titre of blank (ml), S=Titre of sample (ml), T=Titre of undigested blank (ml), D=Dilution factor.

3.3.5 Total suspend solids (TSS) and volatile suspended solids (VSS)

TSS and VSS were determined by standard tests 2540 B and 2540 E respectively [248]. 20 ml of untreated, unfiltered samples were filtered in duplicate through a 9 cm GF/C filter paper with 1.2 µm pores. Each filter paper used was previously weighed to enable before and after calculations. Vacuum

apparatus was used to allow filtration of entire sample. After drying in a desiccator, the filter papers were weighed again and TSS calculated via equation 3-5.

$$\text{TSS (mg } l^{-1}) = -\frac{\text{dried wt.(mg)} - \text{initial wt.(mg)}}{\text{volume used (ml)}} \times 1000 \qquad 3\text{-}5$$

For VSS analysis, the filter papers from the above TSS methodology were placed in a muffle oven for 1 hour at 550 °C. The samples were then weighed and the difference in weight from the TSS weight was used as the weight of VSS present in the sample.

3.3.6 Total phosphorus (TP) and phosphate determination (PO_4)

Standard test 4500 P was used for TP and PO_4 determination. For total phosphorus, a digestion step was first necessary to convert all phosphorus to phosphates. Unfiltered samples treated with 2 ml sulphuric acid were used at the quantities displayed in Table 3-3.

Table 3-3. Required sample size for TP determination

Sample Location	Dilution fraction
Raw WW	1/100
Primary Settlement	1
Activated Sludge Inlet	1/10
Activated Sludge Outlet	1/100
Secondary Clarifier	1
Digestate	1/1000
Digestate Liquor	1/1000
Final Effluent	1

The samples were topped up to 25 ml, where necessary, with distilled water and added to conical flasks containing 0.4 g ammonium persulphate. 1 drop of phenolphthalein indicator, followed by 1 ml 5.6M sulphuric acid were also added. The conical flasks were then placed on a hot plate until a final volume of approximately 10 ml was reached.

Total phosphorus levels could then be measured via spectrophotometry. Digested samples were added to Nessler tubes and topped up to 50 ml with distilled water. 8 ml of combined reagent (containing sulphuric acid, potassium antimonyl tartrate solution, ammonium molybdate solution and ascorbic acid solution) was added to each Nessler tube. The spectrophotometer was set to a wavelength of 880 nm and the spectrophotometer was zeroed with a control solution of distilled water before the absorbance of each sample was recorded.

A calibration curve was created by forming a series of standard phosphate solutions at a series of concentrations ranging from 0-1.25 mg of P per litre using standard phosphate solution and distilled water. The absorbance of each concentration was recorded from the spectrophotometer and used to plot a calibration curve. The total phosphorus concentrations from the samples were then calculated via equation **3-6**:

$$\text{TP (mg l}^{-1}) = \text{P}_{\text{graph measurement}} \text{ (mg l}^{-1}) \times \frac{50}{sample\ size\ (ml)} \qquad \textbf{3-6}$$

Phosphate concentration was determined via the same technique, using filtered samples and without the digestion step.

3.3.7 Interpretation of Mass flow

Internal flow data from Esholt WWTP is unavailable. As such, a steady-state mass and volume flow diagram has been made via a combination of methods. Esholt WWTP takes sewage from an equivalent 750,000 people [249]. The average person in the UK generates 140 litres of wastewater per day, providing an indication of the total incoming flow to the plant.

The internal flow rates of the plant have been interpreted using data from [250], that modelled a plant of similar size (500,000 population served) and also employs a modified Ludzack-Ettinger process set up for nutrient removal in the ASP. Using estimated internal flow rates, the mass flow of individual

components could be created using characterisation data carried acquired in the laboratory.

3.4 Results

3.4.1 Characterisation

The characterisation results are based on data recorded between October 2014 and May 2016. They consist of a combination of first-hand results and data acquired by other members of the BioResource Systems Research Group at the University of Leeds. The mean of each parameter from each sample point has been calculated and displayed in Table 3-4. The raw data, of which, can be found in Appendix A, Table A 1(a-f).

Table 3-4. *Average results for each parameter at each sample point from Esholt WWTP in mg l^{-1} with standard deviation in brackets*

	TSS	**VSS**	**COD**	**TP**	**PO_4**	**TKN**	**TAN**
Raw	322 (130)	264 (112)	788 (381)	6.1 (2.3)	4.2 (1.8)	44.9 (15.6)	24.2 (9.5)
Primary Clarifier	100 (37)	81 (28)	277 (125)	2.0 (1.2)	1.4 (0.7)	27.5 (10.4)	16.2 (8.7)
ASP Inlet	578 (142)	461 (116)	1289 (1164)	10.3 (3.5)	5.3 (3.1)	62.4 (20.6)	20.7 (9.9)
ASP Outlet	3838 (398)	2919 (288)	4281 (2101)	46.6 (25.9)	12.7 (6.3)	251.7 (60.6)	3.4 (2.7)
Secondary Clarifier	36 (28)	28 (17)	54 (26)	0.2 (0.1)	0.1 (0.1)	3.3 (1.4)	1.1 (0.6)
Digestate	38781 (15149)	22412 (9480)	4713 (29609)	289.5 (201)	18.2 (15.8)	3155.4 (710)	1502.1 (262)
Digestate Liquor	349 (137)	303 (104)	3796 (2830)	24.0 (16.2)	18.2 (15.8)	1598.2 (207)	1502.1 (262)
Final Effluent	37 (26)	28 (18)	52 (23)	1.2 (1.2)	1.2 (1.1)	3.0 (1.9)	1.3 (1.1)

3.4.1.1 TSS and VSS

Table 3-4 shows how the treatment facility's operation alters the concentration of solids and volatile solids between operational units. The primary settlement tanks remove over 2/3 of TSS and VSS from the raw wastewater, all of which can be used as feedstock for anaerobic digestion. The concentration of solids increases before entrance to the ASP, with recycling of activated sludge. The solids concentration increases again in the ASP with the pronounced growth of bacteria used to remove COD, phosphorus and nitrogenous compounds. This sludge easily settles in the secondary clarifiers for a final TSS discharge of just 37 mg l^{-1}. The fraction of volatiles within the solids does not alter considerably, falling from 82 % in the plant inlet to just 76 % in its outlet. The digestate holds the greatest concentration of solids which is to be expected after the sludge thickening step which precedes AD. The whole digestate holds the smallest ratio of VSS:TSS because of the utilisation of volatile solids by anaerobic bacteria for the production of biogas. Coefficients of variance, measured as the ratio of the standard deviation to the mean, range between 10 % (activated sludge outlet) and 79 % (secondary settlement outlet) with an average of 43%. This indicates the dynamic nature of solid concentrations within the WWTP.

3.4.1.2 COD

Table 3-4 also highlights the fate of COD at the treatment facility; transforming from a mean initial concentration of 788 mg l^{-1} to just 52 mg l^{-1}. As with the solids, much of the COD is diverted before the ASP via the primary clarification step. The COD concentration increases with the growth of bacteria in the activated sludge tanks but are almost entirely removed during the secondary clarification stage, demonstrating the effectiveness of the ASP in removing COD from the wastewater. However, the digestate retains a considerable amount of COD, much of which remains in the solid (cake fraction). The average coefficient of variance for COD at each sample location was greater than TSS at 58%, again demonstrating the dynamic nature of wastewater treatment.

3.4.1.3 TP and PO_4

The inflow of phosphorus to the treatment facility is considerably smaller than any other components analysed, at a phosphorus concentration of just 6.1 mg l^{-1}. The proportion of phosphate-P is much lower in the activated sludge outlet, which changes from 51% at inlet to 27% after ASP. This shows the effect of biological P removal in the ASP via bacterial assimilation of the phosphate. The phosphorus concentration peaks in the whole digestate at 289.5 mg l^{-1}. 92% of this phosphorus is contained in the solid fraction highlighting one of the reasons the cake is far more marketable than the liquor. Phosphorus recovery from digestate liquor is often promoted as an effective way to help close the phosphorus nutrient cycle with its numerous sinks but finite sources. However, at such small concentrations (24 mg l^{-1}), its applicability at Esholt WWTP may be limited.

3.4.1.4 TKN and NH_3

Table 3-4 also illustrates the effectiveness of the ASP at converting ammonium from the wastewater. The concentration of ammoniacal nitrogen transforms from 20.7 to 3.4 mg l^{-1}. The increase in TKN during ASP is due to the accumulation of bacteria. Nitrogen concentrations peak in the whole digestate with a TKN concentration of 3155 mg l^{-1}. Almost 50% of this nitrogen is retained as ammonium in the digestate liquor at a concentration of 1502 mg l^{-1}. The comparative potency of ammonium in this stream makes it the most applicable of all streams from an ammonia recovery perspective. Thus, an understanding of the volume flow of digestate liquor at Esholt WWTP is required for feasibility and impact analysis of the potential technology introduction.

3.4.2 Mass Flows

Before a mass flow diagram can be produced for the key species characterised in section 3.4.1, analysis of the plant flow rates must be carried out. The facility

does not measure internal (unit to unit) flow rates. However, incoming flow rates have been sourced via personal communications [251,252].

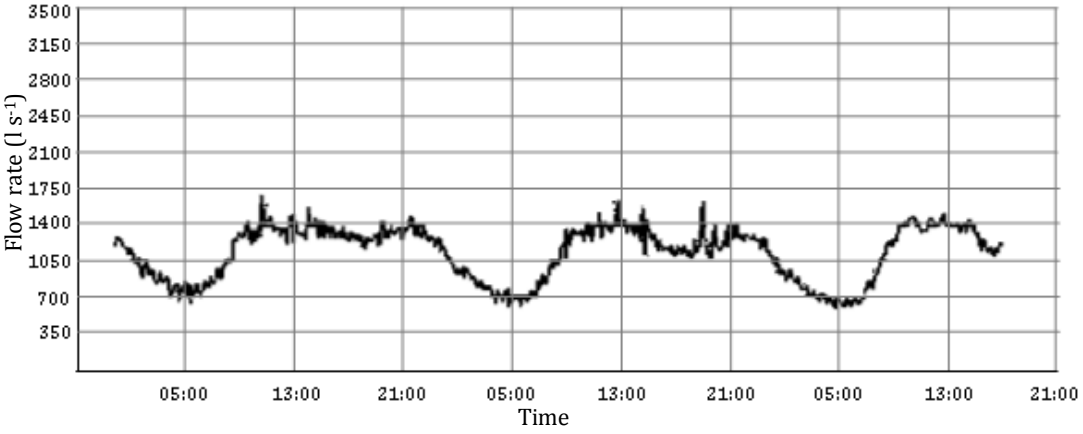

Figure 3-2. Incoming flow data for Esholt WWTP over a 2.5 day period in September 2016

Figure 3-2 perfectly illustrates the nominal incoming flow-rates to Esholt WWTP over 2.5 days. The graph indicates the temporal nature of human daily activities. Flow rate steadily increases during the morning when discharge from showers and other morning activities slowly make it to the treatment facility. The flow-rate tends to drop slowly in the afternoon before experiencing another peak in the evening due to the influence of meal-time and night time preparations. The daily flow rate variations between roughly 600 and 1600 litres per second remain fairly consistent day-to-day. This demonstrates that these data corresponds to a relatively dry-period, where the impact of rain has very little influence on the incoming flow of sewage to the WWTP. The influence of precipitation on plant flow is more starkly highlighted in Figure 3-3:

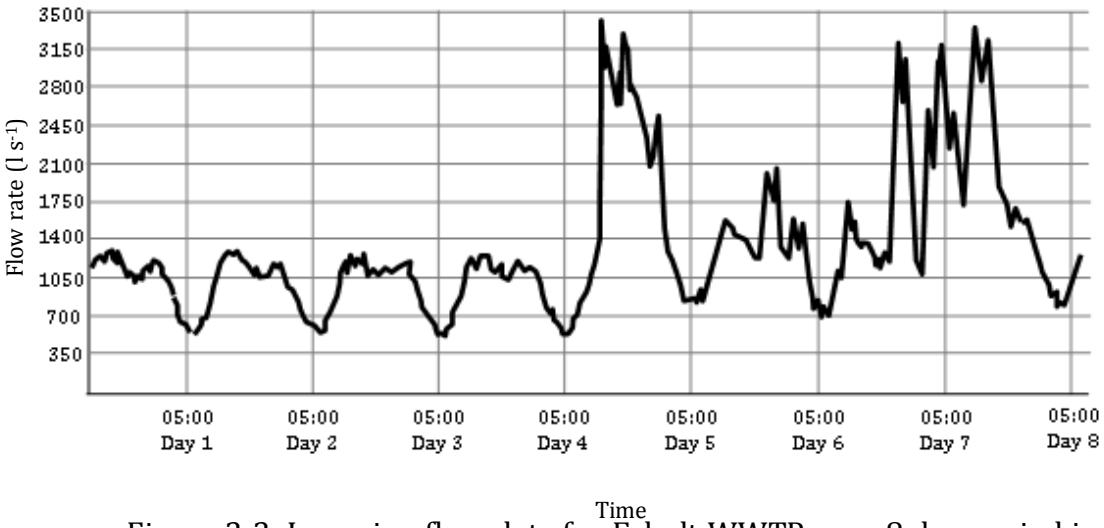

Figure 3-3. Incoming flow data for Esholt WWTP over 8 day period in August 2016.

The first four days in Figure 3-3 show very similar flow-rate patterns to that displayed in Figure 3-2; with daily variations between 600 and 1400 litres per second. However, on the morning of day 4, rain has clearly hit the local area, causing a dramatic increase in the flow of wastewater to the facility to a peak of almost 3,500 l per second. This shows the dramatic impact that weather has on incoming flows and describes, in part, the variations in concentrations of key species described in section 3.4.1.

The variation also makes it difficult to predict a mean flow rate to be used for steady-state modelling. Esholt WWTP serves a population equivalent to roughly 750,000 people that have been assumed to generate 140 litres of sewage per capita per day. Thus, inferring a plant inflow rate of 105,000 m^3 sewage per day or 1,215 l per second. This corresponds fairly well with real flow data, illustrated in Figure 3-2 and Figure 3-3; lying between all daily peaks and troughs.

The results from stream characterisation have been extrapolated to generate a material flow diagram, displayed in Figure 3-4. The internal flow rates shown in Figure 3-4 have been inferred from Minnini et al. [250] as a fraction of the incoming flow rate as follows:

- Primary settlement outlet - 1.009
- ASP inlet - 1..012
- ASP outlet - 1.018
- Final Effluent - 0.999
- Whole Digestate - 0.007
- Digestate Liquor - 0.006

Figure 3-4 details the estimated average flow of digestate liquor at Esholt WWTP at 661 m^3 per day containing an ammonia flow of 993 kg per day. These figures have been used as inputs for process models included in Chapters 4, 5 and 6. The diagram also details that the facility destroys 4,399 kg or 79% of TKN each day. This indicates that the ASP-based biological nitrogen removal is effective in meeting the Water Framework Directive's 75% target [16]. Figure 3-4 also shows an interesting unknown liquor flow from the sludge thickening step. It can be stipulated that this stream contains a considerable flow of ammoniacal nitrogen. As such, it is suggested that future work should evaluate its composition and potential use as a secondary feedstock for ammonia recovery.

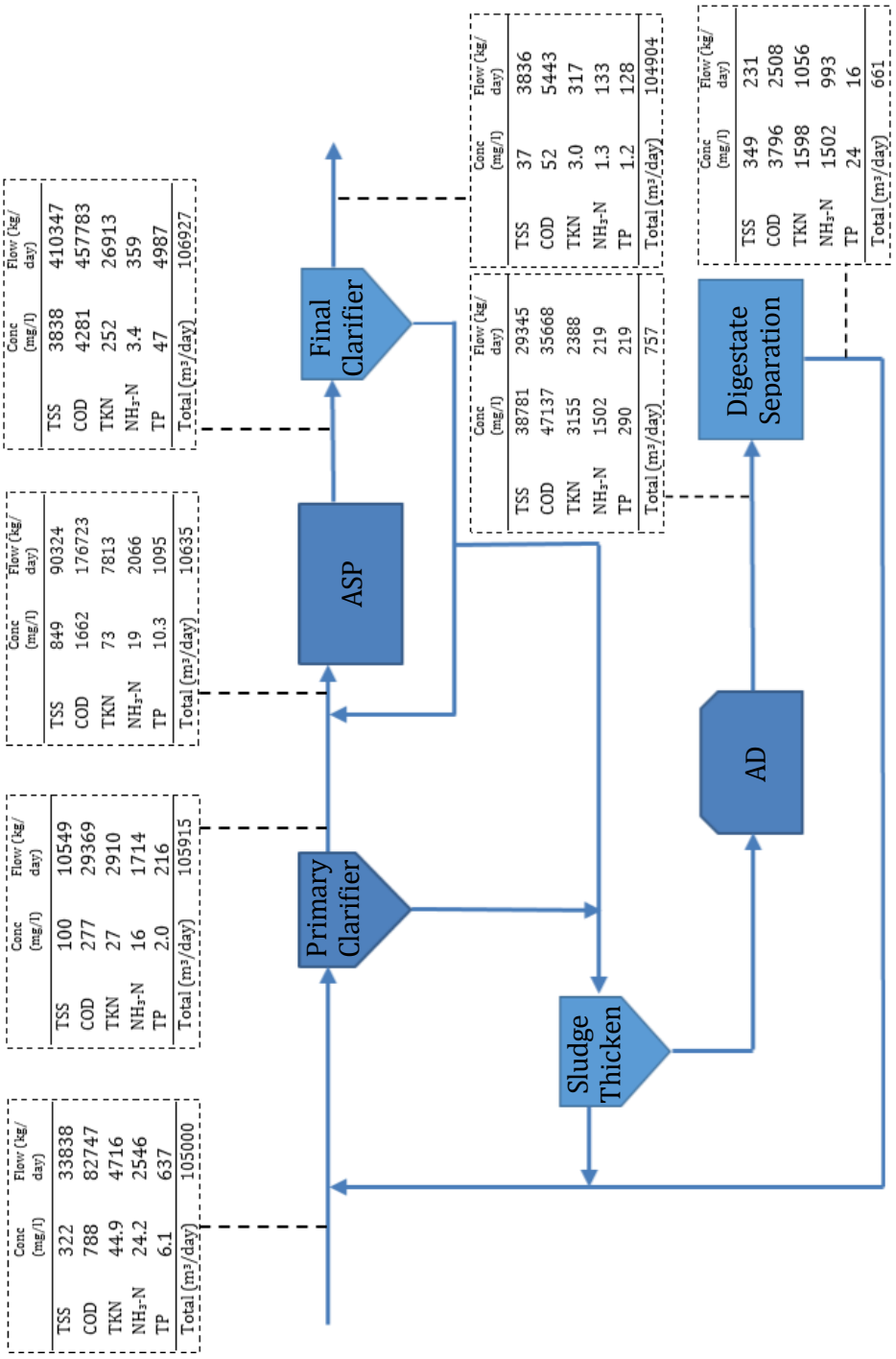

Figure 3-4. Material concentration and flow diagram for Esholt WWTP

3.4.2.1 Material flow validation

As discussed, the volume flow to the WWTP is far from constant. As such, the validity of the predicted material flow diagram has been assessed via comparison with external data. For example, a characterisation of waste activated sludge (WAS), used as the AD feedstock at Esholt WWTP and a stream

that cannot ordinarily be sampled, was carried out by Dr Ramirez Sosa at the university of Leeds [253]. Dr. Ramirez Sosa calculated the WAS to contain 81 g l^{-1} of total solids and that total volatile solids (TVS) were 72% of that. As such, the total flow of volatile solids into the AD at Esholt would be 44,210 kg day^{-1} (see section 3.4.3). Dr Ramirez Sosa also calculated the bio-methane potential to be 0.224 L_{CH4} g^{-1} TVS for the WAS. It has been determined that the facility produces 8,235 kg_{CH4} day^{-1}, meaning the destruction of 26.36 tonnes of TVS day^{-1}. Thus, subtracting the total destroyed TVS by the estimated starting amount, it is predicted that there should be 17.8 tonnes of TVS remaining in the digestate post-AD. This total is just 5% larger than this work's projected figure, shown in Figure 3-4.

Similarly, Yorkshire Water have confirmed they process around 30,000 tonnes of dry solids per year in their thermal hydrolysis plant each year [254]. Thermal hydrolysis is expected to reduce total solids by 25% [255], meaning the outlet flow of solids from the thermal hydrolysis would be 22,500 tonnes per year. This corresponds well with the predicted AD inlet of 22,300 TS per year calculated via extrapolation from [253]. Thus, it is suggested that figures from the predicted mass flow and volume flow diagram can be used with a strong degree of confidence.

3.4.3 Current Esholt energy inventory

In personal communications, information was received that the average daily plant consumption is roughly 60 MWh day^{-1} and electrical power production is roughly 40 MWh per day [256]. These figures correspond with OFGEM data [257], as shown in Table 3-5. The electricity generation between December 2013-March 2018 resulted in a monthly average of 1153 MWh and a daily average of 38.4 MWh. Figures where the capacity factor is under 10% have been excluded as these can mostly be attributed to 'teething' issues with the implementation of the sludge hydrothermal treatment process. Methane production was reverse calculated from the projected energy production of 40 MWh day^{-1} at the facility. With a CH_4 LHV of 50 MJ kg^{-1} and an estimated 35%

electrical efficiency of the internal combustion-based CHP units used at Esholt, the calculated daily generation of biomethane would stand at 8,235 kg.

Table 3-5 Ofgem data for electricity production at Esholt WWTWs between December 2013-March 2018 [257]. (Data excluded where capacity factor is <10%)

Month	Generation (MWh)	Month	Generation (MWh)
Dec-13	1073	Aug-15	523
Jan-14	1025	Sep-15	857
Feb-14	1095	Oct-15	1084
Mar-14	1423	Dec-15	556
Apr-14	1456	Nov-16	654
May-14	1570	Dec-16	982
Jun-14	1172	Jan-17	960
Jul-14	1451	Feb-17	832
Aug-14	1347	Mar-17	1164
Oct-14	1783	Apr-17	1074
Nov-14	930	May-17	1496
Dec-14	1317	Jun-17	723
Jan-15	581	Jul-17	1385
Feb-15	1111	Aug-17	1356
Mar-15	1280	Oct-17	1701
Apr-15	1700	Nov-17	1288
May-15	1335	Dec-17	1429
Jun-15	596	Jan-18	1547
Jul-15	559	Mar-18	1388
		Monthly Mean	**1152.7**

The energy consumption is far more difficult to predict, for there are so many contributing factors. Electrical consumption can range from approximately 0.26-0.84 kWh m^{-3} [258]. For Esholt, that would equate to somewhere between 27.3 MWh day^{-1} and 88.2 MWh day^{-1}. Similarly, the destruction of nitrogen in the plant can be calculated via the TN out of the primary clarifiers plus the flow nitrogen in the digestate liquor minus the outflow of nitrogen in the final effluent. The associated energy use to remove nitrogen in the ASP according to

[57] is 4.57 kWh kg^{-1} of oxidised nitrogen. This would equate to 16.8 MWh day^{-1}, which, if on average is 27% of a plant's energy as described in [57], would make the total plant consumption 62.2 MWh. For these reasons, the figures communicated by Gavin Baker of a plant energy production 40 MWh and consumption of 60 MWh have been accepted [256].

3.4.4 Current Esholt GHG inventory

There are three main gases that contribute to a wastewater treatment facilities greenhouse gases (GHG) footprint. They include nitrous oxide (N_2O), methane (CH_4) and carbon dioxide (CO_2). N_2O is mostly emitted during activated sludge processing and Parravicini et al. [259] built a regression model estimating N_2O emissions based on the % removal of TN during treatment Equation 3-7.

$$y = -0.049x + 4.553 \quad \textbf{3-7}$$

Where x is the % removal of TN which has been calculated as the incoming flow of TN minus the TN contained in the final effluent and solid digestate. This amounts a removal efficiency of 68.4%. Using 3-7, this assigns an emission factor of 0.012 kg N_2O N/ kg $TN_{influent}$; equivalent to 56.5 kg N_2O per day for Esholt WWTP.

Methane emissions occur all over the treatment facility but are significantly increased when anaerobic digestion of sludge is employed at the treatment facility. Like nitrous oxide emissions, estimating the extent of methane emissions is difficult due to plant-to-plant variability. A commonly used conversion factor is 0.87% of incoming COD to the plant as presented in Daelman et al. [260]. This figure will be used for consistency with N_2O emission calculations, as Parravicini et al. also used it in their study [259]. As such, when combined with our mass flow provides a figure of 910 kg_{CH4} day^{-1} for methane emissions.

The final key manner in which GHGs are emitted from WWTPs is via lifecycle emissions from grid electricity use. The emission intensity of UK electricity

currently stands at 107 gCO_2e/ kWh. Given an average daily use of 20 MWh of grid electricity, this adds 2,100 kg CO_2 to the facility's GHG footprint. With GWPs of 298 and 25 times that of CO_2 for N_2O and CH_4 respectively [261], tallied, the plant's total emission of GHG_S is 41.6 tonnes CO_2e per day. The footprint breakdown has been summarised in Figure 3-5, where N_2O contributes 40.4%, CH_4 contributes 54.6% and CO_2 contributes 5%.

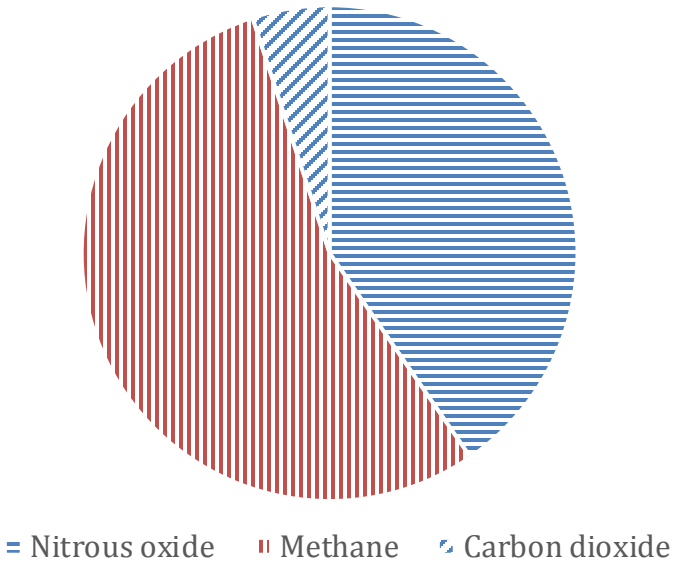

Figure 3-5. GHG footprint for Esholt WWTP

3.5 Concluding Remarks

Internal stream sampling was carried out at Esholt WWTWs between October 2014 and May 2016. Sample characterisation was performed, recording the streams' TSS, VSS, COD, TKN, TAN, TP and PO_4 levels. From characterisation data a steady-state internal mass flow diagram of the treatment facility was generated and validated using a number of methods.

Plant energy production and consumption has been calculated from OFGEM data, mass flow calculations and discussions with plant technicians. It shows that Esholt is able to generate 2/3 of the electricity it consumes. Thus, requires

on average 20 MWh of grid electricity each day. From the energy production figures, biomethane generation has been inferred at 8,235 kg per day.

Emission of greenhouse gases, nitrous oxide, methane and carbon dioxide have been estimated using the mass flow of various species in the facility. Thus, the impact of any changes in GHG emissions caused by the diversion of ammonia on the facility's overall greenhouse gas footprint can be deduced.

Mass flow of ammonia from digestate will be used for ammonia recovery process modelling in the following three chapters. Meanwhile, biomethane flow will be utilised in the solid oxide fuel cell and H_2 production processes models (Chapters 5 and 6).

4 Ammonia Recovery

4.1 Introduction

This chapter focusses on the use of Aspen Plus v8.8 software [262] to design a process that strips ammonia from digestate liquor and recovers it in a way that it is ready for use in a hydrogen production system or direct input alongside biomethane in a SOFC. A range of sensitivity analysis has been carried out in order to optimise the system energetically and provide the versatility required for transfer to the adjoined models of hydrogen generation by steam reforming (SR) and combined heat and power generation via solid oxide fuel cell (SOFC). Work has also been carried out to calculate the requirements to adjust the pH of the liquor to an appropriate stripping level. An economic model has been developed which costs the equipment and determines the financial value of ammonia required in order for the system to be worthwhile.

Examples of process modelling the recovery of ammonia from waste streams in Aspen Plus are limited. Errico et al. [21] simulated recovery of ammonia from digestate liquor, which was present at a concentration of 0.224 mol L^{-1} or 4.04 g l^{-1}. A flash drum was simulated to remove CO_2 from the system before NaOH was added to convert all ammonium to ammonia. An air stripper was used to desorb the ammonia. This preceded an absorption column with a sulphuric acid solvent to re-absorb the ammonia and generate a product of ammonium sulfate. Errico et al. [21] were able to recover over 95% of the initial ammonia concentration, using an air to liquid mass ratio of 0.28, a pH adjustment to 9

and stripping gas at 90 °C. They also found that the plant would be working in profit after 6 years of operation.

Boul et al. [263] also simulated an ammonia stripper in Aspen plus. However, the application was to produce clean water on the moon's surface from human urine. The stripper was preceded by a distillation column which volatilised other volatile organic compounds alongside ammonia. Thedistillate stream, which also contains water, was sent to the top of an air stripper where all of its volatiles were removed, generating a flow of pure water from its bottoms. They achieved 100% ammonia recovery but used an air to liquid mass ratio of 13.6, which would be extremely costly for a wastewater treatment plant. Thus, it is hard to draw too many comparisons with this particular piece of literature.

4.2 Process Design

As discussed in Chapter 2, air and steam stripping are the most mature and preferred techniques in industry for ammonia recovery from digestate liquor [22,170–172]. As such, comparative modelling has been done to designate the fundamental stripping technique. Air stripping is ordinarily combined with substances such as sulphuric or nitric acid to form marketable fertilisers. However, sulphur is a powerful poison for catalysts used in both hydrogen production and SOFCs [136]. Furthermore, the purchasing of substances, such as sulphuric or nitric acid, will only increase operating costs and so have been omitted. Resultantly, the absorption process in this body of work has been carried out using just water and is followed by a final recovery method. A flash separator has first been analysed, the operation of which has been be dictated by downstream feed molar steam to carbon (S:C) ratios for simulated SMR and SOFC plants. Secondly, a distillation column has been considered which will recover ammonia in a far more concentrated form, thus, will not be dictated by downstream S:C ratios. Again, energetic comparisons will be done so a choice can be made on the most appropriate method.

Ammonia concentrations found from the digestate liquor characterisation, carried out in Chapter 3, have been used for input to the model. The pH of liquor

carried out in characterisation analysis has been used to determine the required amount of NaOH to boost pH sufficiently. Meanwhile, the total flow of liquor has been taken from the mass flow analysis done for Esholt WWTP, as also shown in Chapter 3. Three assumptions have been utilised throughout the simulation:

1. Ambient conditions set at 1 bar and 23°C
2. Air composition assumed 79:21 molar split of N_2:O_2 only
3. Digestate consists of just water and ammonia

A 'COMMON' method filter and an 'NRTL-RK' base method have been used throughout. The primary reason this property method has been chosen is that it is applicable for both stripping settings and hydrocarbon processes [264]. A short description of these methods and of the function of blocks used in the simulation can be found in Table 4-1.

The stripper and absorption columns are simulated using Radfrac blocks without condensers and reboilers. Equilibrium calculations have been specified over the alternative rate-based option. Due to the difficulty in simulating packing material, reasonable numbers of stages have been specified. For the stripper, 20 has been used, as it provides adequate ammonia removal for the flow of incoming liquor. The absorption column has a far lower total incoming flow-rate, thus, 10 stages have been specified. A 10% pressure drop has also been specified in the air stripper, meaning stripping air is compressed to 1.1 bar.

The flash separator has been simulated using a 'Flash2' block with 'Vapor-Liquid-DirtyWater' valid phases. A 'RadFrac' column has been used to simulate the distillation column with 15 stages, a 'Partial-Vapor' condenser, a 'Kettle' reboiler at standard convergence. All heaters and coolers have been simulated using 'Heater' blocks with no pressure drop. All heat exchangers are simulated using 'HeatX' blocks, using the 'Shortcut' model fidelity, 'Design' calculation mode and with 'Countercurrent' flows.

Table 4-1 Aspen Plus blocks and property method descriptions

RStoic	Reactor block that calculates output composition based on specified molar conversions of stated reactions
Flash2	Capable of simulating flashes, evaporators, knock-out drums. Calculates thermal and phase conditions for vapour-liquid separation
FSplit	Separates material, heat or work streams into two or more according to specified splits. All outlet streams contain the same fractional composition.
Compr	Simulates both compressors and turbines. In this work both compressors and turbines have been modelled as isentropic. Performs power consumption or production calculations based on desired pressure outlet.
Pump	Models pumps or hydraulic turbines. Designed to handles single-liquid phase inlet streams. Performs power consumption or production calculations based on desired pressure outlet.
HeatX	Capable of simulating a variety of heat exchangers. In this work 'shortcut' option has been used with counter-current flow. Calculates heat transfer capabilities based on properties of hot and cold side flows.
Heater	Capable of simulating heaters and coolers. Calculates thermal and phase conditions for one or more inlet streams under specified conditions (normally temperature and pressure).
RadFrac	Capable of modelling all types of multistage vapour-liquid fractionation operations including stripping and absorption
NRTL-RK Property Method	Component properties are based on NRTL activity coefficient model for liquid phase, Redlich-Kwong equation of state for vapour phase, Rackett model for liquid molar volume and Henry's law for supercritical components

4.2.1 Sensitivity Analysis

Sensitivity analysis was carried out on each of the stripper, absorber and flash separator. For the stripper, the factors requiring sensitivity analysis were air flow-rate and temperature. The processused for stripping sensitivity can be seen in Figure 4-1. The incoming liquor stream, labelled 'LIQ1', contains 1528.56 kmol h^{-1} of water and 2.952 kmol h^{-1} of ammonia, as dictated by characterisation analysis of liquor from Esholt WWTP (Chapter 3). It enters the stripper above stage 1. It is assumed that the liquor has been pre-treated with NaOH to increase the pH to a state where all ammonia is in its free (NH_3) form and all solids have been removed. The liquor is pre-heated before entering the stripper via heat exchange with the bottoms outlet of the stripper (labelled

BTMS1) in the HX1 heat exchanger. HX1 is designed so that BTMS1 outlet temperatures is 1°C greater than the LIQ1 inlet temperature. This ensures maximum heat exchange occurs.

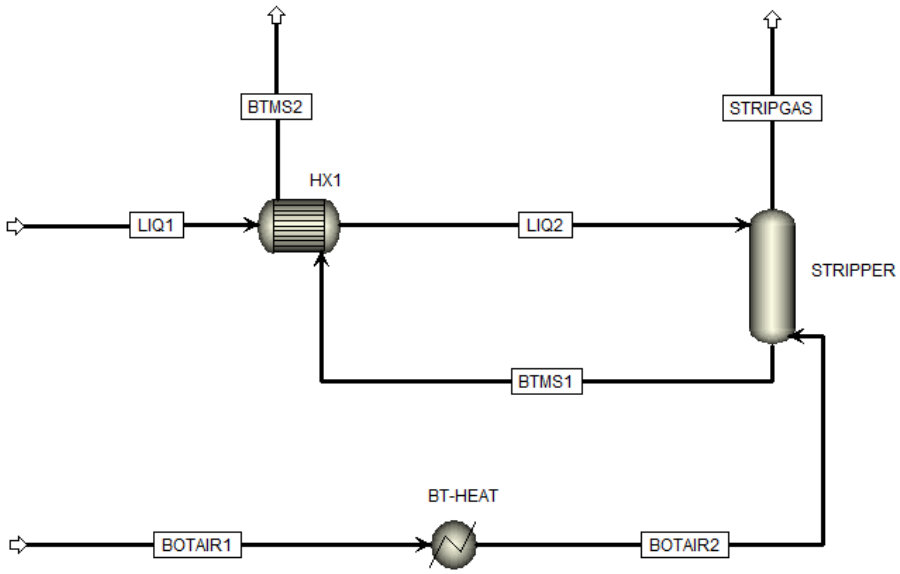

Figure 4-1. Process flow used for stripping sensitivity

Air enters in through stream, 'BOTAIR1', and is preheated in the heater block, 'BT-HEAT'. This hot air stream enters the stripper 'on-stage' 20. Air-flow rate was varied between 200 and 1000 kmol h^{-1} at 50 kmol h^{-1} intervals for sensitivity analysis. Air flow temperatures, set by heater 'BT-HEAT', was varied at 25 °C intervals between 125-800 °C. It should be noted that incoming air temperatures are not equal to the temperature profile of the stripper. The liquor enters at a lower temperature and the heat transfer from air to liquor dictates what temperature the stripper is operating at.

Sensitivity analysis was also carried out for steam stripping. This was done to compare the energetic demand for steam and air stripping, which allows the decision whether steam stripping is the more energetically intensive process, as suggested by literature [172,173]. The analysis was performed using the same process design showcased in Figure 4-9, where the air in stream BOTAIR1 is replaced by water. Two variables were investigated; the incoming temperature of steam and its flow rate. Flow rate was varied between 100-300

kmol h^{-1} at 10 kmol h^{-1} intervals and the temperature (dictated by Heater block 'BT-HEAT') was varied between 100-300 °C at 10 °C intervals.

For the absorber, sensitivity analysis was carried out on incoming air and water flow rate. Temperature contribution analysis was not necessary as literature analysis informed that solubility of ammonia increases with lower temperatures, so ambient temperature was utilised. The process flow used for stripping sensitivity analysis can be found in Figure 4-2. The gaseous exit from the stripper (STRIPGAS) is fed into a 'Heater' block labelled 'COOLER' which cools the stream down to 23°C. 'COOLER' also acts as a condenser, condensing out any water that has vaporised in the stripper. The cool stream (STRIP2) then enters the bottom of the absorption column; 'on-stage' 10.

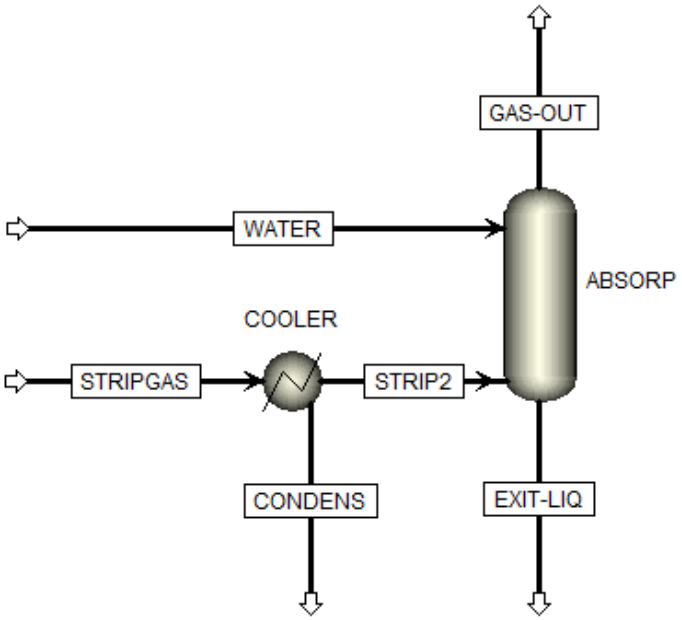

Figure 4-2. Process flow for absorption sensitivity analysis

Analysis was carried out using the stripping column's gaseous outlet for each of the twelve least energy intensive stripping conditions for input to the base of the absorption column. Water flow from the top was also varied between 50 and 800 kmol h^{-1} at 10 kmol h^{-1} intervals.

Flash-based sensitivity analysis involved the variation of incoming temperature, incoming flow rate and operating vapour fraction. The flash separator has two key roles. Firstly, to recover as much ammonia as possible. Secondly to recover ammonia alongside a quantity of water suitable for steam methane reforming (SMR). In Chapter 2, it was calculated that Esholt WWTP generates on average 8,235 kg of CH_4 each day from anaerobic digestion. For the fuel cell process model, all methane will be processed in the internal reforming SOFC, whereas, in the hydrogen production process model, 28% will be used for fuel in the reformer's furnace to meet all thermal demands.

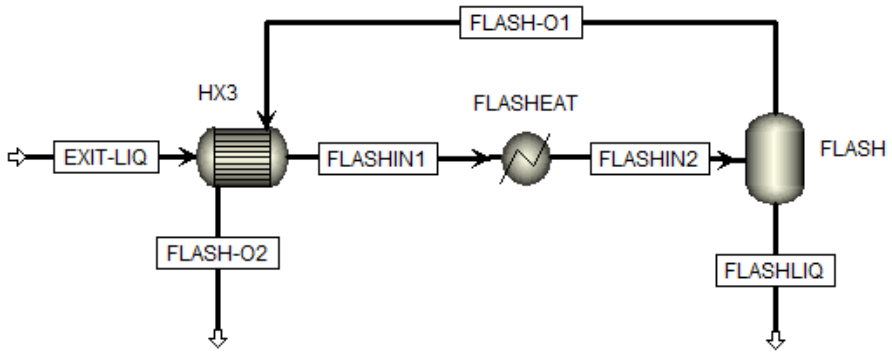

Figure 4-3. Process flow for flash sensitivity analysis

The process flow used for flash sensitivity analysis can be seen in Figure 4-3. The bottoms of the absorption column, 'EXIT-LIQ', is twice pre-heated before entering the flash separator. Firstly, via the heat exchanger, 'HX3', where the hot vaporised outlet from 'FLASH' is used to heat the incoming 'EXIT-LIQ'. HX3 is set up so that the EXIT-LIQ heats up to within 1°C of FLASH-O1. A 'Design Spec' has been set up that dictates the temperature given to 'FLASHIN2' via 'FLASHEAT' so that the heat duty of 'FLASH' is zero. This ensures that no further heating occurs in the flash separator to achieve the set vapour fraction. The required water outlet for downstream feed molar S:C ratios of 2, 3 and 4 for future hydrogen production and SOFC models are shown in Table 4-2.

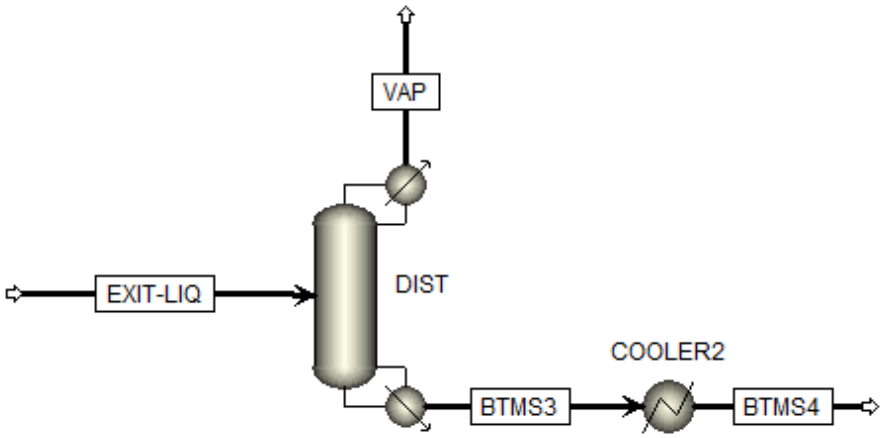

Figure 4-4. Process flow for distillation sensitivity analysis

For sensitivity analysis the distillation column (DIST) has been set up so that EXIT-LIQ from the absorption column enters 'DIST' above stage 2 without pre-heating. The distillate stream (VAP), carrying recovered ammonia exits from the top in gaseous form. The condensed bottoms (BTMS3), leaves at a higher temperature than 'VAP' due to its exit from the reboiler. The heater block, 'COOLER2', cools the stream to ambient conditions so heat recovery potential can be calculated. Two variables underwent sensitivity analysis. Firstly, molar reflux ratio was varied between 0.15 and 1. Secondly, distillate rate was varied between 2.8 and 5 kmol h^{-1}. The reflux ratio can be described as the ratio between the amount of liquid returned down the column and the quantity that is collected in the distillate. The distillate rate can be described as the total flow of fluid as distillate.

The sum of the heat duties of the condenser, reboiler and COOLER2 was used as an indicator for the distiller's energetic consumption. It could then be compared with the energy demand of the flash system in order to appoint the most appropriate final ammonia recovery step.

4.2.2 Economic Costing

Aspen Process Economic Analyzer (APEA) [265] was used to estimate the capital expenditure and was examined under two key areas. Firstly, the 'Equipment Cost' which encompasses the material cost of the equipment unit simulated. Secondly, the 'Total Installed Cost' which includes the material cost plus: above ground piping, poling, concrete, instrumentation underground/above ground electrics, grout and labour costs [266].

4.2.2.1 Cost of Operating Labour

Calculating the total cost of labour began with the consideration of the total required labour for the plant. According to data obtained by Alkhayat & Gerrard [267] and described in Turton et al. [268], the number of operators per shift can be estimated via Equation 4-1:

$$N_{OL} = (6.29 + 31.7{P_P}^2 + 0.23N_{np})^{0.5} \quad 4\text{-}1$$

where, N_{OL} is the number of operators per shift, P_P is the number of processing steps involving the handling of particulate solids and N_{np} is the number of non-particulate processing steps.

An operator would work on average 49 weeks per annum at five 8-hour shifts per week; making 245 shifts per operator per year. For 24 hours/day operation, the plant requires three set of shifts per day or 1,095 shifts per year. This means that approximately 4.5 operators are required per N_{OL}. According to Glass Door, the average salary for a process engineer is £34,523 [269] and has been used as the mean salary for plant operators in this assessment. However, this salary is subject to an annual growth rate of 2.99%; corresponding to data from the UK Office for National Statistics (ONS) for years between 2005-2015 [270].

4.2.2.2 Maintenance costs

Annual maintenance costs have been estimated as 3% of the total installed costs as suggested in both Turton et al. [268] and Rotunno et al. [271].

4.2.2.3 Net Present Value

Net Present Value (NPV) sensitivity analysis has been carried out using speculative values for recovered NH_3 to determine, over a 20 year operating period, what value each unit of recovered NH_3 will need to have in order for the initial investment to be financially viable. For now, speculative ammonia values have been used because its true value cannot be determined without evaluation of its end-use as a fuel for SOFC processing or as a H_2 production feedstock.

NPV takes into account the time value of money; where the value of a sum of money is worth more in the present than the same sum of money will be worth in the future. This is the case because any capital investment is in direct competition with other opportunities that could guarantee a particular rate of return. Thus, NPV analysis applies a discount factor to future cash flows to account for the impact of value over time. The discount factor applied, known as the 'discount rate', equates to alternative potential investment returns. A 10% annual return on investment is a reasonable assumption and, thus, has been used as the discount rate for NPV analysis. Equation 4-2 displays the calculation used for NPV:

$$\boldsymbol{NPV(i,N)} = \sum_{t=0}^{N} \frac{R_t}{(1+i)^t} \qquad 4\text{-}2$$

where; i is the discount rate (as a fraction), N is the plant life time, t is the year of operation and R_t is the net cash flow for the year. Net cash flow includes income based from the speculative value of recovered ammonia minus financial outgoings. For year 0, financial outgoings include capital investment and for operating years include the wage bill, maintenance costs and material costs. If

NPV ≥ 0 within a desired payback period, then process implementation can be viewed financially viable.

Operation expenses such as maintenance costs and caustic soda have been subject to annual inflation of 2.87%, based on the average retail price index (RPI) inflation between 2008-2018, and calculated using data from the office of national statistics (ONS) [272]. Employee salaries have been subject to annual increments of 2.99%, based on the average annual growth between 2005-2015, shown in data from ONS [270].

4.3 Results and Discussion

4.3.1 Stripping Sensitivity Analysis

4.3.1.1 Air Stripping

Review of literature informed that both flow and the temperature of the air feed in the stripper have an impact on the effectiveness of stripping. This has been demonstrated via sensitivity analysis of the process built in Aspen Plus (Figure 4-1), the results for a select number of temperature options can be seen in Figure 4-5. Figure 4-5 shows that where both low flow rates and temperatures of feed air are used, it is not possible to achieve effective ammonia stripping. Whereas, at high flow rates and temperatures, total ammonia recovery can be attained. However, increasing both the temperature and flow rate of feed air impact on the energy requirements of stripping and down-stream process. Thus, it is important for further analysis to choose the most appropriate conditions.

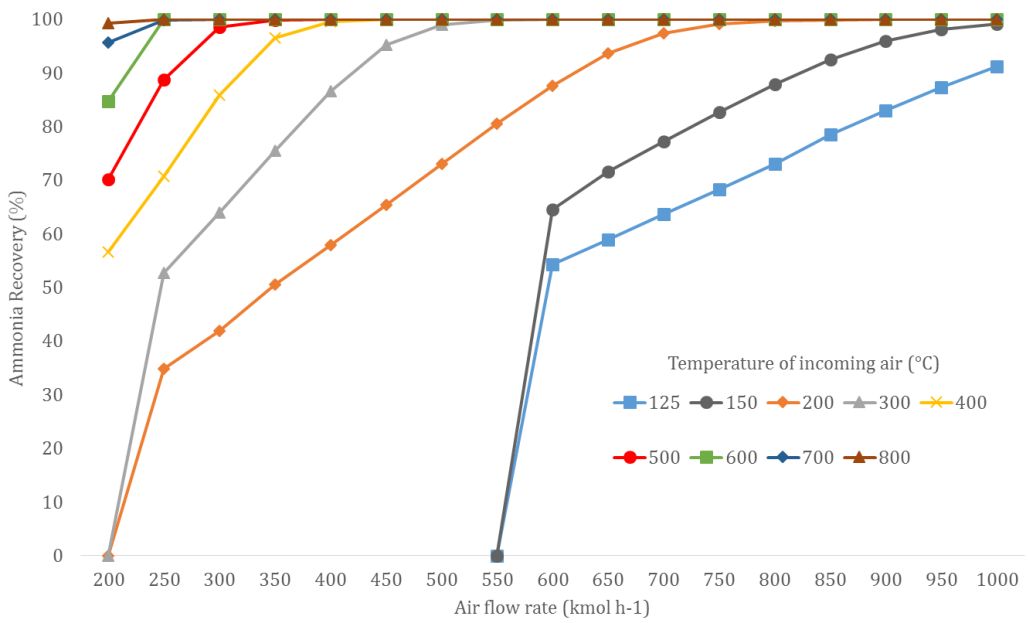

Figure 4-5. Graph illustrating the effect of air temperature and air flow rate on the % of ammonia recovered from digestate liquor.

It was decided that the minimum quantity of ammonia recovery desired in the air stripper is 95%. The sensitivity analysis displayed in Figure 4-5, shows that this is unachievable at the lowest air temperature considered of 125°C. However, at 150°C and an air flow rate of 900 kmol h^{-1}, 96% of ammonia can be recovered. Under these conditions, the gas contained in the stream 'STRIPGAS', leaves at a temperature of 37.4 °C, and the liquid effluent in stream 'BTMS1' leaves at a temperature of 38.7 °C. It also facilitates a mass air to liquid ratio of 0.94 on a mass basis and 799 on a volume basis.

Over 95% of ammonia can be recovered from digestate liquor using the lowest air flow-rate analysed of 200 kmol h^{-1}, if the air is heated to at least 700 °C. Resultantly, the temperature profile of the column is far greater than the high air flow scenarios discussed above. The stripped gas leaves at a temperature of 68.1°C and the liquid bottoms leaves at 70.2°C. The air:liquid ratio under this scenario is much lower, at 0.21 on a mass basis and 178 on a volume basis.

The heater block, 'BT-HEAT', has been used as a proxy to determine the most appropriate conditions for stripping. This is, in essence, the air temperature and air flow rate of the incoming air-stream that requires the lowest energy input. Results from stripping sensitivity that provided >95% recovery were

ordered in terms of heat duty requirements of 'BT-HEAT'. The twelve least energy intensive conditions have been detailed in Figure 4-6.

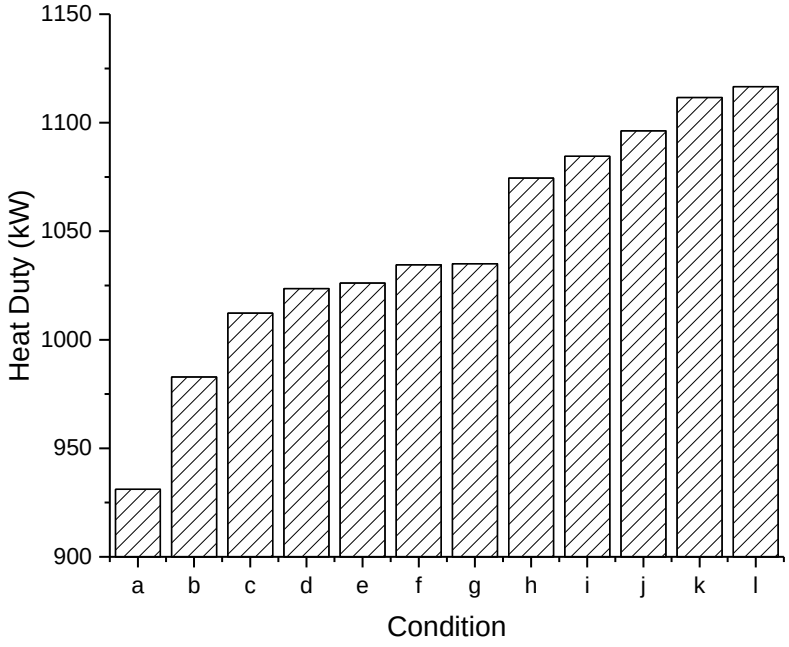

Figure 4-6. Chart comparing the thermal energy requirement to heat incoming stripping air of the twelve least energy intensive conditions. a) 900 kmol h^{-1} at 150°C, b) 950 kmol h^{-1} at 150°C, c) 700 kmol h^{-1} at 200°C d) 550 kmol h^{-1} at 250°C, e) 450 kmol h^{-1} at 300°C, f) 1000 kmol h^{-1} at 150°C, g) 500 kmol h^{-1} at 275°C, h) 650 kmol h^{-1} at 225°C, i) 750 kmol h^{-1} at 200°C, j) 350 kmol h^{-1} at 400°C, k) 250 kmol h^{-1} at 550°C, l) 600 kmol h^{-1} at 250°C

The least energy intensive condition is at 150°C and 900 kmol h^{-1}, which requires 931 kW of heating. There is a general trend that higher flow rates, at lower temperatures are less energy intensive than low flow rates at higher temperatures. It is thought that this amount of heating could be fully met internally when combined with hot streams generated during hydrogen generation or fuel cell process models. However, the high flow rate of air brings with it other issues, firstly the extra energy costs for compression, secondly, the higher flow rates mean a larger column, which facilitates additional capital costs. Lastly, a greater flow of air will require a greater flow of water for the successive absorption step which has its own repercussions, of which will be discussed with further sensitivity analysis.

4.3.1.2 Steam Stripping

Sensitivity analysis was carried out for steam stripping as discussed in section 4.2.1. As with air stripping, 95% ammonia recovery was used as the benchmark to analyse the conditions with the least associated energy demand. As shown in Figure 4-7, the six least energy demanding conditions all had steam flow rates of 110 and 120 kmol h^{-1} at varying temperatures. However, the least energy intensive condition of 110 kmol h^{-1} at 270 °C requires 1,605 kW of thermal power. This is 675 kW or 72% greater than the least energy demanding condition analysed in air stripping. For this reason, air stripping was chosen as the stripping technique of choice going forward.

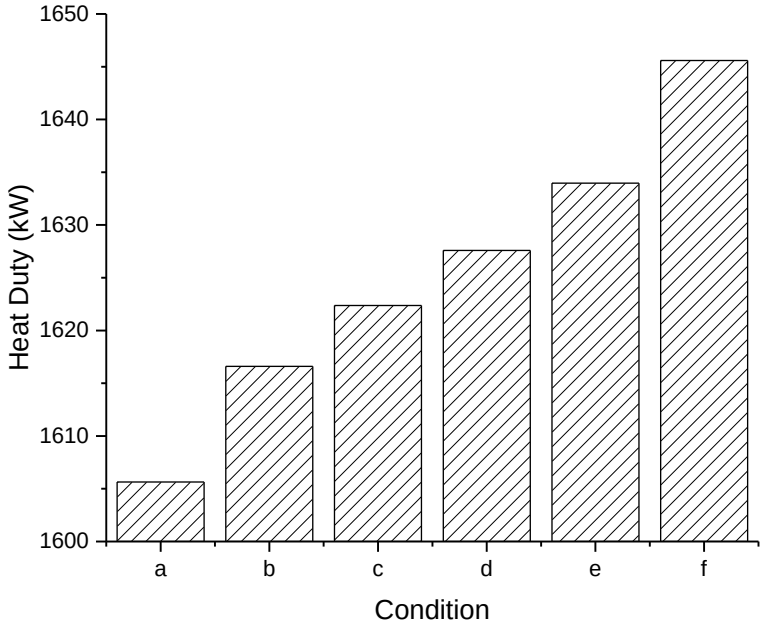

Figure 4-7. Six least energy consuming conditions for steam stripping providing 95% NH_3 recovery. a) 110 kmol h^{-1} at 270°C, b) 120 kmol h^{-1} at 160°C, c) 110 kmol h^{-1} at 280°C, d) 120 kmol h^{-1} at 170°C, e) 110 kmol h^{-1} at 290°C, f) 120 kmol h^{-1} at 180°C.

4.3.2 Absorption and Flash Sensitivity Analysis

Sensitivity analysis of the water flow requirement for ammonia recovery in the absorption column was carried out using the range of flows discussed in section 4.2.1. The flow of water needed to absorb 95% of incoming ammonia for the

twelve scenarios shown in Figure 4-6 were found. The results for each scenario can be found in Figure 4-8. It highlights the fact that, although low temperatures and high-flow rates suit ammonia stripping from an energetic perspective, it has a negative impact on the quantity of water needed to effectively re-absorb the ammonia into solution.

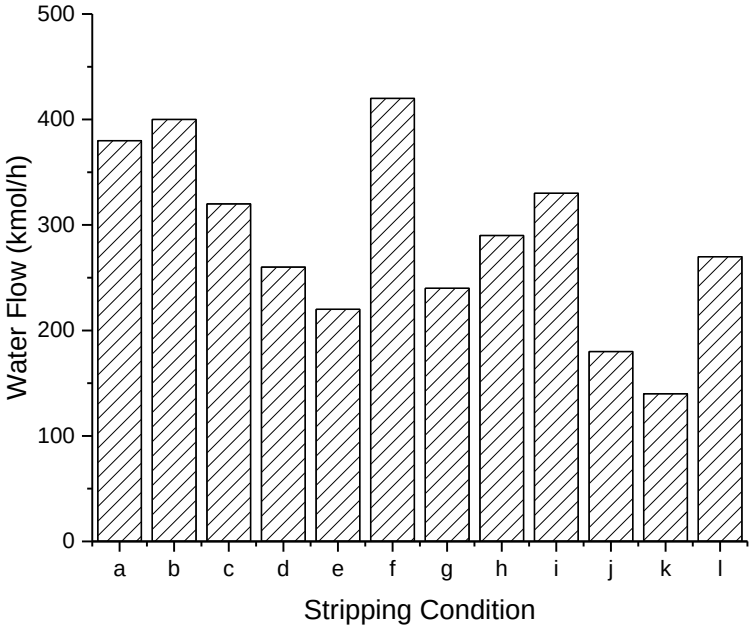

Figure 4-8. Chart comparing the water flow in to the absorption column to absorb 95% of incoming ammonia for the twelve least energy intensive conditions found for air stripping: a) 900 kmol h^{-1} at 150°C, b) 950 kmol h^{-1} at 150°C, c) 700 kmol h^{-1} at 200°C d) 550 kmol h^{-1} at 250°C, e) 450 kmol h^{-1} at 300°C, f) 1000 kmol h^{-1} at 150°C, g) 500 kmol h^{-1} at 275°C, h) 650 kmol h^{-1} at 225°C, i) 750 kmol h^{-1} at 200°C, j) 350 kmol h^{-1} at 400°C, k) 250 kmol h^{-1} at 550°C, l) 600 kmol h^{-1} at 250°C

The workings of Henry's law means that when the partial pressure of ammonia is low in the gas phase, more water is required to absorb ammonia. In order to assess this relationship, the incoming air flow was plotted with the required water flow to recover 95% of the incoming ammonia, as shown in Figure 4-9. The best-fit line shown in Figure 4-9, with an R^2 of 0.998, illustrates the strong linear relationship between incoming flow rate and required water flow for ammonia recovery. For future models with varying quantities of incoming

gaseous flow, a suitable water-flow rate can be predicted using the equation of best-fit.

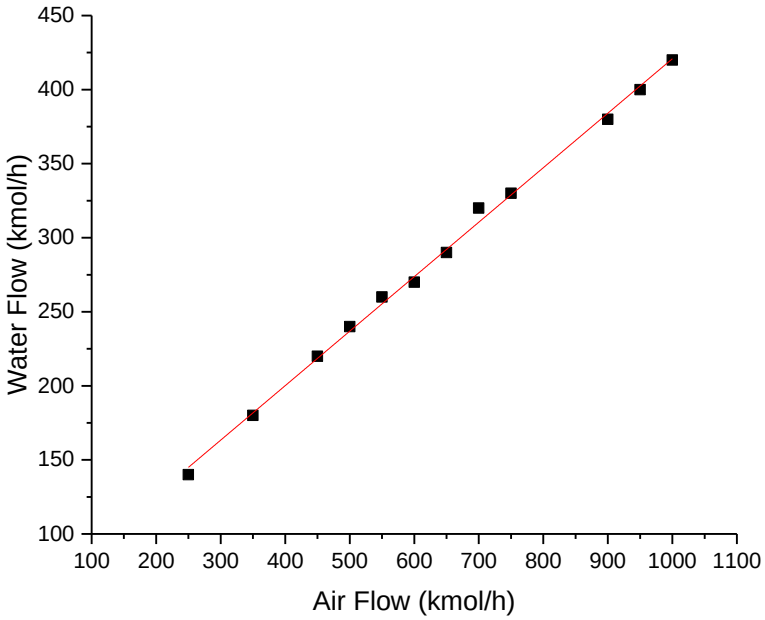

Figure 4-9. Correlation between incoming gaseous flow rate and required water flow to achieve 95% ammonia recovery. Line of best fit; $y = 0.3679x + 52.989$, $R^2 = 0.998$.

The quantity of water required during absorption is also important in terms of whole-process sustainability, due to the impact it has on the operation of the flash separator or distillation column.

4.3.3 Flash Separation

The flash separator manipulates the differing enthalpy of vaporisation points of components in its feed inlet to produce a vapour and a liquid outlet. In the case of the discussed process, it acts to concentrate the ammonia, as its enthalpy of vaporisation is much lower than water's. However, some water still vaporises in the flash separator, meaning its operational conditions are dictated by down-stream feed molar S:C ratios to either the SR or SOFC units. The required water outlet with ammonia is shown in Table 4-2:

Table 4-2. Required water outlet for associated downstream S:C ratios.

SOFC model	Water requirement (kmol h^{-1})
S:C 2	42.8
S:C 3	64.2
S:C 4	85.5
H_2 production model	Water requirement (kmol h^{-1})
S:C 2	30.9
S:C 3	46.4
S:C 4	61.8

Figure 4-10 shows the effect of varying water inlet flows (which corresponds to the water flow used during absorption) on the outlet of vaporised water and ammonia from the flash separator. Each point demonstrates a different set vapour fraction between 0.12-0.5. The objective is to achieve the water flow rates displayed in Table 4-2. In each case, it has been shown that a greater quantity of ammonia recovery is achievable with lower total flow inlet. For example, if the flash is to provide a S:C ratio of 2 for the SOFC model, a set vapour fraction of just above 0.32 for an incoming flow-rate of 140 kmol h^{-1} can be used and will recover 2.32 kmol h^{-1} of ammonia. However, with an incoming flow-rate of 300 kmol h^{-1} a vapour fraction of just below 0.16 would be used and would recover just 1.9 kmol h^{-1} of ammonia.

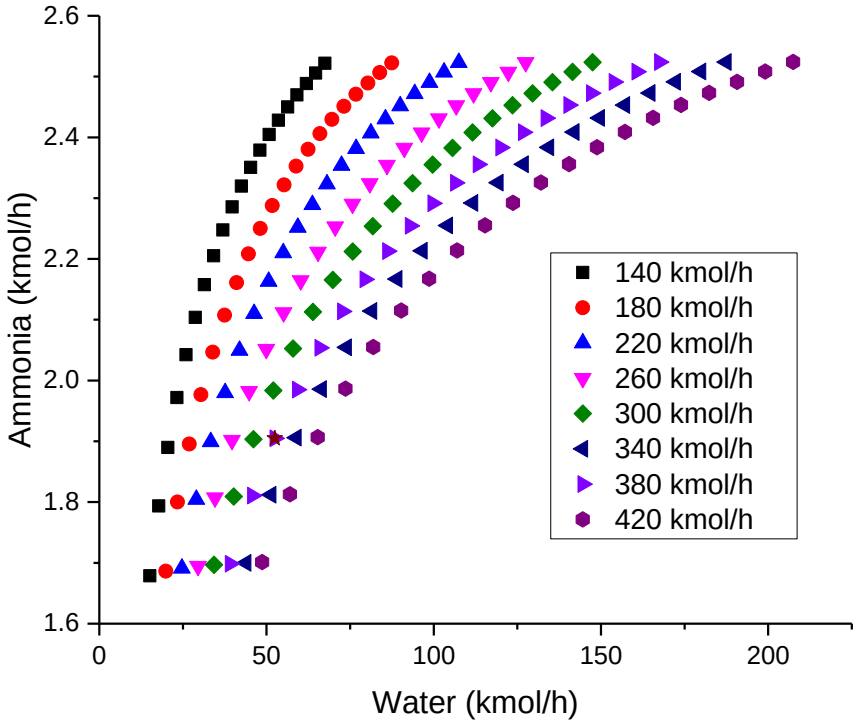

Figure 4-10. Sensitivity analysis results with outlet water and ammonia flow-rates (kmol h^{-1}) from flash separation with varying inlet flow rates between 140-420 kmol h^{-1}.

Lower flow rates in stream 'EXIT-LIQ' also lowers the heat demand of heater block 'FLASHEAT'. The operational preference for lower incoming flow rates to the flash separator, has key knock-on effects. Firstly, it means the absorption column should be operated with the lower flows of incoming water. In turn, previous analysis has shown that in order to recover an adequate quantity of ammonia, this is only possible if higher temperatures with lower air flow rates are used in the air stripper.

Thus, the influence of the lowest incoming flow rate (140 kmol h^{-1}) on the required flash vapour fraction was analysed. This included analysis for the steam requirements of S:C ratios 2, 3 and 4 for both future SOFC and H_2 production models. Regression analysis was performed so that the required vapour fraction, amount of ammonia recovered and associated energy demand were calculated for each downstream S:C scenario. The results from this analysis can be seen in Table 4-3.

Table 4-3. Required vapour fraction operation for the flash separator, quantity of ammonia recovered and heating requirements when quantity of water for future modelling scenarios with differing S:C ratios. Vapour fraction relationship with water vapour outlet: y = 0.00725x + 0.01165. Ammonia recovery relationship with water vapour outlet: y = 0.90037 + 0.06642x - 0.00103x^2 + 5.91E-06x^3. Heat duty relationship with water vapour outlet: y = -4.51775 + 5.46941x + 0.02442x^2.

SOFC model	Water requirement (kmol h^{-1})	Vapour fraction	Ammonia Recovery (kmol h^{-1})	Heat Duty (kW)
S:C 2	42.8	0.32	78.6	274.3
S:C 3	64.2	0.48	84.1	447.3
S:C 4	85.5	0.63	92.9	641.6
H2 Production Model	**Water requirement (kmol h^{-1})**	**Vapour fraction**	**Ammonia Recovery (kmol h^{-1})**	**Heat Duty (kW)**
S:C 2	30.9	0.24	72.6	187.8
S:C 3	46.4	0.35	79.8	301.8
S:C 4	61.8	0.46	83.5	426.8

Table 4-3 illustrates that when fulfilling the requirements of greater downstream S:C ratios, greater vapour fractions must be specified in the flash separator, this also means more ammonia can be recovered. However, the heat demand to achieve this is significantly higher. In essence, it is energetically cheaper to achieve lower S:C ratios but there will be a lower recovery of ammonia. The lowest percentage recovery from the flash separator was 79% for the S:C 2 hydrogen production scenario, whilst the highest was 93% for the SOFC S:C 4 scenario.

4.3.4 Distillation

Distillation could be used in place of stripping technology to recover ammonia straight from digestate liquor. However, due to the low concentrations and quantity of incoming liquid, this was found to be energetically impractical. However, post-absorption, the ammonia concentration is far greater which would make it more feasible. There are very few examples in literature that

have applied distillation post-absorption for ammonia recovery. The RVT group mentions the use of distillation after steam stripping to achieve a highly concentrated ammonia product in their technology overview document [187]. The results shown in the sensitivity analysis carried out in this Chapter look promising. Table 4-4 shows sensitivity results for the least energy consuming runs (in terms of both reboiler duty and combined heat duty for the reboiler, condenser and COOLER2) for eight different incoming flow rates between 140 and 420 kmol h^{-1} at 40 kmol h^{-1} intervals.

Table 4-4. Sensitivity data showing the **l**east energy consuming results for incoming flow rates for distillation at 40 kmol h^{-1} intervals.

Distillate rate (kmol h^{-1})	Reflux ratio	Flow in (kmol h^{-1})	H2O (kmol h^{-1})	NH3 (kmol h^{-1})	Reboiler Duty (kW)	Combined Heat Duty (kW)
3.4	1.5	140	0.10	2.705	348.37	68.19
4.4	0.05	140	1.11	2.700	301.68	82.04
3.6	1.5	180	0.06	2.808	428.31	79.49
4	0.15	180	0.54	2.728	375.40	85.75
3.6	1.5	220	0.00	2.740	472.74	86.82
4.6	0.05	220	0.97	2.769	452.10	102.85
3.8	1.5	260	0.00	2.813	552.03	98.32
4	0.25	260	0.31	2.704	528.61	104.03
4	1.5	300	0.03	2.858	663.16	112.86
5	0.05	300	1.11	2.779	605.70	126.58
4	1.5	340	0.00	2.768	705.40	119.45
4.4	0.25	340	0.40	2.766	683.56	127.74
4.4	1.5	380	0.19	2.860	824.57	136.48
4.8	0.15	380	0.73	2.723	758.16	142.64
4.2	1.5	420	0.00	2.734	859.29	140.71
5	0.15	420	0.79	2.749	835.66	154.57

Under each scenario shown in Table 4-4, over 97% of the incoming ammonia is recovered. This shows a far superior ammonia recovery potential compared to the alternative flash process. Similar to flash processing, the energy consumption of the distiller increases with greater incoming flow. The lowest reboiler duty was found under an inflow of 140 kmol h^{-1} at 301.68 kW. The highest reboiler duty was found under an inflow of 420 kmol h^{-1} at 859.29 kW.

This, again, details the down-stream energetic preference of using lower flow rates of air and water in the air stripper and absorption columns respectively. Thus, if an incoming flow rate of 140 kmol h^{-1} is considered, the reboiler heat duty could stand at 301.68 kW. This is greater than the lowest heat duty requirement for flash processing of 275 kW. However, it is lower than all other flash processing scenarios and guarantees a superior recovery of ammo nia.

The combined heat duty of the condenser, reboiler and COOLER2, labelled in Table 4-4 as 'combined heat duty', describes the energy demand if ideal heat recycling could be achieved. The reboiler is a heat sink whereas the condenser and COOLER2 have the potential to act as heat sources. This explains the disparity shown in Table 4-4 where the lowest reboiler duty doesn't necessarily equate to the lowest combined heat duty. Direct heat transfer between the three is impractical. However, if integrated into a wider process, it could play a part in whole-system sustainability.

Furthermore, a case could be made that the use of higher flow rates during stripping and absorption would be preferential due to the energetic advantages of using higher air flow rates at lower temperatures during stripping (as shown in Figure 4-6), which outweigh the differences in the 'Combined Heat Duty' figures, shown in Table 4-4, between high and low distillation incoming flow rates. However, there are no guarantees that ideal heat recycling can be achieved or is worthwhile, due to the low quality nature of the heat provided and the economic cost of heat exchange equipment. As such, it has been proposed that low flow rate scenarios will be used for the process henceforward.

4.3.5 Ammonia recovery: combined process

The sensitivity analysis carried out has enabled the formation of a combined process where the most appropriate technology methods and process conditions have been implemented. The full process flow combining air stripping, NH_3 absorption, and distillation in achieving the desired S:C for downstream reforming or SOFC can be found in Figure 4-11 and the stream

compositions in Table 4-5. The overall process facilitates an annual recovery of ammonia of 400.7 tonnes.

Table 4-5. Stream composition for final ammonia recovery process.

	LIQ1	LIQ2	BOT AIR	BOT AIR1	BOT AIR2	BTMS 1	BTMS 2	STRIP GAS
H_2O (kmol h^{-1})	1528.6	1528.6	0	0	0	1451.3	1451.3	77.3
O_2 (kmol h^{-1})	0	0	52.5	52.5	52.5	0.6	0.6	51.9
N_2 (kmol h^{-1})	0	0	197.5	197.5	197.5	0.9	0.9	196.6
NH_3 (kmol h^{-1})	3.0	3.0	0	0	0	0.1	0.1	2.8
Total Mole Flow (kmol h^{-1})	1531.5	1531.5	250.0	250.0	250.0	1452.9	1452.9	328.6
Total Mass Flow (kg h^{-1})	27587.7	27587.7	7212.6	7212.6	7212.6	26191	26191	8609.0
Total Volume Flow (l min^{-1})	462.1	480.8	102546	96794	259314	457.9	438.9	153069
Temperature (°C)	23.0	62.4	23.0	34.3	550.0	65.6	24.0	63.5
Pressure (bar)	1	1	1	1.1	1.1	1	1	1
	CONDENS	**STRIP2**	**WATER**	**GAS-OUT**	**EXIT-LIQ**	**BTMS 3**	**BTMS 4**	**VAP**
H_2O (kmol h^{-1})	77.2	0.1	145.5	6.0	139.6	138.5	138.5	1.1
O_2 (kmol h^{-1})	0	51.9	0.0	51.7	0.3	0	0	0.3
N_2 (kmol h^{-1})	0	196.6	0.0	196.3	0.4	0	0	0.4
NH_3 (kmol h^{-1})	0	2.8	0.0	0.1	2.7	0	0	2.7
Total Mole Flow (kmol h^{-1})	77.2	251.4	145.5	254.0	142.9	138.5	138.5	4.4
Total Mass Flow (kg h^{-1})	1390.5	7218.5	2621.2	7260.9	2578.8	2495.1	2495.1	83.7
Total Volume Flow (l min^{-1})	23.2	103124.7	43.9	103106.8	43.1	45.3	41.8	2066.4
Temperature (°C)	23.0	23.0	23.0	20.0	10.8	99.6	23.0	67.4
Pressure (bar)	1	1	1	1	1	1	1	1

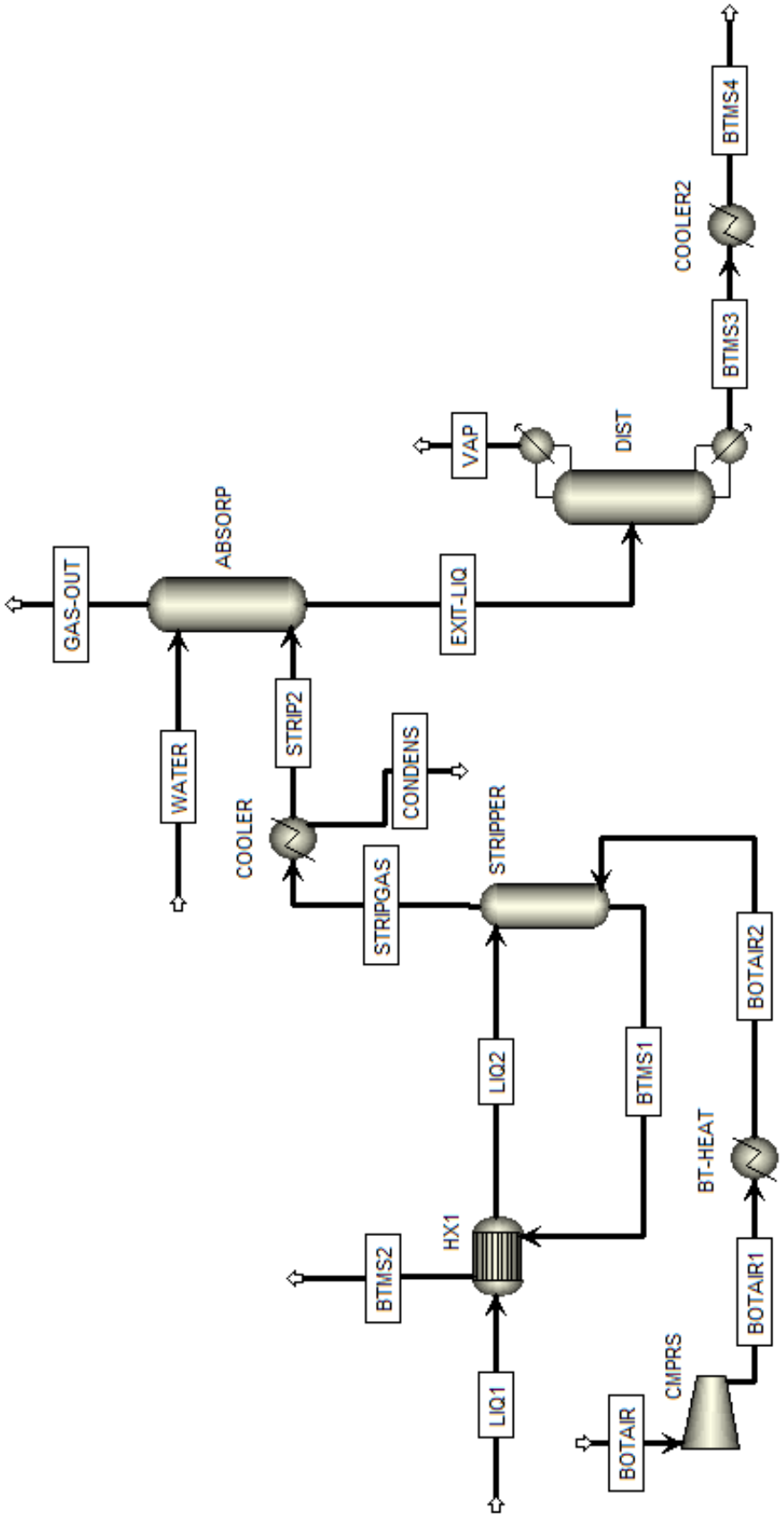

Figure 4-11. Process flow for ammonia recovery.

Figure 4-11 legend

LIQ1	Digestate liquor representative inlet
LIQ2	Preheated digestate liquor
BOTAIR	Air for stripping inlet at ambient temperature and pressure
BOTAIR1	Compressed air for stripping
BOTAIR2	Compressed and preheated air for stripping
BTMS1	Hot liquid outlet from the stripping column
BTMS2	Cooled liquid outlet from the stripping column
STRIPGAS	Gaseous outlet from the stripper containing desorbed NH_3
CONDENS	Water condensed from the stripper's gaseous outlet
STRIP2	Dry gaseous inlet to the absorber
WATER	Water inlet used for NH_3 absorption
GAS-OUT	Gaseous outlet from absorber
EXIT-LIQ	Liquid outlet from absorber containing reabsorbed NH_3
VAP	Gaseous distillate stream from distiller containing recovered NH_3
BTMS3	Hot liquid outlet from distiller
BTMS4	Cool liquid outlet from distiller

4.3.5.1 Stripping conditions

Due to the downstream benefits of using lower flow rates at higher temperatures in the stripping column, the lowest flow rate condition of the 16 least energy intensive conditions found during sensitivity analysis has been chosen (scenario 'k' as displayed in Figure 4-6). This means an incoming air flow rate of 250 kmol h^{-1}, equating to 7,213 kg h^{-1} or 15,558,840 l hr^{-1} at 550°C and 1.1 bar, which facilitates an average column temperature of 64.3°C. These conditions provide the stripping of 95% of the ammonia held in the incoming digestate liquor, which equates to 2.81 kmol h^{-1}. Furthermore, the compression of 'BOTAIR1' stream requires 22.9 kW of power.

4.3.5.2 Absorption conditions

The quantity of water used for absorption has been calculated using the equation presented from the regression analysis in Figure 4-9. This has determined a water flow rate of 145.5 kmol h^{-1} and has led to the absorption of 2.69 kmol h^{-1} of ammonia. This represents a recovery of 98.7% of the ammonia

entering the absorption column and 91% of ammonia held in the initial digestate liquor.

4.3.5.3 Distillation conditions

The stripping conditions with the lowest reboiler duty have been used for the final ammonia recovery process. This means a distillate rate of 4.4 and a reflux ratio of 0.05. This facilitates the recovery of 99.8% of the ammonia held in the distillation feedstock and a final recovery of 91% of ammonia contained in the initial digestate liquor. It has a reboiler duty of 310.1 kW, a condenser "duty" of -2.6 kW and a 'COOLER2' heat "duty" of -226.3 kW. Here, negative heat duties signify the generation of heat (vice versa, positive heat duty represent heat consumption). The true net energy requirement for distillation will only be known when integrated in to a wider process; where the heat generated at 'COOLER2' could be used for heat exchange with other streams. However, if all the heat generated at 'COOLER2' and the column's condenser can be recycled, then the distillation's net energy requirement is just 83.5 kW.

4.3.5.4 Energy Requirements

There are three main components during the proposed ammonia recovery process that consume energy: the air compressor for stripping (CMPRS), the stripping air heater (BT-HEAT) and the distiller's (DIST) reboiler. There are also three main components in the proposed process where cooling is required and could be used for heat recovery or recycling; the unit used to cool the gaseous inlet to the absorption column (COOLER), the distillation (DIST) condenser and cooling unit for the distiller's bottoms stream (COOLER2). The figures, of which, have been displayed in Table 4-6.

Table 4-6. Energy consumption of process and components.

	Energy	Utility
CMPRS (kW)	22.9	Power
BT-HEAT (kW)	1089.3	Heat
COOLER (kW)	-1056.6	Heat
DIST Reboiler (kW)	310.1	Heat
DIST Condenser (kW)	-2.6	Heat
COOLER2 (kW)	-226.3	Heat
Total Energy Consumed (kW)	1422.3	P&H
Potential Energy Export (kW)	1285.5	Heat
Net Power Consumption (kW)	22.9	Power
Net Heat Consumption (kW)	113.9	Heat

Table 4-6 shows that the largest energy consumer in the process is the heater used for pre-heating the stripping gas (BT-HEAT) at 1089.3 kW. This amounts to 78% of all thermal energy requirements, which stands at 1,399.4 kW. The only electrical power sink is during compression at 22.9 kW. The largest potential heat source is from 'COOLER', which could provide 1,056.6 kW of thermal energy if heat can be sensibly exchanged within a wider process. However, it should be noted that this is low quality heat, as the hot stream inlet to 'COOLER' (STRIPGAS) is entering at just 63.5°C. This limits the potential application of this heat in a wider setting but could always be an option for space heating at the WWTP.

Nevertheless, under the assumption that all heat sources from the proposed ammonia recovery process are utilised, the combined net energy consumption is just 136.8 kW. This translates to a net energy consumption of 2.99 kW per kg of recovered ammonia. If none of the energy from the heat sources can be utilised this figure rises to 31 kW per kg of recovered ammonia.

4.3.6 Economic Analysis

4.3.6.1 pH adjustment

The pH target for the ammonia liquor pre-stripping has been set to 10.5 as suggested by Hidalgo et al. [176]. The digestate liquor was found to have an

initial pH of 7.8 which corresponds to a pOH of 6.2 and an OH^- molar concentration of 0.00000063 moles l^{-1}. The reduction of pOH to 3.5 requires the addition of 0.000316 moles of OH^{-1} per litre which equates to 0.0126 g l^{-1} of NaOH. In total this would mean the addition of 8.34 kg of NaOH per day. ICIS report the cost of caustic soda in north-west Europe 310-340 USD/tonne [273], which means an expense in the range of £2.02-£2.22 per day with an exchange rate of 0.78 £/$.

4.3.6.2 Equipment Cost

Results from the Aspen Process Economic Analyzer (APEA) can be found in Table 4-7. The compressor has the highest capital and total installed cost at £416,286 and £688,500 respectively. The reason for this high cost is the large volume of gas required for compression and is another reason to keep the flow of stripping air down with higher temperatures. However, the stripping tower demands the greatest installation costs at £157,950. COOLER2 has the lowest capital and installation costs. However, note that when integrated into the wider process, this is likely to be replaced with a heat exchanger, which could provide different results. APEA was unable to cost the heater block 'BT-HEAT'. As such, a heat exchanger was set up with the same 'cold' input to BT-HEAT, counter-flowing against a stream of steam at 600 °C, which allowed for an appropriate economic proxy.

Table 4-7. Equipment capital costs and total installed costs (includes capital and installation expenditure) from Aspen Process Economic Analyser

Name	Equipment Capital Cost [GBP]	Total Installed Cost [GBP]
CMPRS	416,286	688,500
STRIPPER-tower	116,298	351,600
HX1	96,798	249,000
ABSORP-tower	59,670	231,700
DIST-tower	39,780	191,600
COOLER	23,634	126,700
DIST-cond	12,324	102,700
DIST-reflux pump	10,530	100,700
BT-HEAT	9,360	69,900
DIST-reb	7,722	68,700
COOLER2	3,588	27,700
Total	795,990	1,722,864

4.3.6.3 Net Present Value Analysis

It was found during NPV analysis that the minimum value required for each kg of recovered NH_3, to achieve an NPV of zero over a 20 year operating lifetime, was £1.87. The results of the analysis using this speculative value of recovered ammonia can be found in **Table 4-8**. £1.87 per kg of NH_3 is equivalent to £1.54 per kg of recovered nitrogen. At face value this seems comparatively high compared to the cost of ammonium nitrate fertiliser, for example, which the AHDB reported to be £0.82 per kg of nitrogen in October 2018 [274]. However, by recovering ammonia from digestate liquor the plant will experience energy/expenditure savings from reduced oxygen provision for the facility's activated sludge process (ASP). ASP aeration tanks consume 4.57 kWh kg^{-1} oxidised nitrogen [57]. Thus, the diversion of 329.6 tonnes of nitrogen per year corresponds to 1,506.3 MWh of electricity savings. At a purchasing price of 10p per kWh, this provides annual savings of £150,627 or £0.45 per kg of recovered nitrogen. When this is taken into account, the required value of recovered ammonia seems more viable, considering this is just one example of the added-value the recovery of ammonia can provide wastewater treatment facilities. However, its true value can only be determined when integrated into further

processes for SOFC use or hydrogen production, which is discussed in Chapters 5&6.

Table 4-8. NPV analysis results using a value of £1.87 per kg of recovered ammonia.

	Salaries (£)	Maintenance (£)	Caustic (£)	Total Expense (£)	NH_3 Value (£)	Cashflow (£)	Discount Cashflow (£)	NPV (£)
Yr 0				1,722,864				
Yr 1	507,654	66,264	737	574,656	749,379	174,723	158,840	-1,564,024
Yr 2	522,833	68,251.92	758	591,844	770,892	179,049	147,974	- 1,416,050
Yr 3	538,466	70,299.48	780	609,546	793,023	183,477	137,849	- 1,278,201
Yr 4	554,566	72,408.46	803	627,777	815,789	188,012	128,414	- 1,149,787
Yr 5	571,148	74,580.72	826	646,554	839,208	192,654	119,623	- 1,030,164
Yr 6	588,225	76,818.14	849	665,892	863,300	197,407	111,431	- 918,732
Yr 7	605,813	79,122.68	874	685,809	888,083	202,274	103,798	- 814,934
Yr 8	623,927	81,496.36	899	706,322	913,577	207,256	96,687	- 718,247
Yr 9	642,582	83,941.25	925	727,448	939,805	212,357	90,060	- 628,187
Yr 10	661,795	86,459.49	951	749,206	966,784	217,578	83,886	- 544,301
Yr 11	681,583	89,053.27	979	771,615	994,538	222,924	78,133	- 466,168
Yr 12	701,962	91,724.87	1,007	794,694	1,023,089	228,396	72,774	- 393,394
Yr 13	722,951	94,476.62	1,036	818,463	1,052,460	233,997	67,781	- 325,613
Yr 14	744,567	97,310.92	1,065	842,943	1,082,674	239,730	63,128	- 262,485
Yr 15	766,830	100,230.25	1,096	868,156	1,113,755	245,599	58,794	- 203,691
Yr 16	789,758	103,237.15	1,127	894,122	1,145,728	251,606	54,757	- 148,934
Yr 17	813,372	106,334.27	1,160	920,865	1,178,619	257,754	50,995	- 97,939
Yr 18	837,691	109,524.30	1,193	948,409	1,212,455	264,046	47,491	- 50,448
Yr 19	862,738	112,810.02	1,227	976,776	1,247,261	270,486	44,227	- 6,221
Yr 20	888,534	116,194.33	1,262	1,005,991	1,283,067	277,076	41,186	34,965

If the value for the recovered ammonia shown in Table 4-8 can be achieved then the time taken to pay back the initial investment, using non-discounted cashflow would take just under 9 years. Also using, non-discounted cashflows, a profit over the 20 year period of £2,723,537 could be achieved. Table 4-8 also shows that, by far the largest cost to the facility is the expenditure on salaries, consisting of roughly 88% of all annual outgoings.

4.4 Conclusions

The recovery of ammonia from digestate liquor has been robustly modelled using Aspen Plus process simulation software, utilising thorough sensitivity analysis to provide an energy efficient and proficient method to recover ammonia so that it is ready for processing in SOFCs or as a feedstock for hydrogen production. The final process model discussed and analysed in this chapter has been used as the base ammonia recovery method for models in the following two chapters.

The sensitivity analysis carried out found that air stripping operating at lower temperatures with greater air-flows demanded less heat than higher temperature, lower air flow options. However, using higher flow rates creates multiple down-stream issues. Firstly, more water is required during absorption to recapture the ammonia. This greater load resulted in higher energy demands for the flash separation and distillation steps. Secondly, a greater flow of air resulted in both more energy for compression and capital expenditure for a compression unit that can handle such high flow rates.

As such, the 16 least energy intensive stripping conditions that facilitated >95% ammonia recovery were determined from the sensitivity analysis. The scenario with the lowest air-flow rate was chosen for primary stripping conditions moving forward. This was found to be an incoming air flow rate of 250 kmol h^{-1}, equating to 7,213 kg h^{-1} at 550°C, which recovered 95% of the ammonia held in the digestate liquor. A water flow rate into the absorption column was set at 145.5 kmol h^{-1} which enables the absorption of 91% of the ammonia originally found in the digestate liquor. Sensitivity analysis showed that a final recovery step of distillation was energetically superior to flash separation. The distillation input conditions were set at a distillate rate of 4.4 and a reflux ratio of 0.05. The recovery potential using distillation was extremely effective and very little ammonia was lost, facilitating the overall recovery of 91% of the digestate liquor's ammonia.

Aspen Process Economic Analyser was used to cost the capital and installation costs of the equipment simulated in the discussed process. The total investment cost for installation of the equipment stands at £1,722,864. This was then used

as the year ‘zero’ costs for NPV analysis, where discounted cash-flows were used to determine what value the recovered ammonia would have to represent in order to make the investment financially worthwhile, based on a discount value of 10%. This required value has been determined as £1.87 per kg of recovered ammonia. Whether this figure is achievable will depend on its end use, which is discussed in the following chapters.

5 Solid Oxide Fuel Cell operating on recovered NH_3 and Bio-CH_4

5.1 Introduction

This chapter focusses on the applicability of combining the recovery of ammonia, via methods discussed in Chapter 4, with the operation of an internally reforming solid oxide fuel cell (IR-SOFC) stack, which uses both recovered ammonia and biomethane from the anaerobic digestion unit as fuels. This has been achieved via a number of methods. Firstly, a process model has been built using Aspen Plus to provide mass and thermal flow analysis. A numerical model has also been developed to provide the electrical power and heat generation potentials of the fuel cell. Finally, an economic analysis has been carried out to determine the financial viability of process implementation.

IR-SOFCs are devices that facilitate electricity production via the electrochemical oxidation of hydrogen that is simultaneously generated within the cell. The exothermic nature of the electrochemical oxidation reaction also generates thermal power; making the IR-SOFC a cogeneration device. Figure 5-1 illustrates the layout of a SOFC with the presence of an anode, cathode and electrolyte. The anode, doped with catalyst facilitates the steam reforming of hydrocarbons or the thermal conversion of other hydrogen carriers such as ammonia to produce a hydrogen-rich syngas. The cathode, ordinarily fed with air, enables the reduction of oxygen to its ionic form (O^{2-}) via contact with a circuit of electrons. The oxygen ions cross over the porous electrolyte to react with hydrogen at the anodic triple phase boundary (TPB). Here, water, heat and

electrons are produced. The electrons generated in this reaction provide the power output from the cell and are externally circulated back to the cathode for the reduction of oxygen.

The introduction of high temperature fuel cell systems at wastewater treatment plants (WWTPs) have been endorsed for two key reasons. Firstly, they have the capabilities to achieve superior electrical efficiencies compared to combustion-based cogeneration alternatives as they are not limited by thermodynamic obstructions such as Carnot efficiency [56]. Secondly, their high temperature operation allows for internal thermo-chemical reactions, capable of accepting an abundance of fuels including biogas, biomethane and ammonia [208].

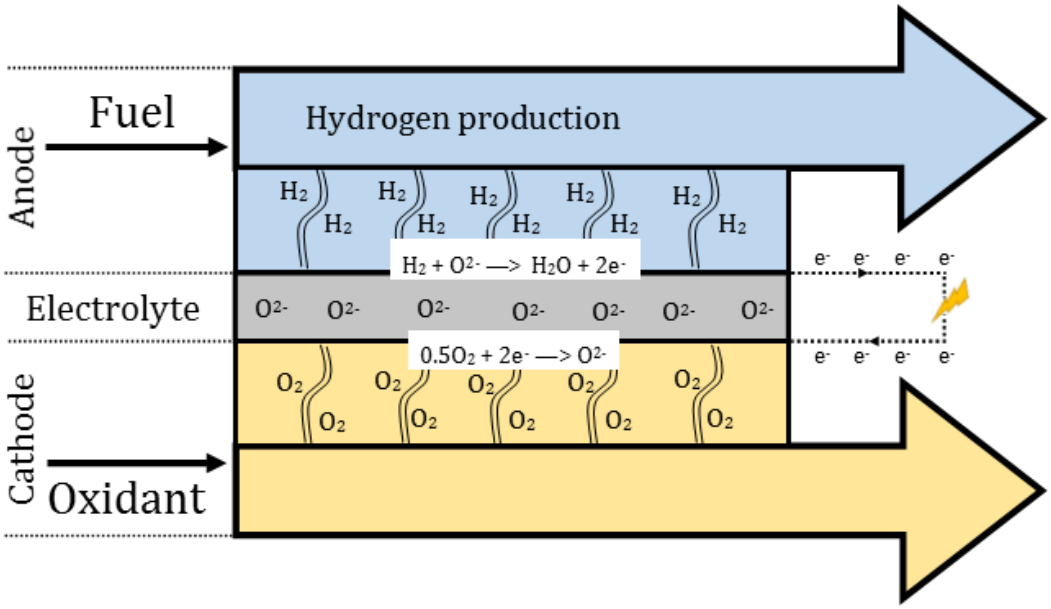

Figure 5-1. Layout of SOFC

The two key types of high temperature fuel cells were discussed for implementation at WWTPS; SOFCs and Molten Carbonate Fuel Cells (MCFCs). However, SOFCs have been chosen as the best option due to their superior electrical efficiency potential. For example, Stuttgart-Möhringen wastewater treatment plant in Germany operated an MCFC using biogas and found it to run with a net electrical efficiency of 44% [275]. On the other hand, a study by Mehr et al. [276] projects that a SOFC stack, using a biogas fuel, to be installed at SMAT Collegno WWTP in Turin will run with a net electrical efficiency of 51.6%.

The main commercially available SOFCs consist of ceramic yttria-stabilised zirconia (YSZ) electrolytes, with Ni/YSZ anodes and Sr- or Ca-doped $LaMnO_3$ cathodes, which operate at temperatures between 900-1000 °C [277]. Efforts have been made in material development to facilitate lower temperature operation using cheaper, metallic interconnects [278]. However, difficulties with overcoming lower electrolyte conductivity, electrode kinetics and sintering temperatures of using such materials has meant the technology readiness levels of 'intermediate temperature' (IT) SOFCs has remained markedly low.

SOFCs have also been identified as an efficient method of using ammonia as a fuel for cogeneration [56,116,279]. The high temperature operation allows for ammonia decomposition to hydrogen and nitrogen, the former being utilised during electrochemical processing. In their review of ammonia applications in SOFCs, Ni et al. [213] found that conventional high temperature SOFCs using Ni/YSZ anodes facilitated full decomposition of ammonia and comparable current densities to pure hydrogen.

However, there is just one other example in the literature, to date, that has studied both the recovery of ammonia from digestate liquor and its use alongside biogas in a SOFC. This was carried out by Xu et al. [157], in which an electrodeionization process was carried out at lab-scale to recover ammonia from synthetic ammonium-rich wastewaters for input to a three-layer button SOFC reactor with biogas produced from a lab-scale AD reactor fed with local sewage sludge. The researchers achieved 95% and 76% ammonium recovery from dilute and concentrated synthetic wastewaters respectively, and predicted a 60% improvement in net energy output compared to conventional CHP systems. However, electrodeionization has been in development for over 60 years and advancements in the fundamental understanding of its operation and application has been extremely slow [280]. Furthermore, its use often needs to be coupled with energy intensive procedures such as reverse osmosis to provide sufficient selectivity [199]. Thus, its pathway to commercialisation may still be some way off and provides further justification of the process discussed in Chapter 4.

5.2 Process Design

Aspen Plus V.8.8 software [262] has been used to process model the system which combines ammonia recovery and cogeneration power from SOFC utilisation. As with the other discussed Aspen Plus simulations (Chapter 4), a 'COMMON' method filter and an 'NRTL-RK' base method have been used throughout. Again, the process model generated in this body of work, associated flow rates of digestate liquor and bio-methane from Esholt WWTP (found in Chapter 3) have been used as primary inputs for the model. The process flow diagram used throughout this Chapter is illustrated in Figure 5-2.

The SOFC could not be simulated with one module or reactor in Aspen Plus due to the contrasting roles performed by the anode and cathode of the SOFC. The anode is where the thermochemical steam reforming (5-2), water-gas-shift (5-3) and ammonia decomposition (5-4) reactions occur, as well as electro-chemical hydrogen oxidation (5-5). These cannot be simulated via an equilibrium-based reactor due to selectivity of hydrogen oxidation at the triple phase boundary over any other type of oxidation. As such, an 'RStoic' reactor labelled 'ANODE' in Figure 5-2 has been used, where reactions and conversions are specified for the given temperature and pressure. The conversion efficiencies of reactions 5-2 to 5-4 were all found via analysis in an 'RGibbs' reactor at the associated temperature and pressure. The conversion of H_2 during reaction 5-5 corresponds to the model's defined utilisation factor (U_F).

$$0.5O_2 + 2e^- \rightarrow O^{2-} \quad \textbf{5-1}$$

$$CH_4 + H_2O \leftrightarrows 3H_2 + CO \quad \textbf{5-2}$$

$$CO + H_2O \leftrightarrows H_2 + CO_2 \quad \textbf{5-3}$$

$$2NH_3 \leftrightarrows 3H_2 + N_2 \quad \textbf{5-4}$$

$$H_2 + O^{2-} \rightarrow H_2O + 2e^- \quad \textbf{5-5}$$

The anode has been fed with compressed biomethane, and according to the desired S:C ratio as discussed in Chapter 4, the mixture of compressed recovered ammonia and compressed water, resulting in streams 'BM1', 'CON-LIQA' and 'H2O' respectively. These streams are combined, pre-heated to 700 °C and fed into the anode via stream 'AN-IN-2'. As with the other streams involved with the SOFC, each block passed through undergoes an assumed 3% pressure drop.

The cathode is simulated via both a 'Sep' block labelled 'CATHODE' and 'Heater' block labelled 'FC-HEAT'. 'Sep' blocks allow the user to partition components of an incoming stream. Thus, the 'CATHODE' block facilitates the simulation of oxygen ion transport across the electrolyte to the anode triple phase boundary. With the oxygen utilisation factor set at 20%, the CATHODE passes this quantity of incoming oxygen to the anode in the stream 'O'. 'FC-HEAT' acts solely as a representation of the heat transfer across the cell. This is vital because the overall exothermic nature of the reactions occurring in the anode dictate the final operating temperature of the fuel cell and the transfer of heat across the cell must be taken into account.

To ensure the heat transfer across the cell is correctly simulated, a 'Design Spec' has been set up that alters the temperature of the incoming air to the cathode (stream 'AIR3') so that heat transfer across the cell fits the energy conservation expression described in equation 5-6. Equation 5-6 details that the heat duty or enthalpy change of reactions experienced in the 'CATHODE' block is equal to the power produced ($P_{AC,net}$), heat transfer across the cell (Q_{trans}) and SOFC internal heat loss (Q_L).

$$-\Delta H_{an} = P_{AC,net} + Q_{trans} + Q_L \qquad 5\text{-}6$$

Thus, by calculating net power production via the numerical model and with the assumption that heat loss is 5%, the Design Spec dictates the temperature of the incoming air in order to alter 'Q_{trans}' accordingly.

The furnace ('FURN') is positioned after the fuel cell and receives gases from both the anode and cathode. These streams contain fuel in the form of

unconverted methane, hydrogen and carbon monoxide from the anode and unused oxygen from the cathode. It has been simulated using an RGibbs reactor, running at 90% thermal efficiency. The furnace exhaust is separated into two streams using an FSplit block (SPLIT). One stream (EXH-B1) is used to pre-heat the cathode inlet via heat exchanger 'HX4'. The other stream (EXH-A1), is used to preheat the anode inlet gases via heat exchanger 'HX5'. The stream, still containing sufficient thermal energy, is then compressed to 1.1 bar via 'CMPRS3' and used as the ammonia stripping gas.

The subsequent ammonia recovery process resembles that detailed in Chapter 4; with the stripping column followed by absorption with water in 'ABSORP' block and distillation in the 'DIST' block. The distillation bottoms stream is comprised almost entirely of water and a small amount of ammonia, making it ideal as the reagent for steam reforming in the SOFC. As such, the stream is split in two via an FSplit block (SPLIT2). The stream labelled 'H_2O' is sent to the SOFC anode at a flow rate that facilitates a feed molar steam to carbon (S:C) ratio of 2.5. The other stream labelled 'BTMS4' can be used along with 'UTILITY 2' for plant heating purposes.

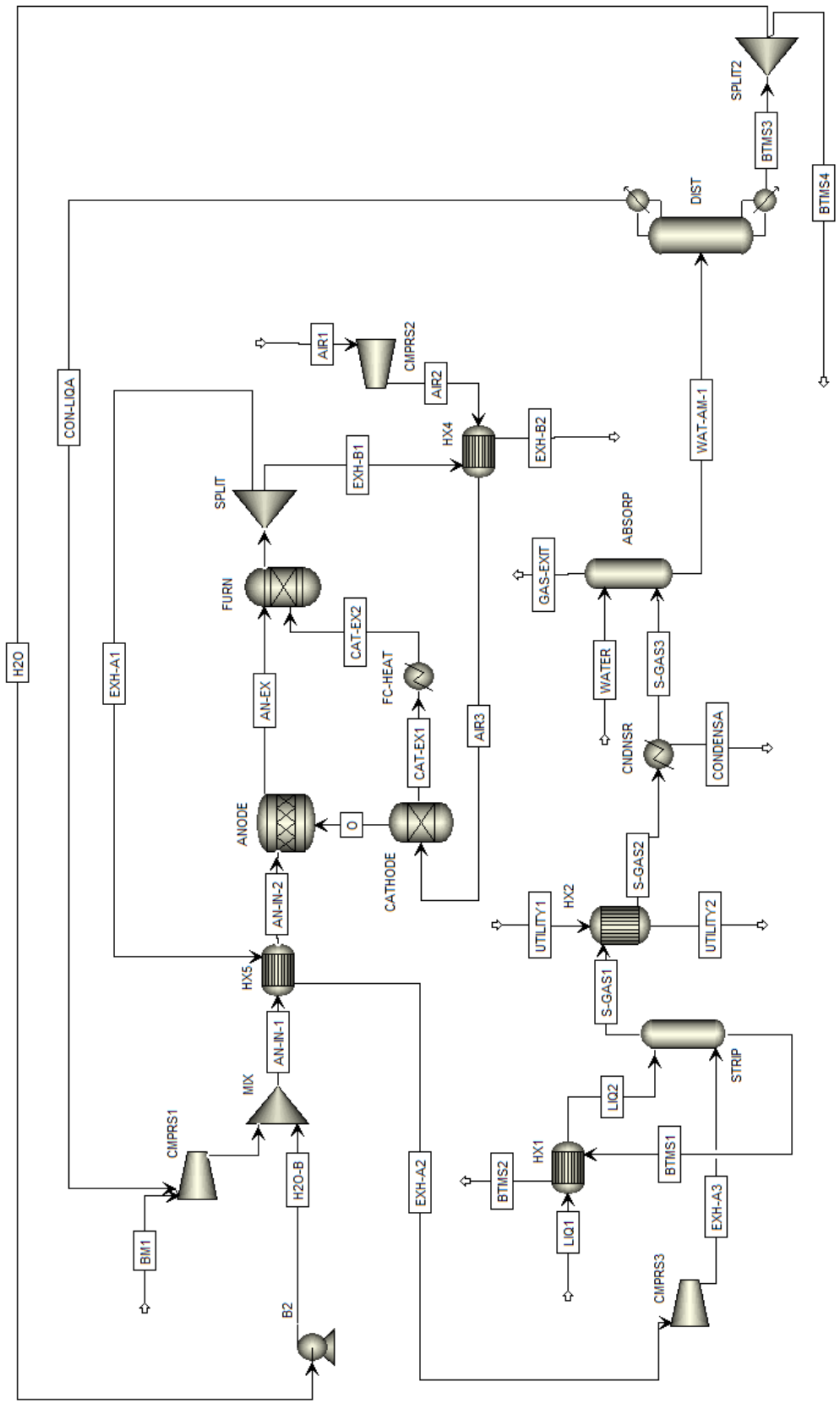

Figure 5-2. Aspen Plus process model flow sheet for SOFC system

Figure 5-2 legend

LIQ1	Digestate liquor representative inlet
LIQ2	Preheated digestate liquor
EXH-A3	Compressed exhaust gas for inlet to stripper
BTMS1	Hot liquid outlet from the stripping column
BTMS2	Cooled liquid outlet from the stripping column
S-GAS1	Gaseous outlet from the stripper containing desorbed NH_3
UTILITY1	Cool water inlet for heat recovery
UTILIT2	Hot water stream used as heating utility
S-GAS2	Cooled gaseous outlet from stripper
CONDENSA	Water condensed from the stripper's gaseous outlet
S-GAS3	Dry gaseous inlet to the absorber
WATER	Water inlet used for NH_3 absorption
GAS-EXIT	Gaseous outlet from absorber
WAT-AM-1	Liquid outlet from absorber containing reabsorbed NH_3
CON-LIQA	Gaseous distillate stream from distiller containing recovered NH_3
BTMS3	Hot liquid outlet from distiller
BTMS4	Hot liquid outlet from distiller used for heat recovery
H2O	Hot liquid outlet from distiller used for internal reforming
H2Ob	Pressurised hot liquid outlet from distiller used for internal reforming
BM1	Biomethane inlet at ambient temperature and pressure
AN-IN-1	Combined stream of biomethane and water
AN-IN-2	Pre-heated anode inlet
AN-EX	Anode exit gases
EXH-A1	Exhaust gas from the furnace diverted for stripping
EXH-A2	Cooler exhaust gas from the furnace diverted for stripping
EXH-B1	Exhaust gas used for heat recovery
EXH-B2	Cooled exhaust gas used for heat recovery

5.2.1 Biogas Clean-up System

A review of biogas purification systems has been carried out in Chapter 2 2.3.2. A clean-up system is essential in order to meet the requirement of the discussed model and ensure the biomethane contains little to no impurities. The presence of H_2S poisons the nickel-based catalyst which enables the internal reforming, thus its removal is of the utmost importance. Of all the reviewed purification technologies, high pressure water scrubbing shows the greatest promise due to its technical maturity and ability to perform both CO_2 and H_2S removal. It has been decided that the negligible (<2%) quantity of CO_2 retained in the biomethane product will have little impact on the operation of the process

model developed in Aspen Plus. A study carried out by Barbera et al. [281] evaluated the installation costs of high pressure water scrubbing technology for an AD facility with a similar biogas output to Esholt WWTP, at 5000 $Nm^3 h^{-1}$. As such, cost data and power usage have been inferred using data from this article. Barbera et al. [281] details that the power consumption during high pressure water scrubbing (HPS) is 0.27 kWh m^{-3} and a total installed cost of €2,647 per $m^3 h^{-1}$.

5.3 Numerical Modelling Method

It should be noted that the methodology for the numerical modelling has been reproduced from Grasham et al. [282]. The SOFC system modelled in this work has been based on SPGI's 120 kW tubular fuel cell, as modelled for example, in [222]. As discussed in Section 5.1, it consists of three key parts; the anode, cathode and electrolyte. Methane, ammonia and steam are fed into the anode, whilst air is fed to the cathode. Oxygen molecules diffuse from the porous cathode to the cathodic triple phase boundary (TPB) where they reduce to ionic O^{2-} (reaction 5-1), then through the electrolyte and on to the anodic TPB. At the anode side, three key reactions occur: (a) steam methane reforming 'SMR' (reaction 5-2), (b) water gas shift 'WGS' (reaction 5-3) and (c) ammonia decomposition 'NH3-DEC' (reaction 5-4). Hydrogen produced diffuses through to the anodic TPB where it reacts with oxygen ions to produce steam and electrons (equation 5-5). The electrons are externally transported via a circuit to the cathode, generating electrical power.

5.3.1 Cell Voltage

The cell voltage is calculated by subtracting the various potential voltage losses from the Nernst Potential, shown in equation 5-7:

$$CV = E - n_{act} - n_{ohm} - n_{conc} \qquad 5\text{-}7$$

Where E is the Nernst voltage potential, n_{act} represents the activation losses, n_{ohm} the ohmic losses and n_{conc} the concentration losses.

5.3.2 Nernst Voltage Potential

The Nernst Potential or the local thermodynamic reversible potential in equation 5-8 determines the theoretical cell voltage potential under given thermodynamic conditions and compositions.

$$E = E_o - \frac{RT_{cell}}{nF} \ln\left(\frac{p_{H2O}}{p_{H2} \cdot \sqrt{p_{O2}}}\right) \quad 5\text{-}8$$

where, according to [212,283]:

$$E_O = 1.2723 - (2.7645 \times 10^{-4}\ T_{cell}) \quad 5\text{-}9$$

E_o is the ideal voltage or reference voltage for hydrogen electro-chemical oxidation at ambient pressure at cell reaction sites, and a function of temperature. R is the universal gas constant, T_{cell} is absolute cell temperature, p_i is partial pressure of relevant gas species 'i' such as H_2O, H_2 or O_2, F is the Faraday constant and n is the number of electrons participating in the reaction. In this case there are two participating electrons as shown in (reaction 5-5). Electrochemical oxidation of CO at the anode is neglected due to the dominance of H_2 over CO in charge transfer kinetics. Other researchers have incorporated the electrochemical oxidation of CO in numerical models, such as Spallina et al. [284]. This was found to be valid under certain conditions by experimental work carried out by Ong et al. [285], but only where high current densities (>1.5 A cm^{-2}) and high CO concentration (>80%) conditions favoured electrochemical oxidation of CO. However, these conditions do not apply to the work presented here and so it can be said with a strong degree of certainty that

CO mostly contributes to the voltage potential via the production of H_2 during WGS, which also takes place at the anode.

5.3.3 Activation Voltage Loss

Activation polarisation (n_{act}) is obtained via manipulation of the Butler-Volmer equation 5-10.

$$j = j_0 \left[exp\left(\frac{\beta n F n_{act}}{RT_{cell}}\right) - exp\left(-(1-\beta)\frac{Zn \cdot n_{act}}{RT_{cell}}\right)\right] \quad 5\text{-}10$$

n_{act} is determined via the equations 5-11 and 5-12, extrapolated from the implicit Butler-Volmer equation and utilised by [222].

$$n_{act,a} = \frac{RT_{cell}}{\beta n F} \cdot sinh^{-1}\left(\frac{j}{2 \cdot j_{0,a}}\right), \quad 5\text{-}11$$

$$n_{act,c} = \frac{RT_{cell}}{\beta n F} \cdot sinh^{-1}\left(\frac{j}{2 \cdot j_{0,c}}\right), \quad 5\text{-}12$$

where j is the current density (A/m^2), j_0 is the exchange current density (A/m^2) and β is the apparaent charge transfer coefficient. Electrodes in the anode and cathode exchange current densities, j_{0a} and j_{0c} respectively, which are determined via 5-13 and 5-14:

$$j_{0a} = \gamma_a \times p_{H_2} \times p_{H2O} \times exp\left(\frac{-E_{aa}}{RT_{cell}}\right) \quad 5\text{-}13$$

$$j_{0c} = \gamma_c \times p_{O2}^{0.25} \times exp\left(\frac{-E_{ac}}{RT_{cell}}\right) \quad 5\text{-}14$$

γ_a and γ_c are activation barrier overpotential coefficients and E_{aa} *and* E_{ac} are activation energies for the anode and cathode respectively, and have each been

obtained from literature. γ_a and γ_c values were taken from [222] and E_{aa} *and* E_{ac} from [209].

5.3.4 Ohmic Voltage Loss

Ohmic losses result from contact resistance, the resistance of ions moving through the electrolyte and electron transfer resistance in electrodes, current collectors and interconnects. Ohmic voltage losses have been determined using equations 5-15 and 5-16:

$$n_{ohmic} = R_{ohmic} \cdot j_{cell} \cdot A_{cell} \quad \text{5-15}$$

$$R_{ohmic} = \rho_a \delta_a + \rho_c \delta_c + \rho_e \delta_e \quad \text{5-16}$$

Where A_{cell} is the area in which the current flows, R_{ohmic} is the global internal resistance which takes into account specific material resistivity (ρ) and component thickness (δ). Figures for ρ and δ have been extrapolated from [222] and subscripts *a*, *c*, and *e* denote the anode, cathode, and electrolyte respectively.

5.3.5 Concentration Voltage Loss

Concentration losses at electrodes occur due to mass transport processes or simplistically where fuel or oxygen is being used by the fuel cell faster than it can be supplied. The concentration losses at the cathode and anode have been calculated via the equations detailed in 5-17 and 5-18.

$$n_{conc,a} = -\frac{RT_{cell}}{n_a F} \cdot \ln\left(1 - \frac{j_{cell}}{j_{l,a}}\right) + \frac{RT_{cell}}{n_a F} \cdot \ln\left(1 + \frac{p_{H_2} j_{cell}}{p_{H_2O} J_{L,a}}\right) \quad \text{5-17}$$

$$n_{conc,c} = -\frac{RT}{n_c F} \cdot \ln\left(1 - \frac{j_{cell}}{j_{l,c}}\right) \quad \text{5-18}$$

$$j_{l,a} = \frac{2F \cdot p_{H_2} \cdot D_{a,eff}}{RT_{cell}} \quad 5\text{-}19$$

$$j_{l,c} = \frac{2F \cdot p_{H_2} \cdot D_{c,eff}}{RT_{cell}} \quad 5\text{-}20$$

$$D_{a,eff} = 1.3103 \times 10^{1.5} \cdot T_{cell}^{1.5} - 0.263382 \quad 5\text{-}21$$

$$D_{c,eff} = D_{O_2} \cdot \left(\frac{T_{cell}}{273}\right)^{1.5} \cdot \frac{\varepsilon}{\tau} \quad 5\text{-}22$$

where, $j_{l,a}$ and $j_{l,c}$ are the anode and cathode limiting current densities respectively and $D_{a,eff}$ and $D_{c,eff}$ are effective diffusivities of H_2 and O_2 (reactant species) for the anode and cathode respectively. D_{O_2} is the ordinary diffusivity of oxygen, ε denotes porosity of the electrode and τ its tortuosity. 5-21 has been provided by [286], whilst 5-22 has been taken from [222].

5.3.6 Efficiency Calculations

The fuel cell voltage as calculated above is based on a 120 kW SOFC using the required fixed variables from [222]. The current was calculated using the formula presented in equation 5-23. Due to the fact that each mole of oxidised hydrogen generates 2 electrons, it is derived that 0.037605 kg H_2 h^{-1} is required to generate 1 kA of current [56]. Thus, the H_2 consumption in each fuel cell was determined via equation 5-24. The fuel requirement in the cell was calculated using a fuel utilisation factor (U_F), as presented in equation 5-25. A DC/AC conversion factor of 0.97 was used to provide power outputs as AC electricity. Net power ($P_{AC,net}$) was calculated by subtracting the consumption in pumps and compressors from the AC production. $P_{AC,net}$ was used to calculate net electrical efficiency as stated in equation 5-26 by dividing net power with LHV flows from methane and ammonia. Thermal efficiency has been calculated via 5-27 and combined efficiency via equation 5-28 where Q_r is the system's thermal output.

$$I_{cell} = \frac{P_{gross}}{CV} \quad 5\text{-}23$$

$$\dot{m}_{H_2,consumed}\,(\mathrm{kg}\,h^{-1}) = I_{cell} \times 0.037605\ (\mathrm{kg}\,h^{-1}\,\mathrm{k}A^{-1}) \quad 5\text{-}24$$

$$\dot{m}_{H_2,in} = \frac{\dot{m}_{H_2,consumed}}{U_F} \quad 5\text{-}25$$

$$\eta_{elec,net} = \frac{P_{AC,net}}{\dot{m}_{CH_4} \cdot LHV_{CH4} + \dot{m}_{NH_3} \cdot LHV_{NH3}} \quad 5\text{-}26$$

$$\eta_{therm} = \frac{Q_r}{\dot{m}_{CH_4} \cdot LHV_{CH4} + \dot{m}_{NH_3} \cdot LHV_{NH3}} \quad 5\text{-}27$$

$$\eta_{CHP,net} = \frac{P_{AC,net} + Q_r}{\dot{m}_{CH_4} \cdot LHV_{CH4} + \dot{m}_{NH_3} \cdot LHV_{NH3}} \quad 5\text{-}28$$

5.3.7 Sensitivity Analysis methodology

Sensitivity analysis of fuel cell temperature, pressure and WGS efficiency has been carried out in order to better understand the impacts of such variables on system efficiency. Operating temperature +/- 90°C, pressure +1bar and WGS CO conversion efficiency +/- 50% have been analysed and compared to the reference model. The anode reaction efficiencies and therefore gas compositions have been assumed the same for temperature and pressure sensitivities but have been adjusted accordingly for WGS efficiency changes, including air flow for a constant oxygen utilisation of 20%.

5.4 Economic Analysis Methodology

The economic study in this work has been carried out under a hypothetical scenario where there is no cogeneration technology in place at Esholt WWTP or one where it is an end-of-life period for the current cogeneration equipment. This has been done to simplify the analysis of the technology's feasibility as an alternative to the current technology. Cost/benefit analysis could then be carried out to discuss how it compares to current conventional technology.

5.4.1 Equipment Costing

As in Chapter 4, Aspen Process Economic Analyzer (APEA) was used to cost the capital and installation expenditure of the majority of process equipment. However, one key piece of equipment that could not be costed using APEA is the SOFC itself. During Chapter 2, a review of literature on the capital cost of SOFCs was carried out. Within this review, the most recent and reliable reference was found to be MosayebNezhad et al. [54]. This reference was used to infer: stack CAPEX, stack replacement and clean-up system CAPEX costs given an assumed manufacturing rate of at least 5,000 units per year by the provider. The cost functions, as a factor of the fuel cell stack's power rating is shown in Table 5-1. The DC/AC inverter has been calculated using cost data presented by the Batelle Memorial Institute for the US Department of Energy [287] given a manufacturing rate of 1,000 units per year for a 250 kW system and shown in Table 5-1. It should be noted that these figures include installation costs.

Table 5-1. SOFC capital cost functions. Currency exchange rates used: £0.78/US$ and £0.9/EUR

	Function (£ kW^{-1})
Stack CAPEX	2,093
Stack replacement	434
Clean-up system CAPEX	450
DC/AC inverter	220

Due to the use of an RGibbs reactor for simulation of a post-fuel cell combustion furnace, labelled 'FURN', APEA was unable to appropriately cost its purchase price and installation expense. As such, cost data for stainless-steel direct-fired heaters from Peters et al. (pg. 692) [288] was used, detailed as a factor of heat duty. The heat duty rating of the furnace was found via analysis in Aspen Plus where the temperature change of the block was kept constant, allowing a heat duty rating to be taken. Inflation from the date of publication (2004) to 2017 was accounted for using the Bank of England's inflation calculator [289] in which the mean was found to be 3% per year. Moreover, dollars were converted to pounds using the rate stated in Table 5-1. Installation costs have

been estimated using the mean of installation costs from Aspen Plus for Equipment types over £100,000, which stands at 34%.

5.4.2 Economic Feasibility Analysis Methodology

The method of analysis for: operating labour, maintenance costs and net present value (NPV) are as described in Chapter 4. The 'product' in the case of this process implementation is the generation of heat and power. As such, the income for the facility is comprised of the financial incentives for the renewable generation of heat and power and the offset costs of the current usage. Income from financial incentives have been projected using tariffs from the UK's Contracts for Difference (CfD) scheme and the renewable heat incentive (RHI) scheme for renewable power and heat respectively. The CfD scheme works on the principle that renewable energy generators should be guaranteed a price for the power they produce to reduce the uncertainty that comes with market fluctuations [239,243]. This value is labelled the 'strike price' and is indexed according to inflation, whilst the average market price of electricity is labelled the 'reference price'. Under CfD, generators will be paid the difference between the strike price and the reference price by the government. The strike price given to generators depends on the technology type employed. The use of the IR-SOFC in the discussed process would make the operators eligible for an 'advanced conversion technology' (ACT) rate. DECC [244] stated an administrative strike price for ACTs at £140 MWh^{-1} during the first auction round. As such, this figure has been utilised in the NPV analysis as the income for electrical power generation from the SOFC, rather than the cost of abated electricity use. However, any additions or reductions to the overall plant demand have been taken into account.

The UK's non-domestic renewable heat incentive (RHI) provides financial support for thermal power production from renewable sources [290]. However, unlike the CfD scheme, there are no unique tariff rates for ACTs. As such, the RHI payments have been based on the tariff rate applied to large biogas combustion systems at 1.16p per kWh_{th}, the lowest of all RHI tariffs

[291]. It has been conservatively estimated that half of the thermal power generated from the fuel cell system will be used to fulfil the onsite WWTP heat requirements. As such, this would offset the facility's need to purchase thermal energy in the form of natural gas. The price of which has been determined via the equation 5-29:

$$E_{heat} = \frac{0.5\ Q_r \times C_{NG}}{\eta_{boiler}} \qquad 5\text{-}29$$

where, E_{heat} is the daily expenditure for heat (£ day^{-1}) Q_r is the system's thermal output (kWh$_{th}$ day^{-1}), C_{NG} is the price of natural gas (£ kWh$_{th}^{-1}$) and n_{boiler} is the standard boiler thermal efficiency at 80%.

5.4.3 Economic Sensitivity Analysis

Sensitivity analysis on the economic study has been carried out to investigate the system's feasibility under a number of different scenarios. Six scenarios have been considered, as detailed in Table 5-2. These scenarios are intended to represent viable circumstances such as the existence of current cogeneration technology or biogas purification technology, receiving a lower CfD strike price or none at all or an over/under projected capital investment cost.

Table 5-2. Economic Sensitivity: Scenario descriptions

	Description
Scenario 1	Plant has existing cogeneration technology in place. - Plant income is based on the economic difference between the current cogeneration and that of the proposed system. - CfD is not provided as the onsite electricity savings (£105 MWh^{-1}) outweighs the potential CfD income of £80 MWh^{-1} - RHI income projected to be equivalent as novel system - Biogas purification not included in projected current technology
Scenario 2	Plant has existing gas purification technology in place. - Capital investment for pressure water scrubbing system omitted. - Additional energy demand also omitted
Scenario 3	CfD strike price reduced to lowest auction price for ACTs - The lowest CfD strike at previous auction: £114 MWh^{-1}.
Scenario 4	CfD unobtainable - There are currently very few ACT schemes that have been awarded CfDs. - Income based on abated electricity use instead
Scenario 5	10% increase in total installation costs - This work has an underestimated the investment costs by 10%.
Scenario 6	10% reduction in total installation costs - This work has overestimated the investment costs by 10%.

5.5 Results and Discussion

5.5.1 Process Modelling Results

5.5.1.1 Ammonia Recovery

Table 5-3 shows the mass flow of various streams involved in the ammonia recovery process. The stripping gas (EXH-A3), originating from the post-fuel cell furnace, enters in at 566.8 °C and a total flow-rate of 230.5 kmol h^{-1}. This

stream has a marginally higher temperature and lower flow-rate than the associated stream discussed in Chapter 4's 'Combined Process'. This is highlighted by the average stripper column temperature changing from 64.3℃ to 72.1°C, as shown in Table 5-4. However, all of the stream's thermal energy requirements are internally met from the heat generated in the fuel cell and furnace.

Table 5-3. Ammonia recovery stream results (streams found in Figure 5-2)

	BTMS 1	BTM S4	CON-LIQA	EXH-A3	H2O	LIQ1	LIQ2	S-GAS1	UTILITY2	WAT-AM-1
CH_4 (kg h^{-1})	0.00	0.00	0.00	0.00	0.00	0.00	0.00	0.00	0.00	0.00
CO (kg h^{-1})	0.00	0.00	0.00	0.00	0.00	0.00	0.00	0.00	0.00	0.00
CO_2 (kg h^{-1})	7.07	0.00	79.14	265.24	0.00	0.00	0.00	258.17	0.00	79.14
H_2 (kg h^{-1})	0.00	0.00	0.00	0.00	0.00	0.00	0.00	0.00	0.00	0.00
H_2O (kg h^{-1})	26197.83	1504.98	18.75	474.45	963.09	27537.44	27537.44	1814.06	28824.45	2486.81
N_2 (kg h^{-1})	19.95	0.00	8.90	4644.03	0.00	0.00	0.00	4624.08	0.00	8.90
NH_3 (kg h^{-1})	0.03	0.01	45.64	0.00	0.01	50.27	50.27	50.25	0.00	45.66
O_2 (kg h^{-1})	10.70	0.00	5.23	1035.24	0.00	0.00	0.00	1024.55	0.00	5.23
Temperature (°C)	72.91	99.65	59.31	566.85	99.65	23.00	69.23	71.16	61.55	15.29
Pressure (bar)	1	1	1	1.1	1	1	1	1	1	1

Post-stripping, a lower flow rate of absorption water has been used, calculated via the line of best fit equation calculated during absorption sensitivity analysis in Chapter 4 (Figure 4-9). Despite, reduced flow-rates throughout the ammonia recovery process, the distillate rate of the distillation column required increasing to 6 kmol h^{-1} to meet sufficient ammonia recovery. This was due to the presence of CO_2, a volatile gas, originating from the furnace and remaining throughout the recovery process, alters the required distillate rate in the distillation column. This has the impact of increasing the heat duty (thermal energy requirements) of the distiller which increases slightly to 332.8 kW, as shown in in Table 5-4.

Table 5-4. Ammonia recovery block conditions

Block	STRIP	ABSORP	DIST
Condenser (°C)	71.2	26.1	59.3
Condenser heat duty (kW)	0	0	-3.7
Reboiler temperature (°C)	72.9	15.3	99.6
Reboiler heat duty (kW)	0	0	332.8

The conditions of the stripping column facilitate the initial recovery of 99.96% of ammonia held in the digestate liquor and a final recovery of 90.8% after distillation As shown in Table 5-3, this equates to a flow rate of 45.64 kg h^{-1}. However, the stream holding the recovered ammonia (CON-LIQA) from the top of the distillation column also contains CO_2. This occurs due to its presence in the furnace exhaust which is used as the initial stripping gas. This could have adverse consequences on the operation of the IR-SOFC. For example, it may alter the power production potential by altering reforming thermodynamics. It could also lead to greater carbon deposition in the anode of the IR-SOFC which can impact the lifetime and catalysts of the stack. As such, it may be preferential in real operation to remove the CO_2 prior to stripping or use an alternate source of stripping gas.

5.5.1.2 SOFC Operation

The mass flow composition of streams involved in the SOFC part of the process model can be found in Table 5-5. The mass flows of water and biomethane provides a molar H_2O:CH_4 (S:M) ratio of 2.5. With the inclusion of the carbon dioxide in the stream CON-LIQA, the molar H_2O:C (S:C) ratio in the SOFC is 2.3. Inside the anode of the fuel cell, 100% of the methane converts through SMR (reaction 5-2), 52% of the CO converts via the WGS (reaction 5-3) and 100% of the ammonia converts via decomposition (reaction 5-4).

Table 5-5. SOFC operation stream results

	H2O-B	BM1	CON-LIQA	AN-IN-2	AIR3	O	AN-EX	CAT-EX2	EXH-A1	EXH-B1
CH_4 (kg h^{-1})	0	343.06	0	343.06	0	0	0	0	0	0
CO (kg h^{-1})	0	0	0	0	0	0	287.51	0	0	0
CO_2 (kg h^{-1})	0	0	79.14	79.14	0	0	568.52	0	265.24	754.91
H_2 (kg h^{-1})	0	0	0	0.00	0	0	23.98	0	0	0
H_2O (kg h^{-1})	963.09	0	18.75	981.84	0	0	1610.47	0	474.45	1350.37
N_2 (kg h^{-1})	0	0	0	0	17815.17	0	46.44	17815.17	4644.03	13217.61
NH_3 (kg h^{-1})	0.01	0	45.64	45.65	0	0	0	0	0	0
O_2 (kg h^{-1})	0	0	0	0	5409.40	1074.31	0	4335.09	1035.24	2946.46
Temperature (°C)	100	23	59	700	867	867	910	910	1075	1075
Pressure (bar)	1.1	1	1	1.1	1.1	1.1	1.08	1.08	1	1

The air enters the cathode of the fuel cell at 867°C, dictated by the design specification discussed in section 5.2. With a 20% oxygen utilisation factor, 1,074.3 kg h^{-1} of oxygen ions (simulated using O_2) transports from the cathode to the anode via stream 'O'. This facilitates the electrochemical oxidation of 85% of the hydrogen generated at the anode; leaving an H_2 outlet flow from the anode of 23.98 kg h^{-1}.

This hydrogen, alongside the unconverted carbon monoxide were used as fuels in the furnace, where combustion takes place using oxygen from the cathode outlet as the oxidant. The RGibbs reactor determines the exhaust temperature via the minimisation of Gibbs free energy and considering a 10% thermal loss. The exhaust, at 1,075°C, has been split into two streams, 'EXH-A1' and 'EXH-B1', used to pre-heat the anode inlet and cathode inlet respectively. The former is also eventually utilised as the stripping gas in the stripping column.

5.5.1.3 Thermal Power Production

There are three streams that are suitable for thermal power contribution to the plant; 'EXH-B2', 'BTMS4' and 'UTILITY2'. Their temperature, composition, flow rate and power potential can be seen in Table 5-6. Note that the thermal power potential of each stream has been calculated via a 'Heater' block which cools the stream to 23°C and 1 bar conditions. The resultant heat duty of the 'Heater'

block at 90% thermal efficiency has been inferred as the thermal power contained in each stream. Table 5-6 also showcases the heat requirement of the distillation column's reboiler.

Table 5-6. Thermal power production analysis (positive values indicate net thermal power production, negative indicate consumption)

	Composition (mass %)		Flow ($kg\ h^{-1}$)	Temperature (°C)	Thermal power (kW)
EXH-B2	N_2 O_2 H_2O CO_2	72 % 16 % 7 % 4 %	18269	121.54	1133.7
BTMS4	H_2O	100 %	1505	99.64	122.9
UTILITY2	H_2O	100 %	23960	69.5	1167.8
DIST Reboiler					-332.8
Total					2,091.6

The total heat output from the process model is shown in Table 5-6 as 2,091.6 kW. Given the quantity of methane and ammonia entering the system, this provides a thermal efficiency of 42% on an LHV basis, calculated via 5-27. This is slightly less than conventional combustion-based CHP systems which classically operate at around 50% thermal efficiency. However, there is rarely a deficit of heat production at wastewater treatment plants and therefore, this reduction should not be problematic.

An issue that could arise, is the quality of heat generated. Table 5-6 shows that only one of the three heat streams generated is above 100°C. Most of the heat required at wastewater treatment plants is for anaerobic digestion and space heating. As such, this shouldn't be much of a concern. However, if high quality heat is required for processes such as thermal hydrolysis, then a form of heat upgrading should be employed.

5.5.2 Numerical Modelling Results

5.5.2.1 Model Validation

The numerical fuel cell model was first validated using data from the operation of a Siemens-Westinghouse Power Generation Inc (SPGI) 120 kW SOFC, as found in Williams et al. [292]. The coefficients used during numerical model calculations and discussed in the methodology (Section 5.3) are detailed in Table 5-7 and correspond to SPGI's 120 kW SOFC.

Table 5-7. Coefficients used in SOFC numerical model

$\mathbf{N_A}$		**2**
$\mathbf{N_C}$		4
$\mathbf{E_{AA}}$	J mol^{-1}	110,000
$\mathbf{E_{AC}}$	J mol^{-1}	120,000
$\mathbf{Y_A}$	A m^{-2}	3.6×10^{8}
$\mathbf{Y_C}$	A m^{-2}	3.5×10^{8}
$\boldsymbol{\rho_a}$	Ω m	$2.98 \times 10^{-5} \exp(1392/T)$
$\boldsymbol{\delta_a}$	m	100×10^{-6}
$\boldsymbol{\rho_c}$	Ω m	$8.114 \times 10^{-5} \exp(600/T)$
$\boldsymbol{\delta_c}$	m	2.2×10^{-3}
$\boldsymbol{\rho_e}$	Ω m	$2.94 \times 10^{-5} \exp(10{,}350/T)$
$\boldsymbol{\delta_e}$	m	40×10^{-6}
$\boldsymbol{D_{O_2}}$	m^2 s^{-1}	4.6×10^{-2}
$\boldsymbol{\varepsilon}$		0.39
$\boldsymbol{\tau}$		5.5

In order to correlate the data, a fuel inlet consisting of 89% H_2 and 11% H_2O was used with a fuel utilisation factor of 0.85 and an operating temperature of 1,000 °C. The current density was altered between 1000-4000 A m^{-2} to produce a polarisation curve with varying cell voltage. This was plotted against operational data, as shown in Figure 5-3.

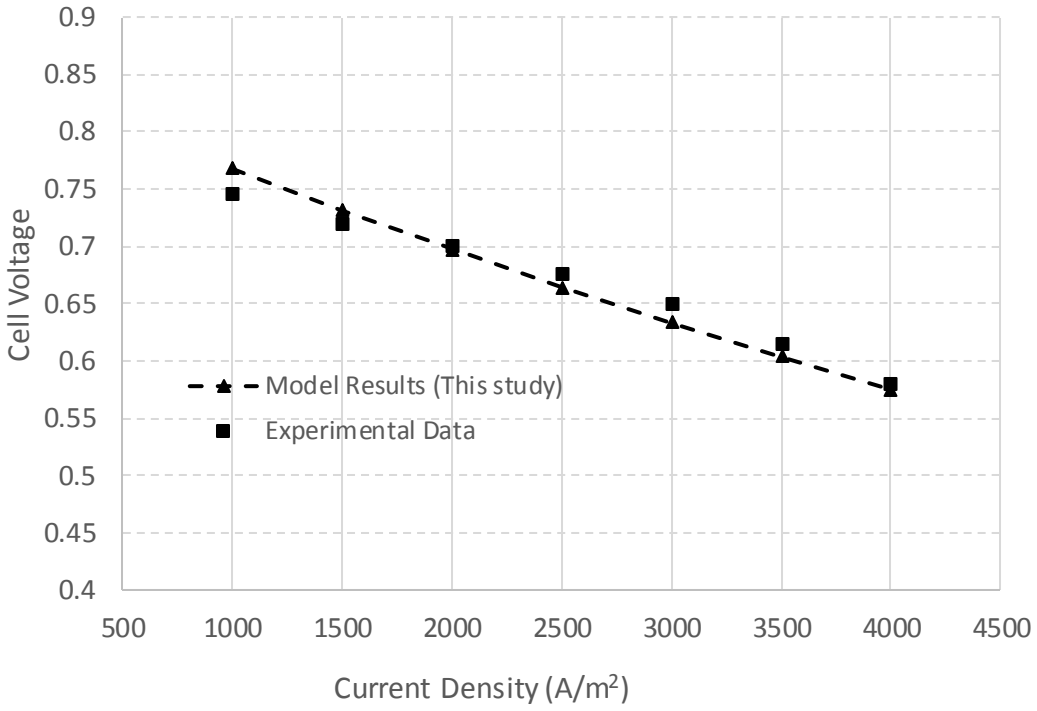

Figure 5-3. Polarisation curve showing experimental data of SPGI's 120 kW SOFC from [292] **and model data (from this work) using fuel composition 89% H_2 11% H_2O, Uf of 0.85 and operating temperature of 1000 °C.**

Figure 5-3 illustrates the close match between model and experimental data with an absolute percentage difference of just 1.15%. As such, it was concluded with a strong degree of certainty that the results from the numerical model are robust and representative of its potential real application.

5.5.2.2 Fuel Cell Operation and Power Production

It was found in the process model that the combination of the hydrogen production reactions occurring in the anode of the IR-SOFC reaction 5-2 to reaction 5-4 generate 159.85 kg of H_2 per hour. This, combined with a fuel utilisation factor of 0.85, creates a scenario where the partial pressure of hydrogen at the anode's TPB (p_{H2}) was 0.678, the partial pressure of the steam

in the anode outlet (p_{H2O}) was 0.765, and the partial pressure of oxygen in the cathode (p_{O2}) was 0.227.

The resultant operating conditions of the fuel cell numerically modelled can be found in Table 5-8. At a temperature of 910 °C and 1.08 bar, the current density was calculated at 1820 A m^{-2}. This provided a cell voltage of 0.74 V and the net production of 58,111 kWh of AC power per day. Thus, using 5-26, it was calculated the IR-SOFC would run with a net electrical efficiency ($n_{elec,net}$) of 48% on an LHV-basis. This is a 37% increase on the efficiency provided by the current CHP system employed at Esholt WWTP. This demonstrates the vast improvement on the power production capable with the use of SOFCs at WWTPs.

Table 5-8. SOFC operating conditions and results

T_{cell}	°C	910
P_{cell}	Bar	1.08
Fuel Utilisation		0.85
Air Utilisation		0.2
Current Density	A m^{-2}	1820
Anode Inlet Temp	°C	700
Cathode Inlet Temp	°C	867
Cell Voltage	V	0.74
$\eta_{elec,net}$	%	48

The main form of voltage losses occurred from activation polarisation at just over 0.1 V. This is due to the relatively low current density employed by the fuel cell which slows the rate of electrochemical reactions and the electrode surface becomes less active [293]. Concentration losses were found to be just under 0.06 V. Ohmic losses proved to be the lowest form of voltage loss at just 0.001

V which is to be expected with the low current density utilised, where ohmic polarisation is directly proportional to current density.

With 100% of ammonia cracking under reaction 5-4 the latter provides the generation of a further 8.1 kg h^{-1} of hydrogen. This equates to 5.07% of the total and corresponds to 2.95 MWh of electricity generated each day at the facility via ammonia cracking at the anode's TPB. Although the decomposition of ammonia has an impact on the molar production of H_2 and therefore overall power output from the stack, its effect on cell voltage is limited because the fractional molar concentration of H_2 does not alter significantly. For every 3 moles of H_2 generated during ammonia decomposition, 1 mole of N_2 is also generated. This helps to regulate the overall molar concentration of H_2 at the anode, which increases by just 0.8% when ammonia decomposition is taken into account. This, in turn, has a similar minimal impact on the concentration of H_2O produced by the electrochemical oxidation of H_2. As such, the introduction of recovered ammonia has a negligible effect on cell voltage and gross efficiency, but does impact significantly on the total power production of the process.

5.5.2.3 Sensitivity Analysis at the SOFC

Various sensitivity analysis was carried out to investigate the impact if a number of variables were changed. The percentage impact on net electrical, thermal and CHP efficiency of each change in variable can be seen in Figure 5-4. Firstly, the conversion of carbon monoxide via the WGS reaction was increased and decreased by 50% of the original value to firstly understand the role the WGS reaction has on the fuel cell's operation and secondly to investigate what would occur if the equilibrium was not facilitated by the fuel cell's catalyst at the anode's TPB. When the WGS reaction efficiency is increased, as is the hydrogen generated in the fuel cell. This boosts the electrochemical oxidation of hydrogen via reaction 5-5 and therefore current generation, hence, the 5.17% increase in net electrical power generation. However, the increase in hydrogen production means more air is required for pre-heating in 'HX4' and

reducing the availability of heat for export downstream thus lowering the thermal efficiency by 4.31 %. Importantly, the opposite occurs if the WGS carbon monoxide conversion efficiency is decreased with a decrease in net electrical efficiency of 5.18% and increase in thermal efficiency of 4.38%.

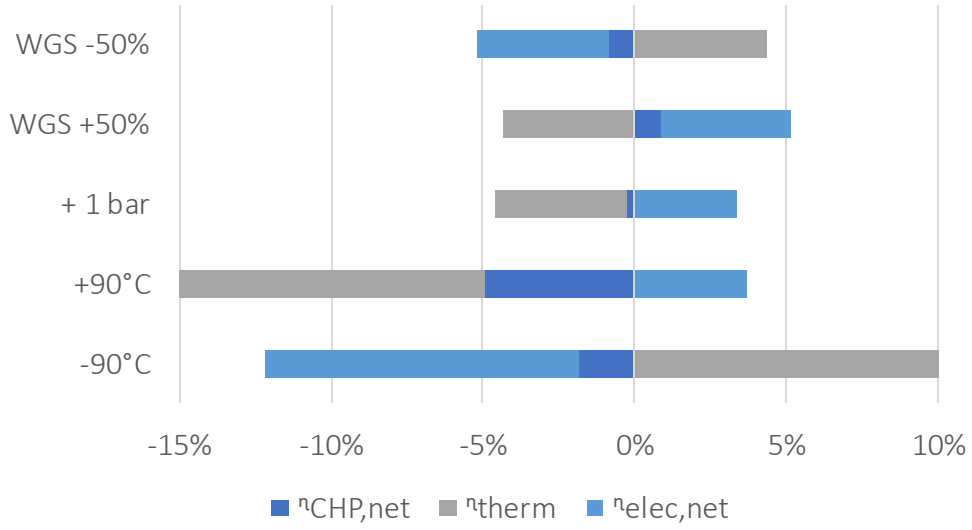

Figure 5-4. Relative percentage impact on thermal (n_{therm}), net electrical ($n_{elect,net}$) and combined efficiency ($n_{CHP,net}$).

With the SOFC operating at just over atmospheric pressure, the sensitivity carried out entailed just increasing it. When the operating pressure is increased by 1 bar, the cell voltage increases by 17.8%, with the partial pressure of contributing reactants and products having such an important impact on the cell voltage. It is important to note that the net electrical efficiency ($n_{elec,net}$) accounts for the power required to compress the streams fed in to the SOFC. Thus, Figure 5-4 showcases that the increase in power from the SOFC outweighs the power required for compression, resulting in a 3.4% increase in net electrical efficiency. However, this increased current production means the fuel cell inlets require more heat to make up for reduction in internal thermal transport. Resultantly, the thermal efficiency of the system reduces by 4.6%, contributing to a small reduction in CHP efficiency of 0.2%.

Reducing the operating temperature by 90°C had the largest impact on net electrical efficiency of all of the altered variables analysed with a reduction of 12.2%. Dropping the temperature causes a drop in the cell voltage and therefore current and net electrical power. The reduced operating temperature means considerably less heat is lost in the cell and less heat needs to be exchanged with the fuel cell inlets. The result of this is a 10.75% increase in the thermal efficiency of the system. The opposite mechanisms occur when cell operating temperature is increased by 90 °C but with a less pronounced impact on electrical efficiency which increases by 3.72% and a more pronounced impact on thermal efficiency which reduced by 15.38%.

5.5.3 Wastewater Treatment Plant Impact: Energy and GHG Emissions

Using Esholt WWTP as a representative case study, the modelled process has the potential to divert 1,095 kg of NH_3 each day. The resultant impact on GHG emissions of doing so can be seen in Table 5-9. In Chapter 3, it was discussed the estimated N_2O emission factor from Esholt lie at 0.012 kg N_2O N/ kg $TN_{influent}$. As such, this diversion of ammonia would decrease nitrous oxide emissions by 10.81 kg per day. This corresponds to equivalent CO_2 savings (CO_2e) of 3,222 kg per day based on a GWP (global warming potential) for N_2O that is 298 times that of CO_2 over a 100 year period. The overall impact of this would be a 19% reduction in N_2O emissions and almost an 8% reduction in total greenhouse gas emissions due to the diversion of ammonia contained in the facility's digestate liquor. It should be noted that studies, such as Kampschreur et al [17], have found vast variation in nitrous oxide emission factors and real emission reductions could be far more or far less pronounced as estimated.

Table 5-9. Table of GHG emission impacts due to ammonia diversion

NH_3 Diversion (kg day^{-1})	1,095.49
N_2O Reduction (kg day^{-1})	10.81
CO_2e Reduction (kg day^{-1})	3,221.91
% of current N_2O	19.14
% of current total GHGs	7.74

As discussed in Chapter 3, the current electricity demand at Esholt WWTP stands at 60 MWh per day. 4.57 kWh of electricity is spent pumping air to oxidise each kg of nitrogen in the facility's activated sludge process (ASP) [57]. As such, the diversion of just over a tonne of ammonia each day reduces the plant's energy demand by a daily 4.12 MWh or just under 7% of its total. The modelling from this chapter showed that the plant could also transition from generating 40 MWh to 58.1 MWh on a daily basis. The pressure water scrubbing unit that has been proposed for implementation at the facility demands 0.27 kWh per Nm^3 of biogas. This equates to 5.24 MWh of electricity each day for Esholt WWTP. As such the facility would transform from requiring 20 MWh of grid electricity each day to just 3 MWh. The ability to attain this transformation would be a colossal achievement for Esholt WWTP or other facilities of a similar size and nature and should not be understated.

The 17 MWh a day of omitted grid electricity further reduces the plant's carbon footprint with the lifecycle emissions of GHGs associated with the UK's electricity grid. The carbon intensity of the electrical grid stands at 107 gCO2e per kWh [294]. Thus, for Esholt WWTP, the reduced electricity consumption would save a total of 1,819 kg CO_2e each day. Combined with the GHG emission savings experienced from the diversion of ammonia, process implementation of the ammonia recovery/SOFC combined processes would reduce Esholt's GHG footprint by a total of 5,041 kg CO_2e per day. This equates to 12.12% of the total or 2.45 kg per year for each person serviced by the facility.

5.5.4 Economic Analysis

5.5.4.1 Equipment Cost

A summary of the equipment and total installation costs can be found in Table 5-10. With the 2.66 MW power requirement of the fuel cell, the total installed cost of the SOFC, including replacement costs and clean-up system, has been found to be £7.9 million. This equates to £2,970 per kW, which is considerably more than the total installation costs for a combined-cycle gas turbine system, as suggested by Leigh Fisher [295] at roughly £500 per kW. The fuel cell represents the greatest capital cost by a considerable distance, comprising of 56% of the total capital investment.

Table 5-10. Equipment cost for combined ammonia-SOFC process

Name	Equipment Cost [£]	Installed Cost [£]
SOFC		5,567,548.18
Biogas purification		1,926,179.71
Stack replacement costs		1,154,474.87
Stack clean-up system		1,197,036.16
CMPRS2	855,426.00	1,028,508.00
DC/AC converter		585,217.68
CMPRS3	416,286.00	537,030.00
CMPRS1	360,594.00	452,634.00
STRIP-tower	167,934.00	346,476.00
HX2	137,046.00	264,264.00
FURN	170,773.93	229,193.17
HX1	97,110.00	201,552.00
ABSORP-tower	59,358.00	178,464.00
DIST-tower	39,780.00	149,448.00
CNDNSR	12,558.00	84,942.00
DIST-cond acc	12,324.00	76,050.00
THERMOUT	10,062.00	64,038.00
DIST-reb	9,438.00	54,600.00
B2	3,198.00	22,074.00
DIST-reflux pump	3,588.00	21,606.00
HX4	7,058.22	9,472.73
HX5	1,764.36	2,367.92
		14,153,176.42

At a total installed cost of just over £1.9 million, the biogas purification system provides the second highest capital expense for the facility. This equates to

13.6% of the total installed cost. For various reasons, process model equipment blocks FURN, HX4, HX5 and CNDNSR could not be costed using APEA. Accordingly, the furnace price was determined using data from Peters et al. [288] estimating a capital cost of £137,046 after inflation adjustments from 2004 levels. Similarly the heat exchangers HX4 and HX5 were costed using Peters et al. [288]. The installation costs of these blocks was estimated at 34% of the capital, as found via the mean of the blocks assessed via APEA. The condenser (CNDNSR) had been simulated using a heater block with a condensate stream, which APEA could not provide cost data for. As such, a 'Flash2' block was set up with the same flow rates to indicate the real cost of the condenser; providing the figure displayed in Table 5-10.

5.5.4.2 Operational Costs

The combined ammonia recovery and SOFC process model consists of 19 different processing steps. There is an addition of 10 processing steps within the biogas purification process; meaning the entire process would entail 29 stages. The labour requirement was calculated as in Equation 4-1 (Chapter 4), providing a figure of the requirement of 16 full time personnel to operate the equipment. This results in a first year wage expenditure of £607,500, rising under the expected salary inflation of 2.99%.

Annual maintenance costs are proposed as 3% of the capital expenditure, as stipulated in Chapter 4, facilitating a first year maintenance cost of £424,595. The caustic requirements to appropriately basify the digestate liquor are as proposed in Chapter 4, with a first year expenditure of £737. With the inclusion of the biogas purification system, the entire electricity usage of the WWTP increases by 1.11 MWh per day. At a purchasing cost of 10.55 p kWh^{-1}, this equates to additional maintenance cost of £42,769 in the first year. In total, this amounts to an initial annual operational cost of £1,075,602, rising by 2.87% per year under inflation.

5.5.4.3 Net Present Value for conventional cogeneration system replacement

Table 5-11 details data generated during NPV analysis carried out for the implementation of the discussed process at Esholt WWTP. The 'income' is comprised of three factors: the revenue from the strike price dictated in a contract for difference scheme (CfD), the abated thermal energy costs and RHI revenue. This totals to £3,445,380 in the first year with CfD comprising roughly 86% of that, heat cost abatement 8% and RHI 6%.

Table 5-11. Net Present Value analysis for SOFC process integration at Esholt WWTP assuming a 10% discount factor

	Annual Expense (£)	Annual Income (£)	Real Net Cash Flow (£)	Net Present Value (£)
Yr 0	14,153,176		-14,153,176	-14,153,176
Yr 1	1,075,602	3,445,380	-11,783,398	-11,998,833
Yr 2	1,063,207	3,544,289	-9,302,316	-9,948,352
Yr 3	1,094,475	3,646,037	-6,750,754	-8,031,325
Yr 4	1,126,664	3,750,707	-4,126,711	-6,239,069
Yr 5	1,159,799	3,858,381	-1,428,129	-4,563,462
Yr 6	1,193,909	3,969,146	1,347,108	-2,996,913
Yr 7	1,229,022	4,083,091	4,201,176	-1,532,324
Yr 8	1,265,169	4,200,307	7,136,314	-163,061
Yr 9	1,302,379	4,320,888	10,154,823	1,117,082
Yr 10	1,340,685	4,444,931	13,259,069	2,313,903
Yr 11	1,380,117	4,572,535	16,451,487	3,432,826
Yr 12	1,420,709	4,703,802	19,734,579	4,478,920
Yr 13	1,462,496	4,838,837	23,110,920	5,456,926
Yr 14	1,505,513	4,977,749	26,583,156	6,371,274
Yr 15	1,549,795	5,120,648	30,154,010	7,226,108
Yr 16	1,595,380	5,267,650	33,826,280	8,025,301
Yr 17	1,642,306	5,418,872	37,602,846	8,772,475
Yr 18	1,690,614	5,574,436	41,486,668	9,471,014
Yr 19	1,740,343	5,734,465	45,480,791	10,124,085
Yr 20	1,791,535	5,899,088	49,588,344	10,734,647

The 'Real Net Cashflow' shown in Table 5-11 describes the cumulative annual income minus the cumulative annual expense. It can be used to detail how long

the initial capital investment is returned in real terms. This has also been visually represented by the dotted line in Figure 5-5 and shows that the initial capital investment would be paid back after 5.5 years. Over the 20 year lifetime of the plant, a profit of £49.5 million can be expected in real terms.

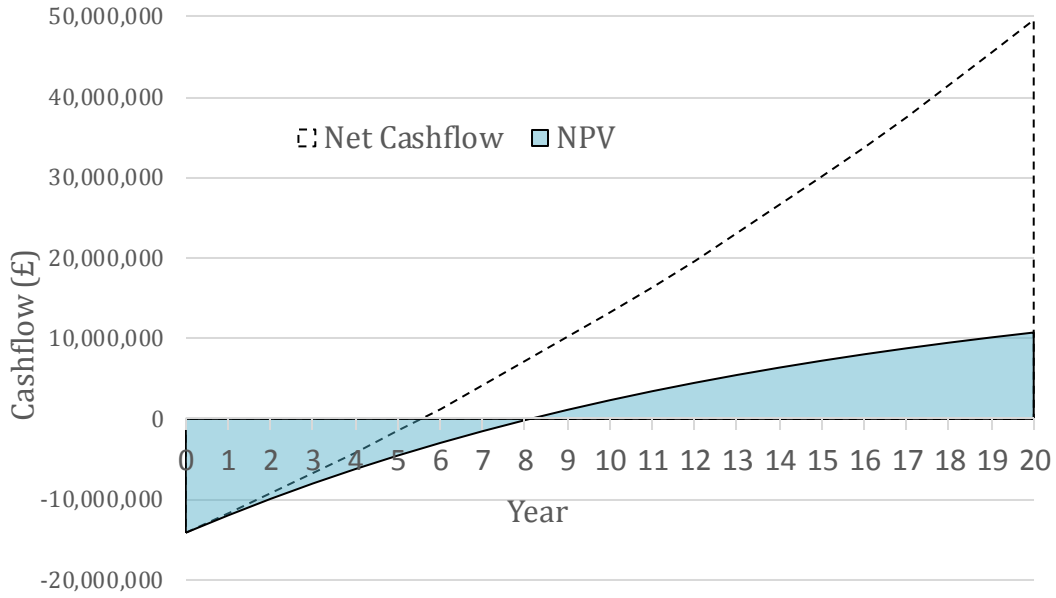

Figure 5-5. Diagram of Net Cashflow and NPV with a 10% discount factor

Table 5-11 and Figure 5-5 also detail the annual NPV derived during analysis. With a 10% discount factor, the system would achieve a positive NPV after a little over 8 years. This means that just after 8 years, the investors will have achieved an average of 10% annual return on their investment. Over the 20 year lifetime of the discussed plant, the operators will have received £10.7 million more than the required 10% annual return. This indicates that at the end of lifetime for their current cogeneration system, the implementation of this process is financially worthwhile.

5.5.4.4 Sensitivity Analysis

The net cashflow and NPV results for each simulated scenario have been illustrated in Figure 5-6. The graph for Scenario 1 clearly shows that if a wastewater treatment facility, with the properties of Esholt WWTP, already has cogeneration technology in place, then the introduction of the combined ammonia recovery and SOFC cogeneration would not be financially viable. In Scenario 1, neither the net cashflow nor NPV turns a profit over the plant's 20 year lifetime. Thus, it can be said with a degree of certainty that this technology should only be introduced to a wastewater treatment facility if at the end of life period of any current cogeneration process or for a new-build site. However, it should be recognised that this analysis did not account for any revenue generated by the sale of current equipment. If a considerable amount of funds could be generated in order to offset the initial capital investment, then its feasibility may look more viable.

Occasionally, biogas purification technology is already in place at wastewater treatment plants, in order to make combustion-based cogeneration a more efficient and cleaner process or bio-methane production for the purpose of grid injection. As such, if the discussed process was introduced without the need to implement biogas purification technology, there would be a significant reduction in the capital and operating expenditure. The results, as shown in the Scenario 2 graph of Figure 5-6, indicate that the potential profitability of process introduction can significantly improve under this scenario. With a pay-back period reduction of a year and a positive NPV after just 6.5 compared to the original 8 years.

During the most recent round of CfD allocation, the lowest strike price awarded to an ACT system was £114 MWh^{-1}. As such, Scenario 3 demonstrates what impact this strike price would have on the process' profitability compared to the referenced strike price of £140 MWh^{-1}. As demonstrated in the scenario 3 diagram of Figure 5-6, there would be a significant reduction in the process' profitability under these circumstances. For example, the time taken to achieve a positive NPV increases by roughly four years to the twelfth year of operation. The end of life profit also reduces by almost £15 million to £35 million.

Nevertheless, even under this scenario an argument could still be made that is financially worthwhile but the investors would require patience before receiving their demands.

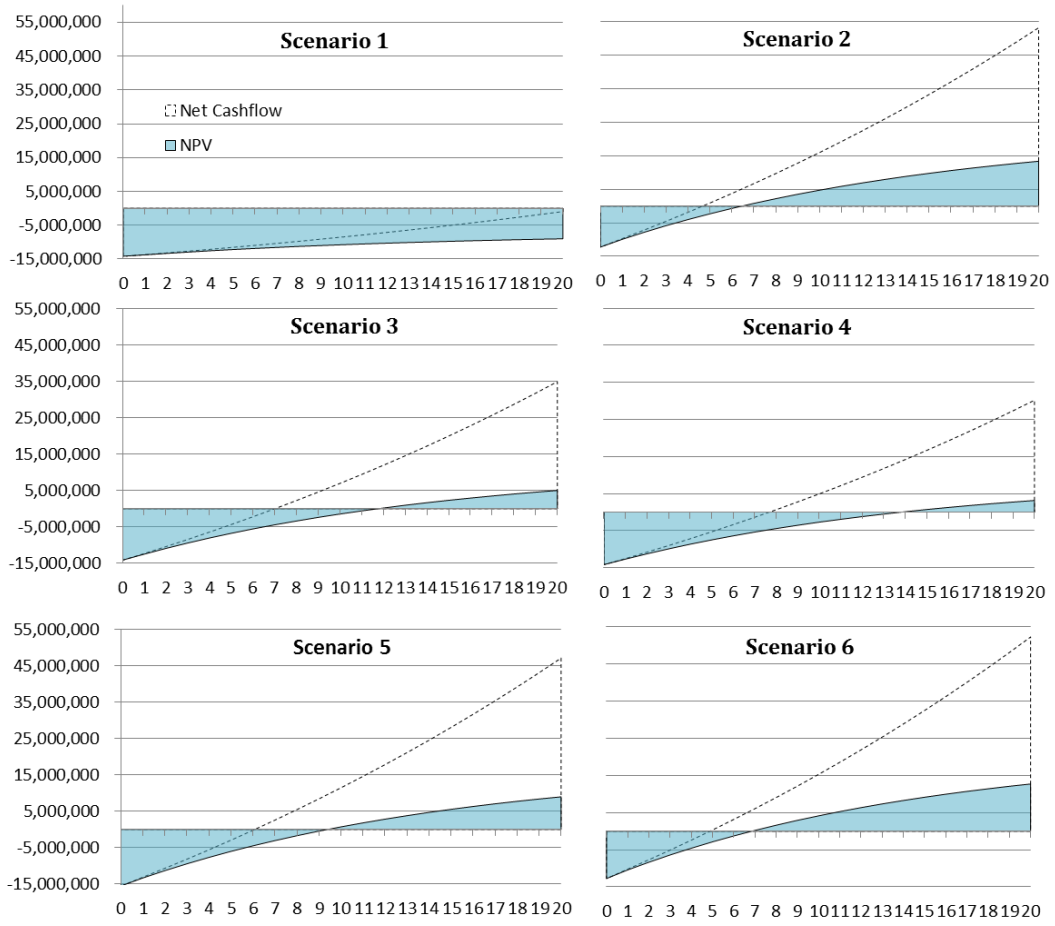

Figure 5-6. Sensitivity analysis: combined cash-flow and NPV diagrams. X-axis in number of years and Y-axis in £. Scenario 1: existing cogeneration technology; Scenario 2: existing biogas purification technology; Scenario 3: CfD contract lowered to £114 MWh^{-1}; Scenario 4: failure to obtain CfD; Scenario 5: 10 % increase in capital expense; Scenario 6 10% decrease in capital expense.

In the case that the operators were unable to secure CfD funding (Scenario 4), then the power-based income for process implementation would instead be the offset purchasing of electricity (as it is with the heat production). At 10.55p per kWh, this would reduce income by £732,000 in the first year. This has the second greatest impact on the financial forecast of all investigated scenarios. NPV does turn positive, but only after 14 years. This limits the attractiveness of

investing in the project as market uncertainties could turn financers away. Under this scenario, real profits are still £30 million which equates to £3.2 million above the required average 10% annual return over the 20 year period.

Scenarios 5 and 6 speculate what the financial implications would be if the capital investment projections were under or over-estimated by 10% (£1.4 million) respectively. As shown in Figure 5-6, the system is still economically viable if investment costs are boosted. However, NPV takes 1.5 years longer to turn positive and real payback takes 0.5 years longer. The fact, that the financial forecast isn't overly sensitive to a 10% rise in total investment costs should provide investors with a sense of security. Alternatively, if the investment figure falls by 10%, which is a plausible scenario in which R&D in SOFCs causes such a reduction, the financial attractiveness of process implementation is even greater. Scenario 6 in Figure 5-6 illustrates that the outlook is only slightly bettered by Scenario 2 of all investigated options under the sensitivity analysis.

5.6 Constraints, Considerations and Further Work

The study carried out in this Chapter has been carried out under the assumption that there is a continuous flow of biogas/biomethane. However, in reality there are temporal variations in quantities of biogas generated and concentrations of methane contained in biogas and ammonia contained in digestate from AD. There are also periods of down-time where repairs or cleaning must occur and with any novel process there is likely to be a settling-in period where operators become accustomed with the system. This hasn't been accounted for in the process model, numerical model or financial analysis. It is suggested that flows of biomethane are controlled as much as possible. This would require an effective storage unit with enough buffering capability to handle fluctuating flows. It is projected that the system would still be financially sound with this addition due to the encouraging nature of economic analysis shown in Figure 5-5. However, analysis with dynamic modelling is suggested in any further work.

Due to the fledgling nature of SOFC technology, it is suggested that similar cogeneration efficiencies will be achievable with lower temperature SOFCs in the future. This could significantly reduce the capital investment expenditure of process implementation and remove some uncertainty that is inevitable when making such a considerable investment. When the technology readiness level of intermediate temperature SOFCs becomes high enough, it is suggested that the numerical modelling is repeated with updated data inputs.

It is also worth noting that this work has focussed on implementation at one particular wastewater treatment facility, serving a sizeable population. Due to the impact of 'economies of scale' theory, process implementation will be far more viable at larger plants than smaller ones. As such, individual assessments need to be carried out in the future for alternative plants to assess the feasibility. For example, the same number of people will be required to run the discussed plant regardless of scale. This would influence the operational expenses considerably more than the plant's income and would become far less feasible.

Furthermore, the GHG emission analysis carried out did not include emissions associated with the construction or embedded material emissions associated with process implementation.. As such, it is recommended that future studies incorporate a thorough lifecycle analysis which incorporates the production and installation of materials associated with the discussed process.

5.7 Conclusions

In this Chapter, a number of analyses have been synthesised to facilitate a thorough investigation into the feasibility and impact of implementing a combined ammonia recovery and biomethane-ammonia fuelled SOFC process at Esholt WWTP in West Yorkshire. The process modelling carried out in Aspen Plus, demonstrated the ability to recover 90% of the ammonia initially contained in the digestate liquor. This ammonia, diverted from the traditional treatment process, was shown to contribute roughly 5% of the total energy production and abates the GHG emissions equivalent to 8% of the WWTP's

total. Combined with the saving of GHG emissions associated with the use of UK grid electricity, implementation of the process is expected to reduce the facility's GHG emissions by 12.12% of its total or 2.45 kg per year for each person serviced by the facility.

The combined ammonia recovery and biomethane-ammonia fuelled SOFC process generates a net production of 58.1 MWh of electricity per day. The diversion of ammonia was found to reduce plant energy demand by 4.12 MWh each day. However, this is eclipsed by the energy demand for biogas purification required to produce biomethane at 5.24 MWh. As such the total plant energy consumption under this process implementation would be 61.1 MWh per day. However, the daily net energy consumption would be just 3 MWh compared to the current 20 MWh.

An economic assessment has been carried out for the implementation of the process at Esholt wastewater treatment plant, under the assumption that no current cogeneration technology is in place. Net present value analysis was performed in order to assess the potential financial attractiveness of process implementation. The system introduction would require a significant initial investment of £14.15 million. However, an initial annual 'income' of £3,445,380 (based on energy expense savings and the renewable incentive schemes of Contracts for Difference and Renewable Heat Incentive) dwarfs any operational expenses and allows for a payback on investment in 5.5 years. Additionally, a positive NPV is achieved after 8 years of operation with a discount rate of 10%.

6 Hydrogen Production Process

6.1 Introduction and background

This chapter focusses on the applicability of utilising biomethane alongside the ammonia recovered via methods discussed in Chapter 4, for the production of H_2. A robust process model has been developed in Aspen Plus to provide mass flow, heat and power analysis. An economic model has also been developed to explore the financial viability of process implementation. Thorough sensitivity analysis has also been carried out to optimise the conditions and illustrate the influence of uncertainty. Esholt WWTP has again been used as a reference plant to give the study context and facilitate comparisons with the process showcased in Chapter 6. There are three key catalytic reactions that occur in the system that will generate H_2; steam methane reforming (SMR), water-gas shift (WGS) and ammonia decomposition.

6.1.1 Steam Methane Reforming

The SMR reaction is described in reaction 6-1. It is a highly endothermic reversible equilibrium reaction, shown by its positive reaction enthalpy change at 298 K (ΔH_{298}). The endothermicity means higher temperatures help shift the reaction to the right, favouring H_2 and CO production. Reaction 6-1 also details how the product contains 4 moles of gas, compared to 2 moles on the reactant side. As such, the forward reaction is also favoured by low pressure conditions.

$$CH_4 + H_2O \leftrightarrows 3H_2 + CO \qquad \Delta H_{298} = +206 \text{ kJ } mol_{CH_4}{}^{-1} \qquad 6\text{-}1$$

Ideally this reaction would be facilitated in a high temperature and low pressure reactor. However, often in industry pressures of 20-30 bar are used to allow the gas to pass over packed-bed reactors and the use of long, thin, tubular reformers (12m, L/D ~100). The reformers, often in their hundreds, help make the plant economically viable due to the large scale production and the smaller piping sizes, reactor volumes and compact fluid movers afforded by the higher pressures [296]. The reformer is typically operated between 800-1000°C in which industry standard nickel-based catalysts can perform unhindered [297]. The use of these temperatures and pressures corresponds to incomplete conversions by steam reforming (60-70%), the unreacted fuel later re-used after separation from the H_2 product as furnace fuel to meet the heat demand of reaction 6-1.

Another important factor to consider when steam reforming methane is the quantity of steam used relative to the fuel feed. This is classically characterised by a feed molar steam : carbon ratio (S:C). In industry, ratios between 2-4 are used, despite a stoichiometric requirement of 1. This is carried out for three key reasons. Firstly, to keep the SMR reaction equilibrium towards the product side of reaction 6-1 under the working of Le Chatelier's principle. As such, a higher S:C enables increased equilibrium methane conversion and, therefore, production of hydrogen as illustrated in Figure 6-1.

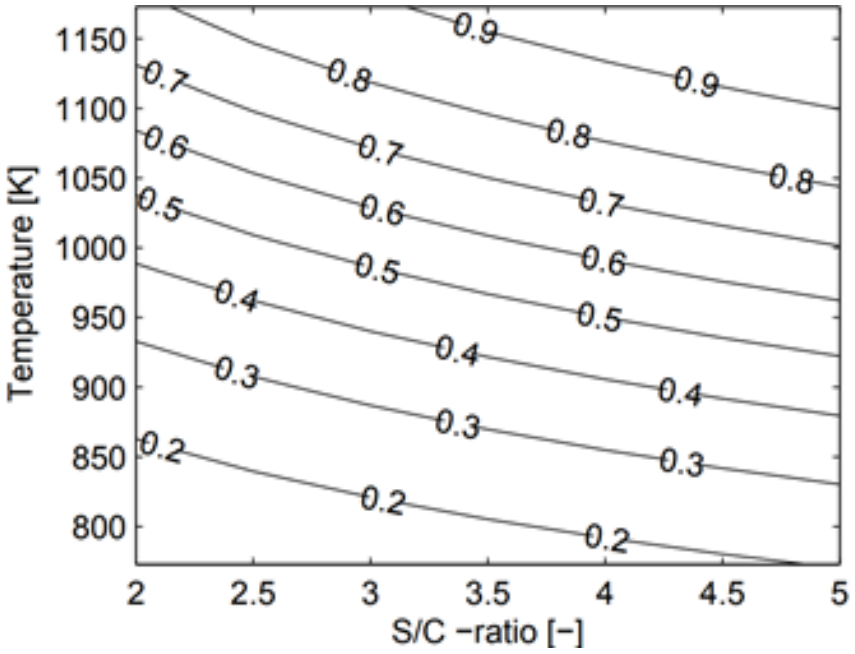

Figure 6-1. Effect of S:C and temperature on equilibrium methane conversions under SMR at 20 bar [136]**.**

Figure 6-1 shows that under 20 bar conditions and a S:C ratio of 5, a temperature of only 1000 K (727 °C)is required to achieve 70% methane conversion. However, at the lower S:C of 2 it requires a temperature of over 1125 K (852 °C) in order to reach the same conversion, thus highlighting that the choice of S:C can be significantly influential on the final yield of hydrogen.

Secondly, the S:C also effects the amount of carbon deposited on the catalyst in real operation. Carbon deposition can occur via three main reactions: thermal decomposition of methane (6-2), the bourdouard reaction (6-3) and the reverse carbon-steam gasification (6-4). By increasing the S:C there will be an equilibrium preference for the destruction of CH_4 and CO from the SMR (6-1) and WGS (6-5) reactions rather than decomposition via reactions 6-2 and 6-3 respectively. Furthermore, if carbon is deposited, a higher S:C will enable in its removal via shifting the equilibrium of reaction 6-4 to the left. Thirdly, a higher S:C allows for additional H_2 production via an equilibrium preference for the WGS reaction (6-5) which will be discussed further in section 6.1.2.

$$CH_4 \leftrightarrows C + H_2 \qquad \Delta H_{298} = 75 \text{ kJ } mol_{CH_4}{}^{-1} \qquad \textbf{6-2}$$

$$2CO \leftrightarrows C + CO_2 \qquad \Delta H_{298} = -172 \text{ kJ } mol_{CO}{}^{-1} \qquad \textbf{6-3}$$

$$CO + H_2 \leftrightarrows C + H_2O \qquad \Delta H_{298} = -41 \text{ kJ } mol_{CO}{}^{-1} \qquad \textbf{6-4}$$

Although there is a clear thermodynamic preference for higher S:C, limitations exist from a thermal efficiency point of view. If endothermic SMR reactions are occurring at 800-1000 °C, a lot of energy and heat exchanger infrastructure is required to get the feedstocks up to temperature and pressure. As such, systems utilising greater S:C will need to spend more energy and money to achieve adequate reforming. Thus, a balance must be struck between thermodynamic and energetic performance of the process for optimal plant thermal efficiency.

6.1.2 Water-gas Shift

In contrast to the SMR reaction, the WGS is exothermic with a reaction enthalpy change of -41 kJ $mol_{CO}{}^{-1}$ at 298 K. As such, to maintain a forward reaction, lower temperatures are preferred compared to SMR. This is why separate reactors are used, manipulating the operating conditions to provide a thermodynamic preference in each reactor.

$$CO + H_2O \leftrightarrows H_2 + CO_2 \qquad \Delta H_{298} = -41 \text{ kJ } mol_{CO}{}^{-1} \qquad 6\text{-}5$$

Typically, two reactors are used to achieve this. Firstly a high temperature catalytic reactor (HT) reactor whereby the feedstock enters between 350°C and 500°C [298]. The exothermic nature of the WGS reaction and the isothermal operation of the reactor creates a boost in the temperature which limits the production of products in reaction 6-5. The syngas is then cooled before entering a low temperature (LT) catalytic reactor between 150°C and 250°C [298] and maximising H_2 generation.

6.1.3 Ammonia Decomposition

The decomposition of ammonia can be seen in reaction 6-6 and is the reverse of the Haber-Bosch ammonia synthesis reaction. The reaction is slightly endothermic and the 2:4 molar ratio between reactants and products means the forward reaction also prefers lower pressures.

$$2NH_3 \leftrightarrows 3H_2 + N_2 \qquad \Delta H_{298K} = +92 \text{ kJ } mol_{NH_3}{}^{-1} \qquad 6\text{-}6$$

A study by Yin et al. [154] showed that at 1 atm and 400 °C the equilibrium will bring about a 99.1% conversion of ammonia. As such, SMR temperatures between 800-1000 °C should bring about a high ammonia conversion. Ammonia is rarely used as a hydrogen production feedstock. However, the narrative has started changing in recent years with the feasibility of utilising ammonia as a hydrogen storage medium with low associated carbon emissions upon release of its H_2 [153].

6.1.4 Economics of thermochemical hydrogen production

NERL have developed an economic model for hydrogen production via SMR technology for a H_2 production rate of 1,500 kg day^{-1} [299]. They have calculated a total installed cost of $1,238,987 for the process in 2016 prices. This includes $265,000 for the furnace and reformer, $216,000 for the WGS reactors and $86,000 for the PSA unit. The NERL model also incorporates a costing methodology for a refuelling station with capital, fixed and operating calculations. The process includes units for compression, storage and dispensing. For the 1,500 kg day^{-1} reference model, a total installed capital cost of $4,495,132 was calculated. Labour, operations and maintenance costs were found to be $0.54 per kg of H_2 processed. Electricity use was found to be 2,230 MWh per year.

Moscowiz et al. [300] state that the current production cost of H_2 production via natural gas reforming is between €1 and €2 kg^{-1}. They also state that the

cost of H_2 produced by electrolysis is €3.50- 5 kg^{-1}. However, Berger's report [301] for the Fuel Cells and Hydrogen Joint Undertaking (FCHJU) states that expected prices for H_2 are extremely variable, ranging €2-13 (£1.80-11.70) kg^{-1} H_2. They continue to state that the average expected H_2 price at the "lower end" of these price ranges would be about €6 (£5.40). Meanwhile, a report by Reuter et al. [302] for the FCHJU calculated the cost of H_2 per kg must be €4-6 (£3.6-5.4) kg^{-1} H_2 in order to be competitive with diesel prices for bus-transport sector. This showcases how uncertain and variable the market price of H_2 is, can be and will be in the future with unpredictable levels of market penetration and technology readiness levels.

6.2 Process Design

A chemical process model has been developed in Aspen Plus v8.8 [23] and sensitivity analysis has been carried out to provide an energetically efficient method of NH_3 recovery from a low concentration ammonia solution, representative of digestate liquor produced at the anaerobic digestion unit at a wastewater treatment plant (as discussed in Chapter 4). This has been combined in the present chapter with a process simulation for H_2 generation via a combination of the catalytic processes of steam bio-methane reforming, water-gas-shift and ammonia decomposition. The following assumptions have been utilised throughout:

- Ambient conditions set at 1 bar, 23°C
- Air composition assumed 79:21 split of N_2:O_2 only

Primary flows of biomethane and digestate liquor flows and ammonia concentrations have been based on data from Esholt WWTP, West Yorkshire, UK – as detailed in Chapter 3. In Aspen Plus, a 'COMMON' method filter with 'ENRTL-RK' base method have been used throughout, in line with the process modelling carried out in Chapters 4 and 5. A short description of this method,

the filter and the function of blocks mentioned throughout can be found in Table 4-1.

The process designed can be seen in Figure 6-2. The liquor enters the system at LIQ-1 and is pre-heated via exchange with the bottoms outlet of the stripping column in 'HX2', as a novel feature of heat integration between integrated processes of ammonia recovery and downstream steam reforming/ammonia cracking. The stripping column (STRIPPER), absorption column (ABSORB) and distillation column (DIST) are all operationally set up as designed in Chapter 3. The gaseous outlet from the distiller, carrying the concentrated ammonia, is pressurised to 31 bar before mixing with a fraction of the distillation bottoms, that quantity of which is dictated by a pre-determined S:C in the reformer. The latter represents yet another novel integrated process feature between the ammonia recovery and the steam reforming/ammonia cracking unit. This combined stream, labelled 'CON-LIQC' is heated via a number of heat exchangers (HX6, HX5 and HX9) before entering the primary reformer/cracker (REFORMER) at 25 bar. Here, it meets a flow of pressurised biomethane in an RGibbs reactor where the minimisation of Gibbs free energy is used to calculate the product yields and syngas composition. The syngas produced from the primary reformer expends heat via transfer with the reformer and furnace inlets via heat exchangers 'HX1' and 'HX4'. The syngas enters the HT-WGS and LT-WGS reactors (also represented as RGibbs reactors) at 350°C and 205°C inlet temperatures respectively, for maximum CO conversion to CO_2 and concurrent production of H_2 from the water co-reactant. Each reactor operates adiabatically, meaning there are no heat losses from the reactor and the exothermic nature of the WGS reaction creates a temperature hike in each reactor. The syngas is then cooled and dried before a PSA unit generates a pure H_2 product containing 90% of the H_2 present in the PSA inlet.

A furnace has been used to generate heat for the process. It has been simulated via an 'RGibbs' reactor and is fuelled by 27.7% of the AD-biomethane product via the stream 'CH4-FUEL' together with any remaining H_2, CH_4 and CO present in the PSA offgas (OFFGAS). The furnace then generates an excess of heat that equates to 110% of the reformer requirements. This fulfils the heating

requirements of the reformer and accounts for 20% thermal losses. A 10% pressure drop is experienced in each of the heat exchangers and reactors where the inlet pressure is greater than atmospheric.

6.2.1 Calculator Blocks

A series of calculator blocks have been designed to fulfil some of the process requirements. Equations 6-7 to 6-10 detail the Fortran statements entered in each of the calculator blocks and describe the air flow required to maintain a combustion excess air of 10%. These then communicate with the model to meet the desired output.

$$\dot{n}_{AIR-1,O_2} = 1.1 \times \begin{pmatrix} \frac{\dot{n}_{OFFGAS,H_2} + \dot{n}_{OFFGAS,CO}}{2} \\ +2\left(\dot{n}_{OFFGAS,CH_4} + \dot{n}_{CH4-FUEL,CH_4}\right) \end{pmatrix} \quad \textbf{6-7}$$

$$\dot{n}_{AIR-1,N_2} = \dot{n}_{AIR-1,O_2} \times 3.791 \quad \textbf{6-8}$$

$$\dot{n}_{BTMS2,H_2O} = (S{:}\,C) \times \dot{n}_{CH_4-COMP,CH_4} \quad \textbf{6-9}$$

$$HD_{FURNACE} = -1.2 \times HD_{REFORMER} \quad \textbf{6-10}$$

In equations 6-7 to 6-10, $\dot{n}_{x,y}$ describes the molar flow of species 'y' in stream 'x'. Equation 6-7 details the requirement of an oxygen flow 1.1 times that of the stoichiometric requirement. This ensures enough oxygen is fed to the furnace to prevent inefficient combustion reactions and maintain an exhaust temperature below 1100°C. Equation 6-8 ensure the quantity of N_2 in stream AIR-1 equates to a 79:21 ratio with oxygen. The calculator block described by equation 6-9 ensures the quantity of water entered to the primary reformer fulfils the predetermined S:C ratio. Equation 6-10 ensures that the heat provided by the furnace is 120% that of the primary reformer requirements (80% heat transfer), where $HD_{FURNACE}$ and $HD_{REFORMER}$ are the heat duties of the furnace and reformer respectively.

6.2.2 Process Modelling Sensitivity Analysis Methodology

A thorough sensitivity analysis has been carried out to optimise the system and unit conditions. As discussed in the Introduction, hydrogen generation can be heightened with increasing reformer temperature and S:C. However, this leads to a greater heat demand for the furnace and therefore less heat to export for air stripping. As such, a study has been carried out which investigates the effect of varying reformer temperature, and heat transfer in HX9 on the heat demand for air stripping (via AIRHT) and the final production of H_2 in stream 'H2'. The sensitivity analysis not only highlights the impact of primary reformer temperature on the system's production of H_2 but indicates whether the increased hydrogen gas generation is worthwhile, given the potential increase in heat duty of AIRHT. The sensitivity study will also dictate optimum operating conditions for each of the proposed S:Cs investigated. The following sensitivity parameters have been utilised:

- Primary reformer temperature: 600-1000°C at 25°C intervals.
- 'CON-LIQF' temperature from 'HX9': 700-1000°C at 25°C
- 'BOTAIR4' temperature from 'HX10': 200-550°C at 25°C

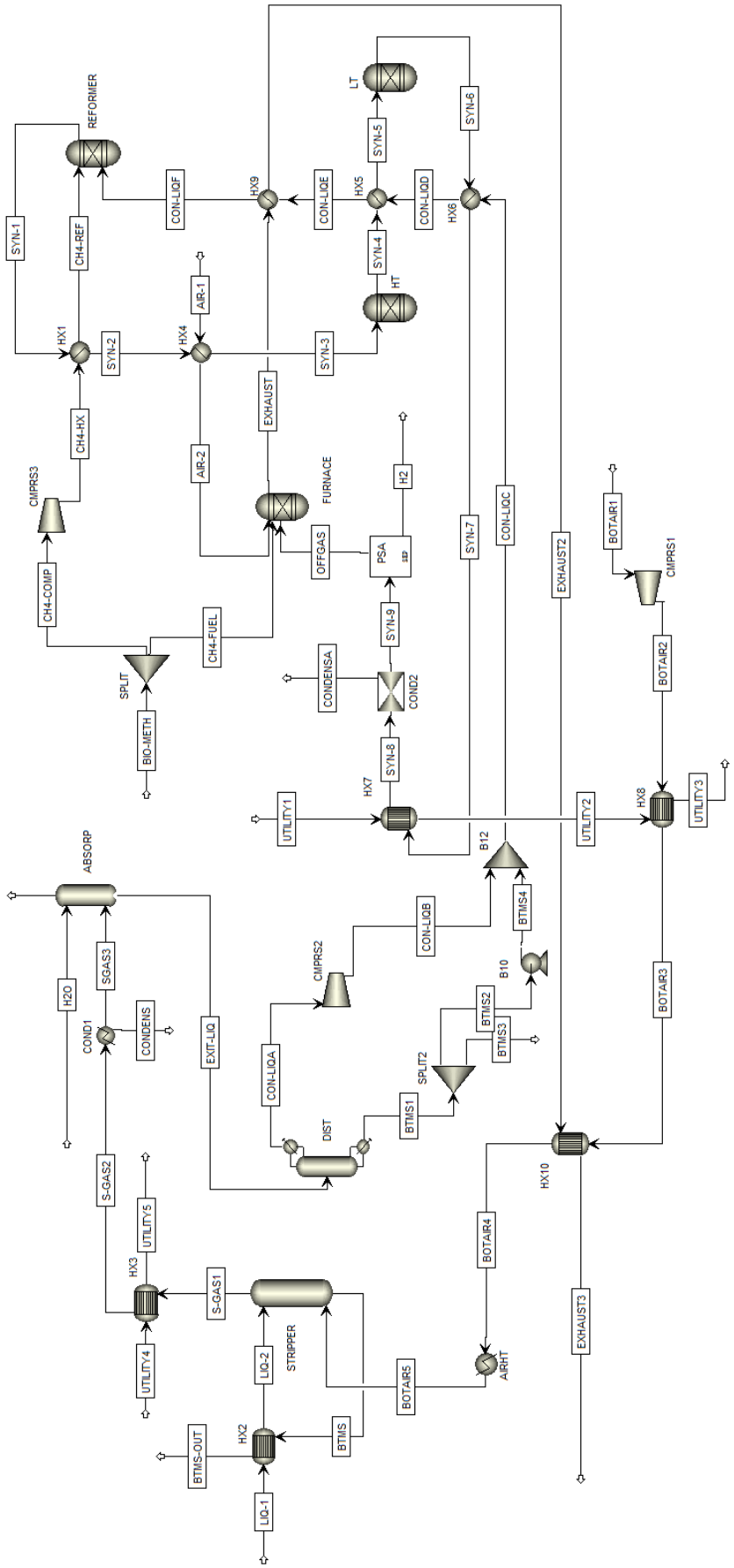

Figure 6-2. Process Flowsheet for ammonia recovery-H_2 production model

Figure 6-2 Legend

LIQ1	Digestate liquor representative inlet
LIQ2	Preheated digestate liquor
EXH-A3	Compressed exhaust gas for inlet to stripper
BTMS	Hot liquid outlet from the stripping column
BTMS-OUT	Cooled liquid outlet from the stripping column
S-GAS1	Gaseous outlet from the stripper containing desorbed NH_3
S-GAS2	Cooled gaseous outlet from stripper
CONDENSA	Water condensed from the stripper's gaseous outlet
S-GAS3	Dry gaseous inlet to the absorber
H2O	Water inlet used for NH_3 absorption
EXIT LIQ	Liquid outlet from absorber containing reabsorbed NH_3
CON-LIQA	Gaseous distillate stream from distiller containing recovered NH_3
CON-LIQB	Compressed distillate
BTMS1	Hot liquid outlet from distiller
BTMS2	Hot liquid outlet from distiller used for steam reforming
BTMS3	Hot liquid outlet from distiller used for heat recovery
BTMS4	Pressurised hot liquid outlet from distiller used for steam reforming
CON-LIQC	Combined ammonia and H_2O stream
UTILITY1	Cool water inlet for heat recovery from syngas
UTILIT2	Hot water stream used as heating utility
UTILITY3	Cooled utility stream
CON-LIQ(D-F)	Combined ammonia and H_2O stream preheated for
BIO-METH	Biomethane inlet at ambient temperature and pressure
CH4-COMP	Split of Bio-CH_4 for reforming
CH4-HX	Compressed Bio-CH_4 for reforming
CH4-REF	Hot and compressed Bio-CH_4 and reformer inlet
CH4-FUEL	Split of Bio-CH_4 for furnace
AIR-1	Air at ambient conditions for furnace
AIR-2	Heated air for furnace inlet
EXHAUST	Exhaust stream from furnace
EXHAUST2	Exhaust stream for heat recovery
EXHAUST3	Cooled exhaust stream
SYN-1	Syngas from primary reformer
SYN-2	Syngas after exchange with biomethane
SYN-3	Cool syngas for entrance to HT-WGS reactor
SYN-4	Syngas from HT-WGS
SYN-5	Syngas for entrance to LT-WGS
SYN-(6-8)	Syngas from LT-WGS used for various heat exchange
SYN-9	Dry syngas for PSA inlet
OFFGAS	Offgas from PSA
H2	High purity H_2 product stream from PSA

6.3 Economic Analysis Methodology

As in Chapters 3, 4 and 5 most of the equipment base and installation costs have been determined using Aspen Plus Economic Analyzer (APEA). However, in order to convert the economic cost of various equipment types that are unable to be accurately calculated by APEA, a method of cost scaling has been implemented to convert the model developed by NREL [303] to the process detailed in this chapter. The calculation to implement the scale estimation, as detailed in [304] is shown in equation 6-11 and is known as the *six-tenths factor rule*:

$$\text{cost of equipment } a = (\text{cost of equipment } b)\ \text{X}^{0.6} \qquad 6\text{-}11$$

where, cost of equipment a and b are the unknown and known unit cost, X is the multiplication factor for the known capacity difference between unit a and unit b $\left(\frac{a}{b}\right)$, 0.6 represent the 'scaling factor' used as a rule of thumb to approximate scaling costs. This cost estimation has been used to estimate the potential equipment costs for the primary reformer, the two WGS reactors, the PSA and the pre-PSA condenser. The 2016 prices detailed in the NREL model [303] have been adjusted for 2018 prices using an annual RPI inflation of 2.87% and a currency conversion of £0.78/US$, as detailed in Chapter 4. Installation costs for these units have been based on the installation factors from similar units in APEA.

Furthermore, the NREL model was also used to estimate equipment replacement costs for each scenario [303]. The NREL model dictates a fixed replacement cost after 5, 10 and 15 years of operation equivalent to 15%, 50% and 15% respectively of the initial capital investment. Additionally, the process model built in Aspen Plus does not account for compression, storage and dispensing (CSD) of the generated hydrogen. As such the associated costs for CSD detailed in the NREL model [303] have been scaled appropriately, using equation 6-11 for the discussed economic analysis. In NREL's model the generated H_2 is compressed to 700 bar ready for storage and eventual dispensing to hydrogen-fuelled vehicles.

Catalyst costs have been estimated at \$0.19 kg^{-1} H_2 as detailed in Kaiwen et al. [305]. Wage expenditure and maintenance costs have been calculated as in Chapters 3, 4 and 5. The capital cost of block AIRHT has been estimated using the cost curve for a stainless steel direct fired heater shown in Peters et al. (pg. 692) [288] adjusted by inflation. The projected market value has been set at £4.50/kg H_2 which is the mean of the values suggested by Reuter et al. [302] for it to be competitive with diesel prices for bus-transport sector.

The required expenditure for heat has been determined using the requirements of blocks AIRHT and DIST with a thermal transfer efficiency of 80% at a cost of 2.33 p/kWh as detailed in the BEIS report on gas and electricity prices in the non-domestic sector [306]. The expenditure on electricity has been estimated via the power consumption of each compressor and pump simulated in Aspen Plus, and the power requirement of CSD calculated from the NREL economic model [303], with the gas clean up system as discussed in Chapter 5, using an electricity cost of 10.55 p kWh^{-1} as detailed by BEIS [306]. Renewable heat incentive (RHI) income has been calculated via the heat generated by EHAUST3, UTILITY3 and UTILIT5 at a price of 1.16 pence kWh^{-1}. The market price of hydrogen has been set at £4.50 kg^{-1} which was determined a reasonable value based on the review of literature discussed in section 6.1.4. NPV analysis has also been carried as detailed in Chapters 3, 4 and 5.

Due to the uncertainty of the economic analysis methodology which meshes a number of techniques and sources, sensitivity analysis has been carried out to indicate which factors will play an important role in the overall feasibility of potential process integration. Figures for the hydrogen selling price, overall annual expense, initial capital investment and catalyst cost have been altered by +/- 15% to show the prospected impact on the systems overall profitability in both non-discounted and NPV terms.

6.4 Results and Discussion

6.4.1 Sensitivity Analysis

Figure 6-3 shows the results of the sensitivity analysis carried out under S:C 4 conditions. Peak hydrogen production occurs at 1000 °C, generating 117 kg per hour which is equivalent to 4.6 MW on a HHV basis, as shown in Figure 6-3. At this reforming temperature, the temperature of CON-LIQF (provided by heat transfer in HX9) was proved to have minimal effect on the amount of heat available for air stripping. By increasing the temperature of CON-LIQF, the heat requirements of the primary reformer decreases, meaning less heat is demanded from the furnace. However, more heat is transferred from the furnace exhaust in HX9 meaning approximately an equivalent amount of heat is left for air stripping.

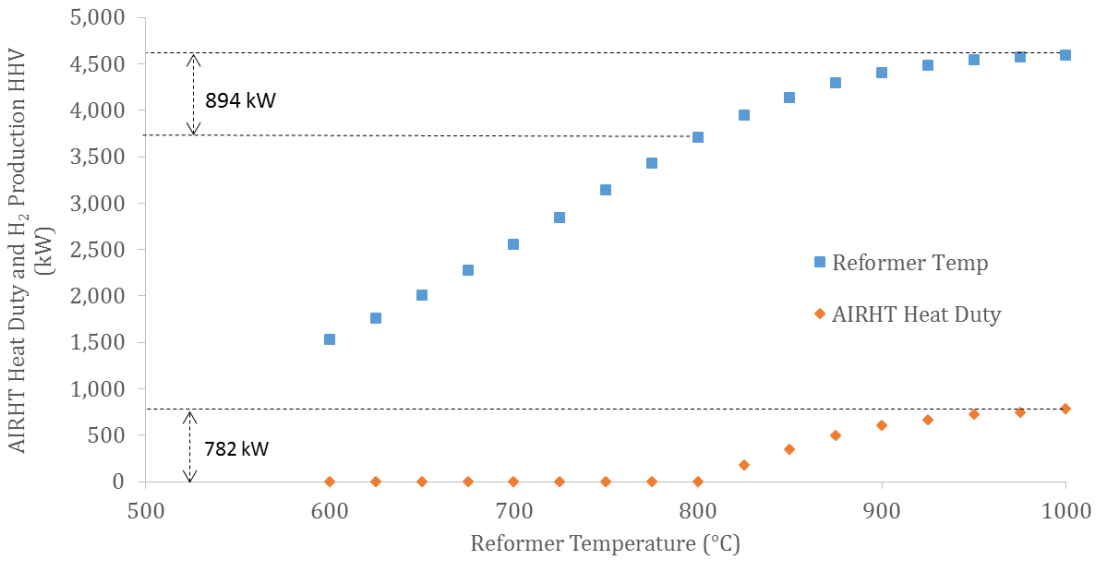

Figure 6-3. S:C 4 sensitivity analysis data detailing the effect of primary reformer temperature on H_2 generation and stripping thermal requirements via AIRHT.

Under the S:C 4 scenario, at 1000 °C reformer temperature, the exhaust from HX9 only carries enough thermal energy to pre-heat the stripping gas to 185°C. As such 782 kW_{th} is required in AIRHT to pre-heat BOTAIR4 to 550°C, as shown in Figure 6-3. However, all of the stripping thermal requirements are met when

primary reformer temperatures below or equal to 800°C are used. At 800°C, 94 kg pf H_2 per hour is generated from the system. This is 894 kW_{HHV} less than at the 1000°C reforming temperature scenario, as illustrated in Figure 6-3. Thus, it can be said that the additional generation of hydrogen at a reformer temperature of 1000°C is worthwhile as the increase in energy content (HHV-basis) is superior to the additional energy used for stripping. Further analysis of the process at this temperature has been shown in section 6.4.2.

Results from the sensitivity analysis under S:C 3 conditions have been illustrated in Figure 6-4. The final production of H_2 peaks at 115 kg per hour (4.5 MW_{HHV}) with a primary reformer temperature of 1000°C. This is 2 kg h^{-1} less than the S:C 4 condition at the same temperature; demonstrating the effect of Le Chatelier's principle in moving the SMR and WGS reactions forward. Under the S:C 3 scenario a maximum temperature of 900°C can be transferred to CON-LIQF via HX9. Above this temperature, not enough heat is left in the exhaust to effectively pre-heat the gas used for air stripping. However, below 900 °C, the change in thermal energy remaining in the exhaust is negligible.

Under the S:C 3 scenario, the thermal requirements for air stripping are met up to a primary reformer temperature of 850°C, in which 97 kg h^{-1} (3.8 MW_{HHV} equivalent) of H_2 is generated from the system. Thus, the primary reformer can operate at 50°C greater than under the S:C 4 scenario before additional energy is required for air stripping. This is the case for two key reasons. Firstly, the additional water/steam in the S:C scenario requires a greater transfer of heat from the furnace exhaust in HX9. Secondly, the reformer has a larger demand of heat from the furnace to maintain its operating temperature. As illustrated in Figure 6-5, this is also demonstrated at a reformer temperature of 1000°C whereby the additional energy requirement for air stripping via AIRHT is 615 kW_{th} compared to 782 kW_{th} at the same temperature under the S:C 4 scenario. However, as under the S:C 4 scenario, the additional energy content of H_2 of 690 kW_{HHV} generated between 850 °C and 1000 °C outweighs the additional thermal demand for air stripping at 615 kW_{th} making the use of higher reformer temperatures acceptable.

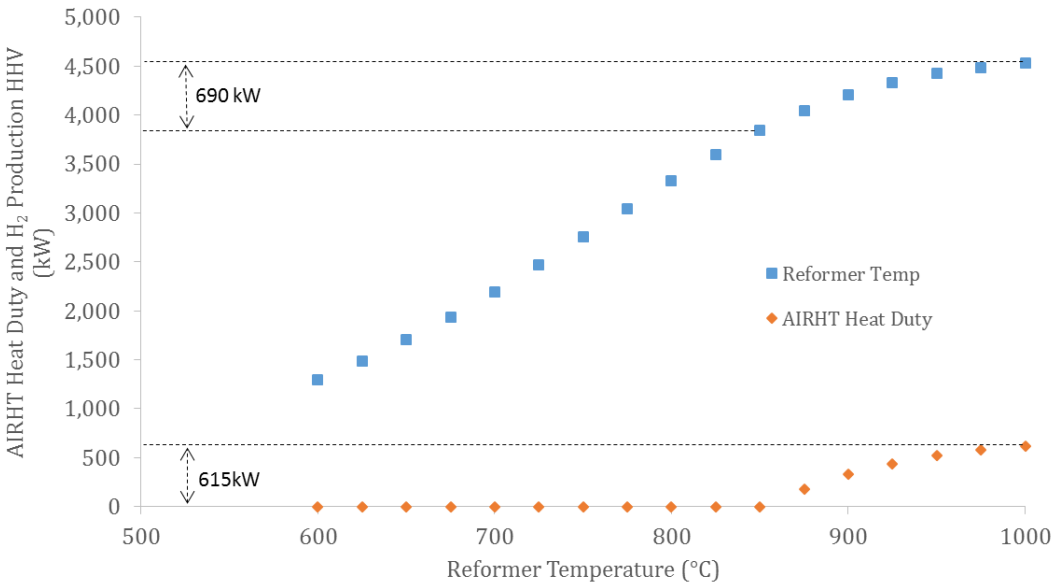

Figure 6-4. S:C 3 Sensitivity analysis data detailing the effect of primary reformer temperature on H_2 generation and stripping thermal requirements via AIRHT.

Results from the sensitivity analysis under S:C 2 conditions have been illustrated in Figure 6-5. As with the S:C 3 and 4 scenarios, peak hydrogen gas production occurred at a primary reformer temperature of 1000 °C. This temperature provided a system output of 108 kg h^{-1} of H_2. This is 7 kg h^{-1} less than the S:C 3 scenario and 9 kg h^{-1} less than the S:C 4 scenario; again showcasing the impact of H_2O flows under the Le Chatelier's principle in moving the SMR and WGS reactions forward. Under the S:C 2 scenario at 1000 °C, the effect of CON-LIQF temperature from HX9 on the energy for air stripping is negligible. At a 1000 °C primary reformer temperature, enough thermal energy is left in the exhaust to heat the stripping gas to 415 °C, meaning 296 kW_{th} must be supplied at AIRHT. This is the lowest energy input for air stripping required for all S:C scenarios considered when a primary reformer temperature of 1000 °C is utilised. Again, this is because less energy from the furnace and its exhaust gas is required to maintain the operating temperature and pre-heat the steam inlet.

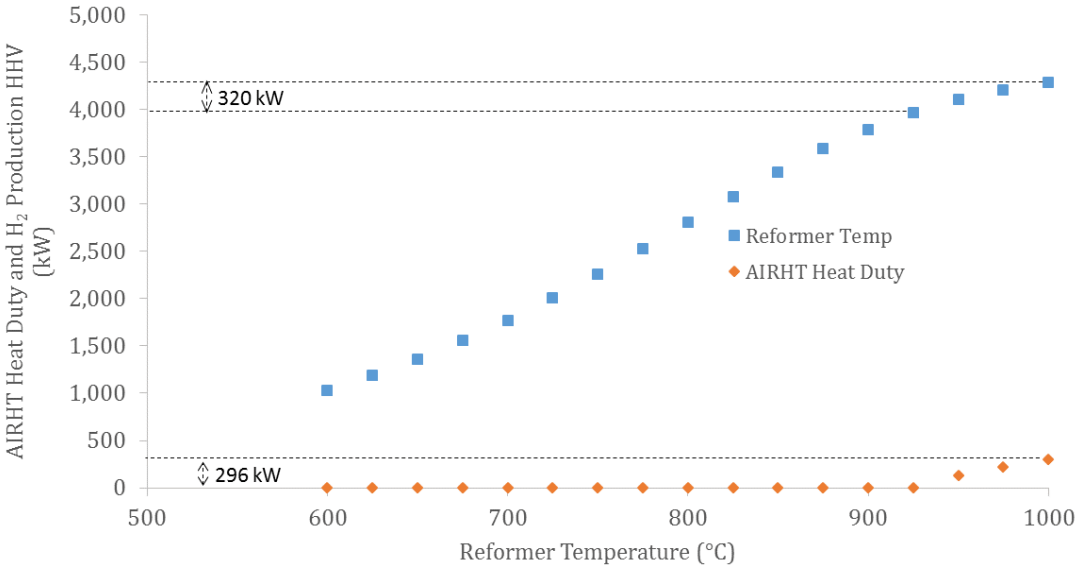

Figure 6-5. S:C 2 Sensitivity analysis data detailing the effect of primary reformer temperature on H_2 generation and stripping thermal requirements via AIRHT.

As shown in Figure 6-5, the thermal requirements for air stripping is met up to a reformer temperature of 925 °C. At this temperature, 101 kg h^{-1} (3.9 MW_{HHV} equivalent) of H_2 is generated from the system. The 320 kW_{HHV} of additional hydrogen generated at 1000°C is greater than the 296 kW_{th} energy required for air stripping. As such, as with the other S:Cs, it has been decided that the higher reformer temperatures should be used for the final process conditions.

If access to thermal power at the facility was limited and all thermal air stripping requirements needed to be met internally, then the lower S:Cs would facilitate a greater production of hydrogen. For example, the greatest H_2 production that can be facilitated is 94 kg h^{-1} at 800°C under S:C 4 conditions, 97 kg h^{-1} at 850°C under S:C 3 conditions and 101 kg h^{-1} under S:C 2 conditions.

6.4.2 Final Process Conditions

6.4.2.1 S:C 4 scenario

Table 6-1 shows the stream compositions and mass flow results from Aspen Plus under S:C 4 conditions with a primary reformer temperature of 1000 °C. 248 kg h^{-1} (15.45 kmol h^{-1}) of methane enters the primary reformer in stream

CH4-REF and 98.9% is destroyed via the SMR reaction (reaction 6-1), exiting via stream SYN-1. Table 6-1 also shows how 99.5% of the ammonia, entering the reformer in stream CONC-LF, undergoes decomposition (reaction 6-6). Furthermore, 32% of the CO generated during SMR reaction is then destroyed via the WGS reaction (reaction 6-5). The recovered ammonia stream 'CONC-LF' contains 9.6 kg h^{-1} (0.3 kmol h^{-1}) of O_2. Each mole of oxygen gas destroys two moles of H_2 generated. The result of this is the generation of 109 kg h^{-1} of H_2 from the primary reformer, as shown in stream SYN-1. 83.7% of this originates from SMR, 9.1% from WGS and 7.2% from NH_3 decomposition.

Table 6-1. H_2 production-based stream compositions and mass flows for S:C 4 scenario

Stream	CH4-COMP	CH4-REF	CONC-LF	SYN-1	SYN-3	SYN-4	SYN-6	H2
H_2O (kg h^{-1})	0	0	1132	777	777	635	596	0
CH_4 (kg h^{-1})	248	248	0	2.6	2.6	2.6	2.6	0
CO (kg h^{-1})	0	0	0	289	289	68	6	0
CO_2 (kg h^{-1})	0	0	0	219	219	567	663	0
H_2 (kg h^{-1})	0	0	0	109	109	125	130	117
C (kg h^{-1})	0	0	0	0	0	0	0	0
O_2 (kg h^{-1})	0	0	9.6	0	0	0	0	0
N_2 (kg h^{-1})	0	0	11.9	48.9	48.9	48.9	48.9	0
N_2O (kg h^{-1})	0	0	0	0	0	0	0	0
NH_3 (kg h^{-1})	0	0	45.3	0.25	0.25	0.25	0.25	0
NO (kg h^{-1})	0	0	0	0	0	0	0	0
NO_2 (kg h^{-1})	0	0	0	0	0	0	0	0
Temperature (°C)	23	995	1000	1000	350	427	228	38
Pressure (bar)	1	25	25	22.5	18	16	13	13
Total mass flow (kg h^{-1})	248	248	1199	1446	1446	1446	1446	117

The syngas is cooled to 350 °C before it enters the HT-WGS reactor in stream 'SYN-3'. 221 kg h^{-1} of the 289 kg h^{-1} (76%) of CO generated in the primary reformer is destroyed in the HT-WGS via reaction 6-5. This produces an additional 15.9 kg h^{-1} (7.9 kmol h^{-1}) of hydrogen. The exothermic nature of this

reaction acts to increase the syngas temperature from 350 °C to 427 °C, as shown in stream SYN-4 in Table 6-1. The syngas is cooled to 205 °C before entering the LT-WGS. Here a further 4.4 kg h^{-1} (2.19 kmol h^{-1}) of H_2 is generated from the conversion of 91% of the incoming CO to the LT-WGS. The syngas from this block (SYN-6), then contains a flow of 130 kg h^{-1} of H_2. The PSA is able to retain 90% of this, producing a final output of 117 kg h^{-1} (57.9 kmol h^{-1}) of H_2.

Table 6-2 showcases the composition and mass flows of key streams surrounding the furnace block (FURN) under the S:C 4 scenario. AIR-1 is preheated to 610 °C containing the oxygen to be used as an oxidising agent for combustion of CH_4, H_2, CO and NH_3 from streams 'OFFGAS' and 'CH4-FUEL'. The combustion facilitates an exhaust temperature of 1025 °C and direct heat for the primary reformer. The exhaust is able to pre-heat air stripping gas to just 185 °C, which leads to a 782 kW_{th} requirement in AIRHT to reach a stripping temperature of 550 °C.

Furthermore, the model has shown that under these furnace conditions, 0.7 kg h^{-1} and 0.002 kg h^{-1} of NO and NO_2 respectively. Collectively termed as NOx, they are known air pollutants, causing smog, ozone and acid rain [307]. It was found via a brief sensitivity analysis, that when H_2 was omitted from the stream 'OFFGAS', the quantity of NOx formed drops by 75%. This could be the case because the presence of hydrogen increases the operating temperature of the furnace, facilitating increased NOx formation. The generation of NOx contained in the exhaust is just 0.02% on a molar basis and should be deemed acceptable. However, the furnace has been simulated by an RGibbs reactor which uses the minimisation of Gibbs free energy to calculate the product yields. NOx formation tends to be kinetically, rather than thermodynamically (equilibrium) determined. Thus, NOx emissions could be greater or lower than what has been predicted by the RGibbs reactor under real operating conditions. Thus, further analysis could deserve attention in future work to better understand the operating conditions required to keep NOx emissions down.

Table 6-2. Furnace-based stream compositions for S:C 4 scenario

Stream	AIR-1	AIR-2	OFFGAS	CH4-FUEL	EXHAUST	EXHAUST2
H_2O (kg h^{-1})	0	0	0.1	0	336	336
CH_4 (kg h^{-1})	0	0	2.6	95.2	0	0
CO (kg h^{-1})	0	0	6.1	0	0.0004	0.0004
CO_2 (kg h^{-1})	0	0	663	0	941	941
H_2 (kg h^{-1})	0	0	13.0	0	0	0
C (kg h^{-1})	0	0	0	0	0	0
O_2 (kg h^{-1})	546	546	0	0	49	49
N_2 (kg h^{-1})	1802	1802	48.9	0	1851	1851
N_2O (kg h^{-1})	0	0	0	0	0	0
NH_3 (kg h^{-1})	0	0	0.2	0	0	0
NO (kg h^{-1})	0	0	0	0	0.7	0.7
NO_2 (kg h^{-1})	0	0	0	0	0.002	0.002
Temperature (°C)	23	803	38	23	1158	270
Pressure (bar)	1	1	13	1	1	1
Total mass flow (kg h^{-1})	2348	2348	734	95	3178	3178

Table 6-3 shows the sources and sinks of heat in the process. Together, the heater used to pre-heat the stripping gas to 550 °C (AIRHT) and the distillation column's reboiler require 1.08 MW of heat. The three streams 'EXHAUST3', 'UTILITY3' and 'UTILITY5' provide the potential for heat export from the system. Their potential heat production have been simulated by cooling them to 23 °C and 1 bar via Heater blocks in Aspen Plus. The respective results shown in Table 6-3 detail the heat duty results from these heater blocks with a 90% efficiency factor. The consequence of this is the potential production of 1.55 MW of heat but a net genearation of 400.9 kW_{th} or 9.6 MWh_{th} per day.

Table 6-3. Heat consumption and production for S:C 4 scenario

	Heat Demand (kW_{th})
Blocks	
AIRHT	781.6
DIST Reboiler	365.5
Streams	
EXHAUST3	-280.4
UTILITY3	-405.3
UTILITY5	-862.3
Net Total (kW_{th})	-400.9
Net Total (kWh_{th} day^{-1})	-9,621.69

Despite producing a reasonable quantity of net heat, the quality of the heat is of a low calibre. Exhaust 3 holds the highest temperature of 120°C under the S:C 4 scenario but holds the lowest quantity of heat, limiting its potential application. UTILITY3 and UTILITY5 are at 95 and 63°C respectively. However, it is proposed that these streams would be suitable for AD and space heating purposes. The AIRHT and distillation column's reboiler will require higher quality heat streams in order to meet their requirements.

Table 6-4 shows the system's power consumption via each compressor and pump. CMPR3 requires the greatest amount of power at 70.5 kW in order to compress the biomethane for reforming to 27.8 bar. Naturally, the pump used for liquid water pumping from the distillation bottoms has the lowest power demand at 3.2 kW. This process produces a product in H_2 gas, rather than CHP as in Chapter 5. As such, the process' power demand will have to be met using grid electricity, simultaneously increasing system operating costs.

Table 6-4. Power consumption for S:C 4 scenario

Blocks	Power Demand (kW)
CMPRS1	64.7
CMPRS2	24.5
CMPRS3	70.5
B10	3.2
Total (kW)	162.8
Total (kWh day^{-1})	3907

6.4.2.2 S:C 3 scenario

Table 6-5 shows the stream compositions and mass flow results from Aspen Plus under S:C 3 conditions with a primary reformer temperature of 1000 °C. 248 kg h^{-1} (15.45 kmol h^{-1}) of methane enters the primary reformer in stream CH4-REF and 97.9% of it is destroyed via SMR (reaction 6-1), exiting via SYN-1. The lower flow of steam in the S:C 3 scenario means its role in shifting the equilibrium of reaction 6-1 to the right is slightly less pronounced. Thus, methane's conversion is slightly less than the S:C 4 scenario's 98.9%.

Furthermore, the effect of the lower S:C has a more significant impact on the role of the WGS reaction (6-5) in the primary reformer. In the S:C 3 scenario, 25% of the CO generated from SMR is converted to hydrogen compared to 32% under S:C 4 conditions. However, the conversion of ammonia is very similar to S:C 4, at 99.4%. The greater concentration of hydrogen in the product syngas, compared to S:C 4 conditions, means the equilibrium of reaction 6-6 is shifted marginally to the left.

The combination of these reactions result in the production of 53.1 kmol h^{-1} of H_2 in the primary reformer. 85.4% from SMR, 7.2% from WGS and 7.5% from NH_3 decomposition. The S:C has a much more pronounced impact on SMR and WGS, thus ammonia decomposition has a greater percentage contribution to the H_2 generated than under the S:C 4 scenario. Again, the O_2 contained in stream CON-LIQF acts to destroy 0.6 kmol h^{-1} of H_2 via combustion, reducing the final output of H_2 from the reformer to 52.5 kmol h^{-1} or 106 kg h^{-1} as shown in Table 6-5.

Table 6-5. H_2 production-based stream compositions and mass flows for S:C 3 scenario

Stream	CH4-COMP	CH4-REF	CONC-LF	SYN-1	SYN-3	SYN-4	SYN-6	H2
H_2O (kg h^{-1})	0	0	854	523	523	387	329	0
CH_4 (kg h^{-1})	248	248	0	5.2	5.2	5.2	5.2	0
CO (kg h^{-1})	0	0	0	317	317	105	14	0
CO_2 (kg h^{-1})	0	0	0	168	168	501	643	0
H_2 (kg h^{-1})	0	0	0	106	106	121	128	115
C (kg h^{-1})	0	0	0	0	0	0	0	0
O_2 (kg h^{-1})	0	0	10	0	0	0	0	0
N_2 (kg h^{-1})	0	0	12	49	49	49	49	0
N_2O (kg h^{-1})	0	0	0	0	0	0	0	0
NH_3 (kg h^{-1})	0	0	45	0.27	0.27	0.27	0.27	0
NO (kg h^{-1})	0	0	0	0	0	0	0	0
NO_2 (kg h^{-1})	0	0	0	0	0	0	0	0
Temperature (°C)	23	995	900	1000	350	438	244	38
Pressure (bar)	1	25	25	23	18	16	13	13
Total mass flow (kg h^{-1})	248	248	920	1168	1168	1168	1168	115

After cooling to 350 °C before entrance to the HT-WGS reactor, 67% of the 317 kg h^{-1} contained in the primary reformer outlet are destroyed in the HT-WGS reactor via reaction 6-5. This creates additional 15 kg h^{-1} of H_2 and leaves a 105 kg h^{-1} flow of CO to the LT-WGS reactor, whilst increasing the syngas temperature to 438 °C. In the LT-WGS reactor, 86% of the incoming CO are converted to H_2 and CO_2, boosting the flow of H_2 to 128 kg h^{-1}. These conversions are lower than under the S:C 4 scenario because the decreased flow of water negatively impacts the placement of equilibrium under the WGS reaction (6-5). This results in the retention of 14 kg h^{-1} of unconverted CO compared to 6 kg h^{-1} under S:C 4 conditions. Furthermore, the final output of H_2 from the PSA is 115 kg h^{1-} compared to 117 kg h^{-1} in the S:C 4 scenario.

Table 6-6 showcases the composition and mass flows of key streams surrounding the furnace block (FURN) under S:C 3 conditions. AIR-1 is

preheated to 641 °C in HX4. The combustion of CH_4, H_2, CO and NH_3 from streams 'OFFGAS' and 'CH4-FUEL' results in an exhaust temperature of 1039 °C and enough heat to meet the demands of the primary reformer. The exhaust is able to preheat stripping gas to 265 °C in HX10, 80 °C greater than under the S:C 4 scenario. This is the case because the lower flow of water required under S:C 3 conditions means less heat is needed to pre-heat CON-LIQE and maintain primary reforming temperature.

Table 6-6. Furnace-based stream compositions for S:C 3 scenario

Stream	AIR-1	AIR-2	CH4-FUEL	OFFGAS	EXHAUST	EXHAUST2
H_2O (kg h^{-1})	0	0	0	0.1	340	340
CH_4 (kg h^{-1})	0	0	95.2	5.2	0	0
CO (kg h^{-1})	0	0	0	14	0	0
CO_2 (kg h^{-1})	0	0	0	643	941	941
H_2 (kg h^{-1})	0	0	0	12.8	0	0
C (kg h^{-1})	0	0	0	0	0	0
O_2 (kg h^{-1})	552	552	0	0	41	41
N_2 (kg h^{-1})	1822	1822	0	49	1871	1871
N_2O (kg h^{-1})	0	0	0	0	0	0
NH_3 (kg h^{-1})	0	0	0	0.3	0	0
NO (kg h^{-1})	0	0	0	0	0.3	0.3
NO_2 (kg h^{-1})	0	0	0	0	0.001	0.001
Temperature (°C)	23	641	23	38	1039	454
Pressure (bar)	1	1	1	13	1	1
Total mass flow (kg h^{-1})	2374	2374	95	725	340	340

Table 6-6 also illustrates how the model predicts the generation of 0.3 and 0.001 kg h^{-1} of NO and NO_2 respectively in the exhaust gas. It is suggested that this less than under the S:C 4 because the furnace is operating at a lower temperature than under the previously discussed scenario, thus dropping the formation of NOx. However, as discussed under S:C 4 conditions, it is

questionable whether this prediction of NOx generation is reliable due to NOx formation being kinetically, rather than thermodynamically determined.

Table 6-7 shows the sources and sinks of heat in the process under the S:C 3 scenario. The thermal requirements in AIRHT is 166.2 kW_{th} less than under the S:C 4 scenario. This is because comparatively more heat is carried in the exhaust gas so the stripping gas is warmer when entering AIRHT. The distillation column's heat demand is constant and irrespective of the S:C. Again, the potential heat production from streams 'EXHAUST3', 'UTILITY3' and 'UTILITY5' have been simulated by cooling them to 23 °C and 1 bar via Heater blocks in Aspen Plus with a 90% efficiency factor. As shown in Table 6-7, 'EXHAUST3', 'UTILITY3' and 'UTILITY5' could produce 250, 292 and 862 kW of thermal power respectively. The result of this is the net generation of 423 kW_{th} or 10.1 MWh day^{-1} of thermal power, 5.4% more than under the S:C 4 scenario.

Table 6-7. Heat consumption and production for S:C 3 scenario

	Heat Demand (kW_{th})
Blocks	
AIRHT	615.4
DIST Reboiler	365.5
Streams	
EXHAUST3	-249.8
UTILITY3	-291.6
UTILITY5	-862.3
Net Total (kW_{th})	-422.8
Net Total (kWh_{th} day^{-1})	-10,147

As under the S:C 4 scenario, the quality of the heat generated is not of the highest calibre. 'EXHAUST3', 'UTILITY3' and 'UTILITY5' hold temperatures of just 88 °C, 75° and 63 °C respectively. As such, they are not of high enough quality to meet the demands of blocks AIRHT and DIST. As such, an external source of high quality heat may be required to meet these demands. However, it is proposed that these streams would be adequate for AD and space heating at the wastewater treatment facility. Thus, suitable for an additional income under the RHI scheme. The system's electrical power requirements are

identical as under the S:C 4 scenario, shown in Table 6-4, totalling at 162.8 kW. Thus the process will still require 3.9 MWh of grid electricity per day.

6.4.2.3 S:C 2 scenario

Table 6-8 shows the stream compositions and mass flow results from Aspen Plus under S:C 2 conditions with a primary reformer temperature of 1000 °C. In the primary reformer, 94.8% of the 248 kg h^{-1} of incoming methane is destroyed via SMR (reaction 6-1). This, again, showcases the influence of the lower flows of steam in moving the SMR reaction forward via the influence of Le Chatelier's principle when compared to the methane conversions of 99.5% and 97.9% under the S:C 4 and S:C 3 scenarios respectively.

The lower S:C ratio also has a significant impact on the WGS reaction (6-5) in the primary reformer. Under S:C 3 conditions, just 16% of the CO produced via SMR is converted to H_2 and CO_2 via WGS compared to 32% and 25% under the S:C 4 and S:C 3 scenarios respectively. The S:C ratio has a more pronounced impact on the WGS reaction compared to the SMR reaction in the primary reformer because the reaction is exothermic, the equilibrium shifts leftwards under high temperatures. Thus, at 1000 °C, the S:C ratio has a greater impact on pushing the equilibrium back right. The conversion of ammonia under the decomposition reaction (6-6) in the primary reformer remains high at 99.3%. It is expected that the conversion is very slightly less than under S:C 4 and S:C 3 scenarios because the higher concentration of hydrogen in the syngas pushed reaction 6-6 marginally to the left.

The combination of reactions 6-1-6-6 produces 50.2 kmol h^{-1} of H_2 in the primary reformer under S:C 2 conditions. Of this, 87.5% originates from SMR, 4.7% from WGS and 7.9% from NH_3 decomposition. However, the O_2 contained in stream CON-LIQF destroys 0.6 kmol h^{-1} of H_2 via combustion, resulting in a release of 49.7 kmol h^{-1} or 100 kg h^{-1} of H_2. This is considerably less than under S:C 4 (109 kg h^{-1}) and S:C 3 (106 kg h^{-1}) conditions. The recovered ammonia has a greater impact on the production of H_2 because SMR and WGS reactions are impacted so significantly.

Table 6-8. H_2 production-based stream compositions and mass flows for S:C 2 scenario

Stream	CH4-COMP	CH4-REF	CONC-LF	SYN-1	SYN-3	SYN-4	SYN-6	H2
H_2O (kg h^{-1})	0	0	575.2	279.8	279.8	167.5	95.0	0
CH_4 (kg h^{-1})	247.9	247.9	0	12.9	12.9	12.9	12.9	0
CO (kg h^{-1})	0	0	0	344.7	344.7	170.1	57.4	0
CO_2 (kg h^{-1})	0	0	0	103.2	103.2	377.5	554.5	0
H_2 (kg h^{-1})	0	0	0	100.1	100.1	112.7	120.8	108.7
O_2 (kg h^{-1})	0	0	9.6	0	0	0	0	0
N_2 (kg h^{-1})	0	0	11.9	48.8	48.8	48.8	48.8	0
N_2O (kg h^{-1})	0	0	0	0	0	0	0	0
NH_3 (kg h^{-1})	0	0	45.2	0.3	0.3	0.3	0.3	0
NO (kg h^{-1})	0	0	0	0	0	0	0	0
NO_2 (kg h^{-1})	0	0	0	0	0	0	0	0
C (kg h^{-1})	0	0	0	0	0	0	0	0
Pressure (bar)	1	25	25	22.5	18.2	16.4	13.3	38
Temperature (°C)	23	995	700	1000	350	439	265	13
Total mass flow (kg h^{-1})	247.9	247.9	641.8	889.7	889.7	889.7	889.7	108.7

Because of the limited impact of the WGS reaction in the primary reformer under S:C 2 conditions, a comparatively large flow of unconverted CO enters the HT-WGS reactor (344.7 kg h^{-1}). 50.7% of this is destroyed in the HT-WGS block, generating 12.6 kg h^{-1} of H_2 and 274.3 kg h^{-1} of CO_2 via reaction 6-5. 66% of the CO entering the LT-WGS are then destroyed, topping the H_2 generation in the syngas to 120.8 kg h^{-1}, leaving a remaining CO flow of 57.4 kg h^{-1}. This is a significantly greater quantity of CO than under the S:C 3 scenario at 14 kg h^{-1} and the S:C 4 scenario at 6 kg h^{-1}. This again demonstrates the significance of S:C ratios on reactions 6-1 and 6-5. The PSA with the ability to recover 90% of the incoming H_2 facilitates a final production of 108.7 kg h^{-1}.

Table 6-9. Furnace-based stream compositions for S:C 2 scenario

Stream	AIR-1	AIR-2	CH4-FUEL	EXHAUST	EXHAUST2	OFFGAS
H_2O (kg h^{-1})	0	0	0	351.15	351.15	0.1
CH_4 (kg h^{-1})	0	0	95.2	0	0	12.9
CO (kg h^{-1})	0	0	0	0	0	57.4
CO_2 (kg h^{-1})	0	0	0	941.10	941.10	554.5
H_2 (kg h^{-1})	0	0	0	0	0	12.1
O_2 (kg h^{-1})	579.5	579.5	0	19.33	19.33	0
N_2 (kg h^{-1})	1912.2	1912.2	0	1961.21	1961.21	48.8
N_2O (kg h^{-1})	0	0	0	0	0	0
NH_3 (kg h^{-1})	0	0	0	0	0	0.3
NO (kg h^{-1})	0	0	0	0.22	0.22	0
NO_2 (kg h^{-1})	0	0	0	0.0005	0.0005	0
C (kg h^{-1})	0	0	0	0	0	0
Pressure (bar)	1	1	1	1	1	12.96
Temperature (°C)	23	460	23	1038	751	38
Total mass flow (kg h^{-1})	2492	2492	95.2	3273.0	3273.0	686

Table 6-9 details key stream compositions and mass flows surrounding the system's furnace under the S:C 2 scenario. Air-1 is pre-heated to 460°C in HX4, enabling the combustion of fuels contained in streams 'CH4-FUEL' and 'OFFGAS'. The exhaust gas, exiting at 1038°C is capable of preheating the stripping gas to 415 °C, 150 °C more than under S:C 3 conditions and 230 °C greater than under S:C 4 conditions. This highlights that although the lower S:C ratios have a negative impact on H_2 generation, there is a far greater ability to retain heat due to the extra demand required for pre-heating water and maintaining its temperature in the primary reformer.

Table 6-10 shows the heat sources and sinks in the process under S:C 2 conditions. The thermal requirements of the AIRHT heater is considerably less than under the other two S:C scenarios at 296.4 kW_{th} which is 38% that of its heat demand under the S:C 4 scenario. The potential heat production from streams 'EXHAUST3', 'UTILITY3' and 'UTILITY5' have been simulated by

cooling them to 23 °C and 1 bar via Heater blocks in Aspen Plus with a 90% efficiency factor. The sum of these three heat streams equates to 1.3 MW_{th}, resulting in a system net production of 627 kW_{th} or 15 MWh_{th} per day. This is 48% greater than under S:C 3 conditions and 56% more than under the S:C 4 scenario.

Table 6-10. Heat consumption and production for S:C 2 scenario

	Heat Demand (kW_{th})
Blocks	
AIRHT	296.4
DIST Reboiler	365.5
Streams	
EXHAUST3	-237.3
UTILITY3	-189.1
UTILITY5	-862.3
Net Total (kW_{th})	-626.8
Net Total ($kWh_{th}\ day^{-1}$)	-15,043

However, as under the other S:C scenarios, the quality of the heat available for export is of fairly low quality. Despite the S:C 2 scenario generating a greater quantity of heat than S:C 3 and 4 scenario, the quality is lower with 'EXHAUST3', 'UTILITY3' and 'UTILITY5' hold temperatures of just 65 °C, 57 °C and 63 °C respectively. These are not of high enough to meet the demands of the AIRHT and distiller's reboiler. However, they are not without use and could be utilised for space and AD heating at the wastewater treatment facility and therefore eligible for RHI income. The system's electrical power requirements are identical as under the S:C 4 scenario, shown in Table 6-4, totalling at 162.8 kW.

6.4.3 Economic Analysis

6.4.3.1 Steam:Carbon 4 scenario

Table 6-11 shows the total installed costs for each equipment block modelled in the discussed Aspen Plus process model along with the estimated cost of gas clean-up and CSD technology under the S:C 4 scenario. It requires the highest

initial capital investment of each S:C scenario at £13,293,229. The additional expense is attributed to the handling of greater flows of steam and H_2 product which require additional material. The highest single unit cost is for the CMPRS2 block at £990,054. The investment for the compression, storage and dispensing system is estimated to make up over 40% of the total installed cost at £5,395,711.

Table 6-11. Total installed cost breakdown for S:C 4 scenario

Equipment block	Installed Cost (£)	Equipment block	Installed Cost (£)
CSD	5,395,711	PSA	173,768
CMPRS2	990,054	HX4	110,526
CMPRS3	988,416	COND1	84,942
Gas Clean Up	933,688	HX5	83,304
AIRHT	761,707	HX10	82,758
CMPRS1	577,902	COND2	74,150
REFORMER	557,643	HX7	58,734
HT	462,953	B10	57,486
LT	462,953	HX8	49,374
STRIPPER	348,348	HX9	49,017
DIST	306,072	HX6	44,694
HX3	204,126	HX1	27,708
HX2	200,382	FURNACE	26,086
ABSORP	180,726		
Total			13,293,229

Figure 6-6 illustrates the temporal change in net cashflow and NPV over the 20 year lifetime of the process under S:C 4 conditions. The full economic breakdown can be seen in Appendix B, Table A 3 H_2 production process economic study data for S:C 4

. The first year yields an income of £4.6 million from the sale of compressed H_2, along with an abated energetic expense of £158,650 from the diversion of ammonia from the activated sludge process and £157,303 from the RHI. Against a total (first year) expense of £2,978,009, allows for a return on investment during the 8th year of operation in real terms and the 15th year in discounted (NPV) terms.

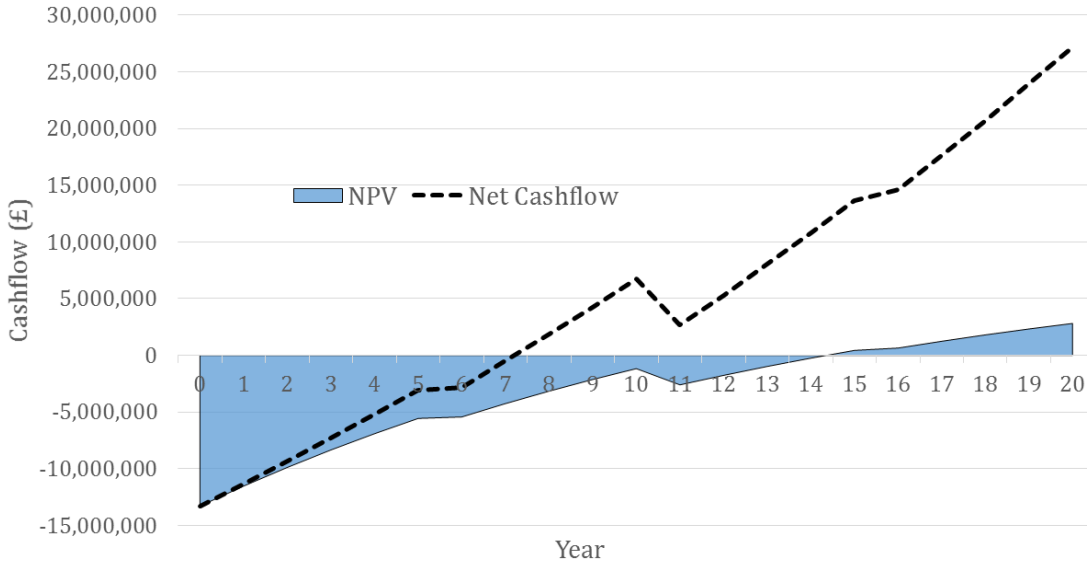

Figure 6-6. SC 4 cash flow and NPV over plant lifetime

After the designated 20 year plant lifetime, a non-discounted profit of £27.2 million can be realised. The NPV analysis has shown that the process could provide £2.8 million more than the desired 10% annual return on investment. Figure 6-7 shows the sensitivity of these profits to changes in a number of model variables. The cost of catalysts, cost of the initial capital investment, the total annual expenditure and the market value of H_2 have all been altered +/- 15% in an attempt to showcase scenarios that represent the uncertainty resulting from the economic analysis methodology.

Figure 6-7 illustrates the impact of altering the market value of H_2 has the most pronounced bearing on the overall profitability and feasibility of process implementation. By decreasing the price of hydrogen by 15% (from £4.50 to £3.83), the non-discounted profit over the plant lifetime decreases by almost £19 million (69%). However, the % impact on the NPV is even more pronounced with a reduction of £7.35 million (261%). Under this scenario, NPV would not turn positive during the plant's 20 year lifetime. In this case, it would be impossible to attract the investors with the knowledge they would not receive their average 10% annual return on investment. Increasing the H_2 value by 15% (to £5.18) has a similar, but reversed, impact increasing the system's profitability by 67% and 254% in non-discounted and NPV terms respectively. This shows how strongly influenced the attractiveness of the process is by the

price of H_2. However, not only is the hydrogen price the most influential variable, it is also the most uncertain one. As discussed previously, the market value could be anywhere between £1.80-11.70 kg^{-1} H_2.

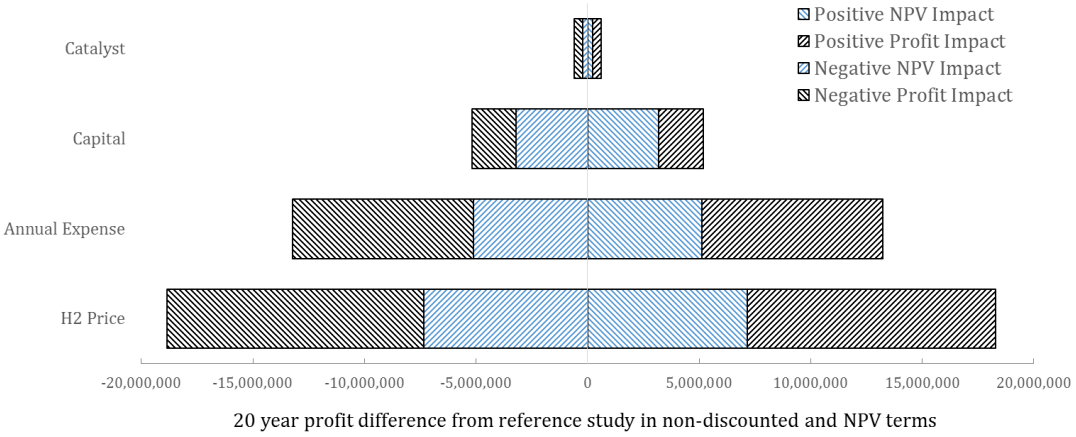

Figure 6-7. Tornado graph showing the results of the sensitivity analysis performed by changing a number of variables by +/- 15 % under S:C 4 process conditions.

Figure 6-7 also shows the total annual expenditure could have considerable influence on the financial viability of process implementation. With a 15% increase in annual costs, the £5.2 million reduction in NPV would mean a positive NPV would not occur during the plant's 20 year lifetime. This would mean investors would not receive the average 10% return dictate in the NPV analysis; considerably reducing the attractiveness of the process. However, if annual expenditure has been overestimated by 15%, then the associated 150% increase in NPV after 20 years of operation would significantly increase the financial outlook. A 15% increase in the estimated initial capital cost would reduce the 20 year NPV by 114% and would not become positive during the plant's lifetime. Meanwhile, a change in the estimated catalyst cost would have a minimal impact on lifetime profitability.

6.4.3.2 Steam:Carbon 3 scenario

Under the S:C 3 scenario, the initial capital investment is £13.01 million, £361,337 less than under the S:C 4 scenario. Figure 6-8 shows the cash flow and annual NPV over the 20 year plant lifetime under S:C 3 conditions. With a slightly lower production of H_2 than under the S:C 4 scenario, the income from compressed H_2 sales drops to £4.5 million in the first year. However, this is countered by a lower total annual expenditure of £2,901,213 (first year) and an RHI income of £142,644 and an equal electricity abatement to the S:C 4 scenario.

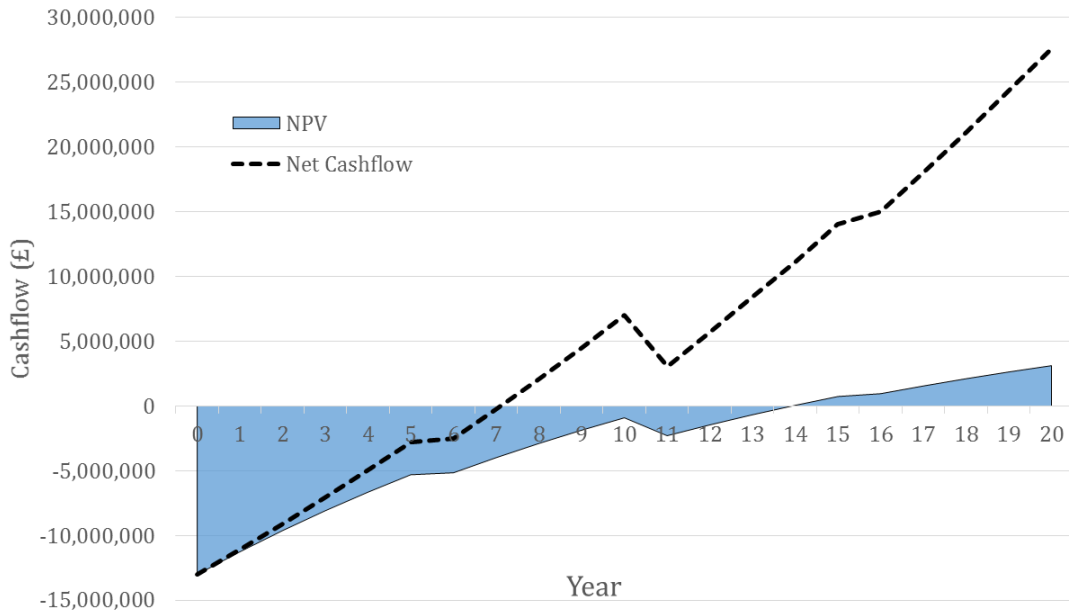

Figure 6-8. S:C 3 cash flow and NPV over plant lifetime

As illustrated in Figure 6-8, the result of the discussed income and expenditure values is a total non-discounted profit of £27.6 million and an NPV of £3.1 million after 20 years of operation. This is over £355,000 more in real terms and £304,000 more in discounted terms compared to the S:C 4 scenario. Figure 6-8 also shows that the payback on the initial investment would occur during the 8th year and would receive a 10% returns on the initial investment (i.e. a positive NPV) during the 14th year; analogous to the S:C 4 scenario.

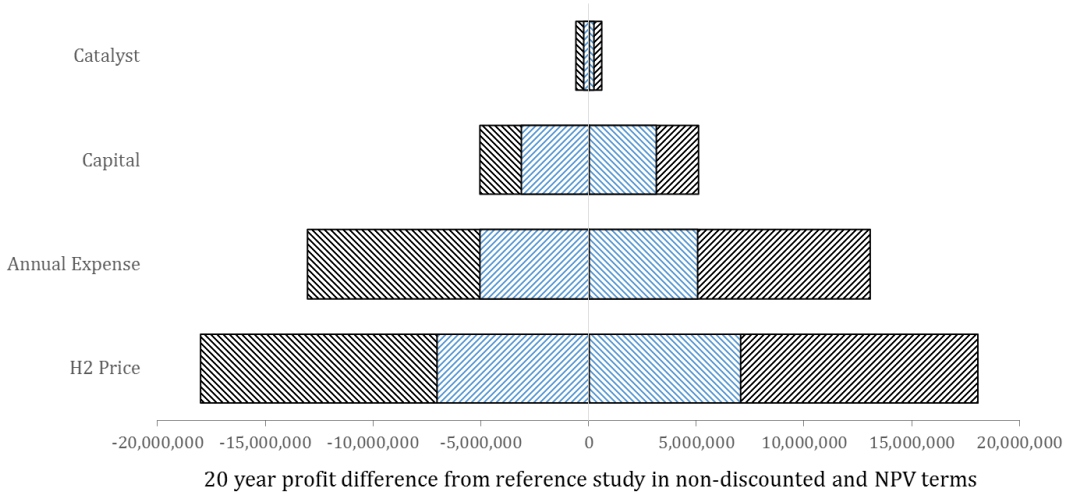

Figure 6-9. Tornado graph showing the results of the sensitivity analysis performed by changing a number of variables by +/- 15 % under S:C 3 process conditions.

Figure 6-9 shows the sensitivity carried out on the economic model for the S:C 3 scenario. The % impact on the profit and NPV is very similar to the associated sensitivity carried out in the S:C 4 scenario. With a H_2 value reduction and annual expense, capital expenditure and catalyst price increase of 15% resulting in a 226%, 163%, 100% and 7% reduction in 20 year NPV respectively. As such, if the estimated value of hydrogen reduces from £4.50 to £3.83, annual expense increases 15% or capital investment increases 15%, then an average annual 10% return on investment cannot be achieved over the 20 year lifetime and would diminish the financial viability of implementing the discussed process.

6.4.3.3 Steam:Carbon 2 scenario

The initial installed cost of the S:C 2 process is the lowest of all three options at £12.53 million. The 952 tonnes of H_2 produced annually under the S:C 2 scenario yield a first year income from sales of £4.28 million. The projected income from RHI has been calculated at £147,468 and electricity abatement equivalent to the other two scenarios. The total (first year) annual expense has been determined as £2,714,393 which is also the lowest of all three considered

scenarios. The result of this is the cash flow and NPV detailed in Figure 6-10 over the plant's lifetime.

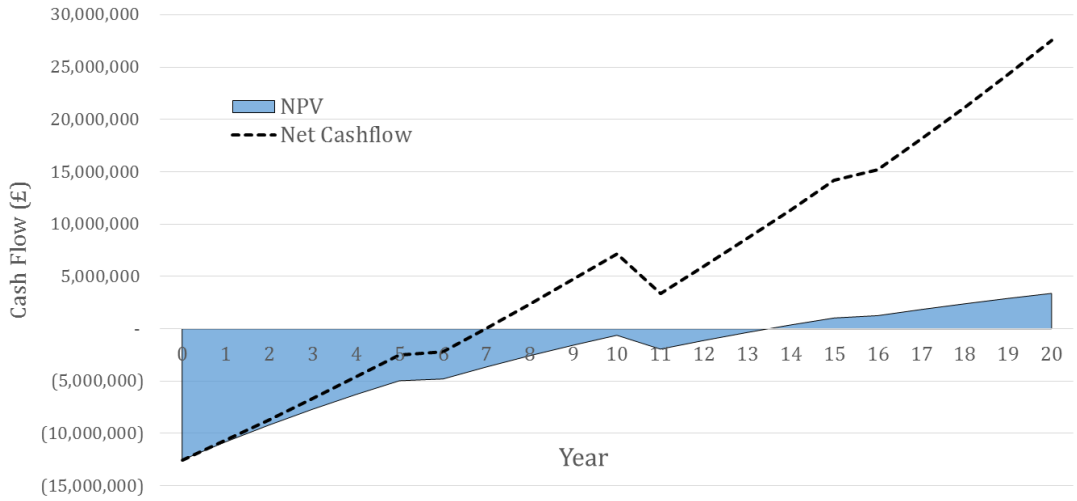

Figure 6-10. S:C 2 cash flow and NPV over plant lifetime

As shown in Figure 6-10, the plant under S:C 2 conditions is projected to end with a final real profit of £26.5 million and an NPV of £3.01 million. Thus, demonstrating the lowest profitability and financial attractiveness of all three scenarios. The plants operating in profit during its 7th year and achieves a positive NPV during the 14th year of operation, as with S:C scenarios 3 and 4. The sensitivity analysis carried out on the S:C 2 financial model showed very similar effects as under the S:C 3 and S:C 4 scenarios with it unable to achieve a positive NPV if the projected H_2 price is lowered, the total annual expense or the initial investment is increased by 15%.

6.4.3.4 Economic analysis general discussion

One of the key outcomes from the economic sensitivity analysis is the influence the market value of H_2 will have on the financial viability of process implementation. Under this uncertainty, it is proposed that it will be difficult to attract investors when a crash in the H_2 market value would diminish the potential for a return on their investment. As such, if 'green hydrogen' is going

to have a significant impact on the UK's transition to a low carbon economy, a controlled market value may need to be put in place akin to the contracts for difference scheme implemented for renewable electricity.

Furthermore, sensitivity analysis carried out on the level of initial capital investment also showed to have a significant effect on the economic feasibility of process implementation. However, a significant proportion (>40%) of the capital investment could be attributed to compression, storage and dispensing (CSD) technology which would facilitate an onsite refuelling station for H_2 fuelled vehicles. As such, there could be an alternative option implemented in the CSD's stead, which would reduce the level of capital investment and improve the financial outlook. It is suggested that this is one area that could be focussed on during future work to clarify whether there are alternative and superior options.

6.5 Wastewater treatment plant energy and GHG emission impacts

The economic analysis has demonstrated that the S:C 3 scenario provides the greatest NPV over the 20 year lifetime of the plant. It is this scenario that will be used for comparative analysis moving forward and has been used to demonstrate the impact on energy and GHG emissions at the reference WWTP. Table 6-12 shows details a breakdown of the power and heat consumption resulting from the proposed introduction of the process at Esholt WWTP.

Table 6-12. Process power and heat consumption for S:C 3 scenario

	Consumption (kWh day^{-1})
Aspen process power consumption	3,888
CSD power consumption	11,234
Gas Clean Up power consumption	5,239
Power abatement from N-diversion	-4,120
Net Power use	16,242
External Heat requirement:	16,071

Table 6-12 shows that although the diversion of ammonia from the ASP facilitates an abatement of 4.1 MWh day^{-1} of electricity. However, this is not enough to counteract the consumption from the process simulated in Aspen Plus, the biogas clean-up and CSD systems. The result of this is the net electricity usage of 16,242 kWh day^{-1} on top of the facility's current power consumption at 60 MWh day^{-1}. The system's external heat requirement is 23,543 kWh day^{-1}, as detailed in Table 6-7 and shown in Table 6-12.

Table 6-13 shows the GHG emissions associated with the potential process introduction at Esholt WWTP. In Chapter 3, it was discussed the estimated N_2O emission factor from Esholt lie at 0.012 kg N_2O N/ kg $TN_{influent}$. The abatement of emissions from the facility's ASP enabled from the diversion of ammonia totals at 3,222 kg day^{-1}, using an N_2O GWP emission factor of 298 times that of CO_2 over a 100 year period. If the H_2 is to be used as a bus transportation fuel, the abated emissions are also shown in Table 6-13. Calculated via a H_2 requirement of 9 kg per 100 km [308] and an emission factor of 1,193 g per km travelled [309].

Table 6-13. System GHG emissions for the S:C 3 scenario

	Emissions (kg CO_2e day^{-1})
ASP abatement	-3,222
Electricity lifecycle emissions	1,738
Heat lifecycle emissions	4,944
Bus transport emission abatement	-14,056
Total (kg CO_2e day^{-1})	-10,596

As shown in Table 6-13, the additional use of grid electricity with a carbon intensity of 107 gCO_2e kWh^{-1} [294], is expected to increase the lifecycle emissions of the plant by 1,738 kg CO_2e day^{-1}. Whilst, the net heat requirement, with a carbon intensity of 210 gCO_2e kWh^{-1} [310], is estimated to contribute an extra 4,944 kg CO_2e day^{-1} to the lifecycle GHG emissions of a plant of Esholt's size. This would result in a net emission of 3,460 kg CO_2e day^{-1} which is

equivalent to 1.25 kg CO_2e per kg of H_2 produced. Therefore, until the gas and electricity grids in the UK are decarbonised, the production of hydrogen via this method will not be entirely 'green'. However, the abatement of CO_2 emissions from bus transport would be 14,056 kg CO_2 per day. As such, Esholt WWTP's associated lifecycle emissions would reduce by 10,596 kg CO_2 day^{-1}.

6.6 Conclusions

In this Chapter thorough process modelling and economic analysis studies have been performed to demonstrate the technical and financial feasibility of implementing this novel method of H_2 production at Esholt WWTP. The sensitivity analysis carried out on the operating temperature of the primary reformer has detailed the effect on both H_2 production potentials and systematic thermal transport to meet the demands of the air stripping unit. It was found that it was worthwhile committing to the maximum temperature of 1,000 °C under each of the S:C 2, 3 and 4 scenarios which, although meant spending external energy to meet the air stripper's heat demand, this was trumped by the additional production of hydrogen from a chemical energy point of view.

Further process modelling analysis detailed the contribution of ammonia decomposition to hydrogen production from the primary reformer at 7.2%, 7.5% and 7.9% under S:C 4, S:C 3 and S:C 2 scenarios respectively. It also detailed the overall impact of S:C ratio on system hydrogen production with higher S:C ratios providing a greater H_2 production potential at 117 kg h^{-1}, 115 kg h^{-1} and 109 kg h^{-1} for S:C scenarios 4, 3 and 2 respectively. On the other hand, it was also shown that the system's net production of heat had an inverse relationship with the S:C ratio at 9.6 MWh day^{-1}, 10.1 MWh day^{-1} and 15 MWh day^{-1} for S:C scenarios 4, 3 and 2 respectively.

The economic analysis showed that the S:C 3 scenario resulted in the greatest return for investors with a positive NPV of over £3.1 million after 20 years of operation. This showcases the balance struck between H_2 production potential and the additional energetic cost of its facilitation. The economic sensitivity

analysis carried out demonstrated the overwhelming impact of the market price of H_2 on the financial viability of process implementation. It showed that with just a 15% reduction on the quoted market value of £4.50 kg^{-1} H_2 led to a bleak economic outlook for the process implementation. On the other hand, a 15% increase on the proposed market value more than doubled the end-of-life NPV.

The production of hydrogen via the discussed process was found to have a significant potential impact on the electricity consumption of the referenced WWTP, increasing it by 16.2 MWh day^{-1} or 20% of its current use. Much of this power demand can also be attributed to the operation of CSD equipment. Meanwhile the proposed introduction of the process was also found to increase the facility's heat demand by 16 MWh day^{-1}. It was also found that the introduction of the process would decrease lifecycle GHG emissions by 10,596 kg CO_2 day^{-1}.

7 Experimental Feasibility of Bio-H_2 Production from AD-generated NH_3 and CH_4 using combined catalytic cracking and steam reforming.

7.1 Background and Introduction

This chapter focusses on the experimental analysis of the potential for combined steam methane reforming (SMR) and ammonia decomposition in a single packed-bed reactor. In Chapter 6, the production of H_2 was studied from a theory-based equilibrium stand-point. The work carried out in this chapter, however, assesses whether equilibrium yields and conversions can be replicated under experimental conditions, or how close practical outputs come to their predicted counterparts.

Catalytic ammonia decomposition occurs via an initial adsorption of ammonia onto the catalyst's active site surface. The ammonia can then undergo successive N-H bond cleavage, releasing hydrogen atoms which combine to make H_2 [153,154]. The final mechanistic stage is the rate-limiting recombinative desorption of nitrogen adatoms to molecular N_2 [153]. Ni-based catalysts (in their reduced metallic form) are generally considered the second most effective (active) catalysts for ammonia decomposition, bettered only by Ruthenium (Ru) [153,154]. However, Ru is an extremely expensive and rare transition metal, making Ni a far more attractive option commercially, if used in fixed bed configuration.

Industrial catalytic steam reforming of hydrocarbons has been carried out for decades to produce hydrogen, ironically, often with the aim of ammonia synthesis [311]. Ru – based catalysts have also been promoted as having the highest activity for steam methane reforming [312]. However, inexpensive Ni catalysts are the most popular in industry, often supported on alumina (Al_2O_3), ceramic magnesium aluminate ($MgAl_2O_4$), cerium oxide, (CeO_2), zirconium oxide (ZrO_2) and silicon dioxide (SiO_2) [297].

As far as this author is aware, there has been no prior experimental work using packed-bed reactors that combine the decomposition of ammonia with the steam reforming of methane. However, there are a number of researchers that have combined the two processes using anodes of solid oxide fuel cells such as Wang et al. [156] and Xu et al. [157]. However, Rollinson et al. [313] examined the use of a urea solution and of aqueous ammonia in a packed-bed reactor that simultaneously reformed the urea and cracked the intermediate or feed ammonia.

7.2 Experimental Rig and Equipment Description

Figure 7-1 and **Figure 7-2** show the bench-scale rig used for the combined ammonia decomposition and steam methane reforming experiments. Three forms of compressed gases are connected to the rig: methane, nitrogen gas and a 5 vol.% H_2/95 vol.% N_2 mix. The flow of each gas is controlled by MKS (US) mass flow controllers. They work via a fast response proportioning valve which adjusts to the required flow depending on the feedback from internal thermal sensors. The gases are passed through electrical pre-heaters before entrance into the reactor. Liquid feedstock (water or aqueous ammonia) is supplied to the system via a 20 ml BD Plastipak (US) syringe with a stainless steel Luer lock needle via a New Era Pump System Inc (US) (model NE-1000). The liquid also passes through a second preheater set at 150°C to vaporise before entrance to the reactor. Heating tape has been used to aid the maintenance of temperature between the base of the preheaters and the reactor. Much of the rig has been insulated to prevent thermal losses as much as possible.

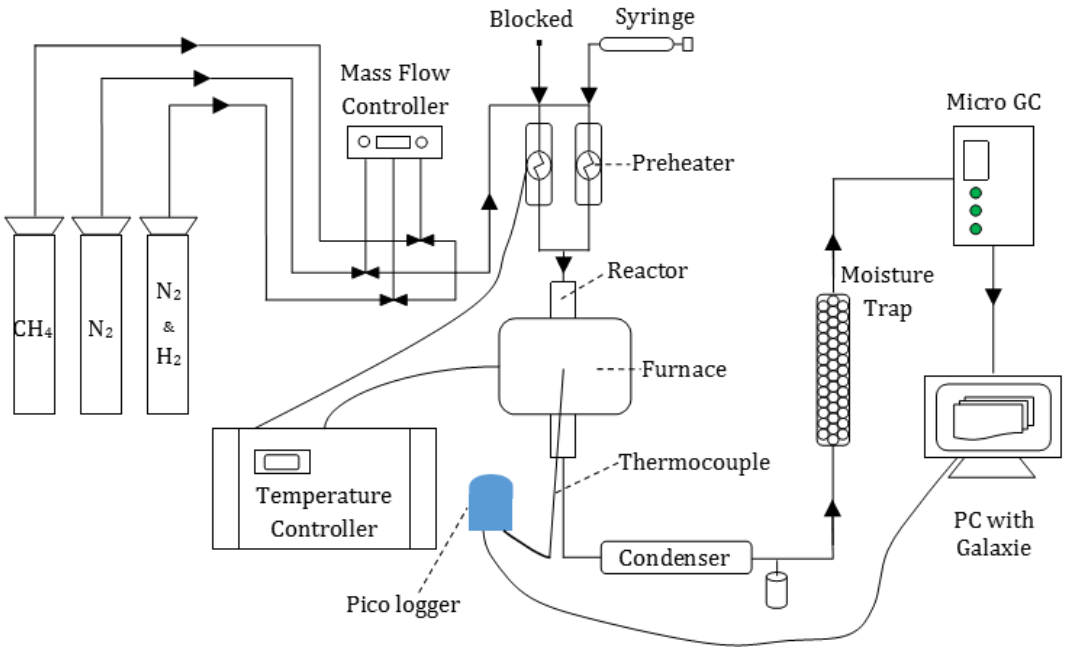

Figure 7-1 Schematic of experimental rig

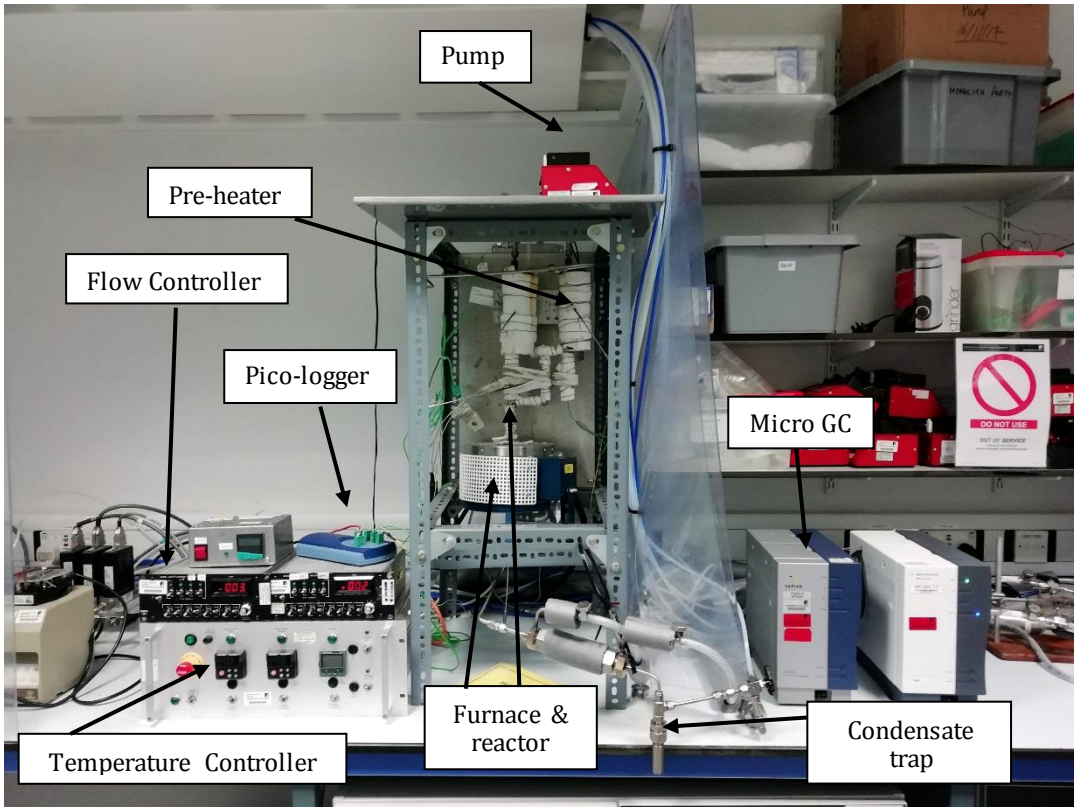

Figure 7-2. Image of rig set up

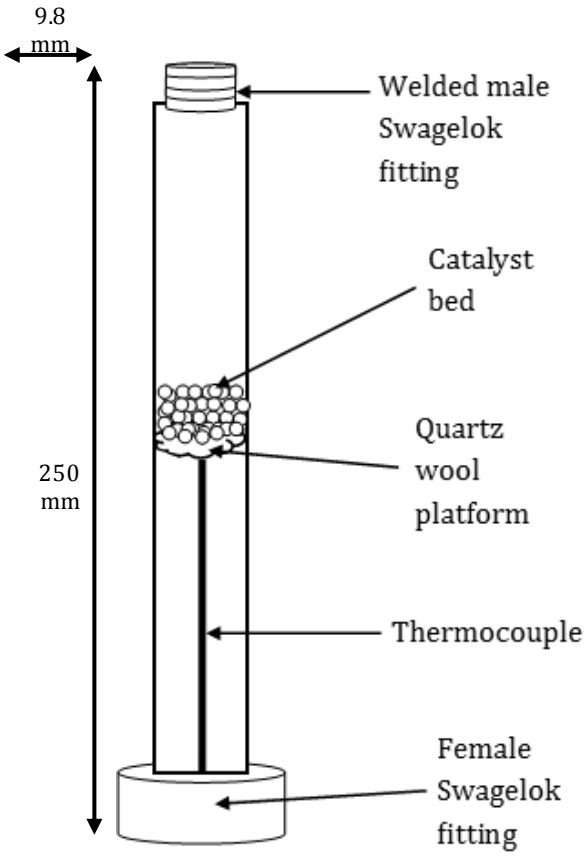

Figure 7-3 Diagram of reactor internal layout. Internal diameter 9.8 mm, length 250 mm.

The reactor is made of a 316 stainless steel tube with an internal diameter of 9.8 mm. The reactor is positioned inside an electric tube furnace (Elite Thermal Systems (UK) TSV10/20/85) which provides the resistive heating to reach the desired reactor temperature. The internal temperature is monitored via a thermocouple connected to a pico-logger console in communication with a PC. Figure 7-3 shows the internal layout of the reactor tube. The thermocouple reaches roughly half way up the tube and provides a support in which a bed of 4 µm quartz wool sits. The quartz wool, in turn, provides a semi-permeable and non-reactive platform in which the powder catalyst can sit.

The outlet from the reactor is fed into a stainless steel condenser which cools the product using a counter-flow of (30 vol. %) ethylene glycol/(70 vol. %) water cooling liquid originating from a Fisher Scientific (US) 3016S chiller set at -2°C. A stainless steel condensate trap is located after the condenser and can be detached in order to remove and store any condensate generated.

Downstream of the condenser, a stainless steel moisture trap, filled with silica gel beads, facilitates the removal of all moisture from the syngas to ensure only a dry gas enters the micro gas chromatograph (GC).

The micro GC utilised is a Varian (US) CP 4900 and provides compositional analysis of the dry product gas from the reactor. It contains two thermal conductivity detectors (TCD) and two columns. The first is a Molecular Sieve 5A plot column and is calibrated to detect the following gases: H_2, O_2, N_2, CH_4 and CO. The second is a Pora Plot Q column which is calibrated for measurement of CO_2, CH_4, C_2H_6, C_2H_4, C_3H_8 and C_3H_6 gas concentrations. The micro GC utilises argon as its carrier for both columns. The comparatively fast run-time of just over 3 minutes makes it more appropriate for continuous sampling than many other conventional multi-species gas analysers.

The micro GC directly communicates with Galaxie™ chromatography data system software from Varian, Inc. The program facilitates shifts between Shutdown, Backflush and Conditioning in a safe and gradual manner. During sampling, the Backflush method operates with a column temperature of 100°C and a pressure of 100 kPa. Over short periods without use (e.g. overnight) the conditioning method is used and increases the column temperature to 180°C, which removes any moisture that may have entered and aids column preservation. For longer periods of time the 'shut-down' method is used and slowly cools the column temperature to ambient ones. The Galaxie program is also operated for calibration of the micro GC. Calibration plots for known gas compositions are loaded so that unknown gas compositions can be accurately measured. The known gas mixtures used for calibration can be seen in Table 7-1. Furthermore, chromatograms are generated in the Galaxie program to be downloaded and prepared for analysis.

Table 7-1 Calibration gas mixtures used for GC calibration in mol %

Mixture 1	CH_4	2.02	%
	CO	4.93	%
	CO_2	15.04	%
	H_2	29.24	%
	N_2	48.77	%
Mix 2	CO	5.1	%
	N_2	94.9	%
Mix 3	H_2	79.5	%
	N_2	20.5	%
Mix 4	CH_4	5.04	%
	CO	10.00	%
	CO_2	4.79	%
	H_2	10.22	%
	N_2	69.95	%

7.3 Catalyst Preparation

A commercial grade 18 wt% NiO/α-Al_2O_3 obtained from Twigg Scientific & Technical Ltd (UK) has been used for each experiment reported in this chapter. In order to prepare for the packed-bed reactor, the pellets were crushed using a pestle and mortar and sieved to a diameter range between 150-250 μm.

Figure 7-4 18wt% NiO/AL_2O_3 catalyst before (left), after crushing (middle) and spent catalyst (right)

7.4 CHN analysis

In order to assess the amount of carbon deposition occurring on the catalyst for each experiment, analysis was carried out using a Thermo Scientific (US) Flash 2000 Elemental Analyzer. The equipment contains a thermal conductivity detector (TCD) which is able to determine elemental weight % of carbon, hydrogen and nitrogen. As such, it is colloquially termed 'CHN'. Spent catalysts were prepared by crushing to make a homogenous sample, weighed to between 15-18 mg, duplicated and placed in small tin capsules. The tin capsules were folded to remove trapped air. The samples were then dropped into the analyser's high temperature furnace (1000-1800 °C). The oxygen-rich atmosphere facilitates the combustion of any carbon, hydrogen and nitrogen to CO_2, H_2O, and NOx which are swept through the furnace via a helium carrier gas. The combustion gases are separated in a gas chromatography column before the TCD measures the mass fraction of C, H and N. High quality calibration using known standards provides assurances on the quality of the output data.

Samples were tested in duplicate and the raw CHN data was converted to usable data by taking the mean of the duplicates. The data is read as a wt% of solid sample so were converted to mass of deposited carbon using the mass of catalyst used in the experiment. A carbon deposition rate per hour could then be calculated using the total duration of the experiment (t_{exp}) and knowledge of feed rate of carbon from the CH_4 source.

7.5 Ammonia analysis

Condensate ammonium analysis was carried out using a Hach (US) AP3900 Laboratory Robot with Hach (US) LCK 303 ammonium calorimetry cuvettes. The analysis was able to measure concentrations within the range of 2-47 mg l^{-1}. The LCK 303 test works by the principle that ammonium ions react at pH 12.6 with hypochlorite ions and salicylate ions in the presence of sodium nitroprusside as a catalyst to form indophenol blue. Calorimetry analysis is

then performed to determine the extent of indophenol blue generation and therefore the implied ammonium concentration of the sample.

Some initial tests were carried out to show the required dilution of samples for concentrations to fall within the detection range. It was found that runs at molar feed steam to carbon ratios (S:Cs) of 2 and 3 in the reformer required a dilution factor of 100 and S:C 4 runs needed a dilution of 10. Sample dilution and preparation was carried out in a fume cupboard where pipettes were used to create 1:9 volume ratios of condensate : deionised water. At this point, the samples obtained from S:C 4 reformer runs were ready with a dilution factor of 10. However, the already diluted samples from S:C 2 and S:C 3 runs underwent another 1:9 volume dilution to facilitate an overall dilution factor of 100. Samples were prepared in duplicate. The automated AP3900 Laboratory Robot proceeded with sample analysis under an automated function, eliminating the chance of human error.

The raw data from the cuvette tests were reported as NH_4-N mg l^{-1} and reconverted to an undiluted concentration via multiplication of their respective dilution factors. The concentrations were then converted to a molar flow of NH_3 using the equations 7-1 to 7-3:

$$\dot{n}_{NH_3-N,condensate} = \mathrm{M}_{\mathrm{NH_3}} \left(\frac{\rho_{NH_3-N,condensate} \times \dot{V}_{H_2O,condensate} \times t_{exp}}{m_{NH_3-N}} \right) \quad \textbf{7-1}$$

$$\dot{V}_{H_2O,condensate} = \frac{\mathrm{M}_{\mathrm{H_2O}} \left(\dot{n}_{H_2O,in} - \dot{n}_{H_2O,destructed} \right)}{1000} \quad \textbf{7-2}$$

$$\dot{n}_{H_2O,destructed} = \dot{n}_{CO,out} + 2\dot{n}_{CO_2,out} \quad \textbf{7-3}$$

where, $\dot{n}_{NH_3-N,condensate}$ is the calculated molar flow (mol h^{-1}) of NH_3 in the experiment's condensate; $\mathrm{M}_{\mathrm{NH_3}}$ is the molar mass of NH_3 (g mol^{-1}); $\rho_{NH_3-N,condensate}$ is the mass concentration of NH_3-N from the Hach (US) LCK 303 analysis (dilution adjusted) (g l^{-1}); $\dot{V}_{H_2O,condensate}$ is the expected volume flow of water in the condensate (l h^{-1}); t_{exp} is the duration of the experiment

(h) or 'time on stream'; M_{H_2O} is the molar mass of H_2O (g mol^{-1}); $\dot{n}_{H_2O,in}$ is molar flow of water into the reactor (mol h^{-1}); $\dot{n}_{H_2O,destructed}$ is the molar destruction rate of H_2O via the SMR and WGS reactions (mol h^{-1}); $\dot{n}_{CO,out}$ is the molar flow of CO produced as determined from the micro GC (mol h^{-1}) and $\dot{n}_{CO_2,out}$ is the molar flow of CO_2 produced as determined from the micro GC (mol h^{-1}). The calculation table of results from the ammonia analysis can be seen in Appendix C, Table A 5.

7.6 Experimental Procedure

Each experiment began with switching on the chiller, set to -2°C and flushing the rig with N_2. Crushed catalysts were weighed out to a weight hourly space velocity (WHSV) of 2 h^{-1}. WHSV is defined as the mass rate of feed to the reactor per hour divided by the mass of catalyst (including support). 0.09 g of quartz wool was weighed and placed in the reactor on top of the thermocouple, as shown in Figure 7-3. The distance of the top of the quartz wool plug from the top of the reactor was measured before the catalyst was placed in the reactor. The distance of the top of the catalyst bed from the top of the reactor was then measured so that the gas hourly space velocity (GHSV) could be determined. GHSV is defined as the total volumetric flow rate under standard conditions (25°C and 1 atm) divided by the volume of catalyst bed (including inter particle and pore voids).

The rig was tested for leaks by flowing 200 ml min^{-1} of N_2 through the system and checking the flow rate downstream at various points using an Agilent Technologies (US) ADM1000 flowmeter. When the chiller reached the desired temperature, the furnace was switched on and the temperature adjusted until the reactor's internal temperature reached 650 °C, whereby the catalyst could be later reduced upon switching the N_2 flow to a reducing flow. The furnace temperature needed to be set roughly at 50 °C greater than the desired reactor temperature due to heat loss between the reactor and furnace walls. Catalyst reduction achieving the conversion of catalytically inert NiO to the catalytically active Ni form was then carried out by switching the N_2 flow to 200 ml min^{-1} of

a 5/95 vol% H_2/N_2 mixture. The micro GC was used to monitor the gaseous outlet and informed on the end of the reduction process when H_2 concentration reached the initial 5 vol%. After catalyst reduction, the system was flushed with N_2 until no traces of H_2 were read by the micro GC.

The furnace temperature was then adjusted to reach the desired experiment temperature and the pre-heaters switched on. The flow of the ammonia solution was set to the desired flow at the syringe pump and 40 ml min^{-1} of N_2 and 21.6 ml min^{-1} of methane were set. The ammonia solution was prepared using a 25 wt% ammonia solution from Fischer Scientific, diluted with deionised water in the ratios displayed in Table 7-2. The amount of ammonia required for S:C ratios 2, 3 and 4 was dictated by ammonia recovery potentials discovered during Aspen Plus process modelling. The quantity is slightly different to those reported in Chapters 3, 4 and 5 as the data were taken from previous models that were improved upon. The samples were prepared in a fume cupboard using pipettes and measured via mass displacement using an analytical balance. The ammonia solution had a density of 0.91 g ml^{-1} which was used to calculate the volume flow required for the prepared ammonia solution.

Table 7-2. Required flow of ammonia solution and deionised water

S:C	Ammonia solution mass flow (g hr^{-1})	Required additional water (g h^{-1})	Total liquid flow rate (ml hr^{-1})
2	0.505	1.531	2.086
3	0.529	2.468	3.049
4	0.559	3.400	4.014

The syringe pump was turned on before the methane feed to prevent methane decomposition occurring. Real time thermocouple data indicated when the ammonia solution entered the reactor because a slight drop in temperature could be seen. At this point, the methane feed was turned on and analysis begun.

After around 50 micro GC sample runs, the experiment was stopped and everything turned off except for the chiller and the N_2 flow, which was

increased to 200 ml min^{-1} in order to flush the rig of all syngas. After two hours, the condensate could be removed and stored in a 10 ml glass vial and placed in the refrigerator to help preserve any remaining ammonium. The reactor was then dismantled and spent catalyst from each experiment was placed in a 10 ml glass vial for CHN analysis.

Equations 7-4 to 7-8 detail the key reactions involved in the experiments. The reader should be familiar with reactions 7-4, 7-5 and 7-8 which detail the SMR, WGS and ammonia decomposition reactions respectively. Reactions 7-6 and 7-7 describe the two main methods in which carbon formation can occur during steam reforming of methane; namely methane decomposition and the Boudouard reaction respectively.

$CH_4 + H_2O$	⇆	$CO + 3H_2$	$\Delta \mathbf{H_{298}} = +\mathbf{206\ kJ\ mol^{-1}}$	**7-4**.
$CO + H_2O$	⇆	$CO_2 + H_2$	$\Delta \mathbf{H_{298}} = -\mathbf{41\ kJ\ mol^{-1}}$	**7-5**.
CH_4	⇆	$C + 2H_2$	$\Delta \mathbf{H_{298}} = \mathbf{75\ kJ\ mol^{-1}}$	**7-6**.
$2CO$	⇆	$C + CO_2$	$\Delta \mathbf{H_{298}} = -\mathbf{172\ kJ\ mol^{-1}}$	**7-7**.
$2NH_3$	⇆	$3H_2 + N_2$	$\Delta \mathbf{H_{298}} = +\mathbf{92\ kJ\ mol^{-1}}$	**7-8**.

At the temperature profile utilised in the experiments discussed in this chapter (700-800 °C), given the reaction enthalpy and kinetics discussed in literature such as Hou & Hughes [314] any carbon formed on the catalyst is expected to arise via methane decomposition (reaction 7-6) but reaction 7-7 may occur in the flow prior to contacting with the catalyst in the lower temperature regions of the reactor.

7.7 Output analysis

The micro GC produces compositional results in specie molar fractions. Ordinarily, the known flow of inert N_2 into the rig would act as a reference so

that flows of other product gases can be inferred. However, although the mole fraction of N_2 is measured, because the decomposition of ammonia also generates N_2, the output flow of N_2 is unknown as it requires knowledge of the total gaseous molar outflow. It was also found that the quantity of ammonia held in the initial feedstock did not remain constant, volatilising over time. As such a method of 'contribution analysis' was employed to determine product yields using equation 7-9 representing the nitrogen elemental balance:

$$\dot{n}_{x(out)} = \frac{\dot{n}_{N_2(in)} + \dot{n}_{N_2(speculative\ NH_3 decomp)}}{y_{N_2(out)}} \times y_{x(out)} \qquad 7\text{-}9$$

where, $\dot{n}_{x(out)}$ is the molar flow of specie x from the reactor, $\dot{n}_{N_2(in)}$ is the known molar flow of N_2 into the reactor, $\dot{n}_{N_2(speculative\ NH_3 decomp)}$ is the speculative quantity of N_2 arising from ammonia decomposition, $y_{N_2(out)}$ is the mole fraction of N_2 given by the micro GC and $y_{x(out)}$ is the mole fraction of specie x given by the GC.

The speculative quantity of NH_3 decomposition was altered between 5% and 100% of its potential to provide hypothetical specie molar flows via equation 7-9. It was put forward that three key reactions were occurring in the reactor: SMR (7-4), WGS (2-14) and NH_3 decomposition (2-18). Stoichiometry dictates that for each mole of CO generated there would be three moles of H_2 and for every mole of CO_2 generated there would be 4 moles of H_2; stipulating equation 7-10 for the production of H_2 from SMR and WGS reactions:

$$\dot{n}_{H_2(SMR\ \&\ WGS\ contribution)} = 3\dot{n}_{CO} + 4\dot{n}_{CO_2} \qquad \textbf{7-10}$$

H_2 production via the contribution of SMR and WGS ($\dot{n}_{H_2(SMR\&\ WGS\ contribution)}$) was calculated for runs with and without ammonia. Doing this enabled the difference in H_2 produced from SMR and WGS reactions to be calculated between runs with and without ammonia present ($\Delta\dot{n}_{H_2(contribution)}$). Equation 7-11 essentially normalises the difference in H_2 production so that the

contribution of ammonia decomposition to H_2 production can be inferred. Equation 7-11 makes the assumption that the contribution to H_2 production via methane decomposition (reaction 7-6) is negligible in comparison to those of reactions 7-4 and 7-5. This assumption will be checked retrospectively upon quantification of the carbon measured on the catalyst and expressed as amount of solid carbon product per amount of carbon fed as CH_4.

$$\dot{n}_{\mathrm{H_2\,(NH_3}\,decomp)} = \Delta\dot{n}_{\mathrm{H_2}(out)} - \Delta\dot{n}_{H_2\,(contribution)} \qquad 7\text{-}11$$

$\Delta\dot{n}_{\mathrm{H_2}(out)}$ describes the difference between $\dot{n}_{\mathrm{H_2}(out)}$ with and without the presence of ammonia. Resultantly, $\dot{n}_{\mathrm{H_2(NH_3}decomp)}$ describes the speculated quantity of H_2 generated from ammonia decomposition (equation 7-11). During ammonia decomposition, for every mole of N_2 generated, 3 moles of H_2 are produced. As such, the true $\dot{n}_{\mathrm{H_2(NH_3}decomp)}$ was determined from the sensitivity analysis when it equalled three times that of $\Delta\dot{n}_{\mathrm{N_2(out)}}$.

7.8 Equilibrium Modelling

Equilibrium modelling was carried out in Aspen Plus V8.8 with equivalent inputs as carried out experimentally. A single equilibrium (RGibbs) reactor was employed to replicate the lab set up. The pressure was set to 1 atm and the temperature was varied between 200°C and 900°C. The inputs can be seen in Table 7-3.

Table 7-3. RGibbs reactor inputs in moles h^{-1}

Description	H_2O (moles h^{-1})	NH_3 (moles h^{-1})	CH_4 (moles h^{-1})	N_2 (moles h^{-1})
S:C 2 no NH_3	0.108	-	0.054	0.100
S:C 2 with NH_3	0.108	0.0076	0.054	0.100
S:C 3 no NH_3	0.162	-	0.054	0.100
S:C 3 with NH_3	0.162	0.0081	0.054	0.100
S:C 4 no NH_3	0.216	-	0.054	0.100
S:C 4 with NH_3	0.216	0.0087	0.054	0.100

Figure 7-5 displays the syngas output from equilibrium modelling of H_2 and CH_4 with and without NH_3 in the feed, under S:C 2, 3 and 4 reforming conditions. H_2 yields peaked at 780°C, 725°C and 695°C for S:C of 2, 3 and 4 respectively. This provides adequate justification of the chosen temperature range examined in the laboratory between 700 °C and 800 °C. Figure 7-5 also shows the methane conversion is influenced by the presence of ammonia at lower temperatures, much more than at higher temperatures. This is because at lower temperatures ammonia decomposition is thermodynamically stronger than SMR. As such, the H_2 from ammonia decomposition shifts the SMR equilibrium backwards, limiting CH_4 conversion.

Furthermore, equilibrium modelling indicated that at 200 °C, over 90% of the ammonia would convert to H_2 under decomposition at equilibrium. Between 700 °C and 800 °C, over 99% of ammonia decomposed in each equilibrium simulation. The influence of this can be seen in Figure 7-5 with the greater yields of H_2 yields compared to runs in the absence of ammonia. Equilibrium modelling indicated no solid carbon as equilibrium product in the conditions monitored. Further results from the equilibrium modelling will be detailed later in the chapter with reference to the experimental results.

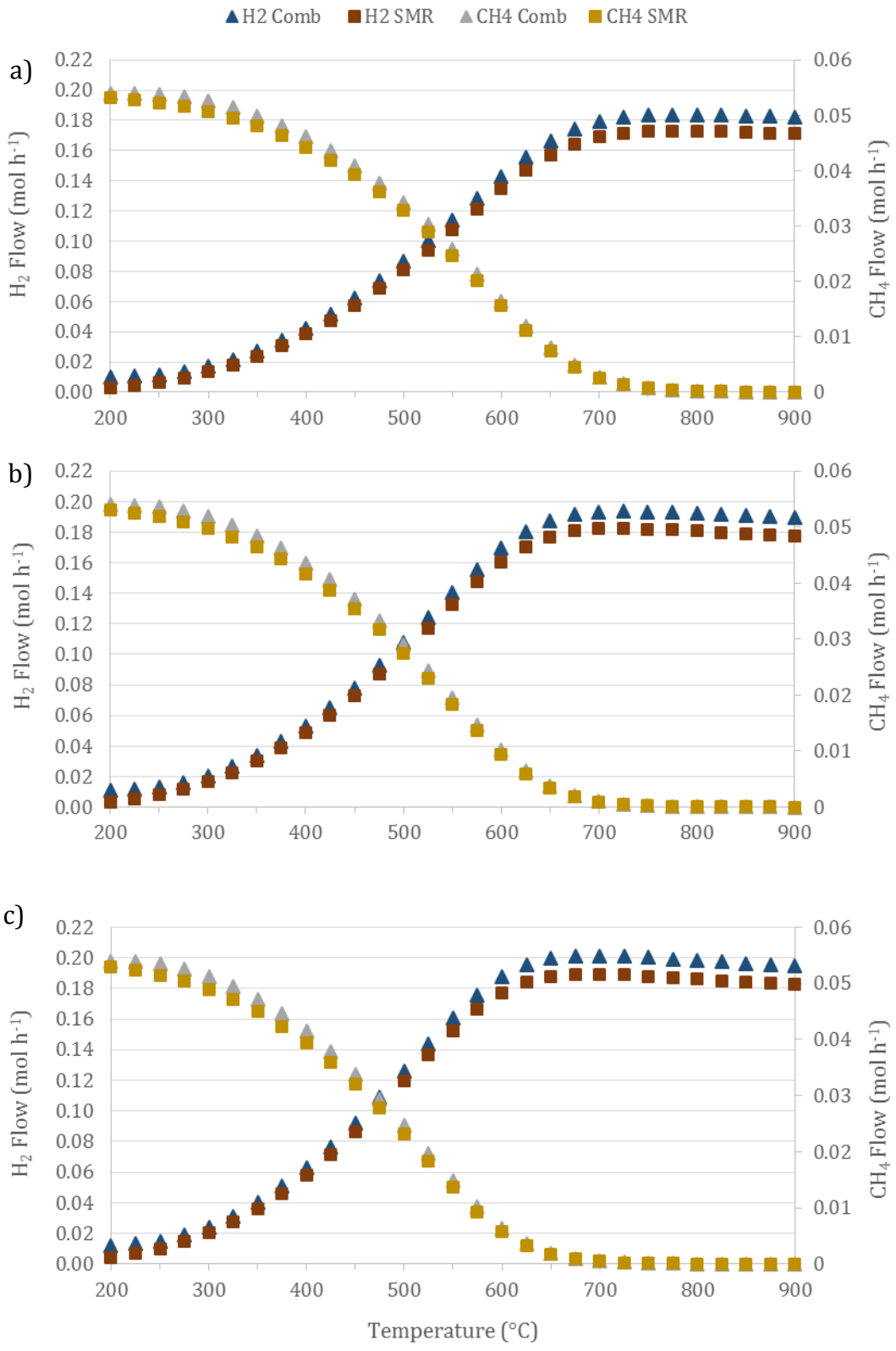

Figure 7-5 (a-c). Graphs detailing the equilibrium syngas flows of H_2 and CH_4 between temperatures 200°C and 900°C and runs with ammonia (labelled 'Comb' for 'combined') and without (labelled 'SMR'). a) S:C 2 conditions, b) S:C 3 conditions, c) S:C 4 conditions

7.9 Experimental Results and Discussion

7.9.1 Syngas Composition

Figure 7-6 illustrates an example of the raw micro GC data over time with results from a SMR test at 700°C and a S:C ratio of 4. It shows that the SMR reaction occurs quickly with a rapid increase of CO and H_2 in mole fraction at the start of the experiment. However, it takes over 10 consecutive sample detections for the mole fraction of CO_2 to increase to a point where it is relatively stable (steady state). This analysis has been carried out for each experiment so that an average for the specie mole fraction can be taken from when the steady state was reached.

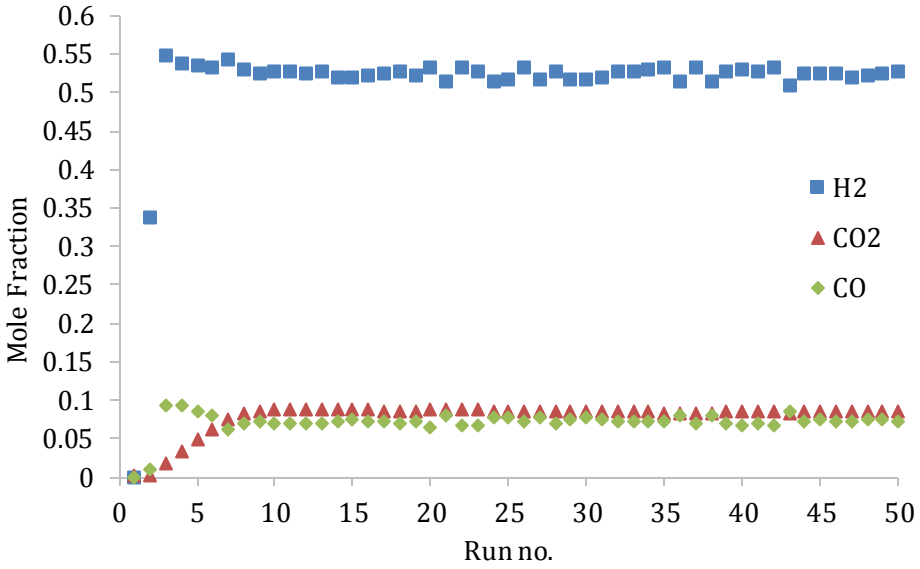

Figure 7-6. Raw GC data example a run without ammonia at S:C 4 and 700°C

Figure 7-6 also illustrates the very slight variation occurring over time in the production of H_2, CO_2 and CO. It is speculated that this occurs due to the intermittent flow of water from the syringe. This happens because the relatively low flow-rate causes the outlet from the syringe to drip, rather than flow continuously. As such, there are periods when there is slightly more and periods where there is slightly less steam in the reactor to facilitate SMR and WGS reactions. However, the standard deviation of H_2 and CO from run 13 (of the experiment displayed in Figure 7-6) is just 0.006 and 0.004 respectively. As

such, it can be stated that the flow intermittency does not have a significant impact on the results. Over three hours of standard operation there were no key signs of catalyst deactivation for any of the experiments. Each experimental condition underwent two experiments and the most stable of each was chosen for further analysis.

7.9.1.1 Hydrogen production and reactants conversion at S:C 2

Figure 7-7 presents the mean flow rates of key species in the syngas when comparing runs with and without ammonia, both experimentally, alongside the calculated equilibrium equivalent. The most obvious differences that can be seen are with H_2 production rates between the experimental (lower) and equilibrium data (higher). This is the case for a number of reasons. Foremost, the experimental methane conversion was not as significant as predicted via equilibrium investigation. For example, at 700 °C the equilibrium model yielded unconverted-CH_4 flow rates in the syngas of 0.0026 mol h^{-1} and 0.0028 mol h^{-1} for runs without and with ammonia respectively compared to 0.0041 mol h^{-1} and 0.0049 mol h^{-1} respectively in the experimental runs. As such, comparatively less H_2 was generated via the SMR reaction.

Figure 7-7 also shows that the CO_2 generation during the experiments was 23.6% and 13.9% less than the equilibrium equivalent during runs without and with feed ammonia respectively. This also explains the comparative lower production of H_2 generated via WGS experimentally. On average, there was 17% less H_2 generated experimentally under S:C 2 conditions than predicted by equilibrium analysis.

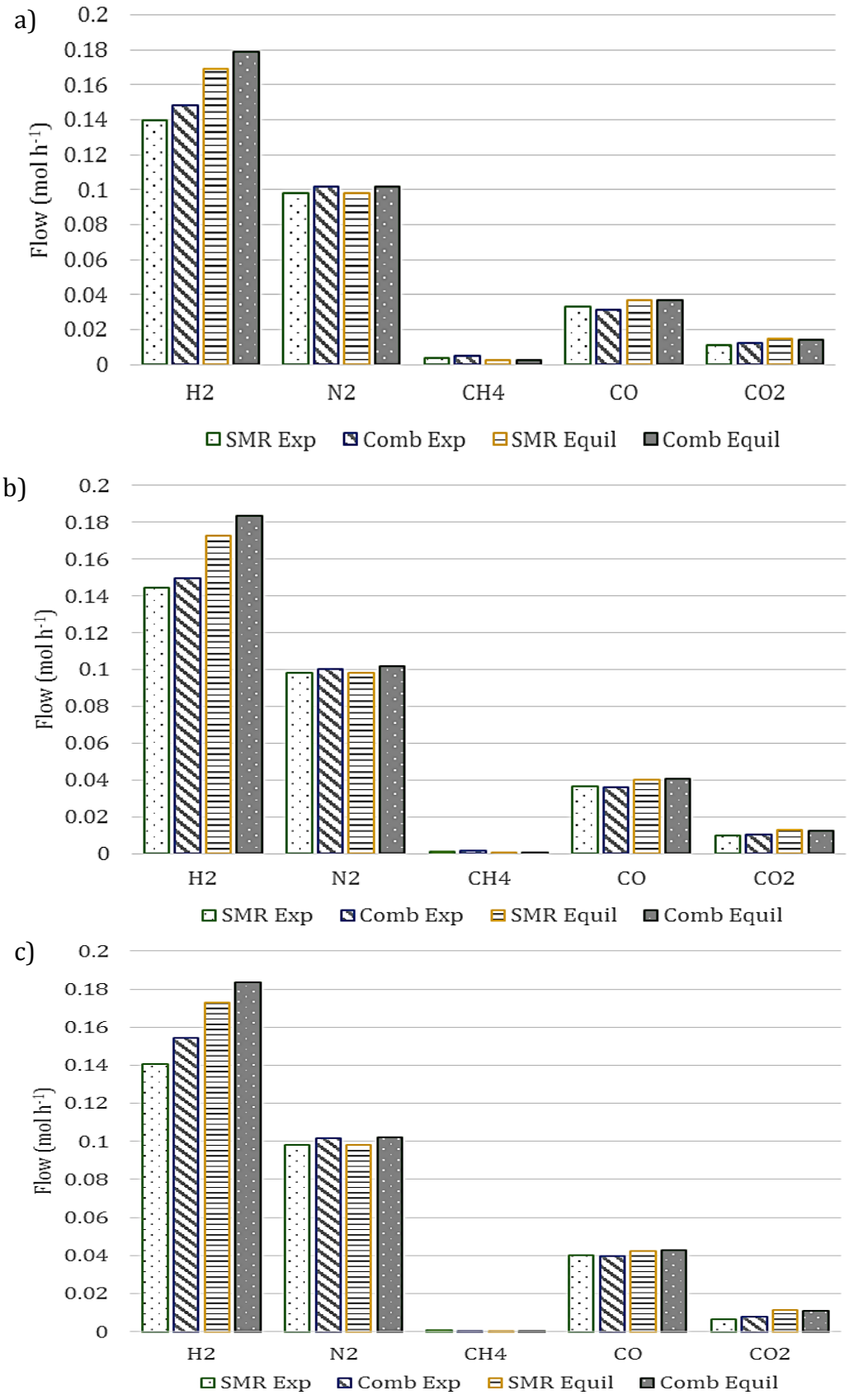

Figure 7-7(a-c). Comparison of dry syngas specie flow from equilibrium modelling and experiments at a S:C ratio of 2. Where 'SMR' describes runs without the presence of ammonia and 'Comb' describes runs with the presence of ammonia. a) 700 °C, b) 750 °C, c) 800 °C

What is clear, however, is that the experimental results follow closely with the general selectivity of products detailed under equilibrium. For example, both experimental and equilibrium investigations detailed that at a S:C of 2, H_2 production should increase with temperature and CO_2 production via the WGS reaction should decrease. This was generally found as shown in Figure 7-8. However, one discrepancy is at 800 °C without feed ammonia (labelled SMR), which had a slightly lower average production of H_2 compared to the 750 °C equivalent. As discussed considerably in Chapter 6, the equilibrium of the forward WGS reaction prefers lower temperatures and higher S:C ratios. The WGS reaction was found to be so limited at 800 °C under S:C 2, that it forced the overall H_2 generation to lower than at 750 °C. For example, the CO_2 generation at 800 °C was just 12.4% of that at 750 °C.

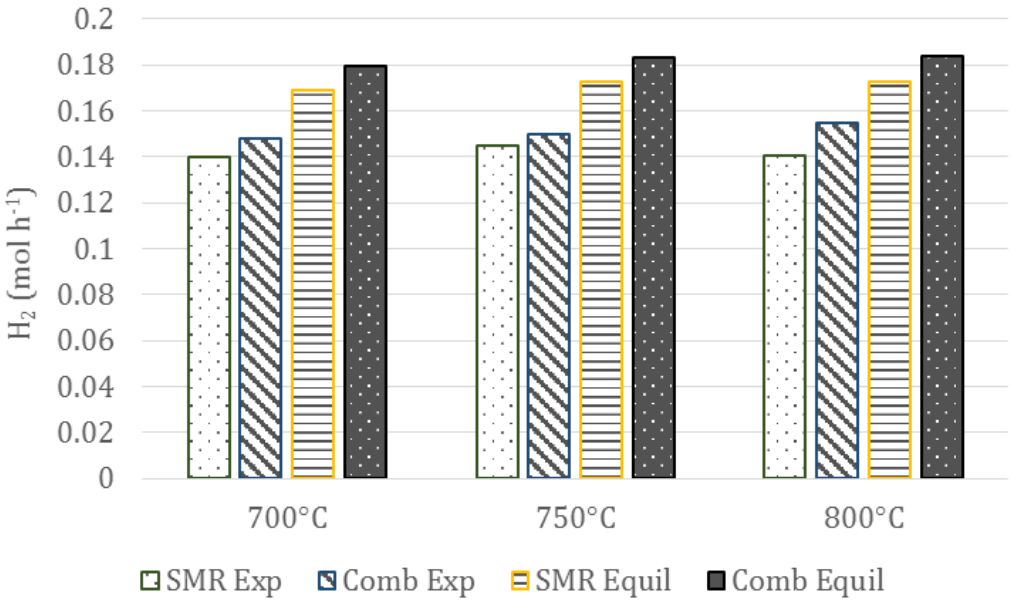

Figure 7-8. Results of H_2 production at S:C 2, 700 °C, 750 °C and 800 °C from experimental and equilibrium studies.

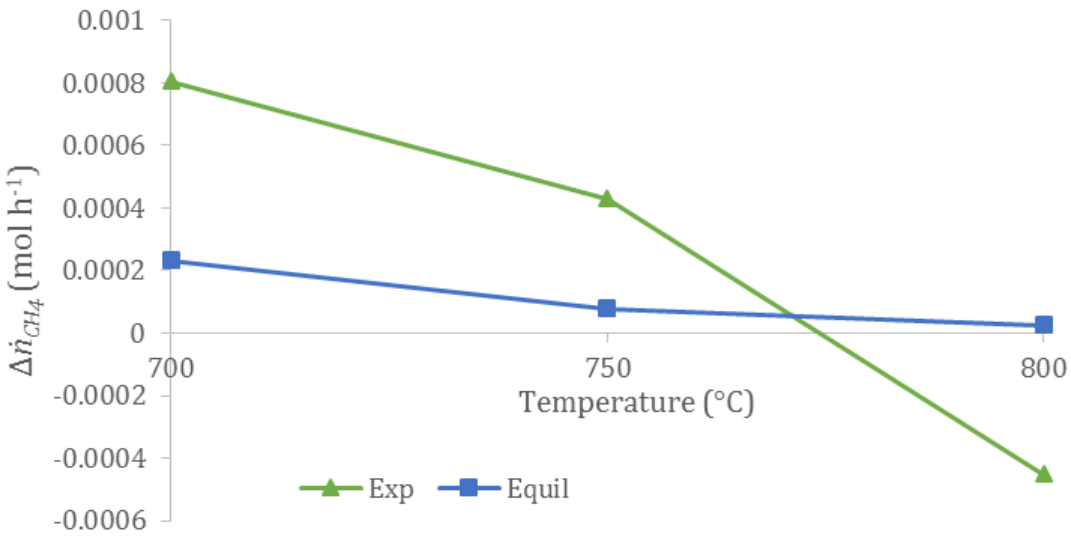

Figure 7-9. Difference in CH_4 flow from the reactor between runs with and without ammonia at S:C 2 $\left(\Delta\dot{\boldsymbol{n}}_{\boldsymbol{CH_4}} = \dot{\boldsymbol{n}}_{\boldsymbol{with,CH_4}} - \dot{\boldsymbol{n}}_{\boldsymbol{without,CH_4}}\right)$.

Equilibrium investigation showed that at lower temperatures, the presence of ammonia reduces methane conversion more so than at higher temperatures. This was another trend that was reproduced in experiments carried out at a S:C 2, as shown by the square plots in Figure 7-9. However, the impact was shown to be far more significant experimentally at temperatures 700 °C and 750 °C, shown by the triangular plots in Figure 7-9. At 800 °C, the runs with ammonia present in the feed, in fact, saw a higher conversion of methane than runs without.

When analysed in detail, the 800 °C S:C 2 SMR experiments resulted in lower than expected methane conversion. Figure 7-10 shows the raw GC data from the more stable of the two experiments carried out with S:C 2 at 800 °C. It illustrates the considerable variability in the syngas composition for H_2, CO_2 and CH_4. This highlights that the SMR and WGS reactions were not proceeding as they should. The cause of this is unknown, but it is speculated that there was an issue with the pump-syringe system (which happened from time to time due to gradual loosening of the Luer lock needle) meaning the flow of water was more inconsistent than usual. As such, it is hypothesized that this was the cause of the higher methane conversions with the presence of ammonia in the feed, rather than a catalytic forcing.

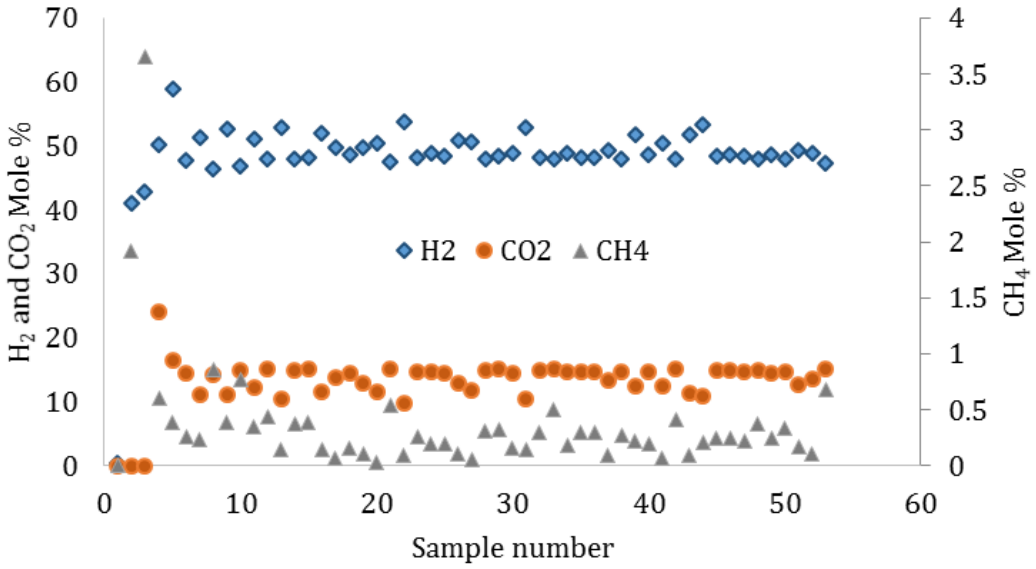

Figure 7-10. Raw GC results in mole % for H_2, CO_2 and CH_4 for a run at S:C 2 and 800 °C.

The raw results of the HACH LCK303 tests and ammonium conversion analysis can be seen in Appendix C, Table A 5. Under and S:C 2 it was found that 93%, 90% and 97% of the ammonia fed into the reactor decomposed to produce H_2 and N_2 at 700 °C, 750 °C and 800 °C respectively. This was less than under equilibrium simulations where over 99% decomposed under each temperature analysed. One reason for this could be that there was not enough residence time in the reactor to volatilise the aqueous ammonium (NH_4^+) contained in solution to free ammonia (NH_3) and to decompose to H_2 and N_2. This could potentially be improved in future experiments by increasing the temperature of the preheaters to above 150 °C. Alternatively, it could be that there are better catalysts to enable the decomposition such as ruthenium-based as discussed in Bell & Torrent-Murciano [153] or bi-metallic alternatives. Regardless, the experiments still demonstrated the ability to combine the steam reforming of methane with a S:C of 2 and the cracking of ammonia within a temperature range of 700-800 °C using a common commercial SMR catalyst formulation.

The CHNS analysis indicated that very little carbon deposition was occurring on the catalyst in any of the experiments occurring at a S:C of 2, as shown in Figure 7-11. It was expected that carbon deposition would decrease with

increasing temperatures [315]. As illustrated in Figure 7-11, the runs with ammonia followed this trend. However, the SMR experiments at 800 ℃ displayed the highest average carbon deposition of all runs carried out at a S:C of 2. This correlates with the lower than expected methane conversion in this run highlighted in Figure 7-9 and Figure 7-10. As aforementioned, it is proposed that these runs experienced some form of human error that prevented effective steam reforming; forcing up the carbon formation.

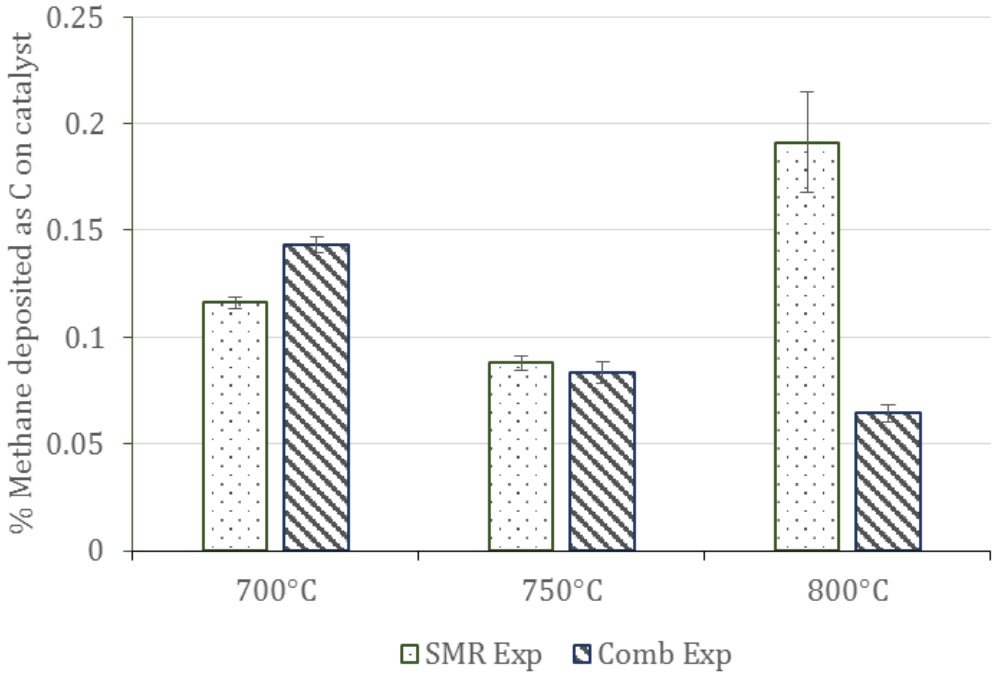

Figure 7-11. Graph showing the molar % of methane depositing as solid C on the catalyst for S:C 2 experiments

Given the very low selectivity to solid carbon obtained in all the experimental runs (less than 0.2% of carbon feed), the assumption that H_2 production via reaction 7-6 was negligible was verified and thus corroborated the methodology for a H_2 production rate caused by the contributions of SMR, WGS and NH_3 decomposition. It was stipulated by Wang et al. [156] that the presence of ammonia during steam methane reforming leads to a suppression of carbon deposition on Ni/Al_2O_3 catalysts due to the occupation of acidic sites by ammonia. However, the results from the S:C 3 runs indicated lower carbon deposition on just 2 of the three temperatures analysed. The investigation

carried out by Wang et al. [156] utilised far higher ammonia concentrations than in this Chapter. As such, further work is required in order to conclude whether the presence of ammonia has much of an impact on carbon deposition at this S:C ratio.

7.9.1.2 Hydrogen production and reactants conversion at S:C 3

Figure 7-12 illustrates the flow rate of syngas species from experimental and equilibrium data at S:C 3 and temperatures 700 °C, 750 °C and 800°C. As with the S:C 2 conditions, the trends and general product selectivity strongly resemble their equilibrium equivalent, with the highest difference being that of H_2 production. Again, this can be mainly attributed to the fact that the methane conversion was not as high as predicted via equilibrium investigation. Figure 7-12 shows the impact of S:C ratios on the WGS reaction, whereby the flow of CO_2 has increased notably from the runs at S:C 2 and are now close to the equilibrium values.

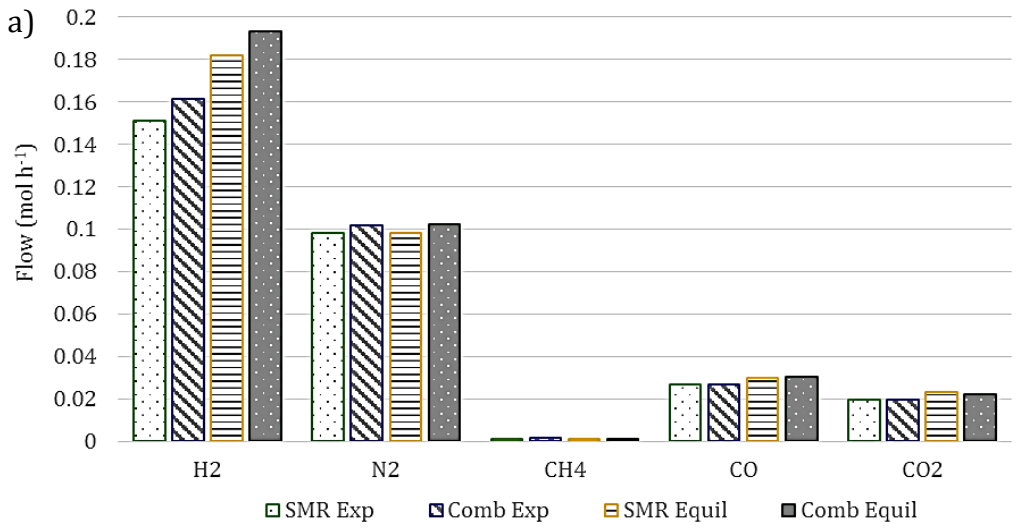

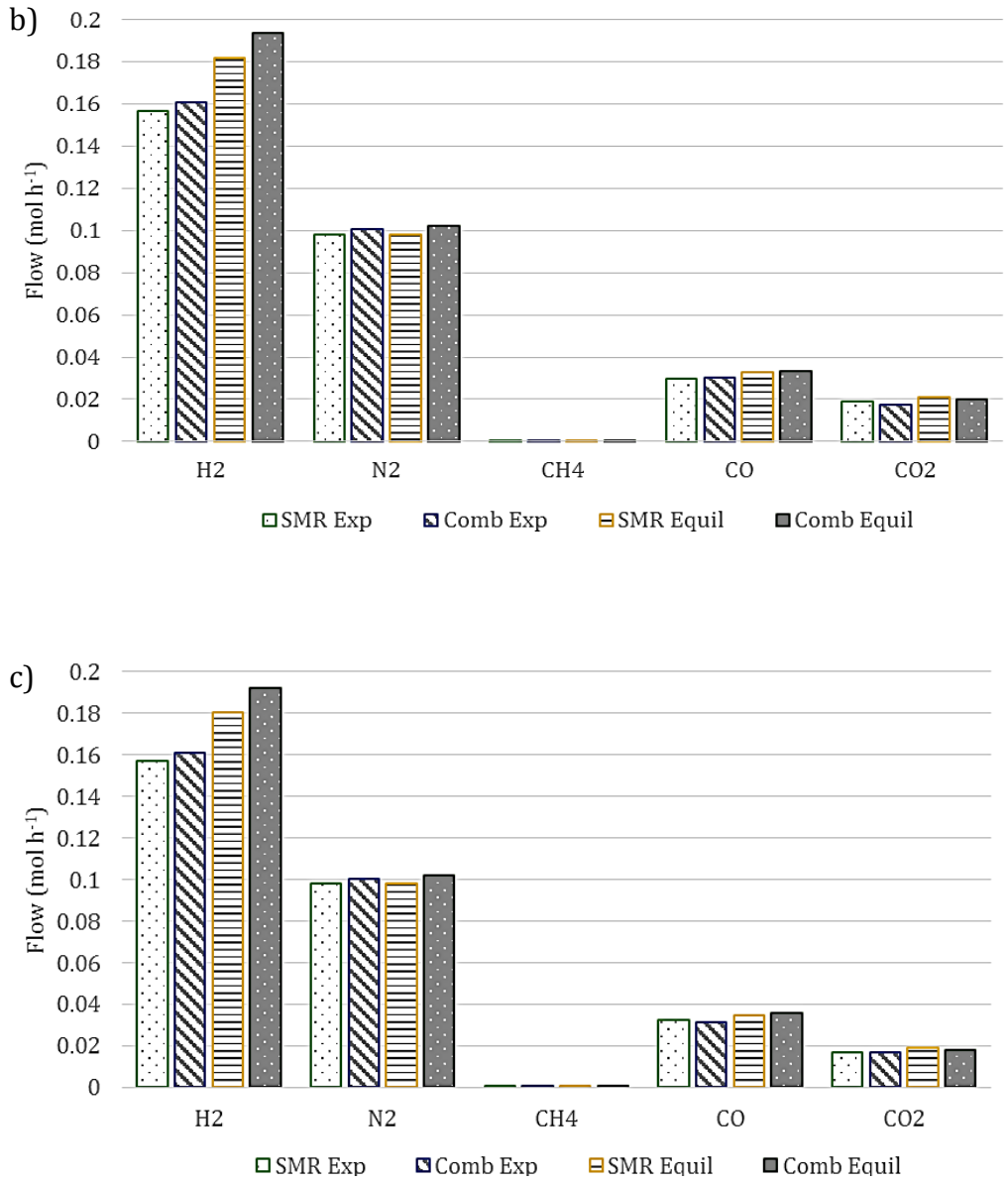

Figure 7-12 Comparison of dry syngas specie flow from equilibrium modelling and experiments at a S:C ratio of 3. Where 'SMR' describes runs without the presence of ammonia and 'Comb' describes runs with the presence of ammonia. a) 700°C, b) 750°C, c) 800°C

Another notable finding can be seen with closer inspection of Figure 7-12 (b) and Figure 7-12 (c), where the increase in H_2 with ammonia in the feed is far less notable from the experimental data than from the equilibrium tests. It was discussed earlier that over time ammonia volatilised from the bottle of the aqueous ammonium solution in which it was stored. Despite attempting to minimise this as much as possible via opening it for the shortest amount of time, the losses proved inevitable. By the time the S:C 3 750 °C and 800 °C

experiments were carried out, just over 40% of the ammonia had volatilised from solution, thus altering the quantity of H_2 produced via the decomposition of ammonia. Via condensate analysis, it was found that, of the ammonia that that was fed into the reactor, 90%, 86% and 92% underwent decomposition at temperatures 700 °C, 750 °C and 800 °C respectively.

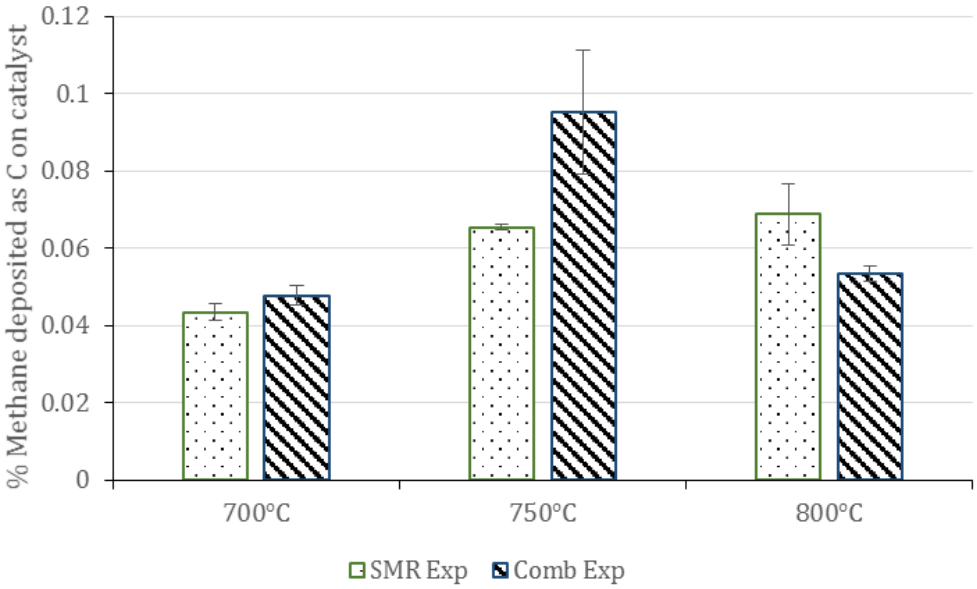

Figure 7-13. Molar % of methane depositing as solid C on the catalyst for S:C 3 experiments

One reason for the lower ammonia conversion could be that there was a higher deposition of carbon during the S:C 3 and 750°C run with ammonia than any other experiment described in this chapter at 0.095% of the initial methane feed, as shown in Figure 7-13. However, there was no definitive correlation between carbon deposition and ammonia conversion amongst the entire dataset, as shown by Figure 7-18. This figure shows a negative regression trend-line (as would be expected) but with an R^2 of just 0.1476 and was found to fail an F-test.

Figure 7-14 illustrates that equilibrium tests with an S:C of 3, the difference between methane conversions with and without ammonia in the feed were much less pronounced than under S:C 2 conditions. The relationship shown

with the experimental data (green markers in Figure 7-14) is not nearly as clear as with the equilibrium study. This is most obviously represented at 750 °C where the outflow of methane in the syngas was -0.00013 mol h^{-1} less with ammonia in the feed than without. However, this can almost certainly be attributed to the additional carbon deposition, as shown in Figure 7-13 via methane decomposition (reaction 7-6).

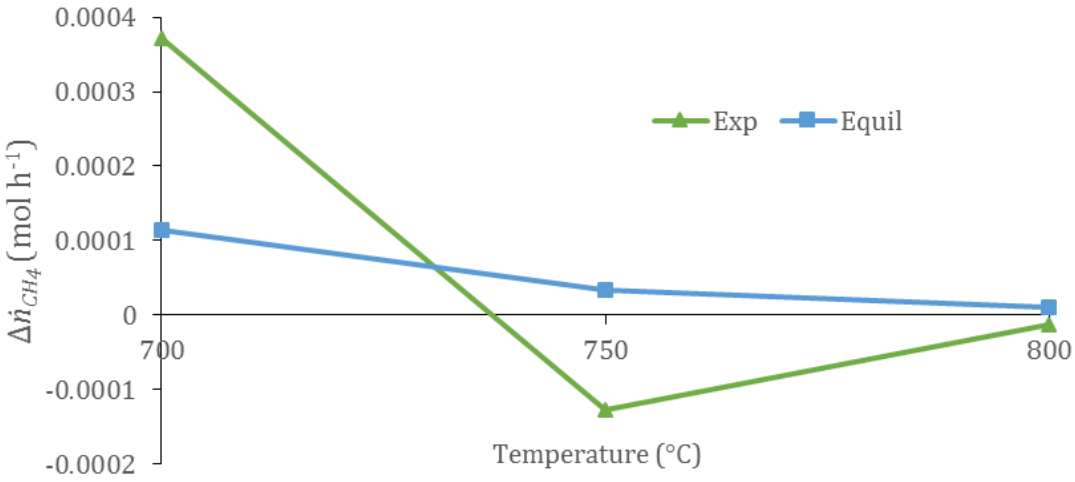

Figure 7-14. Difference in CH_4 flow from the reactor between runs with ammonia in the feed and runs without at S:C 3 $\left(\Delta\dot{\boldsymbol{n}}_{\boldsymbol{CH_4}} = \dot{\boldsymbol{n}}_{\boldsymbol{with,CH_4}} - \dot{\boldsymbol{n}}_{\boldsymbol{without,CH_4}}\right)$.

7.9.1.3 Hydrogen Production and reactants conversion at S:C 4

The syngas produced in the experiments carried out under S:C 4 conditions demonstrated the closest resemblance to equilibrium flow rates, as illustrated in Figure 7-15. It is speculated that the higher flow of water required for S:C 4, meant that the flow from the syringe was less intermittent, which helped maintain steady state. S:C 4 also experienced the lowest average GHSV at 4014 compared to 4235 and 4024 for S:C 2 and 3 respectively. The lower the WHSV, the higher the volume ratio of catalyst to gases. This means there is a greater residence time in the reaction bed, helping reactions to reach conditions closer to equilibrium. The equilibrium study showed that at a reactor temperature of 700 °C under a S:C ratio of 4 the highest production of H_2 for runs with and without ammonia in the feed were facilitated. This was also the case for the

experimental work with a hydrogen production rate of 0.161 mol h^{-1} and 0.168 mol h^{-1} for SMR and combined runs respectively. However, this was still 14.8% and 16.5% less than predicted under equilibrium investigation.

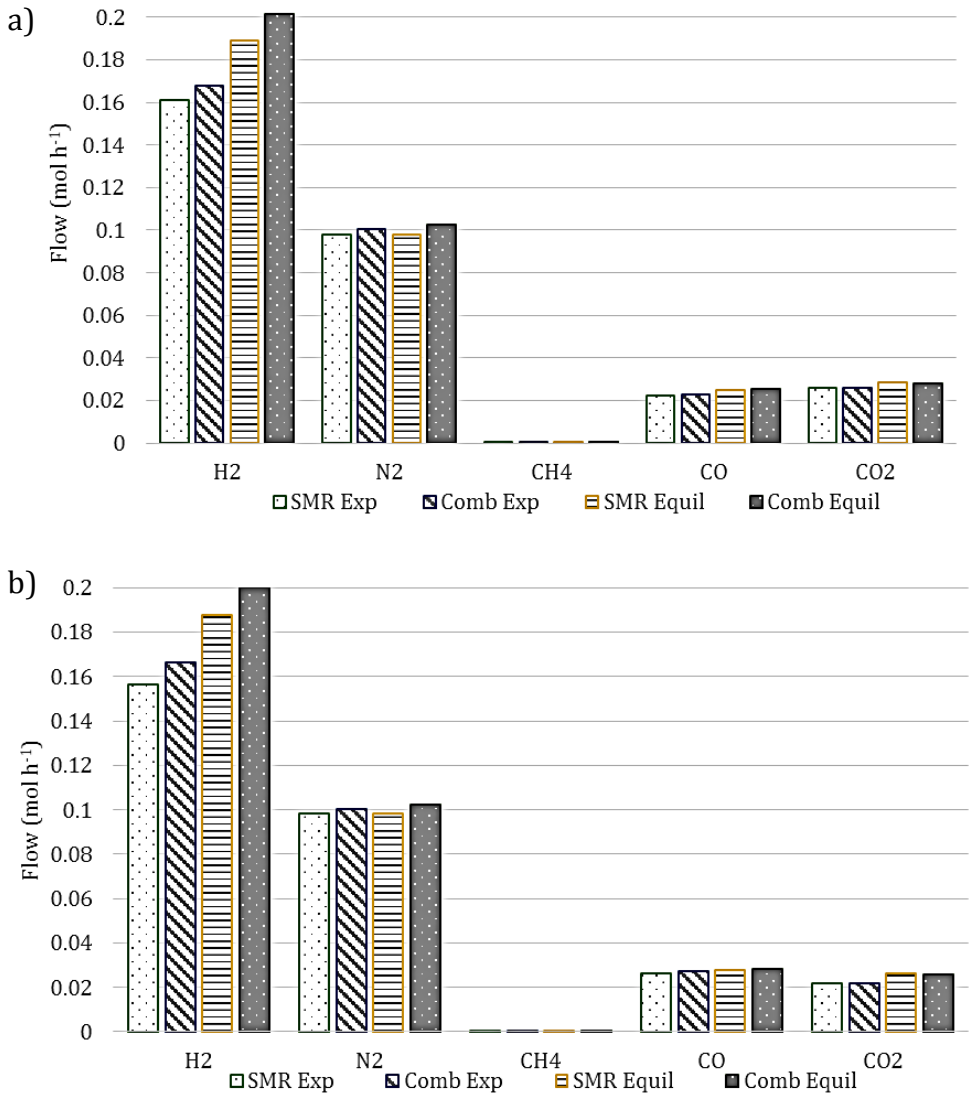

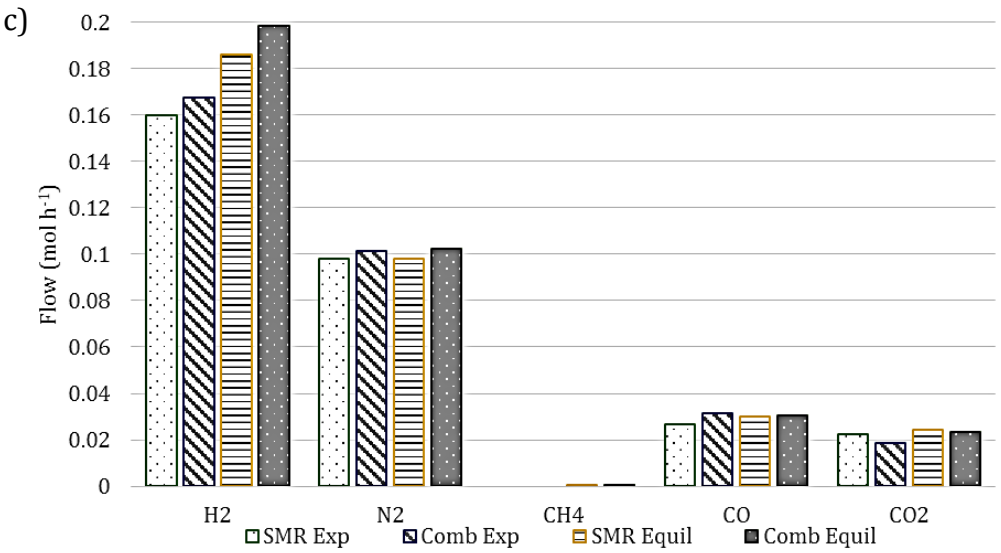

Figure 7-15. (a-c) Comparison of dry syngas specie flow from equilibrium modelling and experiments at a S:C ratio of 3. Where 'SMR' describes runs without ammonia and 'Comb' describes runs with ammonia in the feed. a) 700 °C, b) 750 °C, c) 800 °C

Unlike the other S:C conditions analysed (2 and 3), the methane conversion achieved experimentally at S:C 4 resembles, much more closely, that of the equilibrium. However, the micro GC results for the outlet flow of methane was less than shown via equilibrium studies. For, example at 800 °C the GC exhibited a zero flow of methane in the syngas, whereas equilibrium predicted that there should be a small quantity of CH_4 remaining. One potential reason for this is that the carbon deposited on the catalyst originated from methane decomposition, reducing the final outflow of methane in syngas. Another potential explanation of this could be that the micro GC's detection accuracy at these small concentrations is inhibited. Nonetheless, experiments carried out with a S:C 4 facilitated the highest methane conversion, as hypothesised using equilibrium analysis.

Figure 7-15 indicates that there was a slightly lower generation of CO_2 experimentally than in equilibrium with each of the S:C 4 experiments. This again highlights how the experimental set-up was unable to facilitate the WGS reaction (2-18) at a high enough rate to match equilibrium. This would also have contributed to the lower H_2 yields shown by the laboratory experiments compared to the equilibrium study, as shown in Figure 7-15.

Figure 7-16 details the amount of carbon deposited on the catalyst as a molar % of methane fed into the rig. Runs without ammonia in the feed (labelled 'SMR') showcase the hypothesised trend of reducing carbon deposition with temperature. Conversely, the experiment with ammonia at 700 °C experienced a lower carbon deposition compared to the run at 750 °C.

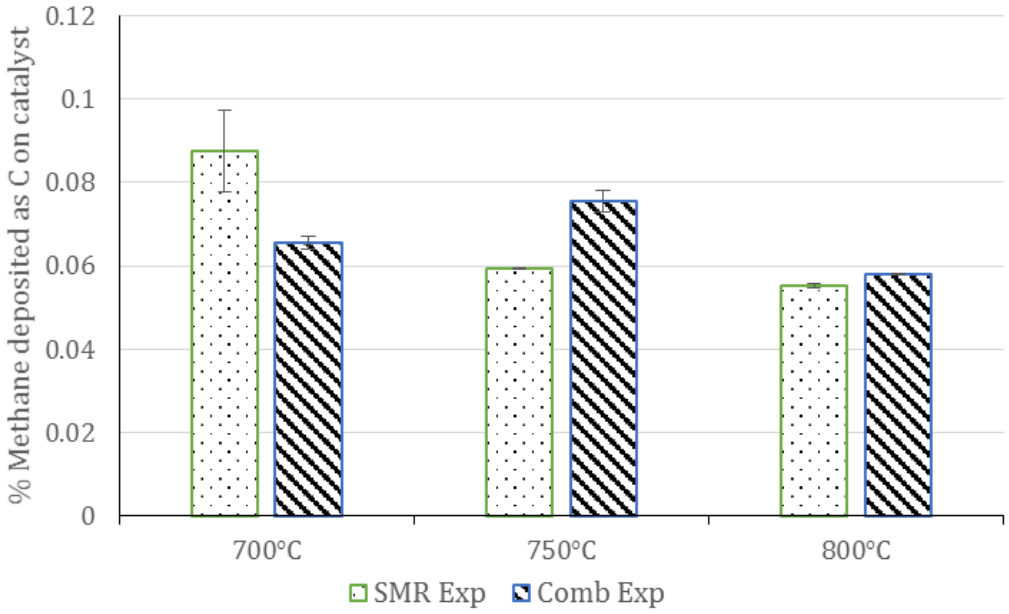

Figure 7-16. Molar % of methane depositing as solid C on the catalyst for S:C 4 experiments with ('Comb') and without ('SMR') NH_3 in the feed.

7.9.2 Overall ammonia contribution

Figure 7-17 details the increase in H_2 calculated via the determined destruction of ammonia alongside the real difference in H_2 flows for runs with and without ammonia in the feed. It also details the calculated % of the expected flow of ammonia that entered the reactor due to loss via volatilisation. It was expected that the real difference in H_2 generation would be less than the contribution of ammonia due to the negative equilibrium effects of introducing ammonia on the SMR and WGS reactions. However, this was found to be the case in just 5 out of the 9 conditions analysed experimentally.

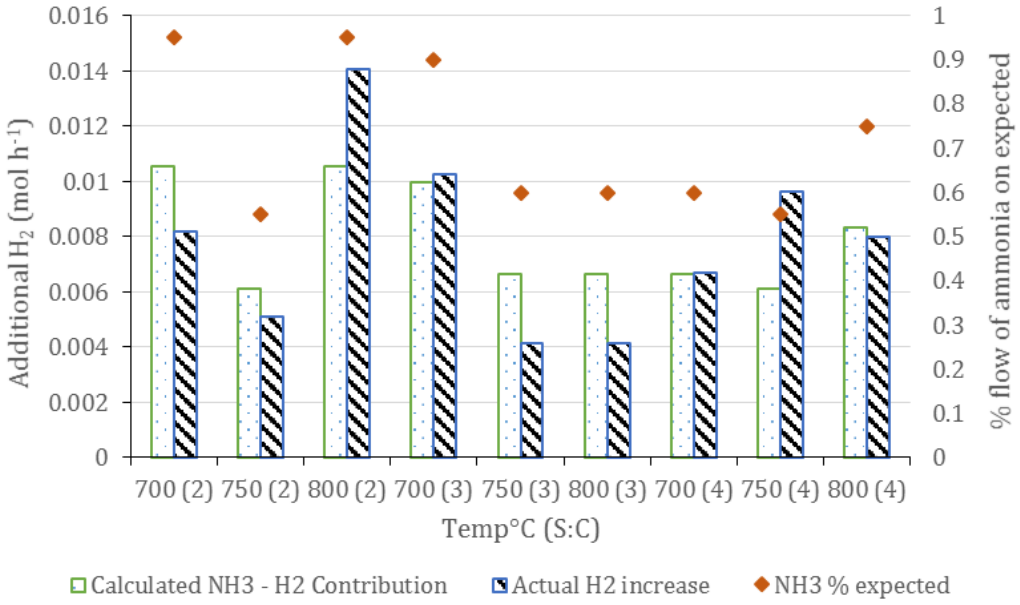

Figure 7-17. Diagram showing the calculated H_2 difference between runs with and without the addition of ammonia ($\Delta\dot{n}_{H_2(out)}$) the H_2 generated from contribution of ammonia decomposition ($\dot{n}_{H_2(NH_3 decomp)}$) as calculated in equation 7-11. Also shown as diamond plots are the % flow of ammonia on expected (due to volatilisation).

Nonetheless, it was found that each experiment with ammonia in the feed increased the flow of H_2 generated in the syngas. It was also found that the conversion of ammonia ranged between 86 % and 98 %. With an average conversion of 91.3%. The conversion followed an increasing trend with temperature with an average conversion of 89.2%, 89.5% and 95.2% for temperatures at 700 °C, 750 °C and 800 °C. This was less than the equivalent equilibrium predictions which predicted conversions over 99%. It is speculated that this occurred because ammonia was fed into the rig in solution and not all of the ammonia had to time to volatilise and decompose. As such, if a gaseous inlet was used instead, the conversions may have been greater.

One potential reason that not all of the experiments resulted with a lower $\Delta\dot{n}_{H_2(out)}$ than $\dot{n}_{H_2(NH_3 decomp)}$ could be the influence of ammonia on the deposition of carbon as shown by Figure 7-18. It shows that there is a slight

negative trend between the % of ammonia decomposition and the deposition of carbon. Showing that at higher rates of ammonia decomposition, there appears to be less carbon deposited on the catalyst, as stipulated by Wang et al. [156]. However, the trend-line displayed in Figure 7-18 has an R^2 of just 0.1476 and the relationship failed an associated F-test. Thus, it is not possible to determine conclusively whether this relationship exists or not.

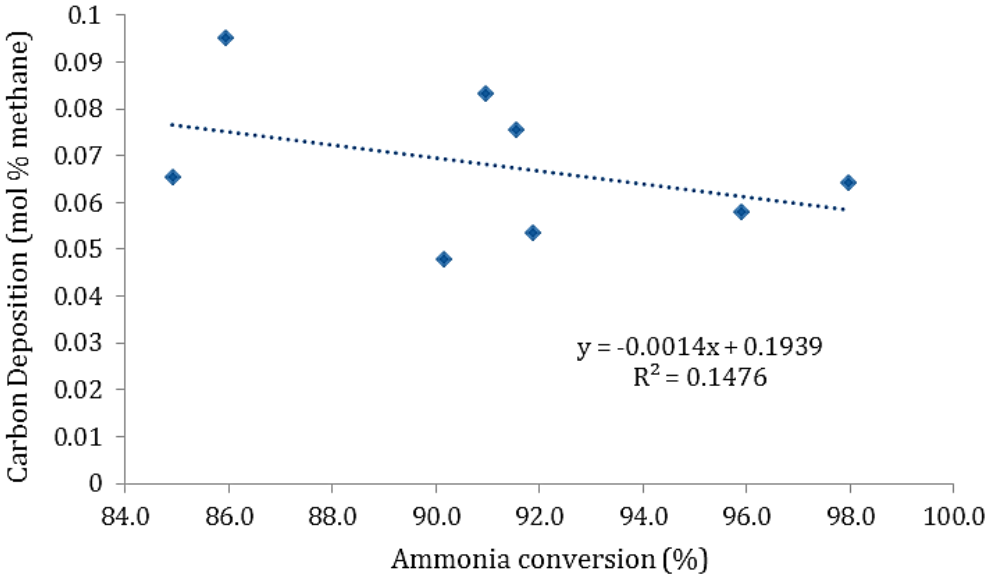

Figure 7-18. Relationship of carbon deposition and ammonia conversion

7.10 Methodological flaws and further work

There was one methodological flaw that affected the results presented in this chapter more than any other; namely the volatilisation of ammonia from prepared solution prior to feed in the reactor. By the end of all of the experiments, the Fischer Scientific ammonia solution had lowered from 25 wt% ammonia to 13.25 wt%; losing over half of its ammonia content. A liquid feed of ammonium solution was required in place of a gaseous flow, as the latter was deemed unsafe for use due to its highly toxic nature if inhaled. Unfortunately, this meant that each time the bottle of 25 wt% ammonia solution was opened, some ammonia was lost due to volatilisation. A gaseous flow would have been preferential as the flow of ammonia could have been

better controlled and its impacts on product yields, decomposition extent and carbon deposition more easily and conclusively determined.

Another issue arose because N_2 was used as the inert carrier/reference gas but it was also generated via the ammonia decomposition reaction, meaning the total outflow of N_2 had to be determined via proxy calculations. In future experiments, another inert carrier gas could be used instead, such as Helium (He). However, the chromatograms generated via the micro GC utilised in this work resulted in H_2 and He peaks extremely close to each other, which could make unique determination difficult.

Furthermore, the experimental work discussed in this chapter utilised just one WHSV (2). As such, its impact on product yields and conversions could not be determined and any further work should assess the impact of multiple WHSVs. Furthermore, by keeping the WHSV constant, the GHSV altered between 4014 and 4235. This may have had an impact on the product yields and extent of reactions. Therefore, any future work should employ examination of varying GHSV.

It was discussed by Yin et al. [154] and Bell & Torrente-Murciano [153] that Ru – based catalysts are superior for ammonia decomposition than Ni – based catalysts, as used in this chapter. Furthermore, Jones et al. [312] found that Ru catalysts are also superior to Ni catalysts for SMR. As such, it could be worth carrying out a similar experimental procedure as done in this Chapter but with Ru or Ru-Ni catalysts to determine the difference in effectiveness. It may also be worth investigating the use of different supports such as monolith catalysts instead of powdered ones, which is also a technology direction being taken in solid oxide fuel cell anode research [316] and would make an interesting bookend to the work carried out in Chapter 5.

7.11 Conclusions

In this chapter, experimental analysis of combined steam methane reforming and ammonia decomposition was carried out in a packed bed reactor using a commercially formulated 18wt% Ni/Al_2O_3 catalyst with a WHSV of 2, for S:C

ratios of 2, 3 and 4 and temperatures 700 °C, 750 °C and 800 °C. It was proved that the combined reactions were possible with respectable conversions of both methane and ammonia. Although general product selectivity was close to equilibrium equivalents, the extent of ammonia decomposition, SMR and WGS reactions did not reach equilibrium comparisons in most cases. For example, ammonia decomposition ranged between 89.2% and 95.2% compared to an expected (equilibrium) conversion of over 99%. Furthermore, H_2 production ranged between 14.8% and 18.3% less in relative terms than expected under equilibrium studies.

It was expected that the presence of ammonia and its decomposition would have a negative impact on the conversion of methane via SMR. However, this was found to be the case in just five of the 9 experimental conditions and no specific trend could be inferred. Fortunately there was very little carbon accumulation found on the catalysts in any of the experiments carried out. It was expected that carbon accumulation would reduce with ammonia conversion due to the theorised occupation of acidic spaces on the catalyst. Despite a trend shown via regression analysis, a very weak relationship was found and was therefore proved inconclusive.

There were multiple methodological issues that were exposed during the experiments reported in this Chapter, the most glaring being the volatilisation of ammonia from the solution sample prior to feed into the reformer. Over half of the originally contained ammonia was lost, which affected syngas compositions and the ability to make assured conclusions as to the relationship of ammonia decomposition with the contributions of other reactions and extent of carbon deposition. A number of suggestions have been made as to potential improvements in the experimental procedure which should be carried out if further experimental work is to be carried out in this field.

8 Conclusions and Future Work

Action on climate change is the most important responsibility humanity has ever experienced. However, innovation, development and uptake requires time and no sector can be left behind, including the wastewater treatment sector. Although the large-scale introduction of anaerobic digestion at WWTPs has much improved their overall sustainability of operation, there is further work to do. Esholt WWTP, the reference facility used throughout this thesis, recovers 2/3 of the energy it consumes, via the combination of anaerobic digestion (AD) and conventional combined heat and power (CHP) technology. This means that 1/3 of its energy is provided by a (mostly) non-renewable electricity grid and the digestate liquor it recycles back into the treatment process, considerably augments the facility's energy consumption and its emission of GHGs with the associated release of N_2O. This begs the question: are there undiscovered methods in which the GHG footprint of the facility can be reduced and/or the generation of power increased?

This thesis has attempted to answer this question with multidisciplinary and multifaceted analysis of the feasibility for the novel utilisation of biogas and recovered ammonia from digestate liquor. This has included the development, optimisation and interpretation of process models that investigate ammonia recovery via air stripping, absorption and distillation with associated economic studies. These have been bookended by experimental work that act as anchor points for the process and economic models. The characterisation of Esholt wastewater treatment plant streams, discussed in Chapter 3, acts as a tangible foundation for the rest of thesis, informing on ammonia concentrations, energy

use and emission of GHGs. The lab-scale generation and analysis of H_2-rich syngas from combined ammonia decomposition and steam methane reforming is discussed in Chapter 7, which evaluates how closely equilibrium model feedstock conversions can be replicated during real operation.

8.1 Ammonia recovery

A review of literature found that the current primary justification for ammonia recovery from digestate liquor is for the generation of fertiliser. However, the fertilisers produced from digestate liquor are inferior to commercial alternatives. This makes it difficult to acquire the profit necessary for wide-scale roll out. In Chapter 4, Aspen Plus process simulation software was used to replicate the conventional initial stage of ammonia recovery informed from literature, air stripping. Sensitivity analysis carried out on the operational conditions of the air stripper detailed the requirements to facilitate a minimum 95% recovery of ammonia and showcased the least energy intensive conditions to use.

After air stripping, the method of ammonia recovery splits from the conventional and a novel process has been developed. The second stage is an absorption step using water, as opposed to sulphuric acid, which would poison downstream catalysts used for thermochemical conversions. Again, sensitivity analysis was performed to determine the most effective and least energy intensive conditions. The final stage utilises a distillation column in which a final recovery of 91% of the ammonia originally found in the digestate liquor is facilitated. At Esholt WWTP, this would provide an annual diversion of 400.7 tonnes of ammonia from the activated sludge process. It was calculated that this quantity was enough to reduce the facility's GHG emissions by 12.12% of its total or 2.45 kg per year for each person serviced by the facility. It was also enough to reduce the plant's energy consumption by 8%.

The associated economic study of the process developed in Aspen Plus, detailed a capital investment requirement of £1.7 million. An NPV analysis, with a 10%

discount rate, indicated that the diverted ammonia would need to have a value of £1.87 per kg for it to be financially attractive to Esholt WWTP. This was found to be more than the equivalent market price of its fertiliser competitor but its added value to the facility as a feedstock for a solid oxide fuel cell (SOFC) stack or H_2 production showed promise.

8.2 SOFC operation

A combination of numerical and process modelling methods were used in Chapter 5 to investigate the production of heat and power from a high temperature, internally reforming SOFC. A review of literature had shown that the combined use of ammonia and methane in a SOFC had been the subject of experimental investigation before. However, the whole-system development and modelling of a process that combines the recovery of ammonia from a renewable source for direct use in a SOFC stack was entirely novel and facilitated the publication of Grasham et al. [282].

The developed process model incorporated the ammonia recovery procedure proposed in Chapter 4 with the simulation of the described SOFC. The material flows of digestate liquor and biomethane as discussed in Chapter 3 were used as inputs for the model so that impacts for process introduction at Esholt WWTP could be thoroughly assessed. A numerical model was built that detailed its ability to operate at a net electrical efficiency of 48%, facilitating a production of 58.1 MWh_{el} per day; equivalent to an increase of 45% of the site's current production total. Of the power produced from the SOFC, it was calculated that the ammonia's contribution was roughly 5%.

The associated economic study found that the process introduction at Esholt WWTP would require a significant initial capital investment of £14.15 million. However, energy expense savings and income from Contracts for Difference and Renewable Heat Incentive schemes would facilitate a payback on investment in just 5.5 years of operation and enable a positive NPV after 8 years (based on a 10% discount rate).

8.3 H_2 production

Thorough sensitivity analysis was performed in order to combine the discussed ammonia recovery process with the thermochemical production of H_2. Three scenarios were analysed for feed molar steam to carbon ratios at the steam reformer (S:C) of 2, 3 and 4 so that a cost-benefit analysis could be performed for determining whether achieving higher yields of H_2 from greater S:Cs can be justified energetically and economically. It was shown that if implemented at Esholt WWTP; 117 kg h^{-1}, 115 kg h^{-1} and 109 kg h^{-1} of H_2 could be produced using S:Cs of 4, 3 and 2 respectively. Net production of heat had an inverse relationship with the S:C at 9.6 MWh day^{-1}, 10.1 MWh day^{-1} and 15 MWh day^{-1} for S:C scenarios 4, 3 and 2 respectively.

Ultimately, the economic NPV analysis detailed that the S:C 3 scenario would be the most profitable; striking a balance between energetic efficiency and H_2 production potential. Using a speculated H_2 market value of £4.50 kg^{-1}, it was calculated that an NPV of £3.1 million could be achieved after 20 years of operation. However, the profitability was found to be highly dependent on the market value of H_2. With the penetration of H_2-based infrastructure expected over the coming years, fluctuations in H_2 value are to be expected. As such, without governmental incentive schemes, it may be difficult to attract investors to back the initial investment of £13.01 million, with the current status of uncertainty.

It was also found that the introduction of the H_2 production process at Esholt WWTP would decrease its lifecycle GHG emissions by 10,596 kg CO_2e day^{-1} if the H_2 was to be used as a bus transportation fuel, displacing emissions associated with combustion of diesel fuel. However, it should be noted that the compression, storage and dispensing system suggested in Chapter 6 has a significant impact on the sustainability and feasibility of the process introduction. Future work should explore alternatives such as grid injection, which would coincide well with the research trend exemplified by H21 Leeds Citygate [33] and HyDeploy [34].

In Chapter 7, an 18wt% Ni/□-Al_2O_3 catalyst was used in a packed-bed reactor with a WHSV of 2 to perform experimental analysis of combined ammonia

decomposition and steam methane reforming (SMR). S:Cs of 2, 3 and 4 and temperatures of 700 °C, 750 °C and 800 °C were analysed. Ammonia decomposition efficiency varied between 89.2% and 95.2% with a slight positive relationship with temperature. However, this was less than the 99% projected via equilibrium investigation. SMR and water-gas shift (WGS) reaction efficiencies were also shown to be less than equilibrium projections, facilitating H_2 production yields between 14.8% and 18.3% less than expected under equilibrium.

However, there are multiple areas in which the experimental procedure could be improved upon; with particular emphasis on the use of a gaseous ammonia inlet rather than an aqueous one. The aqueous feedstock used in the experiments experienced considerable volatilisation of ammonia over time which affected the ability to draw strong and defined conclusions from the work. Regardless, it was showcased that using a catalyst of commercial formulation, enabled combined ammonia decomposition and SMR and facilitated respectable conversions of both ammonia and methane feedstocks.

8.4 Comparison of process routes

One overarching objective of the thesis was to discover whether via novel utilisation of recovered ammonia it would be possible to reduce GHG emissions at wastewater treatment plants. Of the two processes discussed, the H_2 production system showcased the greatest potential reduction in lifecycle emissions at 10,596 kg CO_2e day^{-1} compared to 3,221.91 kg CO_2e day^{-1} for the SOFC process. This was the case due to the significant savings achieved via CO_2 abatement if the H_2 generated was to be used as a bus transportation fuel in replacement of fossil diesel fuel.

However, the SOFC process was shown to be the more financially attractive and viable option of the two, with a payback period of 5.5 years compared to 7 years for the H_2 production system and a 20 year NPV of £10.7 million compared to £3.1 million. With the considerable lifecycle emission improvements under the

H_2 production process, if associated carbon emission reduction incentives can be rolled out, its potential profitability could be much improved.

8.5 Future direction

In this thesis, chemical process modelling has been an invaluable tool in developing integrated systems and analysing their overarching feasibility. This 'whole systems' approach has enabled the development of processes that could be installed into wastewater treatment plants tomorrow, if desired. Despite its virtues, this big picture approach also has its weaknesses in that real-life operation rarely identically mirrors that of a model – as highlighted in Chapter 7 with experimental H_2 production.

As such, there are a number of modelling activities that should be replicated in an experimental environment to determine their true viability in any future work. For example, the ammonia recovery process detailed in Chapters 4, 5 and 6 use a proxy digestate liquor composition, containing just water and ammonia. However, there are many other components that, in real life, could affect the efficiency of recovery. Furthermore, packing material used in the stripping column is known to become contaminated if solids are not effectively removed beforehand and, therefore, would be another interesting area of focus. In conclusion, experimental ammonia recovery data is one particular area where communication with the process model could have a significant impact on results.

There also was no experimental work carried out on SOFC operation. Although combined ammonia and methane feeds have been physically demonstrated before, it would still be interesting to analyse any differences using the inlet compositions described in this thesis. Furthermore, SOFC research is still a fledgling topic, with systematic and material improvements continually transpiring. For example, intermediate temperature (IT) SOFCs are showing the potential to both reduce material costs and maintain high efficiencies. Accordingly, future study in this area may want to focus on analysis of IT-SOFCs rather than the higher temperature stacks discussed in this body of work.

This thesis utilised the operational framework of a singular wastewater treatment plant. Its relatively large size makes for a favourable site in which to implement extensive process additions due to workings of economies of scale. Accordingly, studies into the viability of process integration at other wastewater treatment plants of different sizes and nature should be carried out. Furthermore, normal AD facilities or biorefineries could also be host to the discussed processes and investigation into implementation feasibility in other such industries would make for interesting comparisons.

Both H_2 production and SOFC process routes showcased abilities to markedly reduce GHG emissions at WWTPs. However, with the introduction of carbon capture and storage (CCS) technology, further improvements could be made. Within both discussed processes an exhaust stream containing a considerable quantity of carbon is generated; making them perfectly suited for CCS technology. If financial incentives for CCS are introduced in the UK, its addition to the processes discussed in this thesis could make the wastewater treatment industry a spearhead in the fight against climate change and is, therefore, worth investigation.

9 References

[1] NOAA (National Oceanic and Atmospheric Administration). Global Climate Report - Annual 2017 | State of the Climate | National Centers for Environmental Information (NCEI) 2018. https://www.ncdc.noaa.gov/sotc/global/201713 (accessed May 31, 2018).

[2] WMO (World MeteorologicalOrganisation). The state of the global climatein 2018. 2018.

[3] United Nations. Rio Declaration on Environment and Development. 1992. doi:10.1017/S037689290003157X.

[4] UNFCCC. Finale COP21 2015. http://newsroom.unfccc.int/unfccc-newsroom/finale-cop21/ (accessed March 21, 2016).

[5] Climate Change Act. Climate Change Act 2008: Chapter 27. 2008.

[6] DECC (Department of Energy and Climate Change). The Carbon Plan: Delivering our low carbon future. London: Stationary Office; 2011.

[7] DfT, DECC D. UK Bioenergy Strategy. London: Stationary Office; 2012.

[8] DEFRA & DECC. Anaerobic Digestion Strategy and Action Plan. London: 2011.

[9] Alves HJ, Bley Junior C, Niklevicz RR, Frigo EP, Frigo MS, Coimbra-Araújo CH. Overview of hydrogen production technologies from biogas and the applications in fuel cells. Int J Hydrogen Energy 2013;38:5215–25. doi:10.1016/j.ijhydene.2013.02.057.

[10] Ofwat. Water 2020: Appendix 2 Moving beyond waste - further evidence and analysis 2016. doi:10.1016/j.celrep.2017.09.058.

[11] BEIS (Department of Business Energy & Industrial Strategy). Renewable electricity and capacity generation. 2018.

[12] Lofrano G, Brown J. Wastewater management through the ages: A history of mankind. Sci Total Environ 2010;408:5254–64.

doi:10.1016/j.scitotenv.2010.07.062.

[13] Ludzack FJ, Ettinger MB. Controlling operation to minimize activated sludge effluent nitrogen. Water Pollut Control Vederation 1962;34:920–31.

[14] Barnard JL. Biological nutrient removal without the addition of chemicals. Water Res 1975;9:485–90. doi:10.1016/0043-1354(75)90072-X.

[15] CEC – Council of the European Communities. Directive concerning urban waste water treatment (91/271/EEC). Off J Eur Communities 1991;L135:40-52 (30 May).

[16] CEC – Council of the European Communities. Directive establishing a framework for Community action in the field of water policy (2000/60/EC). Off J Eur Communities 2000;L327:1-72 (22 December).

[17] Kampschreur MJ, Temmink H, Kleerebezem R, Jetten MSM, van Loosdrecht MCM. Nitrous oxide emission during wastewater treatment. Water Res 2009;43:4093–103. doi:10.1016/j.watres.2009.03.001.

[18] Maurer M, Schwegler P, Larsen T. Nutrients in urine: energetic aspects of removal and recovery. Water Sci Technol 2003;48:37–46.

[19] Fux C, Siegrist H. Nitrogen removal from sludge digester liquids by nitrification/denitrification or partial nitritation/anammox: environmental and economical considerations. Water Sci Technol 2004;50:19–26.

[20] Vaneeckhaute C, Lebuf V, Michels E, Belia E, Vanrolleghem PA, Tack FMG, et al. Nutrient Recovery from Digestate: Systematic Technology Review and Product Classification. Waste and Biomass Valorization 2016:1–20. doi:10.1007/s12649-016-9642-x.

[21] Errico M, Fjerbaek Sotoft L, Kjærhuus Nielsen A, Norddahl B. Treatment costs of ammonia recovery from biogas digestate by air stripping analyzed by process simulation. Clean Technol Environ Policy 2017:1–11. doi:10.1007/s10098-017-1468-0.

[22] Fuchs W, Drosg B. Assessment of the state of the art of technologies for the processing of digestate residue from anaerobic digesters. Water Sci Technol 2013;67:1984–93. doi:10.2166/wst.2013.075.

[23] Drosg B, Fuchs W, Al Seadi T, Madsen M, Linke B, Seadi T Al, et al. Nutrient Recovery by Biogas Digestate Processing. IEA Bioenergy 2015:40.

[24] Yuan MH, Chen YH, Tsai JY, Chang CY. Removal of ammonia from wastewater by air stripping process in laboratory and pilot scales using a rotating packed bed at ambient temperature. J Taiwan Inst Chem Eng 2015;60:488–95. doi:10.1016/j.jtice.2015.11.016.

[25] Lebuf V, Accoe F, Van Elsacker S, Vaneeckhaute C, Michels E, Meers E, et al. Techniques for nutrient recovery from digestate: inventory 2013:26.

[26] Bousek J, Scroccaro D, Sima J, Weissenbacher N, Fuchs W. Influence of the gas composition on the efficiency of ammonia stripping of biogas digestate. Bioresour Technol 2016;203:259–66. doi:10.1016/j.biortech.2015.12.046.

[27] Valera-Medina A, Xiao H, Owen-Jones M, David WIF, Bowen PJ. Ammonia for power. Prog Energy Combust Sci 2018;69:63–102. doi:10.1016/j.pecs.2018.07.001.

[28] Klerke A, Christensen CH, Nørskov JK, Vegge T. Ammonia for hydrogen storage: Challenges and opportunities. J Mater Chem 2008. doi:10.1039/b720020j.

[29] Gondal IA, Masood SA, Khan R. Green hydrogen production potential for developing a hydrogen economy in Pakistan. Int J Hydrogen Energy 2018;43:6011–39. doi:10.1016/j.ijhydene.2018.01.113.

[30] Karolyte R. Hydrogen with CCS for decarbonised heat in the Scottish context 2017:1–14.

[31] Demirbas A. Future hydrogen economy and policy. Energy Sources, Part B Econ Plan Policy 2017;12:172–81. doi:10.1080/15567249.2014.950394.

[32] Brandon NP, Kurban Z. Clean energy and the hydrogen econo my. Philos

Trans R Soc A Math Eng Sci 2017;375:20160400. doi:10.1098/rsta.2016.0400.

[33] Northern Gas Networks. H21 Leeds City Gate. Leeds City Gate 2016.

[34] HyDeploy. About HyDeploy 2018. https://hydeploy.co.uk/about/ (accessed May 24, 2018).

[35] Valverde L, Rosa F, Bordons C, Guerra J. Energy Management Strategies in hydrogen Smart-Grids: A laboratory experience. Int J Hydrogen Energy 2016;41:13715–25. doi:10.1016/j.ijhydene.2016.05.279.

[36] Wolf E. Chapter 9 – Large-Scale Hydrogen Energy Storage. Electrochem. Energy Storage Renew. Sources Grid Balanc., 2015, p. 129–42. doi:10.1016/B978-0-444-62616-5.00009-7.

[37] Gabriel García Clúa J, Battista H, Mantz RJ, Gallegos NG. Stabilisation of grid assistance for a renewable hydrogen generation system by min-projection strategy. IET Control Theory Appl 2016;10:183–9. doi:10.1049/iet-cta.2014.1327.

[38] ITM POWER. RWE Power-to-Gas Energy Storage System Launched 2015. http://www.itm-power.com/news-item/rwe-power-to-gas-energy-storage-system-launched (accessed June 19, 2018).

[39] Agency for Natural Resources and Energy. Compilation of the Revised Version of the Strategic Roadmap for Hydrogen and Fuel Cells 2016. http://www.meti.go.jp/english/press/2016/0322_05.html (accessed May 1, 2018).

[40] Air Resources Board. Fuel Cell Electric Vehicle Deployment and Hydrogen Fuel Station Network Development. Calif Environ Prot Agency 2017.

[41] Department for Transport. New greener police cars to run on hydrogen - GOV.UK 2018. https://www.gov.uk/government/news/new-greener-police-cars-to-run-on-hydrogen (accessed May 24, 2018).

[42] Department for Transport and Office for Low Emission Vehicles. £23 million boost for hydrogen-powered vehicles and infrastructure -

GOV.UK 2017. https://www.gov.uk/government/news/23-million-boost-for-hydrogen-powered-vehicles-and-infrastructure (accessed May 24, 2018).

[43] ADBA. Anaerobic Digestion Market report July 2015. 2015.

[44] Tram VO P, Ngo HH, Guo W, Zhou JL, Nguyen PD, Listowski A, et al. A mini-review on the impacts of climate change on wastewater reclamation and reuse. Sci Total Environ 2014;494–495:9–17. doi:10.1016/j.scitotenv.2014.06.090.

[45] Guest JS, Skerlos SJ, Barnard JL, Beck MB, Daigger GT, Hilger H, et al. A new planning and design paradigm to achieve sustainable resource recovery from wastewater. Environ Sci Technol 2009;43:6126–30. doi:10.1021/es9010515.

[46] McCarty PL, Bae J, Kim J. Domestic wastewater treatment as a net energy producer - can this be achieved? Environ Sci Technol 2011;45:7100–6. doi:10.1021/es2014264.

[47] Chudoba P, Sardet C, Palko G, Guibelin E. Main factors influencing anaerobic digestion of sludge and energy efficiency at several large WWTP in central Europe. J Residuals Sci Technol 2011;8:89–96.

[48] Larsen TA, Alder AC, Eggen RIL, Maurer M, Lienert J. Source separation: Will we see a paradigm shift in wastewater handling? Environ Sci Technol 2009;43:6121–5. doi:10.1021/es803001r.

[49] Silva C, Rosa MJ. Energy performance indicators of wastewater treatment: a field study with 17 Portuguese plants. Water Sci Technol 2015;72:510–9. doi:10.2166/wst.2015.189.

[50] Schaubroeck T, De Clippeleir H, Weissenbacher N, Dewulf J, Boeckx P, Vlaeminck SE, et al. Environmental sustainability of an energy self-sufficient sewage treatment plant: improvements through DEMON and co-digestion. Water Res 2015;74:166–79. doi:10.1016/j.watres.2015.02.013.

[51] Siegrist H, Salzgeber D, Eugster J, Joss A. Anammox brings WWTP closer

to energy autarky due to increased biogas production and reduced aeration energy for N-removal 2008.

[52] WERF. Energy Management Exploratory Team Report Executive Summary 2011.

[53] Trendewicz AA, Braun RJ. Techno-economic analysis of solid oxide fuel cell-based combined heat and power systems for biogas utilization at wastewater treatment facilities. J Power Sources 2013;233:380–93. doi:10.1016/j.jpowsour.2013.01.017.

[54] MosayebNezhad M, Mehr AS, Gandiglio M, Lanzini A, Santarelli M. Techno-economic assessment of biogas-fed CHP hybrid systems in a real wastewater treatment plant. Appl Therm Eng 2018;129:1263–80. doi:10.1016/j.applthermaleng.2017.10.115.

[55] Gandiglio M, Torino P, Lanzini A, Torino P, Torino P. Industrial Size Biogas SOFC System in a Wastewater Treatment Plant. Proc. ASME 2016 14th Int. Conf. Fuel Cell Sci. Eng. Technol., Charlotte, North Carolina: 2016.

[56] EG&G Technical Services I. Fuel Cell Handbook. Fuel Cell 2004;7 Edition:1–352. doi:10.1002/zaac.200300050.

[57] Garrido JM, Fdz-Polanco M, Fdz-Polanco F. Working with energy and mass balances: a conceptual framework to understand the limits of municipal wastewater treatment. Water Sci Technol 2013;67:2294. doi:10.2166/wst.2013.124.

[58] IPCC IPOCC. Climate Change 2007 - The Physical Science Basis: Working Group I Contribution to the Fourth Assessment Report of the IPCC. Science (80-) 2007:1009. doi:volume.

[59] Law Y, Ye L, Pan Y, Yuan Z. Nitrous oxide emissions from wastewater treatment processes. Philos Trans R Soc Lond B Biol Sci 2012;367:1265–77. doi:10.1098/rstb.2011.0317.

[60] Hajjaji N, Martinez S, Trably E, Steyer J-P, Helias A. Life cycle assessment of hydrogen production from biogas reforming. Int J Hydrogen Energy

2016;41:6064–75. doi:10.1016/j.ijhydene.2016.03.006.

[61] Reinders M, Beckhaus P, Illing F, Misz U, Rißе H, Schröder M, et al. Biogas as a source for producing hydrogen at wastewater treatment plants – EuWaK – A pilot project. Int J Hydrogen Energy 2015;40:8601–6. doi:10.1016/j.ijhydene.2015.05.042.

[62] Zin RM, Ross a B, Jones JM, Dupont V. Hydrogen from ethanol reforming with aqueous fraction of pine pyrolysis oil with and without chemical looping. Bioresour Technol 2015;176:257–66. doi:10.1016/j.biortech.2014.11.034.

[63] Ni M, Leung DYC, Leung MKH. Mathematical modeling of ammonia-fed solid oxide fuel cells with different electrolytes. Int J Hydrogen Energy 2008;33:5765–72. doi:10.1016/j.ijhydene.2008.07.021.

[64] Yang J, Akagi T, Okanishi T, Muroyama H, Matsui T, Eguchi K. Catalytic influence of oxide component in Ni-based cermet anodes for ammonia-fueled solid oxide fuel cells. Fuel Cells 2015;15:390–7. doi:10.1002/fuce.201400135.

[65] Wojcik A, Middleton H, Damopoulos I, Van Herle J. Ammonia as a fuel in solid oxide fuel cells. J Power Sources 2003;118:342–8. doi:10.1016/S0378-7753(03)00083-1.

[66] Ma Q, Peng R, Tian L, Meng G. Direct utilization of ammonia in intermediate-temperature solid oxide fuel cells. Electrochem Commun 2006;8:1791–5. doi:10.1016/j.elecom.2006.08.012.

[67] Mulder A. The quest for sustainable nitrogen removal technologies. Water Sci Technol 2003;48:67–75.

[68] Heathwaite AL, Johnes PJ, Peters NE. Trends in nutrients. Hydrol Process 1996;10:263–93. doi:10.1002/(SICI)1099-1085(199602)10:2<263::AID-HYP441>3.0.CO;2-K.

[69] Cooper P, Day M, Thomas V. Process Options for Phosphorus and Nitrogen Removal from Wastewater. Water Environ J 1994;8:84–92. doi:10.1111/j.1747-6593.1994.tb01096.x.

[70] Ravishankara AR, Daniel JS, Portmann RW. Nitrous oxide (N2O): the dominant ozone-depleting substance emitted in the 21st century. Science 2009;326:123–5. doi:10.1126/science.1176985.

[71] Forster CF. Wastewater Treatment and Technology. London: Thomas Telford; 2003.

[72] Clay S, Hodgkinson A, Upton J, Green M. Developing acceptable sewage screening practices. Water Sci Technol 1996;33:229–34. doi:10.1016/0273-1223(96)00477-5.

[73] Gerardi M. Nitrification and denitrification in the activated sludge process. New York: John Wiley & Sons, Inc; 2003.

[74] Eckinfelder WW, Argaman Y. Principles of Biological and Physical/Chemical Nitrogen Removal. In: Sedlak RI, editor. Phosphorus Nitrogen Remov. from Munic. Wastewater Princ. Pract., vol. 7. 2nd ed., Boca Raton, Florida: CRC Press; 1991, p. 3–42.

[75] Wu G, Zheng D, Xing L. Nitritation and N2O Emission in a Denitrification and Nitrification Two-Sludge System Treating High Ammonium Containing Wastewater. Water 2014;6:2978–92. doi:10.3390/w6102978.

[76] Colliver BB, Stephenson T. Production of nitrogen oxide and dinitrogen oxide by autotrophic nitrifiers. Biotechnol Adv 2000;18:219–32. doi:10.1016/S0734-9750(00)00035-5.

[77] U.S. Environmental Protection Agency (EPA). Manual: Nitrogen Control EPAl625/R-93/010. Cincinnati; Washington: Office of Research and Development Center for Environmental Research Information Risk Reduction Engineering Laboratory; Office of Wastewater Enforcement and Compliance; 1993.

[78] Strous M, Heijnen JJ, Kuenen JG, Jetten MSM. The sequencing batch reactor as a powerful tool for the study of slowly growing anaerobic ammonium-oxidizing microorganisms. Appl Microbiol Biotechnol 1998;50:589–96. doi:10.1007/s002530051340.

[79] Van Dongen UG., Jetten MSM, Van Loosdrecht MCM. The SHARON®-Anammox® process for treatment of ammonium rich wastewater. Water Sci … 2001;44:153–60.

[80] Hauck M, Maalcke-Luesken FA, Jetten MSM, Huijbregts MAJ. Removing nitrogen from wastewater with side stream anammox: What are the trade-offs between environmental impacts? Resour Conserv Recycl 2016;107:212–9. doi:10.1016/j.resconrec.2015.11.019.

[81] Li Y, Park SY, Zhu J. Solid-state anaerobic digestion for methane production from organic waste. Renew Sustain Energy Rev 2011;15:821–6. doi:10.1016/j.rser.2010.07.042.

[82] Ziemiński K, Frąc M. Methane fermentation process as anaerobic digestion of biomass: Transformations, stages and microorganisms. African J Biotechnol 2014;11:4127–39. doi:10.4314/ajb.v11i18.

[83] Buswell AM, Mueller HF. Mechanism of Methane Fermentation. Ind Eng Chem 1952;44:550–2. doi:10.1021/ie50507a033.

[84] Nayono SE. Anaerobic Digestion of Organic Solid Waste for Energy Production. KIT Scientific Publishing; 2010.

[85] Weiland P. Biogas production: current state and perspectives. Appl Microbiol Biotechnol 2010;85:849–60. doi:10.1007/s00253-009-2246-7.

[86] Niesner J, Jecha D, Stehlík P. Biogas upgrading technologies: State of art review in european region. Chem. Eng. Trans., vol. 35, Italian Association of Chemical Engineering - AIDIC; 2013, p. 517–22. doi:10.3303/CET1335086.

[87] Appels L, Baeyens J, Degrève J, Dewil R. Principles and potential of the anaerobic digestion of waste-activated sludge. Prog Energy Combust Sci 2008;34:755–81. doi:10.1016/j.pecs.2008.06.002.

[88] Dewil R, Appels L, Baeyens J. Energy use of biogas hampered by the presence of siloxanes. Energy Convers Manag 2006;47:1711–22. doi:10.1016/j.enconman.2005.10.016.

[89] Abatzoglou N, Boivin S. A review of biogas purification processes. Biofuels, Bioprod Biorefining 2009;3:42–71. doi:10.1002/bbb.117.

[90] Awe OW, Zhao Y, Nzihou A, Minh DP, Lyczko N. A Review of Biogas Utilisation, Purification and Upgrading Technologies. Waste and Biomass Valorization 2017;8:267–83. doi:10.1007/s12649-016-9826-4.

[91] Daniela Thrän EB, Tobias Persson, Mattias Svensson , Jaqueline Daniel-Gromke, Jens Ponitka MS, Baldwin J. Biomethane Status and Factors Affecting Market Development and Trade. IEA Bioenergy 2014:1–92. http://www.iea-biogas.net/files/daten-redaktion/download/Technical.

[92] Patterson T, Esteves S, Dinsdale R, Guwy A. An evaluation of the policy and techno-economic factors affecting the potential for biogas upgrading for transport fuel use in the UK. Energy Policy 2011;39:1806–16. doi:10.1016/j.enpol.2011.01.017.

[93] Starr K, Gabarrell X, Villalba G, Talens L, Lombardi L. Life cycle assessment of biogas upgrading technologies. Waste Manag 2012;32:991–9. doi:10.1016/j.wasman.2011.12.016.

[94] Muñoz R, Meier L, Diaz I, Jeison D. A review on the state-of-the-art of physical/chemical and biological technologies for biogas upgrading. Rev Environ Sci Biotechnol 2015;14:727–59. doi:10.1007/s11157-015-9379-1.

[95] Persson M, Jonsson O, Wellinger A. Biogas Upgrading to Vehicle Fuel Standards and Grid Injection Task 37 -Energy from Biogas and Landfill Gas. IEA Bioenergy 2006.

[96] Muñoz R, Meier L, Diaz I, Jeison D. A review on the state-of-the-art of physical/chemical and biological technologies for biogas upgrading. Rev Environ Sci Bio/Technology 2015;14:727–59. doi:10.1007/s11157-015-9379-1.

[97] De Arespacochaga N, Valderrama C, Peregrina C, Mesa C, Bouchy L, Cortina JL. Evaluation of a pilot-scale sewage biogas powered 2.8 kW<inf>e</inf> Solid Oxide Fuel Cell: Assessment of heat-to-power ratio

and influence of oxygen content. J Power Sources 2015;300:325–35. doi:10.1016/j.jpowsour.2015.09.086.

[98] Ryckebosch E, Drouillon M, Vervaeren H. Techniques for transformation of biogas to biomethane. Biomass and Bioenergy 2011;35:1633–45. doi:10.1016/j.biombioe.2011.02.033.

[99] EC (European Comission). Report from the Commission to the Council and the European Parliament on the implementation of community waste legislation for the period 2001–2003. COM 406 Final Eur Commision, Brussels 2006.

[100] Smith SR, Alcock RE, Sweetman A, Jones KC, Aranda JM, O'Connor GA, et al. Organic contaminants in sewage sludge (biosolids) and their significance for agricultural recycling. Philos Trans A Math Phys Eng Sci 2009;367:4005–41. doi:10.1098/rsta.2009.0154.

[101] BSI. PAS 110:2014 Specification for whole digestate, separated liquor and separated fibre derived from the anaerobic digestion of source-segregated biodegradable materials. London: British Standards Institution; 2014.

[102] ADBA. Digestate. Pract. Guid. to AD, London: Anaerobic Digestion & Biogas Association; 2013, p. 81–91.

[103] Al Seadi T, Fuchs W. Biogas Digestate Quality and Utilisation. In: Wellinger A, Murphy JD, Baxter D, editors. Biogas Handb. Sci. Prod. Appl., Cambridge, Philadelphia, Delhi: Woodhead Publishing; 2013, p. 267–301. doi:10.1533/9780857097415.2.191.

[104] Dungait JAJ, Cardenas LM, Blackwell MSA, Wu L, Withers PJA, Chadwick DR, et al. Advances in the understanding of nutrient dynamics and management in UK agriculture. Sci Total Environ 2012;434:39–50. doi:10.1016/j.scitotenv.2012.04.029.

[105] Ott C, Rechberger H. The European phosphorus balance. Resour Conserv Recycl 2012;60:159–72. doi:10.1016/j.resconrec.2011.12.007.

[106] Jones DL, Cross P, Withers PJA, DeLuca TH, Robinson DA, Quilliam RS, et

al. REVIEW: Nutrient stripping: the global disparity between food security and soil nutrient stocks. J Appl Ecol 2013;50:851–62. doi:10.1111/1365-2664.12089.

[107] Drosg B, Fuchs W, Al Seadi T, Madsen M, Linke B. Nutrient Recovery by Biogas Digestate Processing. IEA Bioenergy 2015.

[108] Bauer A, Mayr H, Hopfner-Sixt K, Amon T. Detailed monitoring of two biogas plants and mechanical solid–liquid separation of fermentation residues. J Biotechnol 2009;142:56–63. doi:10.1016/j.jbiotec.2009.01.016.

[109] US EPA & US ED. Energy STAR performance ratings. Technical methodology for wastewater treatment plants 2007.

[110] Lidkea TR. Energy use by sewage treatment plants 2007.

[111] Fenu A, Roels J, Wambecq T, De Gussem K, Thoeye C, De Gueldre G, et al. Energy audit of a full scale MBR system. Desalination 2010;262:121–8. doi:10.1016/j.desal.2010.05.057.

[112] Jonasson M. Energy Benchmark for Wastewater Treatment Processes: A comparison between Sweden and Austria. Lund University, Sweden, 2007.

[113] Perry RH, Green DW. Perry's Chemical Engineers' Handbook. 8th ed. New York: McGraw-Hill; 2008. doi:10.1036/0071511334.

[114] Brown & Caldwell. Evaluation of Combined Heat and Power Technologies for Wastewater Facilities. EPA 2012;832-R-10–0.

[115] Kahlbaum GWA, Darbishire FV, editors. Letters of Faraday and Schoenbein 1836-1862. London: Williams and Norgate; 1899.

[116] Ni M, Leung M, Sumathy K, Leung D. Potential of renewable hydrogen production for energy supply in Hong Kong. Int J Hydrogen Energy 2006;31:1401–12. doi:10.1016/j.ijhydene.2005.11.005.

[117] Hacatoglu K, Rosen MA, Dincer I. Comparative life cycle assessment of hydrogen and other selected fuels. Int J Hydrogen Energy 2012;37:9933–40. doi:10.1016/j.ijhydene.2012.04.020.

[118] Holladay JD, Hu J, King DL, Wang Y. An overview of hydrogen production technologies. Catal Today 2009;139:244–60. doi:10.1016/j.cattod.2008.08.039.

[119] Ball M, Wietschel M. The future of hydrogen – opportunities and challenges☆. Int J Hydrogen Energy 2009;34:615–27. doi:10.1016/j.ijhydene.2008.11.014.

[120] Ramachandran R. An overview of industrial uses of hydrogen. Int J Hydrogen Energy 1998;23:593–8. doi:10.1016/S0360-3199(97)00112-2.

[121] Bockris JOM. A hydrogen economy. Science (80-) 1972;176:1323.

[122] Rosen MA. The Prospects for Hydrogen as an Energy Carrier: An overview of Hydrogen Energy and Hydrogen Energy Systems. In: Honnery DR, Moriarty P, editors. Hydrog. Prod. Prospect. Process., New York: Nova Science Publishers; 2012.

[123] Rigas F, Amyotte P. Hydrogen Safety. Boca Raton, Florida: CRC Press, Taylor & Francis Group; 2013.

[124] Crowl DA, Jo Y-D. The hazards and risks of hydrogen. J Loss Prev Process Ind 2007;20:158–64. doi:10.1016/j.jlp.2007.02.002.

[125] DeLuchi MA. Hydrogen vehicles: an evaluation of fuel storage, performance, safety, environmental impacts, and cost. Int J Hydrogen Energy 1989;14:81–130. doi:10.1016/0360-3199(89)90001-3.

[126] Louthan MR. The Hindenburg and the hydrogen economy. Adv Mater Process 2005;163:42.

[127] Edwards PP. Our fear of hydrogen fuel stations. The TImes 2008.

[128] Ricci M, Bellaby P, Flynn R. What do we know about public perceptions and acceptance of hydrogen? A critical review and new case study evidence. Int J Hydrogen Energy 2008;33:5868–80. doi:10.1016/j.ijhydene.2008.07.106.

[129] Yetano Roche M, Mourato S, Fischedick M, Pietzner K, Viebahn P. Public attitudes towards and demand for hydrogen and fuel cell vehicles: A

review of the evidence and methodological implications. Energy Policy 2010;38:5301–10. doi:10.1016/j.enpol.2009.03.029.

[130] Muradov NZ. Production of Hydrogen from Hydrocarbons. In: Gupta RB, editor. Hydrog. Fuel Prod. Transp. Storage, Boca Raton, Florida: CRC Press, Taylor & Francis Group; 2008.

[131] Ersoz A, Olgun H, Ozdogan S. Reforming options for hydrogen production from fossil fuels for PEM fuel cells. J Power Sources 2006;154:67–73. doi:10.1016/j.jpowsour.2005.02.092.

[132] Sircar S, Golden TC. Purification of Hydrogen by Pressure Swing Adsorption. Sep Sci Technol 2006.

[133] Ross J. Heterogeneous Catalysis - Fundamentals and Applications. Amsterdam & Oxford: Elsevier; 2012.

[134] Rostrup-Nielsen J, Hansen JHB. CO2-Reforming of Methane over Transition Metals. J Catal 1993;144:38–49. doi:10.1006/jcat.1993.1312.

[135] Beurden P Van. On the catalytic aspects of steam-methane reforming. ECN 2004:1–27.

[136] Twigg M V., editor. Catalyst Handbook. 2nd ed. London: Wolfe; 1989.

[137] Sehested J, Gelten JAP, Remediakis IN, Bengaard H, Nørskov JK. Sintering of nickel steam-reforming catalysts: effects of temperature and steam and hydrogen pressures. J Catal 2004;223:432–43. doi:10.1016/j.jcat.2004.01.026.

[138] Lakhapatri SL, Abraham MA. Deactivation due to sulfur poisoning and carbon deposition on Rh-Ni/Al2O3 catalyst during steam reforming of sulfur-doped n-hexadecane. Appl Catal A Gen 2009;364:113–21. doi:10.1016/j.apcata.2009.05.035.

[139] Rodriguez JA. The chemical properties of bimetallic surfaces: Importance of ensemble and electronic effects in the adsorption of sulfur and SO2. Prog Surf Sci 2006;81:141–89. doi:10.1016/j.progsurf.2006.02.001.

[140] Samorjai GA. Introduction to Surface Chemistry and Catalysis. New York: Wiley Interscience; 1994.

[141] Trimm DL. Coke formation and minimisation during steam reforming reactions. Catal Today 1997;37:233–8. doi:10.1016/S0920-5861(97)00014-X.

[142] Song C, Ma X. New design approaches to ultra-clean diesel fuels by deep desulfurization and deep dearomatization. Appl Catal B Environ 2003;41:207–38. doi:10.1016/S0926-3373(02)00212-6.

[143] Hoguet J-C, Karagiannakis GP, Valla JA, Agrafiotis CC, Konstandopoulos AG. Gas and liquid phase fuels desulphurization for hydrogen production via reforming processes. Int J Hydrogen Energy 2009;34:4953–62. doi:10.1016/j.ijhydene.2008.11.043.

[144] Ursua A, Gandia LM, Sanchis P. Hydrogen Production From Water Electrolysis: Current Status and Future Trends. Proc IEEE 2012;100:410–26. doi:10.1109/JPROC.2011.2156750.

[145] National Academy of Science. The Hydrogen Economy: Opportunities, Costs, Barriers, and R&D Needs. Washington D.C.: National Academies Press; 2004. doi:10.5860/CHOICE.42-3447.

[146] Winter C-J. Hydrogen energy — Abundant, efficient, clean: A debate over the energy-system-of-change. Int J Hydrogen Energy 2009;34:S1–52. doi:10.1016/j.ijhydene.2009.05.063.

[147] Ntaikou I, Antonopoulou G, Lyberatos G. Biohydrogen Production from Biomass and Wastes via Dark Fermentation: A Review. Waste and Biomass Valorization 2010;1:21–39. doi:10.1007/s12649-009-9001-2.

[148] De Gioannis G, Muntoni A, Polettini A, Pomi R. A review of dark fermentative hydrogen production from biodegradable municipal waste fractions. Waste Manag 2013;33:1345–61. doi:10.1016/j.wasman.2013.02.019.

[149] Hallenbeck PC, Ghosh D. Advances in fermentative biohydrogen production: the way forward? Trends Biotechnol 2009;27:287–97. doi:10.1016/j.tibtech.2009.02.004.

[150] Thauer RK, Jungermann K, Decker K. Energy conservation in

chemotrophic anaerobic bacteria. Bacteriol Rev 1977;41:100–80.

[151] Holladay JD, Hu J, King DL, Wang Y. An overview of hydrogen production technologies. Catal Today 2009;139:244–60. doi:10.1016/j.cattod.2008.08.039.

[152] Premier GC, Kim JR, Massanet-Nicolau J, Kyazze G, Esteves SRR, Penumathsa BKV, et al. Integration of biohydrogen, biomethane and bioelectrochemical systems. Renew Energy 2013;49:188–92. doi:10.1016/j.renene.2012.01.035.

[153] Bell TE, Torrente-Murciano L. H2 Production via Ammonia Decomposition Using Non-Noble Metal Catalysts: A Review. Top Catal 2016;59:1438–57. doi:10.1007/s11244-016-0653-4.

[154] Yin SF, Xu BQ, Zhou XP, Au CT. A mini-review on ammonia decomposition catalysts for on-site generation of hydrogen for fuel cell applications. Appl Catal A Gen 2004;277:1–9. doi:10.1016/j.apcata.2004.09.020.

[155] Schüth F, Palkovits R, Schlögl R, Su DS. Ammonia as a possible element in an energy infrastructure: catalysts for ammonia decomposition. Energy Environ Sci 2012;5:6278–89. doi:10.1039/C2EE02865D.

[156] Wang W, Ran R, Su C, Guo Y, Farrusseng D, Shao Z. Ammonia-mediated suppression of coke formation in direct-methane solid oxide fuel cells with nickel-based anodes. J Power Sources 2013;240:232–40. doi:10.1016/j.jpowsour.2013.04.014.

[157] Xu L, Dong F, Zhuang H, He W, Ni M, Feng SP, et al. Energy upcycle in anaerobic treatment: Ammonium, methane, and carbon dioxide reformation through a hybrid electrodeionization–solid oxide fuel cell system. Energy Convers Manag 2017;140:157–66. doi:10.1016/j.enconman.2017.02.072.

[158] Shiga H, Shinda K, Hagiwara K, Tsutsumi A, Sakurai M, Yoshida K, et al. Large-scale hydrogen production from biogas. Int J Hydrogen Energy 1998;23:631–40.

[159] Appari S, Janardhanan VM, Bauri R, Jayanti S, Deutschmann O. A detailed

kinetic model for biogas steam reforming on Ni and catalyst deactivation due to sulfur poisoning. Appl Catal A Gen 2014;471:118–25. doi:10.1016/j.apcata.2013.12.002.

[160] Chattanathan SA, Adhikari S, McVey M, Fasina O. Hydrogen production from biogas reforming and the effect of H2S on CH4 conversion. Int J Hydrogen Energy 2014;39:19905–11. doi:10.1016/j.ijhydene.2014.09.162.

[161] Cruz PL, Navas-Anguita Z, Iribarren D, Dufour J. Exergy analysis of hydrogen production via biogas dry reforming. Int J Hydrogen Energy 2018;43:11688–95. doi:10.1016/j.ijhydene.2018.02.025.

[162] Wheeldon I, Caners C, Karan K, Peppley B. Utilization of biogas generated from Ontario wastewater treatment plants in solid oxide fuel cell systems: A process modeling study. Int J Green Energy 2007;4:221–31. doi:10.1080/15435070601015585.

[163] Gao Y, Jiang J, Meng Y, Yan F, Aihemaiti A. A review of recent developments in hydrogen production via biogas dry reforming. Energy Convers Manag 2018;171:133–55. doi:10.1016/j.enconman.2018.05.083.

[164] Abdullah B, Abd Ghani NA, Vo DVN. Recent advances in dry reforming of methane over Ni-based catalysts. J Clean Prod 2017;162:170–85. doi:10.1016/j.jclepro.2017.05.176.

[165] Lin C-Y, Lay C-H, Sen B, Chu C-Y, Kumar G, Chen C-C, et al. Fermentative hydrogen production from wastewaters: A review and prognosis. Int J Hydrogen Energy 2012;37:15632–42. doi:10.1016/j.ijhydene.2012.02.072.

[166] Kadier A, Simayi Y, Abdeshahian P, Azman NF, Chandrasekhar K, Kalil MS. A comprehensive review of microbial electrolysis cells (MEC) reactor designs and configurations for sustainable hydrogen gas production. Alexandria Eng J 2016;55:427–43. doi:10.1016/j.aej.2015.10.008.

[167] Zou S, He Z. Efficiently "pumping out" value-added resources from wastewater by bioelectrochemical systems: A review from energy

perspectives. Water Res 2018;131:62–73. doi:10.1016/j.watres.2017.12.026.

[168] Khan MZ, Nizami AS, Rehan M, Ouda OKM, Sultana S, Ismail IM, et al. Microbial electrolysis cells for hydrogen production and urban wastewater treatment: A case study of Saudi Arabia. Appl Energy 2017;185:410–20. doi:10.1016/j.apenergy.2016.11.005.

[169] Cotterill SE, Dolfing J, Jones C, Curtis TP, Heidrich ES. Low Temperature Domestic Wastewater Treatment in a Microbial Electrolysis Cell with 1 m2Anodes: Towards System Scale-Up. Fuel Cells 2017;17:584–92. doi:10.1002/fuce.201700034.

[170] Liu L, Pang C, Wu S, Dong R. Optimization and evaluation of an air-recirculated stripping for ammonia removal from the anaerobic digestate of pig manure. Process Saf Environ Prot 2015;94:350–7. doi:10.1016/j.psep.2014.08.006.

[171] Collivignarelli C, Bertanza G, Baldi M, Avezzu F. Ammonia stripping from MSW landfill leachate in bubble reactors: process modeling and optimization. Waste Manag Res 1998;16:455–66. doi:10.1177/0734242X9801600508.

[172] Larsen T a., Udert KM, Lienert J. Source Separation and Decentralization for Wastewater Management. IWA Publ 2013:491. doi:10.1017/CBO9781107415324.004.

[173] Jardin N, Thöle D, Wett B. Treatment of sludge return liquors: Experiences from the operation of full-scale plants. Weftec 2006 2006;1991:5237–55.

[174] Bonmatí A, Flotats X. Air stripping of ammonia from pig slurry: Characterisation and feasibility as a pre- or post-treatment to mesophilic anaerobic digestion. Waste Manag 2003;23:261–72. doi:10.1016/S0956-053X(02)00144-7.

[175] Lide D, editor. CRC Handbook of Chemistry and Physics. A Ready-reference Book of CHemical and Physical Data. Boca Raton: CRC Press; 1993.

[176] Hidalgo D, Corona F, Martín-Marroquín JM, del Álamo J, Aguado A. Resource recovery from anaerobic digestate: struvite crystallisation versus ammonia stripping. Desalin Water Treat 2016. doi:10.1080/19443994.2014.1001794.

[177] Siegrist H, Laureni M, Udert KM. Transfer into the gas phase: ammonia stripping. In: Larsen TA, Udert KM, Lie, editors. Source Sep. Decentralization Wastewater Manag. 1st ed., London: IWA Publishing; 2013, p. 337–50.

[178] Lei X, Sugiura N, Feng C, Maekawa T. Pretreatment of anaerobic digestion effluent with ammonia stripping and biogas purification. J Hazard Mater 2007;145:391–7. doi:10.1016/j.jhazmat.2006.11.027.

[179] Collings GH. Commercial Fertilizers. 5th ed. New Delhi: Tata McGraw-Hill; 1955.

[180] Heffer P, Prud'homme M. Global Nitrogen Fertiliser Demand and Supply: Trend, Current Level and Outlook. Int Fertil Assoc 2016.

[181] Perry RH, Green DW. Chemical Engineers' Handbook Seventh. 7th ed. New York: McGraw-Hill; 1997. doi:10.1021/ed027p533.1.

[182] Metcalf & Eddy Inc. Wastewater Engineering: Treatment and Reuse. 4th ed. Boston: McGraw-Hill; 2003.

[183] Huang J, Shang C. Air stripping. Adv Physicochem Treat Process 2006;4:47–79. doi:10.1016/S0166-1116(08)70529-6.

[184] Kinidi L, Ai I, Tan W, Binti N, Wahab A, Fikri K, et al. Recent Development in Ammonia Stripping Process for Industrial Wastewater Treatment. Int J Chem Eng 2018;2018.

[185] Saracco G, Genon G. High temperature ammonia stripping and recovery from process liquid wastes. J Hazard Mater 1994;37:191–206. doi:10.1016/0304-3894(94)85048-8.

[186] Liu B, Giannis A, Zhang J, Chang VWC, Wang JY. Air stripping process for ammonia recovery from source-separated urine: Modeling and optimization. J Chem Technol Biotechnol 2015;90:2208–17.

doi:10.1002/jctb.4535.

[187] RVT. Ammonia recovery Removal from liquids and gases 2015. http://www.rvtpe.net/wp-content/uploads/prospekte/RVT_Ammonia_Recovery_120529.pdf (accessed September 14, 2018).

[188] SSM (Solids Sewage Manure). ANAStrip Technology 2009. http://www.ssm-technology.com/ (accessed February 11, 2019).

[189] ACWA. Air Stripping 1996. http://www.acwa.co.uk/air_stripping (accessed February 11, 2019).

[190] Anaergia. Nutrients and Digestate Management n.d. https://www.anaergia.com/what-we-do/wastewater-resource-recovery/nutrient-recovery-and-biosolids-management (accessed February 11, 2019).

[191] Monroe Environmental. Air Strippers. 2018.

[192] Branch Environmental Corp. Ammonia Strippers 2018. https://www.branchenv.com/ammonia-stripper/ (accessed February 11, 2019).

[193] CECO-HEE Environmental Engineering. Air Stripped Tower Model HAST. 2018.

[194] Nijhuis Industries. NIJHUIS AECO-NAR Efficient ammonia removal from digestate and production of green fertilizer. 2017.

[195] Colsen. AMFER - Removal of ammonia from digestate and waste water. 2015.

[196] CMI. Expert of AIR STRIPPING SOLUTIONS. 2016.

[197] Teichgräber B, Stein A. Nitrogen elimination from sludge treatment reject water – comparison of the steam-stripping and denitrification processes. Water Sci Technol 1994;30:41–51.

[198] Zeng L, Mangan C, Li X. Ammonia recovery from anaerobically digested cattle manure by steam stripping. Water Sci Technol 2006;54:137–45.

doi:10.2166/wst.2006.852.

[199] Mondor M, Masse L, Ippersiel D, Lamarche F, Massé DI. Use of electrodialysis and reverse osmosis for the recovery and concentration of ammonia from swine manure. Bioresour Technol 2008;99:7363–8. doi:10.1016/j.biortech.2006.12.039.

[200] McCutcheon JR, McGinnis RL, Elimelech M. Desalination by ammonia-carbon dioxide forward osmosis: Influence of draw and feed solution concentrations on process performance. J Memb Sci 2006;278:114–23. doi:10.1016/j.memsci.2005.10.048.

[201] Reeves TG. Nitrogen removal: a literature review. Water Pollut Control Fed Water Environ Fed 1972;44:1895–908.

[202] Maurer M, Pronk W, Larsen TA. Treatment processes for source-separated urine. Water Res 2006;40:3151–66. doi:10.1016/j.watres.2006.07.012.

[203] Cath TY, Childress AE, Elimelech M. Forward osmosis: Principles, applications, and recent developments. J Memb Sci 2006;281:70–87. doi:10.1016/j.memsci.2006.05.048.

[204] Xie M, Shon HK, Gray SR, Elimelech M. Membrane-based processes for wastewater nutrient recovery: Technology, challenges, and future direction. Water Res 2016;89:210–21. doi:10.1016/j.watres.2015.11.045.

[205] Zarebska A, Nieto DR, Christensen K V., Norddahl B. Ammonia recovery from agricultural wastes by membrane distillation: Fouling characterization and mechanism. Water Res 2014;56:1–10. doi:10.1016/j.watres.2014.02.037.

[206] Thygesen O, Hedegaard MAB, Zarebska A, Beleites C, Krafft C. Membrane fouling from ammonia recovery analyzed by ATR-FTIR imaging. Vib Spectrosc 2014;72:119–23. doi:10.1016/j.vibspec.2014.03.004.

[207] Ellamla HR, Staffell I, Bujlo P, Pollet BG, Pasupathi S. Current status of fuel cell based combined heat and power systems for residential sector. J

Power Sources 2015;293:312–28. doi:10.1016/j.jpowsour.2015.05.050.

[208] Hajimolana SA, Hussain MA, Daud WMAW, Soroush M, Shamiri A. Mathematical modeling of solid oxide fuel cells: A review. Renew Sustain Energy Rev 2011;15:1893–917. doi:10.1016/j.rser.2010.12.011.

[209] Nagel FP, Schildhauer TJ, Biollaz SMA. Biomass-integrated gasification fuel cell systems - Part 1: Definition of systems and technical analysis. Int J Hydrogen Energy 2009;34:6809–25. doi:10.1016/j.ijhydene.2009.05.125.

[210] Park J, Li P, Bae J. Analysis of chemical, electrochemical reactions and thermo-fluid flow in methane-feed internal reforming SOFCs: Part i - Modeling and effect of gas concentrations. Int J Hydrogen Energy 2012;37:8512–31. doi:10.1016/j.ijhydene.2012.02.110.

[211] Lee AL, Zabransky RF, Huber WJ. Internal reforming development for solid oxide fuel cells. Ind Eng Chem Res 1990;29:766–73. doi:10.1021/ie00101a009.

[212] Lisbona P, Corradetti A, Bove R, Lunghi P. Analysis of a solid oxide fuel cell system for combined heat and power applications under non-nominal conditions. Electrochim Acta 2007;53:1920–30. doi:10.1016/j.electacta.2007.08.046.

[213] Ni M, Leung MKH, Leung DYC. Ammonia-fed solid oxide fuel cells for power generation - A review. Int J Energy Res 2009;33:943–59. doi:10.1002/er.

[214] Lin Y, Ran R, Guo Y, Zhou W, Cai R, Wang J, et al. Proton-conducting fuel cells operating on hydrogen, ammonia and hydrazine at intermediate temperatures. Int J Hydrogen Energy 2010;35:2637–42. doi:10.1016/j.ijhydene.2009.04.019.

[215] Gao H, Scherson YD, Wells GF, Rockstrom J, Steffen W, Noone K, et al. Towards energy neutral wastewater treatment: methodology and state of the art. Environ Sci Process Impacts 2014;16:1223. doi:10.1039/c4em00069b.

[216] Gandiglio M, Lanzini A, Soto A, Leone P, Santarelli M. Enhancing the Energy Efficiency of Wastewater Treatment Plants through Co-digestion and Fuel Cell Systems. Front Environ Sci 2017;5:1–21. doi:10.3389/fenvs.2017.00070.

[217] Qadir Z. DEMOSOFC: Turning waste into energy in Turin, Italy | Sustainable Gas Institute. Sustain Gas Inst 2018. https://www.sustainablegasinstitute.org/demosofc-turning-waste-into-energy-in-turin-italy/ (accessed September 17, 2018).

[218] Vakouftsi E, Marnellos GE, Athanasiou C, Coutelieris F. CFD modeling of a biogas fuelled SOFC. Solid State Ionics 2011;192:458–63. doi:10.1016/j.ssi.2010.05.051.

[219] Zakrzewska B, Pianko-Oprych P, Jaworski Z. Multiscale Modeling of Solid Oxide Fuel Cell Systems. Chemie Ing Tech 2014;86:1029–43. doi:10.1002/cite.201400022.

[220] Beale SB. Numerical models for planar solid oxide fuel cells. In: Sundén B, Faghri M, editors. Transp. Phenom. fuel cells, vol. 10, Southampton, UK: WIT Press; 2005. doi:10.2495/1-85312-840-6/02.

[221] Perna A, Minutillo M, Jannelli E, Cigolotti V, Nam SW, Yoon KJ. Performance assessment of a hybrid SOFC/MGT cogeneration power plant fed by syngas from a biomass down-draft gasifier. Appl Energy 2017:1–13. doi:10.1016/j.apenergy.2017.08.077.

[222] Minutillo M, Perna A, Jannelli E. SOFC and MCFC system level modeling for hybrid plants performance prediction. Int J Hydrogen Energy 2014;39:21688–99. doi:10.1016/j.ijhydene.2014.09.082.

[223] Costamagna P, Selimovic A, Del Borghi M, Agnew G. Electrochemical model of the integrated planar solid oxide fuel cell (IP-SOFC). Chem Eng J 2004;102:61–9. doi:10.1016/j.cej.2004.02.005.

[224] Ameri M, Mohammadi R. Simulation of an atmospheric SOFC and gas turbine hybrid system using Aspen Plus software. Int J Energy Res 2013;37:412–25. doi:10.1002/er.

[225] Wiranarongkorn K, Im-Orb K, Ponpesh P, Patcharavorachot Y, Arpornwichanop A. Design and evaluation of the sorption enhanced steam reforming and solid oxide fuel cell integrated system with anode exhaust gas recirculation for combined heat and power generation. Chem Eng Trans 2017;57:97–102. doi:10.3303/CET1757017.

[226] Doherty W, Reynolds A, Kennedy D. Process simulation of biomass gasification integrated with a solid oxide fuel cell stack. J Power Sources 2015;277:292–303. doi:10.1016/j.jpowsour.2014.11.125.

[227] Bao C, Wang Y, Feng D, Jiang Z, Zhang X. Macroscopic modeling of solid oxide fuel cell (SOFC) and model-based control of SOFC and gas turbine hybrid system. Prog Energy Combust Sci 2018;66:83–140. doi:10.1016/j.pecs.2017.12.002.

[228] Colantoni A, Giuseppina M, Buccarella M, Cividino S, Vello M. Economical Analysis of SOFC System for Power Production. Comput. Sci. Its Appl. - ICCSA, Santander, Spain: 2011, p. 270–6.

[229] Wei M, Smith SJ, Sohn MD. Analysis of Fuel Cell Markets in Japan and the US : Experience Curve Development and Cost Reduction Disaggregation. ERNEST ORLANDO LAWRENCE BERKELEY Natl Lab 2016.

[230] Siefert NS, Litster S. Exergy & economic analysis of biogas fueled solid oxide fuel cell systems. J Power Sources 2014;272:386–97. doi:10.1016/j.jpowsour.2014.08.044.

[231] Ammermann H, Hoff P, Atanasiu M, Ayloor J, Kaufmann M, Tisler O. Advancinng Europe's energy systems: Stationary fuel cells in distributed generation: A study for the Fuel Cells and Hydrogen Joint Undertaking. Luxemberg: Publications Office of the European Union; 2015.

[232] Arsalis A. Thermoeconomic modeling and parametric study of hybrid SOFC – gas turbine – steam turbine power plants ranging from 1 . 5 to 10 MWe. J OfPower Sources 2008;181:313–26. doi:10.1016/j.jpowsour.2007.11.104.

[233] Cheddie DF. Integration of A Solid Oxide Fuel Cell into A 10 MW Gas Turbine Power Plant 2010:754–69. doi:10.3390/en3040754.

[234] Naja B, Shirazi A, Aminyavari M, Rinaldi F, Taylor RA. Exergetic , economic and environmental analyses and multi-objective optimization of an SOFC-gas turbine hybrid cycle coupled with an MSF desalination system 2014;334:46–59. doi:10.1016/j.desal.2013.11.039.

[235] Farooque M, Daly J, Leo T, Pais C, Venkataraman R, Wang J-Y, et al. Direct Fuel Cell Experience on Renewable Biogas. ECS Trans 2011;30:261–70. doi:10.1149/1.3562481.

[236] Gabrielli P, Gazzani M, Mazzotti M. Electrochemical conversion technologies for optimal design of decentralized multi-energy systems: Modeling framework and technology assessment. Appl Energy 2018;221:557–75. doi:10.1016/j.apenergy.2018.03.149.

[237] Lanzini A, Madi H, Chiodo V, Papurello D, Maisano S, Santarelli M, et al. Dealing with fuel contaminants in biogas-fed solid oxide fuel cell (SOFC) and molten carbonate fuel cell (MCFC) plants: Degradation of catalytic and electro-catalytic active surfaces and related gas purification methods. Prog Energy Combust Sci 2017;61:150–88. doi:10.1016/j.pecs.2017.04.002.

[238] Newbery DM. Towards a green energy economy? The EU Energy Union's transition to a low-carbon zero subsidy electricity system – Lessons from the UK's Electricity Market Reform. Appl Energy 2016. doi:10.1016/j.apenergy.2016.01.046.

[239] Garton G, Grimwood, Ares E. Energy : The Renewables Obligation Briefing paper. London: 2016.

[240] Wood G, Dow S. What lessons have been learned in reforming the Renewables Obligation? An analysis of internal and external failures in UK renewable energy policy. Energy Policy 2011;39:2228–44. doi:10.1016/j.enpol.2010.11.012.

[241] Ofgem. Feed-in Tariffs: Essential guide to closure of the scheme 2018.

[242] BEIS. The Future for Small-scale Low-carbon generation - a call for evidence. 2018.

[243] DECC. Electricity market reform: policy overview. 2012. doi:10.1109/CONECCT.2013.6469293.

[244] DECC. CFD Auction Allocation Round One 2015.

[245] Department of Energy & Climate Change. National Renewable Energy Action Plan for the United Kingdom Article 4 of the Renewable Energy Directive. 2009. doi:1st July 2010.

[246] Ofgem. Tariffs and payments: Non-Domestic RHI 2019. https://www.ofgem.gov.uk/environmental-programmes/non-domestic-rhi/contacts-guidance-and-resources/tariffs-and-payments-non-domestic-rhi (accessed February 14, 2019).

[247] Carrère H, Dumas C, Battimelli A, Batstone DJ, Delgenès JP, Steyer JP, et al. Pretreatment methods to improve sludge anaerobic degradability: A review. J Hazard Mater 2010;183:1–15. doi:10.1016/j.jhazmat.2010.06.129.

[248] APHA. Standard Methods for the Examination of Water & Wastewater. 21st ed. Washington D.C.: American Public Health Association; 2005.

[249] Yorkshire Water. Green Apple Award for Esholt Waste Water Treatment Works 2016. https://www.yorkshirewater.com/about-us/newsroom-media/green-apple-award-2016 (accessed July 30, 2018).

[250] Mininni G, Laera G, Bertanza G, Canato M, Sbrilli A. Mass and energy balances of sludge processing in reference and upgraded wastewater treatment plants. Environ Sci Pollut Res Int 2015;22:7203–15. doi:10.1007/s11356-014-4013-2.

[251] Baker G. Email to Oliver Grasham, 23 August. 2016.

[252] Baker G. Email to Oliver Grasham, 13 September. 2016.

[253] Ramirez Sosa DR. Resource recovery from co-digestion of organic waste with surplus activated sludge via the carboxylate platform. University of Leeds, 2017.

[254] Yorkshire Water. Thermal Hydrolysis Project 2013. https://yorkshirewater.com/sites/default/files/downloads/Thermal

Hydrolysis.pdf.

[255] Abu-Orf M, Goss T. Comparing Thermal Hydrolysis Processes (CAMBI™ and EXELYS™) For Solids Pretreatmet Prior To Anaerobic Digestion. Proc Water Environ Fed 2012;2012:1024–36. doi:10.2175/193864712811693272.

[256] Baker G. Email to Oliver Grasham, 19 December. 2016.

[257] Renewables-UK. Project Details from OFGEM: Esholt STW CHP 2018. http://renewables-uk.co.uk/subscriber/details_ofgem.asp?ofgemid=G01258SGEN (accessed August 15, 2018).

[258] Guerrini A, Romano G, Indipendenza A. Energy efficiency drivers in wastewater treatment plants: A double bootstrap DEA analysis. Sustain 2017;9:1–13. doi:10.3390/su9071126.

[259] Parravicini V, Svardal K, Krampe J. Greenhouse Gas Emissions from Wastewater Treatment Plants. Energy Procedia 2016;97:246–53. doi:10.1016/j.egypro.2016.10.067.

[260] Daelman MRJ, Van Voorthuizen EM, Van Dongen LGJM, Volcke EIP, Van Loosdrecht MCM. Methane and nitrous oxide emissions from municipal wastewater treatment - Results from a long-term study. Water Sci Technol 2013;67:2350–5. doi:10.2166/wst.2013.109.

[261] IPCC. Climate Change 2013: The Physical Science Basis 2013.

[262] Aspen Plus. Aspen Technology. Inc, Version, 88 2015.

[263] Boul PJ, Langez KE, Conger B, Anderson M. Air Stripping Designs and Reactive Water Purification Processes for the Lunar Surface. Am Inst Aeronaut Astronaut 2010.

[264] Aspen-HYSYS. Aspen HYSYS - Aspen Physical Property System 2001.

[265] Aspen Plus Economic Analyzer. Aspen Technology. Inc, Version, 10 2017.

[266] Aspen Technology. Aspen Capital Cost Estimator: User Guide 2017.

[267] Alkhayat WA, Gerrard AM. Estimating Manning Levels for Process Plants.

Trans. Am. Assoc. Cost Eng., Montreal, Canada: 1984, p. 1.2.1-1.2.4.

[268] Turton R, Bailie RC, Whiting WB, Shaeiwitz JA. Estimation of Manufacturing Costs. In: Turton R, Bailie RC, Whiting WB, Shaeiwitz JA, editors. Anal. Synth. Des. Chem. Process. 3rd ed., Upper Saddle River, N.J.: Prentice Hall; 2008.

[269] Glass Door. Salary: Process Engineer 2018. https://www.glassdoor.co.uk/Salaries/process-engineer-salary-SRCH_KO0,16.htm (accessed November 27, 2018).

[270] Office for National Statistics (ONS). Wages and salaries annual growth rate % 2018. https://www.ons.gov.uk/economy/grossdomesticproductgdp/timeseries/kgq2/qna (accessed November 27, 2018).

[271] Rotunno P, Lanzini A, Leone P. Energy and economic analysis of a water scrubbing based biogas upgrading process for biomethane injection into the gas grid or use as transportation fuel. Renew Energy 2017;102:417–32. doi:10.1016/j.renene.2016.10.062.

[272] Office for national statistics (ONS). RPI All Items: Percentage change over 12 months n.d. https://www.ons.gov.uk/economy/inflationandpriceindices/timeseries/czbh/mm23 (accessed December 4, 2018).

[273] ICIS. ICIS Pricing: Caustic Soda (Europe). 2014.

[274] Agriculture & Horticulture Development Board (ADHB). UK Fertiliser Price Market Update Monthly average prices for October 2018. 2018.

[275] Locher C, Meyer C, Steinmetz H. Operating experiences with a molten carbonate fuel cell at Stuttgart-Möhringen wastewater treatment plant. Water Sci Technol 2012;65:789–94. doi:10.2166/wst.2012.463.

[276] Mehr AS, Gandiglio M, MosayebNezhad M, Lanzini A, Mahmoudi SMS, Yari M, et al. Solar-assisted integrated biogas solid oxide fuel cell (SOFC) installation in wastewater treatment plant: Energy and economic analysis. Appl Energy 2017;191:620–38.

doi:10.1016/j.apenergy.2017.01.070.

[277] Singhal SC. Solid oxide fuel cells for stationary, mobile, and military applications. Solid State Ionics 2002;152–153:405–10. doi:10.1016/S0167-2738(02)00349-1.

[278] Krishnan VV. Recent developments in metal-supported solid oxide fuel cells. Wiley Interdiscip Rev Energy Environ 2017;6. doi:10.1002/wene.246.

[279] Borello D, Del Prete Z, Marchegiani A, Rispoli F, Tortora E. Analysis of an Integrated PEMFC/ORC Power System Using Ammonia for Hydrogen Storage. Vol 3 Cycle Innov Educ Electr Power; Fans Blowers; Ind Cogener 2012;3:143. doi:10.1115/GT2012-68599.

[280] Alvarado L, Chen A. Electrodeionization: Principles, strategies and applications. Electrochim Acta 2014;132:583–97. doi:10.1016/j.electacta.2014.03.165.

[281] Barbera E, Menegon S, Banzato D, D'Alpaos C, Bertucco A. From biogas to biomethane: a process simulation-based techno-economic comparison of different upgrading technologies in the Italian context. Renew Energy 2018;135:663–73. doi:10.1016/j.renene.2018.12.052.

[282] Grasham O, Dupont V, Camargo-Valero MA, García-Gutiérrez P, Cockerill T. Combined ammonia recovery and solid oxide fuel cell use at wastewater treatment plants for energy and greenhouse gas emission improvements. Appl Energy 2019;240:698–708. doi:10.1016/j.apenergy.2019.02.029.

[283] Campanari S, Iora P. Definition and sensitivity analysis of a finite volume SOFC model for a tubular cell geometry. J Power Sources 2004;132:113–26. doi:10.1016/j.jpowsour.2004.01.043.

[284] Spallina V, Mastropasqua L, Iora P, Romano MC, Campanari S. Assessment of finite volume modeling approaches for intermediate temperature Solid Oxide Fuel Cells working with CO-rich syngas fuels. Int J Hydrogen Energy 2015;40:15012–31. doi:10.1016/j.ijhydene.2015.08.101.

[285] Ong KM, Lee WY, Hanna J, Ghoniem AF. Isolating the impact of CO concentration in syngas mixtures on SOFC performance via internal reforming and direct oxidation. Int J Hydrogen Energy 2016;41:9035–47. doi:10.1016/j.ijhydene.2016.03.107.

[286] Lee TS, Chung JN, Chen YC. Design and optimization of a combined fuel reforming and solid oxide fuel cell system with anode off-gas recycling. Energy Convers Manag 2011;52:3214–26. doi:10.1016/j.enconman.2011.05.009.

[287] Batelle Memorial Institute. Manufacturing Cost Analysis of 100 and 250 kW Fuel Cell Systems for Primary Power and Combined Heat and Power Applications. Columbus, OH: U.S. Departmentof Energy; 2017.

[288] Peters MS, Timmerhaus KD, West RE. Heat-Transfer Equipment - Design and Costs. Plant Des. Econ. Chem. Eng. 5th ed., New York: McGraw-Hill; 2004, p. 642–754. doi:10.1080/00137915908965075.

[289] Bank of England. Inflation calculator | Bank of England 2018. https://www.bankofengland.co.uk/monetary-policy/inflation/inflation-calculator?number.Sections%5B0%5D.Fields%5B0%5D.Value=150000&start-year=736.5&end-year=1075 (accessed January 11, 2019).

[290] Ofgem. About the Non-Domestic RHI 2019. https://www.ofgem.gov.uk/environmental-programmes/non-domestic-rhi/about-non-domestic-rhi (accessed February 1, 2019).

[291] Ofgem. Tariffs and payments: Non-Domestic RHI 2019. https://www.ofgem.gov.uk/environmental-programmes/non-domestic-rhi/contacts-guidance-and-resources/tariffs-and-payments-non-domestic-rhi (accessed February 1, 2019).

[292] Williams MC, Strarkey JP, Singhal SC. US distributed generation fuel cell program. In: Brandon N, Thompsett D, editors. Fuel Cells Compend. 1st ed., Oxford, UK: Elsevier Ltd; 2005, p. 4.

[293] Kaur G. Cell Voltages , Polarisations and Performances. Solid Oxide Fuel Cell Components, Cham: Springer; n.d. doi:10.1007/978-3-319-25598-9.

[294] BEIS, Department for Business E& IS. Updated Energy and Emissions Projections 2017 2018.

[295] Leigh Fisher. Electricity Generation Costs and Hurdle Rates. 2016.

[296] Ogden JM. Review of Small Stationary Reformers for Hydrogen Production. Environ Stud 2001:63. doi:IEA/H2/TR-02/002.

[297] Iulianelli A, Liguori S, Wilcox J, Basile A. Advances on methane steam reforming to produce hydrogen through membrane reactors technology: A review. Catal Rev - Sci Eng 2016;58:1–35. doi:10.1080/01614940.2015.1099882.

[298] Chen WH, Lin MR, Jiang TL, Chen MH. Modeling and simulation of hydrogen generation from high-temperature and low-temperature water gas shift reactions. Int J Hydrogen Energy 2008;33:6644–56. doi:10.1016/j.ijhydene.2008.08.039.

[299] Melaina M, Penev M. Hydrogen Station Cost Estimates. 2013.

[300] Moscoviz R, Trably E, Bernet N, Carrère H. The environmental biorefinery: State-of-the-art on the production of hydrogen and value-added biomolecules in mixed-culture fermentation. Green Chem 2018;20:3159–79. doi:10.1039/c8gc00572a.

[301] Roland B. Fuel Cells and Hydrogen for Green Energy in European Cities and Regions. 2018.

[302] Reuter B, Faltenbacher M, Schuller O, Whitehouse N, Whitehouse S. New Bus ReFuelling for European Hydrogen Bus Depots: High-Level Techno-Economic Project Summary Report. 2017.

[303] Penev M, Saur G, Hunter C, Zuboy J. H2A Hydrogen Production Model : Version 3 . 2018 User Guide (DRAFT). NREL 2018.

[304] Peters M, Timmerhaus KD, West RE. Analysis of Cost Estimation. Plant Des. Econ. Chem. Eng. 5th ed., New York: McGraw-Hill; 2004, p. 226–78.

[305] Kaiwen L, Bin Y, Tao Z. Economic analysis of hydrogen production from steam reforming process: A literature review. Energy Sources, Part B Econ Plan Policy 2018;13:109–15.

doi:10.1080/15567249.2017.1387619.

[306] BEIS. Gas and electricity prices in the non-domestic sector 2018. https://www.gov.uk/government/statistical-data-sets/gas-and-electricity-prices-in-the-non-domestic-sector (accessed March 8, 2019).

[307] Clean Air Technology Center. Nitrogen Oxides (NOx), Why and How They Are Controlled. Epa-456/F-99-006R 1999:48. doi:EPA 456/F-99-006R.

[308] Willmann V. Aberdeen Hydrogen Bus Project. LowCVP Low Emiss Bus Work Glas 08/03/2018 2018.

[309] Hill N, Bonifazi E, Bramwell R, Karagianni B, Harris B. 2018 Government GHG Conversion Factors For Company Reporting: Methodology paper for emission factors: final report 2018:141.

[310] Parliamentary Office of Science and Technology. Carbon Footprint of Heat Generation. Postnote Updat 2016;523:1–6.

[311] Rostrup-Nielsen J. Steam reforming of hydrocarbons. A historical perspective. Stud Surf Sci Catal 2007;147:121–6. doi:10.1016/s0167-2991(04)80038-7.

[312] Jones G, Jakobsen JG, Shim SS, Kleis J, Andersson MP, Rossmeisl J, et al. First principles calculations and experimental insight into methane steam reforming over transition metal catalysts. J Catal 2008;259:147–60. doi:10.1016/j.jcat.2008.08.003.

[313] Rollinson AN, Rickett GL, Lea-Langton A, Dupont V, Twigg M V. Hydrogen from urea–water and ammonia–water solutions. Appl Catal B Environ 2011;106:304–15. doi:10.1016/j.apcatb.2011.05.031.

[314] Hou K, Hughes R. The kinetics of methane steam reforming over a Ni / alpha -Al2O3 catalyst. Chem Eng J 2001;82:311–28. doi:http://dx.doi.org/10.1016/S1385-8947(00)00367-3.

[315] Saberimoghaddam A, Nozari A. A kinetic and statistical model for carbon deposition on Ni/Al2O3 catalyst in the steam methane reforming. Res Chem Intermed 2018;44:201–15. doi:10.1007/s11164-017-3098-x.

[316] Yamaguchi T, Shimizu S, Suzuki T, Fujishiro Y, Awano M. Design and fabrication of a novel electrode-supported honeycomb SOFC. J Am Ceram Soc 2009;92. doi:10.1111/j.1551-2916.2008.02688.x.

10 Appendices

10.1 Appendix A

Data referenced in Chapter 3

Table A 1. Characterisation from various Esholt WWTP streams

a) Raw wastewater

Date	Temp (°C)	pH	TSS (mg L^{-1})	VSS (mg L^{-1})	COD (mg L^{-1})	TKN (mg L^{-1})	TAN (mg L^{-1})	NO_3-N (mg L^{-1})	TP (mg L^{-1})	PO_4^{3-}P (mg L^{-1})
Oct-14	18.0	6.97	200	168	1373	24.6	15.7	2.0	0.9	0.9
Nov-14	22.5	7.59	216	180	140	21.3	14.6	1.9	2.8	1.9
Dec-14	15.0	7.75	394	262	276	42.6	24.6	0.2	8.2	6.3
Jan-15	7.5	7.65	206	180	408	34.7	21.3	0.5	5.4	4.3
Feb-15	9.0	7.69	266	232	741	53.8	29.1	0.5	6.2	5.4
Mar-15	10.0	7.67	276	194	1071	59.4	33.6	0.2	7.1	7.1
Jul-15	10.0	6.81	298	252	680	35.3	21.3	ND	5.3	5.8
Oct-15	8.5	7.13	528	458	968	49.3	30.8	0.3	7.1	2.8
Nov-15	16.5	7.34	552	442	507	44.8	14.6	1.5	6.3	4.0
Dec-15	12.0	7.19	148	102		16.2	5.0	2.0		
Jan-16	18.5	7.40	192	154	1221	48.2	18.5	0.5	3.8	1.9
Feb-16	13.0	7.62	416	360	1172	54.9	28.8	0.7	7.2	4.4
Mar-16	14.2	7.77	500	422		63.3	34.2	0.6	9.2	5.8
Apr-16	14.8	7.81	284	234	956	59.4	31.9	0.1	7.4	4.8
May-16	8.2	6.90	358	318	732	66.1	39.8	ND	8.0	4.1
Mean	13.2	7.4	322.3	263.9	788.1	44.9	24.2	0.9	6.1	4.2
Min	8.2	6.8	148.0	102.0	507.2	16.2	5.0	0.1	3.8	1.9
Max	18.5	7.8	552.0	458.0	1221	66.1	39.8	2.0	9.2	7.1
STDEV	4.4	0.3	130	112	381	15.6	9.5	0.7	2.3	1.8

b) Primary Clarifier

Date	Temp (°C)	pH	TSS (mg L^{-1})	VSS (mg L^{-1})	COD (mg L^{-1})	TKN (mg L^{-1})	TAN (mg L^{-1})	NO_3-N (mg L^{-1})	TP (mg L^{-1})	PO_4^{3}-P (mg L^{-1})
Oct-14	18.0	6.74	60	52	242	17.1	7.8	2.8	0.1	0.4
Nov-14	22.0	7.46	142	114	154	14.6	3.4	1.8	1.9	1.2
Dec-14	14.5	7.41	178	94	241	26.0	15.1	0.3	3.3	1.8
Jan-15	7.0	7.46	102	78	143	21.8	9.0	0.5	2.8	1.4
Feb-15	9.0	7.13	136	114	370	38.1	26.3	0.0	2.4	2.2
Mar-15	9.5	7.42	42	22	402	38.1	23.0	0.3	2.2	2.2
Jul-15	9.0	6.98	116	106	354	33.0	24.6	ND	2.5	2.1
Oct-15	7.5	7.39	128	110	500	45.9	34.2	0.4	4.5	2.1
Nov-15	16.0	7.42	64	58	123	12.3	5.6	2.2	0.5	0.2
Dec-15	13.0	7.17	92	84		15.4	9.0	1.0		
Jan-16	18.5	7.34	84	52	198	20.7	11.8	0.8	ND	0.8

Feb-16	12.5	7.30	60	60	258.0	24.6	14.8	1.0	0.6	0.6
Mar-16	14.5	7.30	90	88		37.8	17.9	0.9	1.7	1.4
Apr-16	14.5	7.25	120	110	449	35.3	19.6	0.9	2.8	2.1
May-16	8.1	6.94	80	80	171	31.4	20.7	ND	1.2	0.7
Mean	12.9	7.2	99.6	81.5	277.3	27.5	16.2	1.0	2.0	1.4
Min	7.5	6.9	42.0	22.0	123.2	12.3	5.6	0.0	0.5	0.2
Max	18.5	7.4	136.0	114.0	500.0	45.9	34.2	2.2	4.5	2.2
STDEV	4.5	0.2	37	28	125	10.4	8.7	0.8	1.2	0.7

c) ASP inlet

Date	Temp (°C)	pH	TSS (mg L^{-1})	VSS (mg L^{-1})	COD (mg L^{-1})	TKN (mg L^{-1})	TAN (mg L^{-1})	NO_3-N (mg L^{-1})	TP (mg L^{-1})	PO_4^{3-}P (mg L^{-1})
Feb-15	9.0	7.18	496	396	696	53.2	33.6	0.0	3.0	2.9
Mar-15	12.5	6.76	3566	2734	4643	183.7	6.2	0.5	18.9	13.6
Jul-15	10.0	6.86	706	570	1224	101.9	28.0	ND	11.8	10.0
Oct-15	9.5	7.35	692	528	1129	81.8	38.6	ND	12.9	8.9
Nov-15	16.5	7.46	488	390	4058	39.2	10.6	2.1	6.3	3.0
Dec-15	14.5	7.24	300	242		34.2	11.2	0.7		
Jan-16	18.5	7.24	446	328	763	50.4	11.8	0.7	5.2	1.1
Feb-16	12.5	7.21	636	510	1094	57.1	14.8	1.1	10.4	3.5
Mar-16	14.1	7.37	736	588		76.7	17.4	0.7	12.2	4.5
Apr-16	15.2	7.28	694	564	1103	59.4	17.9	0.3	11.0	4.2
May-16	7.9	6.91	582	492	244	70.6	23.5	ND	11.3	1.6
Mean	12.7	7.2	849.3	667.5	1662	73.5	19.4	0.8	10.3	5.3
Min	7.9	6.8	300.0	242.0	243.9	34.2	10.6	0.0	3.0	1.1
Max	18.5	7.5	736.0	588.0	4058	101.9	38.6	2.1	12.9	10.0
STDEV	3.4	0.2	142	116	1164	20.6	9.9	0.7	3.5	3.1

d) ASP outlet

Date	Temp (°C)	pH	TSS (mg L^{-1})	VSS (mg L^{-1})	COD (mg L^{-1})	TKN (mg L^{-1})	TAN (mg L^{-1})	NO_3-N (mg L^{-1})	TP (mg L^{-1})	PO_4^{3-}P (mg L^{-1})
Feb-15	9.0	6.49	3594	2736	3704	173.6	4.5	1.9	2.8	1.3
Mar-15	10.5	6.69	3490	2640	5357	148.4	1.7	1.6	18.3	13.8
Jul-15	10.0	6.49	4174	3222	1361	249.8	2.5	ND	27.0	15.6
Oct-15	10.0	6.82	3442	2626	2419	184.8	3.4	9.3	41.0	15.5
Nov-15	16.5	6.81	3930	2916	5072	217.3	2.8	4.9	30.8	13.2
Dec-15	14.0	6.75	3622	2690		298.2	1.7	2.1		
Jan-16	19.0	6.54	4408	3312	5344	305.2	11.2	2.3	60.8	11.0
Feb-16	13.0	6.55	4168	3114	7031	280.0	3.1	8.0	69.3	18.5
Mar-16	15.4	6.65	4374	3346		312.2	2.2	2.7	73.3	19.0
Apr-16	15.3	6.55	3766	2922	6618	288.4	2.2	3.8	70.9	16.9

May-16	8.7	6.68	3246	2580	1626	310.8	1.7	1.7	72.2	2.3
Mean	12.9	6.6	3838	2919	4281	251.7	3.4	3.8	46.6	12.7
Min	8.7	6.5	3246	2580	1361	148.4	1.7	1.6	2.8	1.3
Max	19.0	6.8	4408	3346	7031	312.2	11.2	9.3	73.3	19.0
STDEV	3.4	0.1	398	288	2101	60.6	2.7	2.7	25.9	6.3

e) Secondary Clarifier

Date	Temp (°C)	pH	TSS (mg L^{-1})	VSS (mg L^{-1})	COD (mg L^{-1})	TKN (mg L^{-1})	TAN (mg L^{-1})	NO_3-N (mg L^{-1})	TP (mg L^{-1})	PO_4^{3-}-P (mg L^{-1})
Oct-14	19.5	6.09	22	22	85	2.0	2.1	5.5	0.0	0.0
Nov-14	22.5	6.89	84	76	71	7.0	2.1	7.2	0.3	0.0
Dec-14	14.0	6.83	112	42	41	1.4	1.8	1.9	0.4	0.3
Jan-15	7.0	6.98	16	12	7	4.5	0.7	1.3	0.4	0.2
Feb-15	11.0	6.61	24	20	74	1.7	1.4	2.4	0.1	0.2
Mar-15	9.0	6.72	34	28	54	3.1	1.4	2.0	0.2	0.1
Jul-15	9.0	6.74	16	14	27	2.0	0.6	1.0	0.1	0.1
Oct-15	9.0	7.06	20	20	105	3.4	0.8	15.1	ND	0.1
Nov-15	17.0	6.90	26	26	43	2.2	0.6	7.1	0.1	0.1
Dec-15	15.0	6.72	48	48		3.6	0.6	4.6		
Jan-16	18.5	6.74	46	26	53	3.9	1.1	3.8	ND	ND
Feb-16	13.0	6.65	10	10	31	2.2	0.3	9.4	ND	0.1
Mar-16	14.3	6.75	42	42		3.1	1.1	5.6	ND	0.1
Apr-16	14.3	6.70	16	16	59	4.5	1.1	6.2	ND	0.1
May-16	7.9	6.54	22	22	57	4.5	1.1	5.2	ND	0.0
Mean	13.4	6.73	35.8	28	54	3.3	1.1	5.2	0.2	0.1
Min	7.0	6.1	10.0	10.0	6.8	1.4	0.3	1.0	0.0	0.0
Max	22.5	7.1	112.0	76.0	104.8	7.0	2.1	15.1	0.4	0.3
STDEV	4.6	0.2	28	17	26	1.5	0.6	3.7	0.1	0.1

d) Whole digestate

Date	Temp (°C)	pH	TSS (mg L^{-1})	VSS (mg L^{-1})	COD (mg L^{-1})	TKN (mg L^{-1})	TAN (mg L^{-1})	NO_3-N (mg L^{-1})	TP (mg L^{-1})	PO_4^{3-}-P (mg L^{-1})
Oct-14	27.0	7.10	46500	28500	104575	2475.2	1523.2	4.56129	80.6	3.8
Nov-14	23.0	8.15	45300	23250	69930	3427.2	1456.0	ND	247.7	29.8
Dec-14	17.5	7.82	52000	31500	68966	4032.0	2284.8	ND	334.8	40.3
Jan-15	12.5	7.68	44125	24275	34014	3348.8	1489.6	ND	354.3	15.9
Feb-15	13.0	7.58	52965	33995	74074	3796.8	1355.2	0.4	210.9	18.8
Mar-15	17.0	7.79	35815	11760	26786	2251.2	1500.8	ND	248.0	18.4
Jul-15	13.0	7.97	37500	22500	27211	2772.0	1540.0	ND	262.1	56.1

Oct-15	12.0	7.90	44500	28000	48387	3332.0	1680.0	ND	189.5	ND
Nov-15	22.5	7.85	40500	26000	50725	3108.0	1372.0	ND	238.3	18.4
Dec-15	22.0	6.62	33615	19750		2926.0	1232.0	ND		
Jan-16	21.5	7.45	38000	23500	22901	2604.0	1232.0	ND	275.4	0.0
Feb-16	14.0	7.58	8000	5000	7812	1736.0	1162.0	0.1	177.5	5.8
Mar-16	17.4	7.51	50000	28000		3486.0	1540.0	ND	537.2	12.4
Apr-16	18.0	7.59	51500	29080	72059	3612.0	1596.0	ND	853.3	11.5
May-16	18.9	8.18	1396	1072	5344	4424.0	1568.0	ND	43.4	5.5
Mean	18.0	7.7	38781	22412	47137	3155.4	1502.1	1.7	289.5	18.2
Min	12.0	6.6	1396.0	1072.0	5343.5	1736.0	1162.0	0.1	43.4	0.0
Max	22.5	8.2	52965	33995	74074	4424.0	1680.0	0.4	853.3	56.1
STDEV	4.5	0.4	15149	9480	29609	710	262	2.5	201.0	15.8

e) Digestate Liquor

Date	Temp (°C)	pH	TSS (mg L^{-1})	VSS (mg L^{-1})	COD (mg L^{-1})	TKN (mg L^{-1})	TAN (mg L^{-1})	NO_3-N (mg L^{-1})	TP (mg L^{-1})	PO_4^{3-}P (mg L^{-1})
Oct-14			408	372	11765	1702.4	1523.2	4.6	7.4	3.8
Nov-14	21.0	8.06	540	470	4895	1612.8	1456.0	ND	38.4	29.8
Dec-14	21.5	7.86	492	402	6897	1792.0	2284.8	ND	46.3	40.3
Jan-15	22.0	7.79	656	496	2041	1612.8	1489.6	ND	27.4	15.9
Feb-15	20.0	7.59	396	350	2963	1433.6	1355.2	0.4	18.2	18.8
Mar-15	24.0	7.90	282	246	2679	1624.0	1500.8	ND	28.0	18.4
Jul-15	16.0	8.09	268	252	680	1652.0	1540.0	ND	64.1	56.1
Oct-15	11.0	7.88	336	310	2419	1876.0	1680.0	ND	22.1	ND
Nov-15	27.0	7.95	360	310	3623	1568.0	1372.0	ND	24.2	18.4
Dec-15	23.5	7.65	308	288		1442.0	1232.0	ND		
Jan-16	23.5	7.53	210	160	2290	1232.0	1232.0	ND	7.2	0.0
Feb-16	27.0	7.71	174	174	2344	1176.0	1162.0	0.1	10.7	5.8
Mar-16	24.4	7.62	308	274		1638.0	1540.0	ND	16.5	12.4
Apr-16	22.3	7.69	352	302	3824	1708.0	1596.0	ND	15.5	11.5
May-16	16.1	8.02	150	144	2927	1904.0	1568.0	ND	9.9	5.5
Mean	21.4	7.8	349.3	303.3	3795.8	1598.2	1502.1	1.7	24.0	18.2
Min	11.0	7.5	150.0	144.0	680.3	1176.0	1162.0	0.1	7.2	0.0
Max	27.0	8.1	396.0	350.0	3823.5	1904.0	1680.0	0.4	64.1	56.1
STDEV	4.4	0.2	137	104	2830	207	262	2.5	16.3	15.8

f) Final Effluent

Date	Temp (°C)	pH	TSS (mg L^{-1})	VSS (mg L^{-1})	COD (mg L^{-1})	TKN (mg L^{-1})	TAN (mg L^{-1})	NO_3-N (mg L^{-1})	TP (mg L^{-1})	PO_4^{3-}P (mg L^{-1})

Oct-14	19.0	6.15	14	14	85	3.6	0.0	4.8	0.2	0.3
Nov-14	22.5	7.21	58	58	49	8.7	0.6	7.8	0.7	0.6
Dec-14	14.0	7.07	94	22	28	1.4	1.1	1.8	1.3	1.6
Jan-15	7.0	7.07	14	10	7	1.7	0.6	1.3	0.6	0.7
Feb-15	11.0	7.11	30	22	44	1.7	2.5	2.7	2.2	2.2
Mar-15	9.5	7.02	24	22	80	1.4	1.1	9.3	0.3	0.5
Jul-15	11.0	6.92	8	8	27	1.4	1.1	1.9	1.2	1.3
Oct-15	7.5	7.47	14	14	56	3.1	1.7	13.4	2.6	2.2
Nov-15	17.0	7.23	12	12	36	2.2	1.1	7.3	0.4	0.6
Dec-15	14.5	6.95				3.1	4.5	4.5		
Jan-16	18.0	7.15	64	30	69	2.2	1.7	3.8	1.1	2.2
Feb-16	13.0	7.07	68	68	55	2.2	0.8	7.7	4.5	4.1
Mar-16	14.5	7.08	46	46		3.1	0.6	6.7	0.3	0.5
Apr-16	14.5	6.99	36	36	81	5.0	1.1	6.6	0.5	0.3
May-16	8.5	6.52	30	30	57	4.5	0.6	5.6	ND	0.2
Mean	13.4	7.0	36.6	28.0	51.9	3.0	1.3	5.7	1.2	1.2
Min	7.0	6.2	8.0	8.0	6.8	1.4	0.0	1.3	0.2	0.2
Max	22.5	7.5	94.0	68.0	85.0	8.7	4.5	13.4	4.5	4.1
STDEV	4.5	0.3	26	18	23	1.9	1.1	3.3	1.2	1.1

10.2 Appendix B.

Data referred to in Chapter 6

Table A 3 H_2 production process economic study data for S:C 4

													HI income	Cashflow	Cum Cashflow	Net Cashflow	Discounted Cash Flow	Cumulative DCF		NPV
Yr 0								13,293,228.57								- 13,293,228.57				-13,293,228.57
Yr 1	644,130.05	398,796.86		293,103.45	791,288.51	699,233.33	151,456.96	2,978,009.16	16,271,237.72	4,598,895.60	158,650.90	157,303.31	1,936,840.66	1,936,840.66	- 11,356,387.91	1,760,764.23	1,760,764.23		-11,532,464.33
Yr 2	663,389.53	410,245.39		301,517.77	814,004.58	719,306.71	155,804.94	3,064,268.93	19,335,506.65	4,730,919.28	163,205.40	161,819.13	1,991,674.88	3,928,515.54	- 9,364,713.03	1,646,012.30	3,406,776.53		- 9,886,452.04
Yr 3	683,224.88	422,022.59		310,173.65	837,372.77	739,956.34	160,277.74	3,153,027.98	22,488,534.64	4,866,733.06	167,890.65	166,464.58	2,048,060.31	5,976,575.84	- 7,316,652.72	1,538,738.02	4,945,514.55		- 8,347,714.01
Yr 4	703,653.30	434,137.89		319,078.02	861,411.81	761,198.78	164,878.95	3,244,358.76	25,732,893.39	5,006,445.73	172,710.40	171,243.39	2,106,040.78	8,082,616.62	- 5,210,611.95	1,438,454.19	6,383,968.74		- 6,909,259.83
Yr 5	724,692.54	446,600.98		328,238.01	886,140.96	783,051.04	169,612.24	3,338,335.78	29,071,229.17	5,150,169.24	177,668.52	176,159.40	2,165,661.38	10,248,277.99	- 3,044,950.57	1,344,705.33	7,728,674.06		- 5,564,554.50
Yr 6	746,360.85	459,421.87	1,993,984.28	337,660.97	911,580.02	805,530.63	174,481.42	5,429,020.04	34,500,249.21	5,298,018.71	182,768.98	181,216.53	232,984.17	10,481,262.17	- 2,811,966.40	131,513.49	7,860,187.56		- 5,433,041.01
Yr 7	768,677.03	472,610.81		347,354.44	937,749.38	828,655.56	179,490.38	3,534,537.59	38,034,786.80	5,450,112.60	188,015.85	186,418.83	2,290,009.69	12,771,271.86	- 521,956.71	1,175,137.06	9,035,324.62		- 4,257,903.94
Yr 8	791,660.48	486,178.38		357,326.18	964,670.00	852,444.35	184,643.13	3,636,922.51	41,671,709.32	5,606,572.76	193,413.35	191,770.49	2,354,834.09	15,126,105.95	1,832,877.38	1,098,547.48	10,133,872.10		- 3,159,356.46
Yr 9	815,331.13	500,135.43		367,584.19	992,363.45	876,916.06	189,943.81	3,742,274.07	45,413,983.38	5,767,524.52	198,965.80	197,275.78	2,421,492.04	17,547,597.98	4,254,369.42	1,026,949.01	11,160,821.11		- 2,132,407.46
Yr 10	839,709.53	514,493.17		378,136.68	1,020,851.91	902,090.29	195,396.66	3,850,678.24	49,264,661.63	5,933,096.84	204,677.65	202,939.11	2,490,035.36	20,037,633.34	6,744,404.78	960,016.42	12,120,837.53		- 1,172,391.03
Yr 11	864,816.84	529,263.08	6,646,614.28	388,992.12	1,050,158.22	927,987.22	201,006.04	10,608,837.81	59,873,499.43	6,103,422.36	210,553.48	208,765.02	- 4,086,096.95	15,951,536.40	2,658,307.83	- 1,432,152.05	10,688,685.48		- 2,604,543.09
Yr 12	890,674.87	544,457.00		400,159.18	1,080,305.84	954,627.60	206,776.46	4,077,000.94	63,950,500.38	6,278,637.53	216,597.98	214,758.19	2,632,992.75	18,584,529.15	5,291,300.58	838,952.63	11,527,638.11		- 1,765,590.45
Yr 13	917,306.04	560,087.11		411,646.83	1,111,318.92	982,032.75	212,712.54	4,195,104.19	68,145,604.57	6,458,882.73	222,816.01	220,923.40	2,707,517.94	21,292,047.09	7,998,818.52	784,271.50	12,311,909.62		- 981,318.95
Yr 14	944,733.49	576,165.91		423,464.26	1,143,222.33	1,010,224.64	218,819.02	4,316,629.66	72,462,234.23	6,644,302.34	229,212.54	227,265.60	2,784,150.82	24,076,197.91	10,782,969.34	733,153.93	13,045,063.54		- 248,165.02
Yr 15	972,981.03	592,706.31		435,620.94	1,176,041.60	1,039,225.86	225,100.81	4,441,676.55	76,903,910.78	6,835,044.93	235,792.70	233,789.87	2,862,950.95	26,939,148.86	13,645,920.29	685,367.70	13,730,431.24		437,202.68
Yr 16	1,002,073.16	609,721.54	1,993,984.28	448,126.61	1,209,803.04	1,069,059.64	231,562.94	6,564,331.21	83,468,242.00	7,031,263.30	242,561.77	240,501.44	949,995.29	27,889,144.15	14,595,915.58	206,746.65	13,937,177.89		643,949.33
Yr 17	1,032,035.15	627,225.24		460,991.29	1,244,533.69	1,099,749.87	238,210.58	4,702,745.82	88,170,987.82	7,233,114.64	249,525.16	247,405.68	3,027,299.65	30,916,443.80	17,623,215.24	598,935.10	14,536,112.99		1,242,884.43
Yr 18	1,062,893.00	645,231.43		474,225.29	1,280,261.38	1,131,321.16	245,049.05	4,838,981.30	93,009,969.12	7,440,760.67	256,688.45	254,508.12	3,112,975.94	34,029,419.74	20,736,191.18	559,896.09	15,096,009.08		1,802,780.51
Yr 19	1,094,673.50	663,754.53		487,839.20	1,317,014.73	1,163,798.77	252,083.84	4,979,164.59	97,989,133.71	7,654,367.74	264,057.38	261,814.46	3,201,075.00	37,230,494.74	23,937,266.18	523,401.34	15,619,410.42		2,326,181.85
Yr 20	1,127,404.24	682,809.39		501,843.94	1,354,823.19	1,197,208.75	259,320.59	5,123,410.10	103,112,543.81	7,874,106.97	271,637.86	269,330.55	3,291,665.29	40,522,160.03	27,228,931.46	489,285.07	16,108,695.49		2,815,466.92

Table A 2. H_2 production process economic study data for S:C 3

	Wage Expenditur	Maintenance	Replacement Cost	Heat Costs	Electricity costs	Operating Cost of C&S	Catalyst Cost	Annual Expense	Cumulative Total (£	Income H2 Sales	Income abated (	RHI income	Cashflow	Cum Cashflow	Net Cashflow	Discounted Cash Flow	Cumulative DCF		NPV
Yr 0								13,011,385.70							- 13,011,385.70				-13,011,385.70
Yr 1	644,130.05	390,341.57		250,647.75	784,076.86	682,795.21	149,221.69	2,901,213.12	15,912,598.82	4,531,022.97	158,650.90	142,644.56	1,931,105.32	1,931,105.32	- 11,080,280.39	1,755,550.29	1,755,550.29		-11,255,835.41
Yr 2	663,389.53	401,547.38		257,843.27	806,585.90	702,396.68	153,505.50	2,985,268.26	18,897,867.08	4,661,098.19	163,205.40	146,739.56	1,985,774.89	3,916,880.21	- 9,094,505.49	1,641,136.28	3,396,686.56		- 9,614,699.14
Yr 3	683,224.88	413,074.88		265,245.35	829,741.12	722,560.87	157,912.29	3,071,759.38	21,969,626.47	4,794,907.56	167,890.65	150,952.11	2,041,990.94	5,958,871.15	- 7,052,514.55	1,534,178.02	4,930,864.58		- 8,080,521.12
Yr 4	703,653.30	424,933.30		272,859.93	853,561.07	743,303.93	162,445.59	3,160,757.12	25,130,383.59	4,932,558.29	172,710.40	155,285.60	2,099,797.18	8,058,668.33	- 4,952,717.37	1,434,189.73	6,365,054.31		- 6,646,331.40
Yr 5	724,692.54	437,132.16		280,693.11	878,064.84	764,642.47	167,109.02	3,252,334.14	28,382,717.72	5,074,160.66	177,668.52	159,743.49	2,159,238.54	10,217,906.87	- 2,793,478.84	1,340,717.25	7,705,771.56		- 5,305,614.15
Yr 6	746,360.85	449,681.21	1,951,707.86	288,751.16	903,272.05	786,593.59	171,906.34	5,298,273.06	33,680,990.78	5,219,828.10	182,768.98	164,329.36	268,653.38	10,486,560.25	- 2,524,825.46	151,647.83	7,857,419.38		- 5,153,966.32
Yr 7	768,677.03	462,590.52		297,040.54	929,202.91	809,174.87	176,841.37	3,443,527.26	37,124,518.03	5,369,677.32	188,015.85	169,046.88	2,283,212.79	12,769,773.04	- 241,612.67	1,171,649.18	9,029,068.56		- 3,982,317.14
Yr 8	791,660.48	475,870.43		305,567.89	955,878.18	832,404.42	181,918.08	3,543,299.48	40,667,817.51	5,523,828.36	193,413.35	173,899.82	2,347,842.06	15,117,615.10	2,106,229.40	1,095,285.65	10,124,354.21		- 2,887,031.49
Yr 9	815,331.13	489,531.57		314,340.04	983,319.24	856,300.83	187,140.53	3,645,963.33	44,313,780.84	5,682,404.73	198,965.80	178,892.08	2,414,299.29	17,531,914.38	4,520,528.68	1,023,898.58	11,148,252.79		- 1,863,132.91
Yr 10	839,709.53	503,584.89		323,364.02	1,011,548.06	880,883.25	192,512.90	3,751,602.65	48,065,383.49	5,845,533.46	204,677.65	184,027.66	2,482,636.12	20,014,550.51	7,003,164.80	957,163.70	12,105,416.49		- 905,969.21
Yr 11	864,816.84	518,041.65	6,505,692.85	332,647.05	1,040,587.27	906,171.37	198,039.50	10,365,996.55	58,431,380.03	6,013,345.23	210,553.48	189,310.67	- 3,952,787.17	16,061,763.34	3,050,377.64	- 1,385,427.79	10,719,988.70		- 2,291,397.00
Yr 12	890,674.87	532,913.43		342,196.58	1,070,460.13	932,185.46	203,724.76	3,972,155.23	62,403,535.27	6,185,974.50	216,597.98	194,745.35	2,625,162.59	18,686,925.92	5,675,540.22	836,457.70	11,556,446.40		- 1,454,939.30
Yr 13	917,306.04	548,212.15		352,020.26	1,101,190.57	958,946.36	209,573.23	4,087,248.60	66,490,783.87	6,363,559.55	222,816.01	200,336.04	2,699,462.99	21,386,388.91	8,375,003.21	781,938.27	12,338,384.67		- 673,001.03
Yr 14	944,733.49	563,950.05		362,125.95	1,132,803.21	986,475.49	215,589.59	4,205,677.79	70,696,461.66	6,546,242.66	229,212.54	206,087.22	2,775,864.63	24,162,253.54	11,150,867.84	730,971.91	13,069,356.59		57,970.89
Yr 15	972,981.03	580,139.76		372,521.75	1,165,323.38	1,014,794.93	221,778.67	4,327,539.51	75,024,001.17	6,734,170.18	235,792.70	212,003.51	2,854,426.88	27,016,680.43	14,005,294.72	683,327.10	13,752,683.69		741,297.99
Yr 16	1,002,073.16	596,794.23	1,951,707.86	383,215.98	1,198,777.12	1,043,927.35	228,145.43	6,404,641.13	81,428,642.29	6,927,492.66	242,561.77	218,089.64	983,502.94	28,000,183.37	14,988,797.67	214,038.90	13,966,722.59		955,336.88
Yr 17	1,032,035.15	613,926.82		394,217.23	1,233,191.25	1,073,896.09	234,694.95	4,581,961.49	86,010,603.78	7,126,364.99	249,525.16	224,350.49	3,018,279.15	31,018,462.52	18,007,076.82	597,150.44	14,563,873.02		1,552,487.32
Yr 18	1,062,893.00	631,551.24		405,534.30	1,268,593.32	1,104,725.17	241,432.50	4,714,729.53	90,725,333.32	7,330,946.48	256,688.45	230,791.08	3,103,696.47	34,122,158.99	21,110,773.29	558,227.09	15,122,100.12		2,110,714.41
Yr 19	1,094,673.50	649,681.62		417,176.25	1,305,011.71	1,136,439.28	248,363.47	4,851,345.83	95,576,679.15	7,541,401.04	264,057.38	237,416.55	3,191,529.14	37,313,688.14	24,302,302.44	521,840.52	15,643,940.63		2,632,554.93
Yr 20	1,127,404.24	668,332.48		429,152.42	1,342,475.59	1,169,063.83	255,493.42	4,991,921.96	100,568,601.11	7,757,897.26	271,637.86	244,232.24	3,281,845.39	40,595,533.53	27,584,147.83	487,825.41	16,131,766.04		3,120,380.34

Table A 4 H_2 production process economic study data for S:C 2

	Wage Expenditu	Maintenance	Replacement Costs	Heat Costs	Electricity costs	Operating Cost of C&S	Catalyst Cost	Annual Expense	Cumulative Total (E	Income H2 Sales	Income abated (	RHI income	Cashflow	Cum Cashflow	Net Cashflow	Discounted Cash	Cumulative DCF		NPV
Yr 0								12,530,090.07							- 12,530,090.07				- 12,530,090.07
Yr 1	644,130.05	375,902.70		169,125.20	759,805.85	624,327.43	141,102.00	2,714,393.23	15,244,483.31	4,284,954.00	158,650.90	130,949.71	1,860,161.38	1,860,161.38	- 10,669,928.70	1,691,055.80	1,691,055.80		- 10,839,034.28
Yr 2	663,389.53	386,694.00		173,980.39	781,618.12	642,250.43	145,152.71	2,793,085.20	18,037,568.51	4,407,965.14	163,205.40	134,708.97	1,912,794.32	3,772,955.69	- 8,757,134.38	1,580,821.75	3,271,877.54		- 9,258,212.53
Yr 3	683,224.88	397,795.09		178,974.97	804,056.58	660,687.96	149,319.71	2,874,059.19	20,911,627.70	4,534,507.65	167,890.65	138,576.16	1,966,915.26	5,739,870.95	- 6,790,219.12	1,477,772.55	4,749,650.09		- 7,780,439.98
Yr 4	703,653.30	409,214.87		184,112.93	827,139.19	679,654.79	153,606.34	2,957,381.42	23,869,009.12	4,664,682.90	172,710.40	142,554.36	2,022,566.25	7,762,437.20	- 4,767,652.88	1,381,439.96	6,131,090.05		- 6,399,000.02
Yr 5	724,692.54	420,962.49		189,398.38	850,884.44	699,166.11	158,016.02	3,043,119.98	26,912,129.10	4,798,595.18	177,668.52	146,646.76	2,079,790.48	9,842,227.68	- 2,687,862.39	1,291,386.26	7,422,476.31		- 5,107,613.76
Yr 6	746,360.85	433,047.35	1,879,513.51	194,835.57	875,311.37	719,237.55	162,552.30	5,010,858.50	31,922,987.60	4,936,351.77	182,768.98	150,856.65	259,118.90	10,101,346.58	- 2,428,743.49	146,265.86	7,568,742.17		- 4,961,347.90
Yr 7	768,677.03	445,479.14		200,428.85	900,439.54	739,885.20	167,218.80	3,222,128.57	35,145,116.17	5,078,063.04	188,015.85	155,187.40	2,199,137.72	12,300,484.30	- 229,605.77	1,128,505.37	8,697,247.55		- 3,832,842.52
Yr 8	791,660.48	458,267.82		206,182.70	926,289.08	761,125.60	172,019.26	3,315,544.95	38,460,661.12	5,223,842.51	193,413.35	159,642.47	2,261,353.39	14,561,837.69	2,031,747.62	1,054,938.05	9,752,185.60		- 2,777,904.48
Yr 9	815,331.13	471,423.63		212,101.73	952,880.70	782,975.76	176,957.54	3,411,670.49	41,872,331.62	5,373,806.98	198,965.80	164,225.44	2,325,327.73	16,887,165.42	4,357,075.35	986,165.95	10,738,351.55		- 1,791,738.53
Yr 10	839,709.53	484,957.11		218,190.69	980,235.71	805,453.19	182,037.58	3,510,583.81	45,382,915.42	5,528,076.57	204,677.65	168,939.97	2,391,110.39	19,278,275.81	6,748,185.74	921,876.57	11,660,228.11		- 869,861.96
Yr 11	864,816.84	498,879.11	6,265,045.04	224,454.44	1,008,376.02	828,575.89	187,263.46	9,877,410.80	55,260,326.22	5,686,774.89	210,553.48	173,789.85	- 3,806,292.57	15,471,983.24	2,941,893.16	- 1,334,082.33	10,326,145.79		- 2,203,944.29
Yr 12	890,674.87	513,200.78		230,898.01	1,037,324.16	852,362.39	192,639.36	3,717,099.57	58,977,425.79	5,850,029.08	216,597.98	178,778.96	2,528,306.44	18,000,289.68	5,470,199.61	805,596.35	11,131,742.13		- 1,398,347.94
Yr 13	917,306.04	527,933.59		237,526.55	1,067,103.35	876,831.75	198,169.60	3,824,870.88	62,802,296.67	6,017,969.91	222,816.01	183,911.29	2,599,826.33	20,600,116.01	8,070,025.94	753,077.08	11,884,819.22		- 645,270.86
Yr 14	944,733.49	543,089.35		244,345.39	1,097,737.42	902,003.56	203,858.59	3,935,767.81	66,738,064.48	6,190,731.94	229,212.54	189,190.96	2,673,367.63	23,273,483.64	10,743,393.57	703,981.25	12,588,800.47		58,710.39
Yr 15	972,981.03	558,680.19		251,359.99	1,129,250.93	927,898.00	209,710.90	4,049,881.03	70,787,945.51	6,368,453.57	235,792.70	194,622.19	2,748,987.43	26,022,471.08	13,492,381.00	658,085.74	13,246,886.20		716,796.13
Yr 16	1,002,073.16	574,718.61	1,879,513.51	258,575.95	1,161,669.12	954,535.81	215,731.21	6,046,817.37	76,834,762.88	6,551,277.18	242,561.77	200,209.35	947,230.92	26,969,701.99	14,439,611.92	206,145.05	13,453,031.25		922,941.17
Yr 17	1,032,035.15	591,217.45		265,999.07	1,195,017.96	981,938.34	221,924.36	4,288,132.32	81,122,895.20	6,739,349.22	249,525.16	205,956.89	2,906,698.96	29,876,400.95	17,346,310.87	575,074.89	14,028,106.14		1,498,016.07
Yr 18	1,062,893.00	608,189.94		273,635.29	1,229,324.17	1,010,127.52	228,295.29	4,412,465.21	85,535,360.41	6,932,820.39	256,688.45	211,869.44	2,988,913.07	32,865,314.02	20,335,223.95	537,582.29	14,565,688.43		2,035,598.36
Yr 19	1,094,673.50	625,649.67		281,490.73	1,264,615.23	1,039,125.95	234,849.13	4,540,404.20	90,075,764.60	7,131,845.66	264,057.38	217,951.72	3,073,450.57	35,938,764.59	23,408,674.52	502,533.73	15,068,222.16		2,538,132.08
Yr 20	1,127,404.24	643,610.63		289,571.68	1,300,919.41	1,068,956.86	241,591.10	4,672,053.91	94,747,818.51	7,336,584.49	271,637.86	224,208.62	3,160,377.06	39,099,141.65	26,569,051.58	469,769.91	15,537,992.07		3,007,902.00

10.3 Appendix C.

10.4 Data referred to in Chapter 7

Table A 5. Ammonium analysis results

Temp	S:C	CO	CO2	moles H2O	mole H2O in	mole H2O out	run time /hr	total moles out	mass out	Litres	mg/L N out	mg/L NH3 out	g NH3 out	g adjusted NH3 in	% conversion
700	2	0.031	0.012	0.056	0.106	0.050	3.730	0.186	3.346	0.003	829.500	10085.719	0.034	0.448	92.461
750	2	0.036	0.010	0.056	0.111	0.055	3.180	0.174	3.139	0.003	522.500	6352.970	0.020	0.221	90.972
800	2	0.039	0.010	0.059	0.108	0.050	3.330	0.165	2.981	0.003	224.000	2723.570	0.008	0.400	97.968
700	3	0.027	0.019	0.066	0.160	0.094	3.120	0.293	5.274	0.005	569.500	6924.433	0.037	0.371	90.162
750	3	0.031	0.018	0.066	0.162	0.097	3.250	0.314	5.656	0.006	527.000	6407.684	0.036	0.258	85.940
800	3	0.032	0.016	0.064	0.162	0.098	3.350	0.327	5.898	0.006	301.500	3665.876	0.022	0.266	91.863
700	4	0.023	0.026	0.074	0.217	0.142	3.100	0.441	7.950	0.008	406.000	4936.470	0.039	0.260	84.906
750	4	0.024	0.025	0.073	0.216	0.143	3.100	0.443	7.978	0.008	207.500	2522.950	0.020	0.238	91.554
800	4	0.032	0.018	0.068	0.215	0.147	3.220	0.473	8.527	0.009	169.000	2054.836	0.018	0.428	95.902